DE GRUYTER

Chérif F. Matta, Lulu Huang, Lou Massa

QUANTUM CRYSTALLOGRAPHY

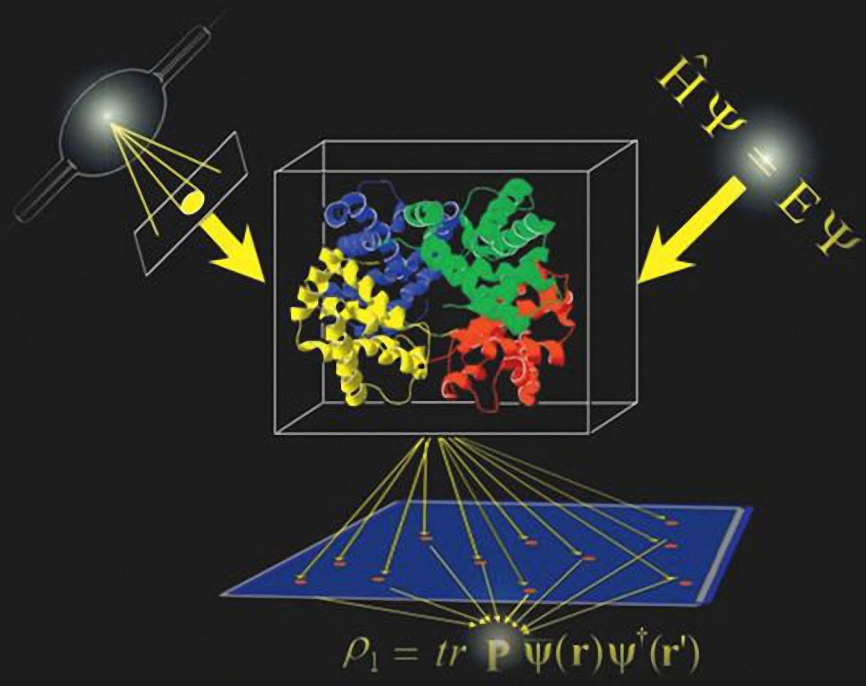

DE
G

Chérif F. Matta, Lulu Huang, Lou Massa
Quantum Crystallography

Also of interest

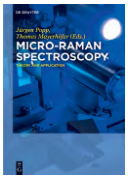

Micro-Raman Spectroscopy.
Theory and Application
Popp, Mayerhöfer (Eds.), 2020
ISBN 978-3-11-051479-7, e-ISBN (PDF) 978-3-11-051531-2

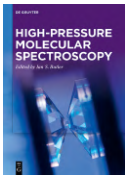

High-pressure Molecular Spectroscopy
Butler (Ed.), 2022
ISBN 978-3-11-066528-4, e-ISBN (PDF) 978-3-11-066861-2

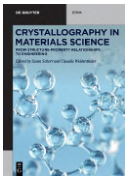

Crystallography in Materials Science.
From Structure-Property Relationships to Engineering
Schorr, Weidenthaler (Eds.), 2021
ISBN 978-3-11-067485-9, e-ISBN (PDF) 978-3-11-067491-0

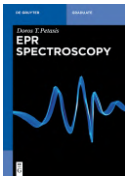

EPR Spectroscopy
Petasis, Hendrich, 2022
ISBN 978-3-11-041753-1, e-ISBN (PDF) 978-3-11-041756-2

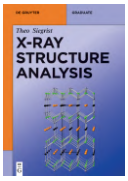

X-Ray Structure Analysis
Siegrist, 2021
ISBN 978-3-11-061070-3, e-ISBN (PDF) 978-3-11-061083-3

Chérif F. Matta, Lulu Huang, Lou Massa

Quantum Crystallography

DE GRUYTER

Authors

Professor Chérif F. Matta
Department of Chemistry and Physics
Mount Saint Vincent University
Halifax, Nova Scotia
Canada B3M 2J6
&
Department of Chemistry
Saint Mary's University
Halifax, Nova Scotia
Canada B3H 3C3
&
Département de chimie
Université Laval
Québec, Québec
Canada G1V 0A6
&
Department of Chemistry
Dalhousie University
Halifax, Nova Scotia
Canada B3H 4J3

Dr. Lulu Huang
Department of Chemistry
Hunter College
The City University of New York (CUNY)
New York, NY 10021
USA
&
Retired from
Center for Computational Materials Science
Naval Research Laboratory
Washington, DC 20375
USA

Professor Lou Massa
Department of Chemistry and
Department of Physics,
Hunter College and the Graduate Center
The City University of New York (CUNY)
New York, NY 10021
USA

ISBN 978-3-11-056566-9
e-ISBN (PDF) 978-3-11-056667-3
e-ISBN (EPUB) 978-3-11-056571-3

Library of Congress Control Number: 2022945742

Bibliographic information published by the Deutsche Nationalbibliothek
The Deutsche Nationalbibliothek lists this publication in the Deutsche Nationalbibliografie; detailed bibliographic data are available on the Internet at http://dnb.dnb.de.

Cover image: © Chérif F. Matta; A graphical representation illustrating how the interplay of experiment (represented by an X-ray beam falling on a crystallographic unit cell) and quantum theory (epitomized by the Schrödinger equation) lead to more than just an experimentally-derived electron density (ρ). The union of theory and experiment deliver more, that is, a density matrix (ρ_1) which is represented in a chosen basis set by its surrogate **P.** (Graphic art courtesy of C. F. Matta).
Typesetting: Integra Software Services Pvt. Ltd.
Printing and binding: CPI books GmbH, Leck

www.degruyter.com

This book is dedicated to Jerome Karle (Nobel Laureate 1985) and Isabella Karle (US National Medal of Science 1995), important supporters of quantum crystallography.

Isabella and Jerome as graduate students, sometime during the World War II years, with their Ph.D. mentor Lawrence Brockway (left) (courtesy of the U.S. Naval Research Laboratory).

Acknowledgements

Chemists should naturally be the first and greatest appreciators. Research is appreciation. Willis R. Whitney (1921)

("The Biggest Things in Chemistry", *Journal of Industrial & Engineering Chemistry*, 13 (2), 161–166).

L. M. thanks his wife Mary for her constant support. C. F. M. is grateful to Maged Matta, Hebatallah Habib, and Sara and Nadine Matta. L. H. thanks her family.

The authors are indebted to too many people to mention here who have helped them to complete this work. Of those many people, the authors are particularly grateful to the following scholars for directly and personally influencing their thoughts over the years: William L. Clinton, Jerome and Isabella Karle, William N. Lipscomb Jr., Ada Yonath, Richard F. W. Bader, John C. Polanyi, Claude Lecomte, Russell J. Boyd, Philip Coppens, Todd A. Keith, André D. Bandrauk, Sason Shaik, Tina A. Harriott, Daniel Majaess, Paul W. Ayers, Leon Cohen, Viraht Sahni, Rafik A. Matta, Ashraf W. El-Miniawy, Bhakta Rath, Samuel Lambrakos, Nagwa El-Badry, Mahmoud Abdel-Aty, Hugo Bohórquez, Eva Knoll, Ángel Martín-Pendás, Labiba K. El-Khordagui, Abdel-Aziz Saleh, Mohamed El-Raey, Ignacy Cukrowski, Thanh-Tung Nguyen-Dang, Jesús Hernández-Trujillo, Fernando Cortés-Guzmán, Aurora Costales Castro, Olimpia Lombardi, Eric Scerri, and James S. M. Anderson.

The authors' appreciation is also directed to Piero Macchi, Alessandro Genoni, Simon Grabowsky, Dylan Jayatilaka, Carlo Gatti, Naganami Sukumar, and Paulina M. Dominiak, and all the members and consultants, past and present, of the *Commission on Quantum Crystallography* of the *International Union of Crystallography* (IUCr) for furthering the subject of quantum crystallography.

Much gratitude is due to the publisher de Gruyter, its editorial office, and handling editors, especially Ria Sengbusch, for supporting this monograph. The authors also thank Laura Gamble for helping with typesetting parts of this book.

Most importantly of all, the authors deeply appreciate the many students who have contributed their work to the study of quantum crystallography over the years and whose work this monograph is largely based upon.

Finally, much of the work in this monograph has been enabled through the support of the U.S. Naval Research Laboratory, Hunter College (and its President Jennifer J. Raab) - The City University of New York (CUNY), the Natural Sciences and Engineering Research Council of Canada (NSERC), Canada Foundation for Innovation (CFI), Compute Canada, and Mount Saint Vincent University, a support much appreciated by the authors.

https://doi.org/10.1515/9783110566673-202

Preface

> [*T*]*he task of physics as of all science is found in the coherent* description *of experience*. Robert Bruce Lindsay & Henry Margenau (1936)
>
> (*Foundations of Physics*, p. 2, Dover Publications, Inc., New York (1963)).

Readers are presented information about the authors' experience in the developing field of quantum crystallography (QCr). Their inspiration which underlies the subject is the fundamental idea of *N*-representability and its implementation by derivation of the Clinton equations. The purpose of the discussion includes a reference to the historical context in which QCr was developed.

This monograph introduces the reader to the core ideas that led to the development of *quantum crystallography* (QCr). This field of science lies at the intersection of crystallography, as commonly known, and quantum mechanics. In this monograph, some aspects of this exciting field are reviewed with special focus on the contributions and interests of the writers. It is made clear from the outset that *this is not a textbook on crystallography or quantum mechanics, nor on QCr*, rather it is a *topical review* focused on the authors' interests and contributions. This means that several important topics are omitted or alluded to in passing.

Crystallography is very old. But, modern crystallography begins when X-rays were discovered by Wilhelm C. Röntgen in 1895, and their wave nature was exploited by Max von Laue and the Braggs (William and Laurance) in 1912 and 1913, respectively. Quantum mechanics begins in the latter half of the 1920s with Werner Heisenberg, Erwin Schrödinger, and Paul A. M. Dirac.

Soon after the discovery of quantum mechanics, its application to crystallography came about in increments. It was implemented in the solution of crystal structures by using as a model the sum of the spherical atoms that occupy the crystal unit cell. Of course, the overlap of orbitals associated with chemical bonding is not well represented in that way. This led to a representation of directional bonding and lone pair density achieved by placing multipoles at atomic centers. The extraordinary success of such multipole representation placed ever-increasing emphasis upon electron density as the source of scattering. At the same time, it led to looking away from the density matrix, whose diagonal elements are the electron density. And, the density matrix is required to be *N*-representable in order that it, and the electron density corresponding to it, can both be quantum mechanically valid. For a density matrix to be *N*-representable simply means it can be derived from an antisymmetric *N*-body wave function.

What occurred at about the same time as the ever-increasing prominence of multipole representations was the invention of a fully quantum mechanical X-ray formalism. Its goal was that of extracting from the X-ray scattering experiment of the crystallized molecule a representation of exactly the same formalism as would be obtained by

https://doi.org/10.1515/9783110566673-203

solving the Schrödinger equation within a single determinant approximation. Such single determinants underlie the Hartree–Fock approximation and the Kohn–Sham equations of density functional theory. For the first time the density matrix of theory and experimental crystallography would have exactly the same parameters and physical interpretation. They could therefore be compared one to another in the same way.

It was the *N*-representable density matrix X-ray formalism that came to be called *quantum crystallography*. It is perhaps a subtle point that *an "accurate" electron density can, at the same time, be not quantum-mechanically valid*. As discussed in a recent paper [1], a leader in the field of experimental X-ray density opined that to be accurate is to be quantum mechanical. But that misses the point that accuracy in the density does not mean the same as quantum mechanical validity of the density matrix. Fortunately, something is known about the quantum mechanical validity of the density matrix. In particular, the mathematical requirements for *N*-representability by a single determinant are exactly known. There is another factor sometimes not sufficiently appreciated regarding the difference between having an accurate electron density and a quantum mechanically valid density matrix. The difference is that all quantum properties can be calculated from *N*-representable density matrices, but only some properties follow from the electron density, no matter how accurate that density may be.

Having "grown up" in the field of quantum mechanics, as it were, it would be natural to look for *N*-representability of the density matrix in an attempt to extract its elements from the X-ray scattering data. The emphasized *N*-representability is after all just an acknowledgment of the experimental indistinguishability of the electrons which scatter X-rays. Thus, it was natural evolution that we would introduce *N*-representability into the formalism of QCr. On the other hand, a crystallographer searching for a representation of chemical bonding might be drawn to increasingly accurate densities represented by, say, multipoles. As it happens, both "*N*-representability" and accuracy are important.

C. F. Matta, Halifax, NS
L. Huang, Alexandria, VA
L. Massa, New York City, NY
July 2022

Reference

[1] Massa L. A zigzag path through quantum crystallography. *Struct. Chem.* 28, 1293–1296 (2017).

Foreword

Quantum crystallography, the field of this book, aims at expanding crystallography by combining scattering experiments with quantum mechanics. The field has been launched more than 50 years ago and is now a fast-developing area of research to which dozens of research groups around the world are contributing. The authors, Chérif F. Matta, Lulu Huang, and Lou Massa, are well known among these scientists. They are known to me through their meaningful contributions to understanding ribosome's function and origin through crystallography, documented in a small number of papers we published together. Perhaps of more importance to the reader, the authors have published a great number of papers reaching back to what they call the start of quantum crystallography. It may be worth something to know of the authors' description of that start to understand better the present state of the field. They follow a line of progress which begins with *extraction* of quantum information from X-ray scattering of small systems and follow it through to what they refer to as *injecting* quantum information into the classical structure of large systems.

Molecules, small or large, need validity in their quantum mechanical representation. This book claims to find it in the universal requirement of *N*-representability, a term whose definition and enlightenments I leave to the book itself. Importantly, those electron density matrices, which have the required validity, provide exactly the underpinning needed to understand the system in accordance with the theory created by Richard F. W. Bader and his school, namely the Quantum Theory of Atoms in Molecules (QTAIM). In this respect, this book also contains an excellent review of QTAIM in the context of quantum crystallography.

I can recommend this book to those readers interested in the union of two fields, experimental crystallography and the theory of quantum mechanics, that developed separately for a time and now can be seen coming together as quantum crystallography.

Ada Yonath
Professor
Weizmann Institute of Science
Nobel Laureate in Chemistry (2009)

https://doi.org/10.1515/9783110566673-204

Contents

About the authors

Chérif F. Matta, B.Pharm.Sci., Dipl., PhD, HDR, FRSA, FRSB, FInstP, FRSC, FAAS, FAAAS, is Professor and Chair/Head of the Department of Chemistry & Physics at Mount Saint Vincent University and an Adjunct Professor at Dalhousie, Laval, and Saint Mary's Universities. He holds frequent Visiting Professorships at Zewail City for Science and Technology (Egypt). Professor Matta has a Bachelor of Pharmaceutical Science from Alexandria University (Egypt), a PhD in theoretical chemistry from McMaster University (Canada), and a Habilitation to Direct Research from the Université de Lorraine (France). He held postdoctoral fellowships at the University of Toronto and at Dalhousie University. Prof. Matta's research ranges from theoretical and computational chemistry to mitochondrial biophysics. He has been named "*Distinguished Visiting Professor*" by the Polish Ministry of Science and Higher Education (2022). Matta's accolades include his University's Award for Research Excellence (2017), the Lady Davis Visiting Fellowship (2016), the NSERC-Acfas "Preuve par l'image" Prize for 2016, the Molecular Graphics and Molecular Simulation Society Silver Jubilee Prize for 2009, the John C. Polanyi Prize in Chemistry for 2004, and the Izaak Walton Killam Fellowship in 2002–2004. He was named the 2021–2022 "*Science Atlantic Speaker of the Year*". Chérif Matta is *Fellow of the American Association for the Advancement of Science*, *Fellow of the African Academy of Sciences*, *Fellow of the Royal Society of Chemistry*, *Fellow of the Institute of Physics*, *Fellow of the Royal Society of Biology*, and *Fellow of the Royal Society of the Arts*. He is the outgoing Chair/Head of the Interdisciplinary Adjudication Committee of the Canada Research Chairs Programme and is the current Director of Accreditation & member of the Board of Directors of the Canadian Society for Chemistry. He is also, currently, a member of the Commission for Quantum Crystallography of the International Union of Crystallography (IUCr) and outgoing Associate Editor for the journal "*Foundation of Chemistry*".

Lulu Huang, earned both an M.A. and a PhD in analytical chemistry with a thesis devoted to quantum crystallography from City University of New York (CUNY). Dr. Huang held a postdoctoral appointment to further study quantum crystallography with Professor Lou Massa and Dr. Jerome Karle (Nobel Laureate in Chemistry, 1985). She then made a career at the US Naval Research Laboratory (NRL) as a Senior Scientist in the Laboratory for the Structure of Matter. Since 1995 she has worked with Dr. Jerome Karle until his retirement from NRL in 2009. As a co-creator of the kernel energy method (KEM) - along with J. Karle and L. Massa, she applied it extensively to biological macromolecules. She is also credited for inventing a theoretical protocol for discovering explosive molecules. Her recent work using density functional calculations to predict (IR and UV-Vis spectra) of water clusters and of explosives is well-documented. She received Alan Berman Research Publication Award in 1996, 2002, and 2006 at the US Naval Research Laboratory. Dr. Huang retired from NRL in 2015 and subsequently she has served as "Distinguished Scholar" at the Department of Chemistry of Hunter College, The City University of New York (CUNY).

https://doi.org/10.1515/9783110566673-206

Lou Massa is Professor of Chemistry and Physics at Hunter College & the Graduate School, The City University of New York. He obtained a B.Sc. from Le Moyne College, an M.Sc. from Clarkson University, and a PhD from Georgetown University – all three degrees in physics – followed by a Postdoctoral Fellowship at Brookhaven National Laboratory. He has also received an Honorary Doctorate of Humane Letters (D.H.L.) from Mount Saint Vincent University. In 2017, the journal "*Structural Chemistry*" published a special issue in his honor titled "*A Path through Quantum Crystallography*" with articles contributed by some 80 authors including Nobel Laureate Ada Yonath. His awards include, the American Society of Engineering Education's "Distinguished Visiting Professor" at the US Naval Research Laboratory (NRL), the Hunter College President's Award for Excellence in Research, the NRL Berman Award for Outstanding Science Paper, and the Westchester Branch of the American Chemical Society 2019 Award as "Distinguished Scientist". His research interests include quantum crystallography. He currently serves as Consultant for the Commission on Quantum Crystallography of the International Union of Crystallography. He served as co-guest editor for two special issues of the *Journal of Computational Chemistry* on quantum crystallography. Professor Massa is also interested in the dissemination of science to the general public and has served as host of his televised broadcast on CUNY-TV interviewing prominent scientists about their recent books. A subset of the transcripts of these interviews appears in Prof. Massa's Oxford University Press book "*Science and the Written Word*". He has had Visiting in Residence Appointments at Harvard University, Université de Bordeaux, University of London, IBM Watson Research Laboratory, University of North Carolina (Chapel Hill), Grumman Aerospace, Naval Surface Warfare Center (Carderock, MD). His membership in learned societies includes the American Crystallographic Association, the American Physical Society, and the American Chemical Society.

Introduction

There is no more basic enterprise in chemistry than the determination of the geometrical structure of a molecule. Such a determination, when it is well done, ends all speculation as to the structure and provides us with the starting point for the understanding of every physical, chemical and biological property of the molecule. Roald Hoffmann (1981)

(Foreword of L. V. Vilkov, V. S. Mastryukov, N. I. Sadova, *Determination of the Geometrical Structure of Free Molecules* (English Translation), p. 5, Mir Publishers, Moscow (1981))

The problem which this book presents for the reader is how to understand the creation of a (relatively) new borderline field of scientific importance, namely, *quantum crystallography* (QCr). The solution resides in the idea of *N*-representability. Imposing it upon the analysis of experimental X-ray scattering data follows from the Clinton equations. Various applications using experimental crystallography, for example, the X-ray scattering data of the beryllium crystal, prove the point. The reader of these chapters will understand the origin of the field and its recent expansion and possible paths forward into the future.

Experimental crystallography is important because in the briefest of words *structure implies function*. And quantum mechanics is regarded as the most important theoretical conception of the chemical material world. Were it possible to join these two studies, experimental and theoretical, within a common formalism, would not that advance the understanding to flow from the exercise of both? To visualize the creation of that field of adjoining scientific borders, quantum crystallography is the challenge and reward a reader may anticipate in consideration of the pages which herein follow.

A logical course of action is to recollect for starters a few fundamentals of crystallography. In particular, the measured intensities of the scattered X-rays determine the structure factors. These are related to the electron density from which the scattering occurs. The structure factors and the electron density are Fourier transforms of one another, and as such are information equivalents, in principle. To know one is to know the other. Crystal structures are determined by placing atoms at such positions with assigned vibrational motions to minimize the difference between measured and calculated structure factors as judged by the crystallographic *R*-factor. For in-depth elaboration of these points and more, the reader can consult standard textbooks such as Refs. [1–6] or introductory expositions such as Refs. [7–12].

In a similar way, one is motivated to recollect the main points of quantum mechanics intended to calculate the properties, particularly the energetics, of crystalline materials. The crux of the matter is that the fundamental equation of motion for most of chemistry is the nonrelativistic time-independent Schrödinger equation whose solutions are antisymmetric *N*-body wave functions. The antisymmetry expresses the experimental indistinguishability of the electrons and their Pauli correlation. The one-

https://doi.org/10.1515/9783110566673-001

and two-particle density matrices are obtained by successive integrations over the square of the wave function until all coordinates are "averaged out," except for those of particle one, or particles one and two, respectively. That the density matrices are descendants of antisymmetric wave functions is the property called *N*-representability. To be fully quantum mechanical is to be *N*-representable. The density matrices are simpler than the wave function and still allow for the calculation of all one- and two-electron properties including the molecular energy. For a general introduction to quantum mechanics, there exists an abundance of excellent texts including Refs. [13–18], while for a specialized discussion about the density matrix formalism within quantum chemistry we direct the reader to Refs. [19–24].

The energy variational principle will hold so long as the density matrices are *N*-representable. Importantly, the Clinton equations have been derived for the purpose of imposing *N*-representability upon the density matrix while simultaneously ensuring the accuracy of the electron density [25–28]. The Clinton equations, at first, were explored with simple cases involving theoretically produced X-ray structure factors [29]. In one case, based on an approximate sum of spherical atomic densities to represent the H_2 molecule due to Stewart, Davidson, and Simpson (SDS) [30], the data was fit by least squares to a density matrix in two different ways. First, the Clinton equations were used to find a best single determinant *N*-representable density fit to the SDS data. Second, using the same atomic orbital basis as before, but without imposition of any forced relation to *N*-representability, an optimum least squares fit to the data was obtained. The result indicated that in the first case, the density matrix was quantum mechanically valid, but not so in the second case. Coleman's theorem that *N*-representability can be judged by an inequality condition satisfied by the eigenvalues of the density matrix [23] was used to reach that conclusion. The meaning of that application of the Clinton equations is that best least squares fit to X-ray data leads toward density accuracy without, at the same time, guaranteeing quantum validity of the density matrix. The density and the density matrix are related, but different.

Our first application of the Clinton equations using real experimental X-ray scattering data occurred with the beryllium crystal [31] using the highly accurate data of Larsen and Hansen [32]. This was perhaps the most accurate diffraction data of that time. How we rather accidentally came upon these data has been discussed elsewhere [33].

The density matrix was framed in the context of a ligand field model [34]. Each Be atom was given a fixed Hartree–Fock inner shell orbital. The valence orbital was a sum of two atomic orbitals: one attached to the Be nucleus and one allowed to "float" to a position minimizing the *R*-factor. The resulting idempotent density matrix produced by solution of the Clinton equations was highly accurate as judged by the calculated structure factors. Our experimental density contours were compared to highly accurate theoretical contours which were available for the Be crystal and displayed impressive similarity. We understood the publication of these Be results to be a strong

indication of the quantum mechanical importance of both *N*-representability and the Clinton equation as a method for its imposition utilizing X-ray scattering data.

Now clearly Be forms a small "molecular" crystal, with only a few electrons per unit cell. Several other papers investigated the use of projector density matrices for description of small-molecule X-ray scattering. In our view, there is no doubt a projector density matrix is adequate to represent X-ray scattering of a molecule sufficiently small, that is to say, the number of X-ray data must be considerably larger than the number of elements in the projector matrix they are meant to determine. But actually as the size of a molecule grows, there comes a point at which the number of X-ray data is insufficient to determine every element of the density matrix. Our experimental investigation of the maleic anhydride crystal was the occasion for realizing a way to circumvent the problem of too few scattering data for the system under consideration [35].

Maleic anhydride is a small flat molecule composed of nine atoms. Its structure was determined by Louis Todaro, the crystallographer in charge of the Laboratory for Quantum Crystallography at Hunter College (City University of New York, CUNY) at the time (*ca*. 1999). The scattering data were fit to a density matrix corresponding to a full molecular orbital model accounting, in that way, for both the core and valence contributions. The *R*-factor associated with the *N*-representable density matrix was about 1%. We calculated a density difference map based upon using multipoles at atomic positions. The result was striking in the sense that it showed quite beautifully a flow of electrons consistent with the formation of chemical bonds and lone pairs consistent with chemical knowledge of the molecule.

Indeed, multipoles are conveniently useful in achieving *accuracy* of a molecular density. What they miss is *N-representability*. This led to the idea applicable to very large molecules that the quantum crystallography can be broken into two parts: (1) the classical structure of a crystalline molecule, that is, the Cartesian coordinates of the atoms can be determined with high accuracy based upon a multipole representation of atomic densities; and (2) the *N*-representability, that is, the quantum validity of the density matrix can be ensured by its quantum chemical calculation using the classical structure. In the case of very large structures, one would be *injecting* quantum mechanics into the crystallography, whereas for small structures one speaks of *extracting* quantum mechanics from the scattering data.

Calculating the *ab initio* wave function or the density matrix of a very large molecule is not easy. The computational difficulty to do so rises as a high power of the number of atoms in the system. Surmounting this difficulty, in order to "inject" quantum mechanics into the crystallography of large molecules required us to invent a time-saving – but still accurate – method of *ab initio* calculation which came to be called the *kernel energy method* (KEM) [36–46].

KEM makes *ab initio* calculations on very large molecules practicable by the simple device of breaking such molecules into small pieces (so-called kernels). The

kernels are chosen to be small enough to calculate quickly. The sum of kernels would not accurately replicate the entire whole molecule. But the KEM includes the interaction between kernels by including all possible double kernels in the final summation (see Chapter 5, or any of the following Refs. [36–46]). The KEM has been tested on a variety of large biological molecules, including proteins, DNA, and RNA examples. It is accurate. Interestingly, "accurate" KEM is *not* mandated to be "*N*-representable". However, if the kernels, like puzzle pieces, are used to build up the full molecule puzzle, that is, the density matrix of the full system, *N*-representability can be restored by using the Clinton equations [47]. The result is a density matrix projector of a size corresponding to the full system. However, to make energy calculations practicable, that full projector can be decomposed into subspace projectors corresponding again to the size of the smaller kernels.

Topology and its underlying topography play an important role in the analysis of both classical and quantum crystallography, as shall be seen in this book. Rickard F. W. Bader and his school introduced topological analysis into the study of electron density [48–50] as presented in the results of crystallography [3–6]. Thus, the importance of critical points, bond paths, and Bader partitioning became much discussed in papers displaying highly accurate experimental densities. Bader was also convinced that his zero flux condition for defining individual atoms or functional groups of atoms could be related to kernels of the KEM (private communication to the present authors, *ca*. 2007).

Finally, we come to a discussion of the calculation of the energy associated with an experimentally derived electron density matrix. The energy cannot be obtained from an electron density alone. Some portions of the energy are given up by the density, that is, the classical electrostatic part, but not its entirety which includes quantum terms. For example, an energy quantity much calculated in crystallography papers is the classical potential energy of repulsion between two electron clouds. This is possible because, in this case, the energy operator is purely multiplicative, simply involving multiplication by the inverse distance between points. However, the kinetic energy cannot be obtained from the density alone. Its quantum operator is not purely multiplicative as it requires a second derivative sandwiched between coordinates arriving from wave functions on the left and right. The density matrix or the wave function is required for the kinetic energy expectation values.

Importantly, the variational theorem, which is crucial in calculations of the energy, only holds true if the density matrix is *N*-representable. In the case of single determinants, the two-body density matrix is a known functional of the one-body density matrix. Therefore the *N*-representability of ρ_1 determines that of ρ_2 and guarantees the variational theorem. We used the functional relation between ρ_2 and ρ_1 to derive the variational energy associated with *N*-representable ρ_1 in KEM form (see Chapter 9). The formalism for calculation of energy is one example of the general case

that every quantum operator, including the operators representing the momentum and the energy, flow from the density matrix, but not generally from the density alone.

It may interest readers to realize that there has been a recent expansion in understanding and practicing of quantum crystallography. Perhaps the demarcation of this change was the publication of a paper in 2017 by Grabowsky, Genoni, and Burgi (GGB) [51]. The paper outlines the nature of the original ideas in quantum crystallography and an indication of their path forward. The paper must be considered the ground for discussion at the contemporaneous meeting held in Nancy (France).[1] A result of that conference was an agreement to suggest the renaming of one of the permanent commissions of the *International Union of Crystallography* (IUCr) from its old name (*Commission on Charge, Spin and Momentum Densities*) to its new and current name (*Commission on Quantum Crystallography*), a name change approved at IUCr's General Assembly held in Hyderabad (India) in August 2017. This Commission is highly active and has provided the overarching umbrella under which several international conferences and journal special issues on the topic have already been organized indicating the influential presence of quantum crystallography on the international scene. The importance of the GGB paper is recognized by discussing of some of its aspects in Appendix 2 of this book. Along similar lines, namely, an expanded view of quantum crystallography, we also suggest that the reader may consult Simon Grabowsky and Alessandro Genoni's paper [52] and Piero Macchi's paper [53].

Chapters 3 and 4 of this monograph emphasize the importance of *N*-representability as a foundation of the field of quantum crystallography. Appendix 1 reviews the historical development of the concept of *N*-representability and provides important references for that history of ideas [54]. Also, an indication of a possible generalization of density matrices beyond single determinants is considered [55–57], a topic of interest which we have not been able to consider within the scope of these chapters.

Appendix 3 is a list of papers related to development of quantum crystallography, all by the authors of this monograph. These references may be used to pursue in further detail the ideas of quantum crystallography presented in the chapters of this monograph. As authors of this book we are not simply describing the field of quantum crystallography so much as *reviewing our participation* in its development as we have experienced it. Needless to say, our collaborations with many others have been important. These include Professors William Clinton, William Lipscomb, Jerome Karle, and Richard F. W. Bader. Students who have worked the field include Carol Frishberg, Pat Oldfield, Maria Flocco, Arnaud Soirat, Sonjae Wallace, and Walter Polkosnik.

1 Centre Européen de Calcul Atomique et Moléculaire (CECAM) Discussion Meeting – Quantum Crystallography: Current Developments and Future Perspectives, Nancy, France (19–20 June 2017).

References

[1] Stout, GH, Jensen, LH. *X-Ray Structure Determination: A Practical Guide, (Second Edition)*. John-Wiley and Sons, New York, (1989).

[2] Giacovazzo, C, Monaco, HL, Viterbo, D, Scordari, F, Gilli, G, Zanotti, G, Catti, M. *Fundamentals of Crystallography (International Union of Crystallography Book Series, No. 2)*. Oxford University Press, Oxford, UK, (1992).

[3] Tsirelson, VG, Ozerov, RP. *Electron Density and Bonding in Crystals: Principles, Theory and X-ray Diffraction Experiments in Solid State Physics and Chemistry*. Institute of Physics Publishing, New York, (1996).

[4] Coppens, P. *X-ray Charge Densities and Chemical Bonding*. Oxford University Press, Inc, New York, (1997).

[5] Coppens, P. Electron density from X-ray diffraction. *Annu. Rev. Phys. Chem.* 43, 663–692 (1992).

[6] Koritsanszky, TS, Coppens, P. Chemical applications of X-ray charge-density analysis. *Chem. Rev.* 101, 1583–1628 (2001).

[7] Rhodes, G. *Crystallography Made Crystal Clear: A Guide for Users of Macromolecular Models (Third Edition)*. Elsevier, Inc. and Academic Press, Inc, San Diego, (2006).

[8] Sands, DE. *Introduction to Crystallography*. Dover Publications, Inc, New York, (1975).

[9] Brown, PJ, Forsyth, JB. *The Crystal Structure of Solids (Series: The Structures and Properties of Solids – Vol. 2)*. Edward Arnold (Publishers), Ltd., London, (1973).

[10] Zachariasen, WH. *Theory of X-Ray Diffraction in Crystals*. Dover Publications, Inc., Mineola, NY, (1945).

[11] Guinier, A. *X-Ray Diffraction: In Crystals, Imperfect Crystals, and Amorphous Bodies*. Dover Publications, Inc, New York, (1994).

[12] Aubert, E, Lecomte, C. Illustrated Fourier transforms for crystallography. *J. Applied Cryst.* 40, 1153–1165 (2007).

[13] Merzbacher, E. *Quantum Mechanics (Third Edition)*. John Wiley and Sons, Inc, New York, (1998).

[14] Townsend, JS. *A Modern Approach to Quantum Mechanics*. McGraw-Hill, Inc, New York, (1992).

[15] Griffiths, DJ. *Introduction to Quantum Mechanics (Second Edition)*. Pearson, Prentice Hall, Upper Saddle River, NJ, (2005).

[16] Fock, VA. *Fundamentals of Quantum Mechanics (English Translation of the Second Russian Edition of 1976 – the First Russian Edition was Published in 1931)*. Mir Publishers, Moscow, (1978).

[17] Landau, LD, Lifshitz, EM. *Quantum Mechanics*. Pergamon Press, New York, (1965).

[18] Dirac, PAM. *The Principles of Quantum Mechanics, Third Edition*. Oxford University Press, Oxford, (1958).

[19] McWeeny, R, Sutcliffe, BT. *Methods of Molecular Quantum Mechanics*. Academic Press, New York, (1969).

[20] McWeeny, R. The nature of electron correlation in molecules. *Int. J. Quantum Chem.* 1s, 351–359 (1967).

[21] McWeeny, R. Some recent advances in density matrix theory. *Rev. Mod. Phys.* 32, 335–369 (1960).

[22] Löwdin, P-O. Quantum theory of many-particle systems. I. Physical interpretations by means of density matrices, natural spin-orbitals, and convergence problems in the method of configurational interaction. *Phys. Rev* 97, 1474–1489 (1955).

[23] Coleman, AJ, Yukalov, VI. *Reduced Density Matrices: Coulson's Challenge*. Springer, Berlin, (2000).
[24] Parr, RG, Yang, W. *Density-Functional Theory of Atoms and Molecules*. Oxford University Press, Oxford, (1989).
[25] Clinton, WL, Frishberg, CA, Massa, LJ, Oldfield, PA. Methods for obtaining an electron-density matrix from x-ray data. *Int. J. Quantum Chem.* 7, 505–514 (1973).
[26] Massa, LJ, Clinton, WL. Antisymmetric wavefunction densities from coherent diffraction data. *Trans. Am. Cryst. Ass.* 8, 149–153 (1972).
[27] Clinton, WL, Massa, LJ. Determination of the electron density matrix from X-ray diffraction data. *Phys. Rev. Lett.* 29, 1363–1366 (1972).
[28] Clinton, WL, Galli, AJ, Massa, LJ. Direct determination of pure-state density matrices. II. Construction of constrained idempotent one-body densities. *Phys. Rev.* 177, 7–12 (1969).
[29] Huang, LS. *X-Ray Orthonormal Orbital Model of Crystallography*, *PhD Thesis*; Graduate Center, City University of New York (CUNY): New York, NY, 1993.
[30] Stewart, RF, Davidson, ER, Simpson, WT. Coherent X-ray scattering for the hydrogen atom in the hydrogen molecule. *J. Chem. Phys.* 42, 3175–3187 (1965).
[31] Massa, L, Goldberg, M, Frishberg, C, Boehme, R, LaPlaca, S. Wave functions derived by quantum modeling of the electron density from coherent X-ray diffraction: beryllium metal. *Phys. Rev. Lett.* 55, 622–625 (1985).
[32] Larsen, FK, Hansen, NK. Diffraction study of the electron density distribution in beryllium metal. *Acta Cryst. B* 40, 169–179 (1984).
[33] Massa, L. A zigzag path through quantum crystallography. *Struct. Chem.* 28, 1293–1296 (2017).
[34] Figgis, BN, Hitchman, MA. *Ligand Field Theory and Its Applications*. Wiley-VCH, New York, NY, (2000).
[35] Huang, L, Massa, L, Karle, J. Quantum crystallography applied to crystalline maleic anhydride. *Int. J. Quantum Chem.* 73, 439–450 (1999).
[36] Huang L, Massa L, Karle J. Quantum kernels and quantum crystallography: Applications in biochemistry. Chapter 1 in: *Quantum Biochemistry: Electronic Structure and Biological Activity – Vol. 1*; Matta CF (Ed.), Wiley-VCH, Weinheim (2010), pp 3–60.
[37] Massa, L, Huang, L, Karle, J. Quantum crystallography and the use of kernel projector matrices. *Int. J. Quantum. Chem.* 56, 371–384 (1995).
[38] Huang, L, Massa, L, Karle, J. Kernel energy method illustrated with peptides. *Int. J. Quantum Chem.* 103, 808–817 (2005).
[39] Huang, L, Massa, L, Karle, J. Kernel energy method: Application to DNA. *Biochemistry* 44, 16747–16752 (2005).
[40] Huang, L, Massa, L, Karle, J. Kernel energy method: Application to insulin. *Proc. Natl. Acad. Sci. USA* 102, 12690–12693 (2005).
[41] Huang, L, Massa, L, Karle, J. The kernel energy method: Application to a tRNA. *Proc. Natl. Acad. Sci. USA* 103, 1233–1237 (2006).
[42] Huang, L, Massa, L, Karle, J. Kernel energy method applied to vesicular stomatitis virus nucleoprotein. *Proc. Natl. Acad. Sci. USA* 106, 1731–1736 (2009).
[43] Huang, L, Bohórquez, H, Matta, CF, Massa, L. The kernel energy method: Application to graphene and extended aromatics. *Int. J. Quantum Chem.* 111, 4150–4157 (2011).
[44] Huang, L, Krupkin, M, Bashan, A, Yonath, A, Massa, L. Protoribosome by quantum kernel energy method. *Proc. Natl. Acad. Sci. USA* 110, 14900–14905 (2013).
[45] Huang, L, Massa, L, Matta, CF. A graphene flake under external electric fields reconstructed from field-perturbed kernels. *Carbon* 76, 310–320 (2014).

[46] Timm, MJ, Matta, CF, Massa, L, Huang, L. The localization-delocalization matrix and the electron density-weighted connectivity matrix of a finite graphene nanoribbon reconstructed from kernel fragments. *J. Phys. Chem. A* 118, 11304–11316 (2014).
[47] Polkosnik, W, Massa, L. Single determinant *N*-representability and the kernel energy method applied to water clusters. *J. Comput. Chem.* 39, 1038–1043 (2018).
[48] Bader, RFW. *Atoms in Molecules: A Quantum Theory*. Oxford University Press, Oxford, U.K., (1990).
[49] Popelier, PLA. *Atoms in Molecules: An Introduction*. Prentice Hall, London, (2000).
[50] Matta, CF, Boyd, RJ (Eds.). *The Quantum Theory of Atoms in Molecules: From Solid State to DNA and Drug Design*. Wiley-VCH, Weinheim (2007).
[51] Grabowsky, S, Genoni, A, Bürgi, H-B. Quantum crystallography. *Chem. Sci.* 8, 4159–4176 (2017).
[52] Genoni, A, Bučinský, L, Claiser, N, Contreras-García, J, Dittrich, B, Dominiak, PM, Espinosa, E, Gatti, C, Giannozzi, P, Gillet, J-M, Jayatilaka, D, Macchi, P, Madsen, AØ, Massa, L, Matta, CF, Merz, KM, Jr, Nakashima, P, Ott, H, Ryde, U, Scherer, W, Schwarz, K, Sierka, M, Grabowsky, S. Quantum crystallography: Current developments and future perspectives. *Chem. Eur. J.* 24, 10881–10905 (2018).
[53] Macchi, P. The connubium between crystallography and quantum mechanics. *Crystallogr. Rev.* 26, 209–268 (2020).
[54] Massa, L. Approximate *N*-representability by correlated-determinant wavefunctions. In: *Reviews of Modern Quantum Chemistry: A Celebration of Robert G. Parr, Vol. 1*; Sen, KD (Ed.), *World Scientific*, *New Jersey* (2002), 666–683.
[55] Soirat, A, Flocco, M, Massa, L. Approximately *N*-representable density functional density matrices. *Int. J. Quantum Chem.* 49, 291–298 (1994).
[56] Soirat, A, Flocco, M, Massa, L. Approximately *N*-representable density functional density matrices: The case of large N. *Proc. Ind. Acad. Sci. (Chem. Sci.)* 106, 209–216 (1994).
[57] Massa, L, Flocco, M, Soirat, A. Reduced density matrices *N*-representable by correlated determinant wavefunctions. *J. Mol. Struct. (THEOCHEM)* 199, 337–342 (1989).

Chapter 1
Some basic concepts of crystallography

The examination of crystal structure, with the aid of X-rays has given us for the first time an insight into the actual arrangement of the atoms in solid bodies. The study of structure by means of a microscope is limited by the coarseness of the light which illuminates the object, for we can never hope to see details smaller than the wavelength of the light. By using X-rays with their very short wavelengths, this limit of minuteness has at one step been decreased ten thousand times, for the wavelength of the X-rays is of a smaller order than the dimensions of the atomic structure. We are actually looking into the interior of the molecule and the atom with this fine-grained form of light. William Lawrence Bragg (1922)

(Nobel Lecture, delivered at the Technical University of Stockholm on 6 September 1922. Note that the Nobel Prize has been awarded in 1915)

Classical crystallography concerns atomic structure, that is, specifying the position of atoms in a crystal. This is usually achieved by minimization of the *R*-factor, which is a numerical measure of the accuracy of atomic positions. The basic data of the X-ray scattering experiment is the collection of experimental structure factors which are the square roots of the measured intensities. The structure factors $F(\mathbf{K})$ are Fourier transforms of the electron density $\rho(\mathbf{r})$ in the crystal. The essential crystalline structure can be obtained assuming that the electron density can be modeled as a sum of spherical atoms in the unit cell. But, as noted by Robert Stewart, Philip Coppens, Claude Lecomte, and others, a realistic model of the bonding electron density can be obtained by modeling the atomic density contributions as multipoles. This is a great advance in electron density accuracy but it is not mandated to be *N*-representable.

1.1 Introductory remarks

Crystallography is a science of structure. At first it is concerned with structure at the macroscopic level. Using X-ray diffraction, crystallography provides a tool for exposing the structure at the atomic level. Macroscopic chemical, physical, and biological properties of the material under study can then be understood in terms of the underlying structural regularity associated with atoms. This atomic structure is revealed by X-ray diffraction crystallography, which will be referred to as simply "classical crystallography" in this monograph – which is concerned with single-crystal crystallography.

At a deeper level than the atomic geometrical arrangement, the structure of electronic orbitals underlies that of the atoms. X-ray experiments provide the scattering data, and quantum theory the language, ideas, and mathematics required to expose the detailed structure associated with a density matrix of electronic orbitals [1]. We refer to this approach as "*quantum crystallography*," QCr for short [2–18], the topic of this monograph.

https://doi.org/10.1515/9783110566673-002

Before engaging into a description of QCr, it is important to contextualize the work: What subbranch of crystallography encompasses this new development? What are the basic assumptions? And what are the approximations and levels of theoretical treatments used? Hence, in the next two sections, some aspects of elastic scattering, within single-crystal X-ray diffraction experiments, are briefly reviewed first. This is followed by a discussion on the nature and origin of structure factors. These two sections are a prelude to the description of QCr, the subject of subsequent chapters.

1.2 Elastic scattering and Bragg's law

In the following development, we will rely on a semiclassical description of radiation–matter interaction in which matter is treated quantum mechanically and the electromagnetic radiation field classically. In contrast to spectroscopy, where absorption or emission is recorded as a function of wavelength/frequency, in the type of crystallographic experiments referred to in this book, the wavelength/frequency is fixed (in fact, it is, ideally, monochromatic) and it is the scattering intensity as a function of the angle, or as a function of position in reciprocal space, that is being recorded.

Thus, only coherent elastic scattering is considered and not Compton scattering in which the incident and the scattered radiation have slightly different frequencies. In the case of Compton scattering, it is the sum of the *intensities* rather than the sum of the *amplitudes* which determines the scattered intensity. The sum of intensities does not generate relative information about atomic positions in the unit cell since intensities, as opposed to amplitudes, do not give rise to phase-dependent interference effects.

Bragg's law of X-ray diffraction itself is based on such interference effects among beams reflected from a set of atomic planes defined by the Miller indices (h, k, l):

$$2d_{hkl} \sin\theta = n\lambda, \tag{1.1}$$

where d_{hkl} is the distance between pairs of atomic planes, θ is the angle of incidence and of reflection, n is an integer, and λ is the wavelength of the radiation. Reflections are observed only when the condition in eq. (1.1) is satisfied. This is precisely the condition of maximally constructive interference of the amplitudes of the scattered waves. Given that the source of X-rays is infinitely far from the atomic planes, the X-ray electromagnetic waves are considered as plane waves, as is implicitly assumed in deriving Bragg's law.

According to electromagnetic theory, the intensity of radiation is proportional to the square of the amplitude of the electromagnetic wave. The relative amplitude, in this case, along with an unknown phase, is called a "*structure factor*." Because QCr extracts quantum mechanical information from X-ray structure factors, it is fitting to start this book with a brief review of their origin and nature.

1.3 Structure factors

The problem in contemporary crystallography is that of determining the Cartesian coordinates of the atoms in the unit cell [19, 20]. Consider the X-ray scattering by the electron density of a single crystal followed by the detection of the reflection using a photon detector. The main steps of this type of diffraction experiments are summarized in Fig. 1.1 and its caption.

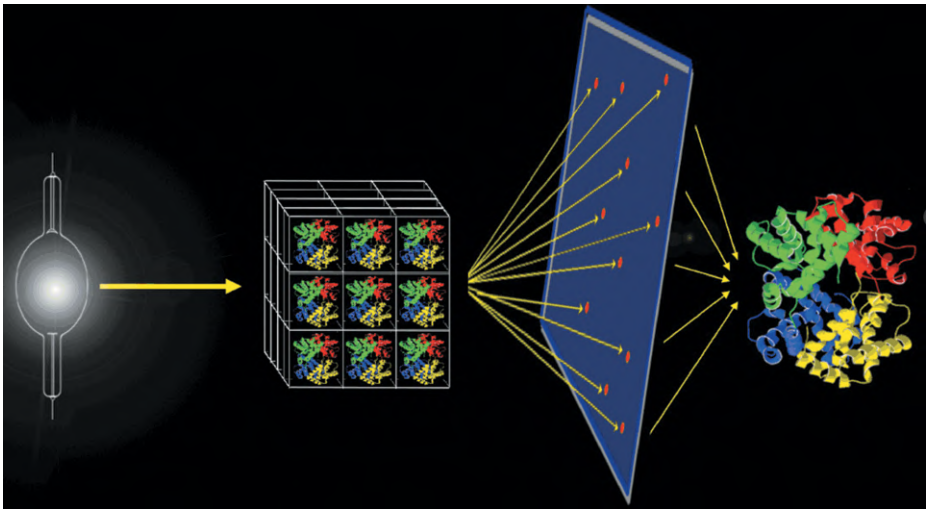

Fig. 1.1: The essentials of an X-ray diffraction experiment. (*Left*) A collimated X-ray beam is generated whether from a traditional single-element X-ray tube or a bright coherent light source such as a contemporary fourth-generation synchrotron. (*Middle*) The beam is diffracted from a crystal mounted on a goniometer rotating in the three spatial directions. The "reflections" are detected for each combination of three goniometer angles to swipe the accessible region of the reciprocal space, sampled at the positions of the reflections. In the past, the detection of the intensities was made using a photographic emulsion, but nowadays, it is almost exclusively performed using a charged coupled device (CCD) detector. The indexed intensities, each labeled with a unique ($\mathbf{K} \equiv (h, k, l)$) index that specifies its "address" in reciprocal space, are then channeled to a computer for an iterative refinement comparing the experimental and calculated structure factors (after solving the phase problem). The result is an electron density map, with a resolution that depends on the reach of the data in the reciprocal space. (*Right*) A "fleshed-out" ribbon representation of the geometry based on the electron density map of a small peptide consisting of four domains depicted in the traditional ribbon representation after guessing the missing residues, atoms, and so on from the knowledge of the peptide's primary structure.

An ideal crystal is made up of a repetition of the unit cell in three dimensions. The periodicity is, hence, manifested along each of the three spatial axes of the crystal. The periodicity of the arrangement of the nuclei gives rise to a periodic external

potential which, in its turn, is reflected in the three-dimensional periodicity of the electron density. Thus, the electron density in the crystal must satisfy [21]

$$\rho(x+p,\, y+q,\, z+r) \;=\; \rho(x,y,z), \tag{1.2}$$

where p, q, and r are arbitrary integer multiples of the dimensions of the unit cell, and x, y, and z are fractional coordinates.

One can regard the crystal as exhibiting three independent periodicities, one along each of the three Cartesian axes. The Miller indices (h, k, and l) are effectively the frequencies by which the periodic electron density function oscillates along each of the principal Cartesian axes [22], and also correspond to the coordinates of a given reflection in reciprocal space.

Any periodic function can be expanded in terms of a Fourier series [23–25]. Such an expansion of the electron density in a crystal can be written as [20]

$$\rho(xyz) = \frac{1}{V}\sum_{h}\sum_{k}\sum_{l} F(hkl)\exp\left[-2\pi i(hx+ky+lz)\right], \tag{1.3}$$

where V is the volume of the unit cell and $F(hkl)$ are the Fourier expansion coefficients. These dimensionless coefficients are the *structure factors* that must be obtained from the experiment.

The X-ray diffraction experiment measures the indexed intensities of the various reflections. These intensities are proportional to the square of the magnitude of the structure factors, that is:

$$I(hkl) \propto |F(hkl)|^2. \tag{1.4}$$

The squaring in eq. (1.4) results in the loss of phase information since the structure factors are, in general, complex numbers. This is the crux of the well-known *phase problem* of crystallography. That problem has several solutions (reviewed, e.g., in Ref. [19]). At this point in the discussion, for simplicity, we will defer the effects of thermal vibrations on the scattering.

The triple sum (rather than an integral) in eq. (1.3) (over h, k, l) reflects the reality that the reciprocal space is only *sampled* at the observed reflections, which is a direct result of Bragg's condition. The equation represents a discrete Fourier transform of $F(hkl)$. To invert this procedure and obtain an expression for a general structure factor *given* an electron density, one has to resort to the inverse Fourier transform. The inverse transform of the electron density, as it has been expressed in eq. (1.3), is [21]

$$F(hkl) \;=\; \int_0^1\int_0^1\int_0^1 \rho(xyz)\;\exp\left[2\pi i(hx+ky+lz)\right]\,dx\,dy\,dz, \tag{1.5}$$

where each integral spans one of the three principal axes of the unit cell, and the sign of the exponential factor has been inverted. In this reverse Fourier transform,

the (continuous) electron density within the unit cell plays the role of the Fourier expansion coefficients. Written in this manner (eq. (1.5)), the electron density in the unit cell, in its entirety, contributes to every observed structure factor in the set $\{F(hkl)\}$.

The quality of a crystallographic refinement is gauged by the agreement of the observed and calculated structure factors (F_{obs} and F_{calc}), which is improved in an iterative procedure. Structure factors are calculated from a model of the electron density (eq. (1.5)) obtained by superposing spherical atomic densities (or in more accurate modeling, aspherical/multipolar atomic densities, *vide infra*). These atomic densities are predetermined from theory and placed in assumed geometrical positions in the unit cell that are systematically varied during the refinement until the agreement is maximized.

"Solving a structure" is achieved when the difference between the observed and the calculated structure factors is minimized. This minimum is reached, in a least-square sense, in what came to be known as the residual factor (*R*-factor) defined as

$$R\text{-factor} = \frac{\sum \big|\, |F_{obs}| - |F_{calc}| \,\big|}{\sum |F_{obs}|}. \tag{1.6}$$

In a typical crystallographic refinement, the electron density in the studied crystal is guessed on the basis of external information that may be available such as the unit cell composition.

In the spherical atom approximation the atoms are placed in their assumed positions in the unit cell. The densities of these atoms are allowed to overlap in a *promolecule* in accordance with the assumptions of an *independent atom model* [26, 27]. In this approximation [26],

$$\rho^{pro} = \sum_{i=1}^{M} \rho_i, \tag{1.7}$$

where ρ_i is a spherically symmetrical atomic electron density of the *i*th atom placed at its position in the target molecule to obtain the approximate promolecular density ρ^{pro}.

The promolecule has proven time and again to be extremely useful in providing good geometries for thousands of molecular structures. A structure factor based on the superposition of spherical atoms, a promolecular density, can be written as a sum of *j* atomic densities as follows [21]:

$$F(hkl) = \sum_j \int_0^1 \int_0^1 \int_0^1 \rho_j(xyz)\ \exp\left[2\pi i(hx + ky + lz)\right] dx\, dy\, dz, \tag{1.8}$$

where j runs over the atoms in the unit cell, each placed at its relative position within the cell, and the integral is over the volume of the unit cell. A coordinate transformation for atom j, centered at x_j, y_j, z_j, is introduced such that:

$$\left.\begin{aligned} x' &= x - x_j \\ y' &= y - y_j \\ z' &= z - z_j \end{aligned}\right\}, \tag{1.9}$$

where the primed coordinates move the origin to the position of the jth nucleus. Applying this coordinate transformation, we get

$$F(hkl) = \sum_j \underbrace{\int_0^1\int_0^1\int_0^1 \rho_j(x'y'z') \exp\left[2\pi i(hx' + ky' + lz')\right] dx'dy'dz'}_{f_j(hkl)} \exp\left[2\pi i\left(hx_j + ky_j + lz_j\right)\right], \tag{1.10}$$

where

$$f_j(hkl) = \int\int\int \rho_j(x'y'z') \exp\left[2\pi i(hx' + ky' + lz')\right] dx'dy'dz' \tag{1.11}$$

is the atomic scattering factor, that is, atom j's contribution to the structure factor. Equations (1.10) and (1.11) can then be combined into

$$F(hkl) = \sum_j f_i \exp\left[2\pi i(hx_j + ky_j + lz_j)\right]. \tag{1.12}$$

The vibrational motion of nuclei, which is a function of temperature, diminishes the scattering power of a given atom by smearing its density over the amplitude of the vibrational motion. This effect can be accounted for by introducing the Debye–Waller factor, also known as the temperature factor, the displacement parameter, or the B-factor, B_j. This temperature factor, for a given atom, is proportional to the squared average displacement of that atom from its equilibrium position. Such a temperature factor modifies the structure factor expression (eq. (1.10)) to read as follows [21]:

$$F(hkl) = \sum_j f_j(hkl) \exp\left[2\pi i(hx_j + ky_j + lz_j)\right] \exp\left[-B_j\left(\frac{\sin\theta}{\lambda}\right)^2\right], \tag{1.13}$$

where θ and λ are, respectively, the scattering angle and the wavelength of the X-ray radiation, respectively, and the B-factor is defined as follows:

$$B_j = 8\pi^2\langle u^2\rangle, \tag{1.14}$$

where the angular brackets indicate the temporal and spatial averaging, and $\langle u^2 \rangle$ is the mean square isotropic (i.e., averaged over all directions) displacement of the given atomic position.

The temperature factor is determined from the difference between calculated and observed intensities. The *B*-factor is isotropic (i.e., is not directionally sensitive), but in more accurate work, the temperature factor is anisotropic and captures, simultaneously, the directionality and the amplitudes of atomic vibrations. The latter anisotropic temperature factor is graphically displayed in the familiar thermal ellipsoids around atomic positions in ORTEP (Oak Ridge Thermal-Ellipsoid Plot Program) diagrams of crystallographic structures.

The atomic scattering factor, also known as the atomic form factor, f_i, defined in eq. (1.11), appears in eq. (1.10) as the pre-exponential factor. The atomic scattering factor is assumed completely transferable for any given atom regardless of its electronic environment in the crystal. The value of this factor is a function of the Bragg angle θ, scaled to yield the number of electrons in the neutral atom for $\theta = 0$. The scattering factors of all atoms, obtained from quantum chemical calculations, are available in the *International Tables for X-Ray Crystallography* [28].

The spherical atom approximation underlying the promolecular modeling is less severe, the heavier the atom of interest. As a corollary, this approximation can introduce errors that are reflected in inaccurate bond lengths, especially involving hydrogen atoms. As a result, promolecular models often yield X–H bonds (X = second row atom) that are systematically shorter than measured by neutron diffraction [29, 30]. Other than this shortcoming, this modeling yields reasonable molecular geometries and is, and has been, used routinely to solve the structures of thousands of molecules. However, this promolecular modeling is inherently inadequate if an analysis of the electron density at the bonding regions is of interest [29–35].

In 1967, Philip Coppens, with the molecule *s*-triazine, showed that spherical atomic modeling misses the details of the electron density in the chemical bonding region [29] (Fig. 1.2). The sum of spherical atoms does not flow as much charge into the bonding region as actually occurs. To compensate for that, the temperature factors can drive the hydrogen atoms into the bonding region.

Since the neutron scattering is independent of the bonding electron density, it determines more accurate hydrogen positions. Coppens used the atomic positions delivered from neutron diffraction to build a “neutron-based promolecule” and then subtracted its electron density from that obtained from the traditional X-ray promolecule [29]. The electron density difference map showed regions that are consistent with the expected positions of the lone electron pairs at the back of the nitrogen atoms and bonding density within the C–N bonding region [29] (Fig. 1.2). This early work underscores the importance of going beyond the spherical atom approximation as Coppens himself reminisces in a memoir published in 2015 [36]:

The work helped to silence the skeptics who consistently described the small band of upstarts active in X-ray Electron Density Analysis somewhat derisively as 'electron seers'.

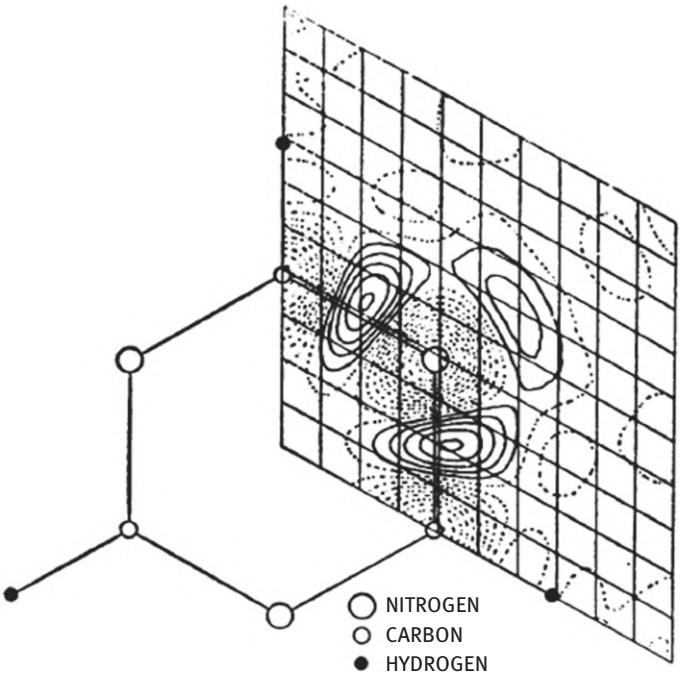

Fig. 1.2: An early difference map of *s*-triazine obtained between the X-ray electron density and that of a spherical model centered at atomic positions determined with neutron diffraction, including the experimental temperature factors. The difference map shows distinct regions ascribable to the nitrogen atom's lone pairs and to the chemical bonding between carbon and nitrogen atoms (reproduced from Ref. [29] with permission of the copyright holder. © 1967 American Association for the Advancement of Science).

To remedy for the limitations of the promolecular modeling, several workers, including prominently Robert Stewart, and Coppens and Niels Hansen, introduced the multipolar (nonspherical) modeling of the electron density on the crystallographic scene [30–37]. Among the popular aspherical modeling algorithms is Hansen and Coppens' MOLLY [33] and Lecomte *et al.*'s MOPRO [30, 35, 41]. In the Hansen–Coppens formalism, an atomic electron density is expressed in terms of the polar coordinates **r**, θ, and φ [33]:

$$\rho_{\text{atom}} = P_{\text{core}}\,\rho_{\text{core}} + P_{\text{valence}}\,\kappa^3\rho_{\text{valence}}(\kappa r) + \sum_{l=0}^{l_{\max}} \kappa'^3 R_l(\kappa' r) \sum_{m=0}^{l} P_{lm\pm}\, d_{lm\pm}(\theta,\varphi), \quad (1.15)$$

where

$$N(\Omega) = P_{\text{core}} + P_{\text{valence}} + \sum_{m=0}^{l} P_{lm\pm}, \tag{1.16}$$

where P is a population coefficient, $N(\Omega)$ is the total number of electrons associated with the atom or ion Ω, ρ_{core} and ρ_{valence} are probability densities of the free atom or ion, and R_l is an exponential radial function.

In expression (1.15), the spherical core and valence densities, represented by the first two terms, are followed by the third term that enables the deformation of the valence electron density from its spherical symmetry. The electron density of the atomic core is left unchanged during the refinement, while the κ and κ' parameters are adjustable to allow for the radial flexibility of the valence electron density. The latter is included in the first summation of the third term to improve the description of outer *s*-electrons of transition metal atoms since these are often more diffuse than the valence *d*-electrons. Finally, $d_{lm\pm}(\theta, \varphi)$ are the usual spherical harmonics which are introduced to capture the nonspherical features of the atomic electron density.

Inserting eq. (1.15) into eq. (1.11) gives an expression for the nonspherical (multipolar) atomic form factor. The nonspherical form factor can then be placed within the structure factor expression (eq. (1.10)) to obtain the multipolar structure factor [30, 33, 35]:

$$\begin{aligned} F(hkl) = \sum_{j} \Big[& P_{j,\text{core}}\, f_{j,\text{core}}(H) + P_{j,\text{valence}}\, f_{j,\text{valence}}(H/\kappa) \\ & + 4\pi \sum_{l=0}^{l_{\max}} \sum_{m=0}^{l} P_{lm\pm}\, i^l \langle j_l \rangle d_{lm\pm}(\beta, \gamma) \Big] \exp\left[2\pi i (hx_j + ky_j + lz_j)\right]\, T_j(hkl), \end{aligned} \tag{1.17}$$

where $f_{j,\text{core}}$ and $f_{j,\text{valence}}$ are the Fourier transforms of $\rho_{j,\text{core}}$ and $\rho_{j,\text{valence}}$, respectively, $\langle j_l \rangle$ is the lth-order Fourier–Bessel transform of the radial part of R_l, $d_{lm\pm}(\beta, \gamma)$ are spherical harmonics in reciprocal space polar coordinates, and $T_j(hkl)$ are anisotropic temperature factors which quantify the jth atom's thermal vibration around its equilibrium position.

Atomic coordinates, temperature factors, and $P_{j,\text{valence}}$, P_{lm}, κ, and κ' are all optimized during the multipolar refinement. The multipolar model yields accurate electron densities that agree well with those calculated at high level of quantum chemical theory especially when the modeling is performed on data collected from good quality crystals at low-to-very low temperatures (N_2 or He gas temperatures) [35].

1.4 The electron density

Quantum crystallography is a phrase made up by borrowing the word "quantum" from quantum mechanics and the word "crystallography" from the field of single-

crystal X-ray diffraction crystallography.[1] This phrase has been coined in a 1995 article [3] and the theory developed in a series of subsequent papers and book chapters (see, e.g., early developments of the field in Refs. [4–6, 8]). Figure 1.3 is a display of the title page of the paper that introduced the term in 1995 [3] scanned from a hard copy reprint sent to the then graduate student of Professor Richard F. W. Bader, Chérif F. Matta, by Dr. Jerome Karle with his signed dedication (also see brief historical notes in Ref. [42]).

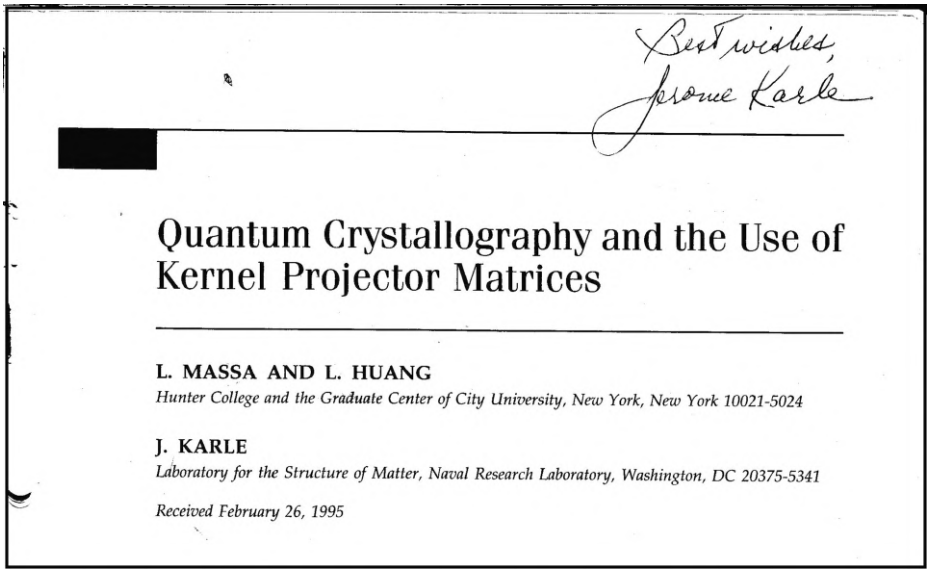
Best wishes,
Jerome Karle

Quantum Crystallography and the Use of Kernel Projector Matrices

L. MASSA AND L. HUANG
Hunter College and the Graduate Center of City University, New York, New York 10021-5024

J. KARLE
Laboratory for the Structure of Matter, Naval Research Laboratory, Washington, DC 20375-5341

Received February 26, 1995

Fig. 1.3: Title page of the paper that introduced the term "quantum crystallography" in 1995 (*Int. J. Quantum. Chem.* 56, 371–384) [3] with Dr. Jerome's Karle's signed dedication.

The merging of the terms "quantum" and "crystallography" is not coincidental. The object being determined in crystallography is the electron density, $\rho(\mathbf{r})$. This quantity is also accessible from theory through applied quantum mechanics. By virtue of the first Hohenberg–Kohn theorem (HK-1 theorem) [43], the nondegenerate ground-state electron density carries all the information about the electronic system whether in the ground or in excited states. This theorem is the foundation of modern density functional theory (DFT) [44].

The HK-1 theorem states that the nondegenerate ground-state electron density, $\rho(\mathbf{r})$, determines the external potential (V) uniquely [43]. The term "external potential"

1 The term "crystallography" is used in this book to imply single-crystal X-ray diffraction crystallography unless otherwise explicitly stated.

means the potential *external* to the system of electrons, namely, the bare nuclear potential and any potential associated with an externally applied field.

The electron density also determines the total number of electrons (N) in the system, which, along with V, completely specifies the system's Hamiltonian. The Hamiltonian then fixes all the system's eigenfunctions (e.g., the set of wave functions in position space) and eigenvalues, that is, the energies of the different states. Specifying the eigenfunctions uniquely fixes all the properties of the system, ground and excited, since these are obtained through the averaging of linear Hermitian operators on the eigenstates. These arguments retrace the E. Bright Wilson justification of the HK-1 theorem (see Refs. [45–47] and the literature cited therein). Thus,

$$\rho(\mathbf{r}) \;\rightarrow\; \left\{ \begin{matrix} V[\rho(\mathbf{r})] \\ N[\rho(\mathbf{r})] \end{matrix} \right\} \rightarrow \hat{H} \rightarrow \{\Psi_i\}, \tag{1.18}$$

where $i = 0, 1, 2, \ldots, \infty$, and the square brackets indicate a functional dependence on the electron density. While a function $f(x, y, z, \ldots)$ delivers a scalar or a vector when fed with one or more variables $(x, y, z, \ldots)$, a functional $F[f(x, y, z, \ldots)]$ delivers a number when fed with a given function $f(x, y, z, \ldots)$ as its argument. An important example of a functional is the action integral, $S[L]$, the time integral of the Lagrangian (the kinetic energy minus the potential energy), which delivers a specific value for the action of each chosen spatiotemporal trajectory. The motion of the particle always follows the path that extremizes (here minimizes) the action integral.

While the energy of *any* electronic state, ground or excited, is a functional of the nondegenerate ground-state density, the same cannot be said about an excited-state density as has been shown by Gaudoin and Burke [48]. In other words, the energy of any state is *not* a functional of the excited-state density, that is, it is possible to have more than one external potential consistent with one and the same excited-state density [48].

Importantly, we note that the arrows in the mapping expressed in (1.18) are invertible, through the following equation, which we also use to provide the definition of the term "electron density":

$$\rho(\mathbf{r}) = N \sum_{\omega_i} \int \ldots \int \Psi^* (\mathbf{x}_1, \ldots, \mathbf{x}_N)\, \Psi(\mathbf{x}_1, \ldots, \mathbf{x}_N)\, d\mathbf{r}_2, \ldots, d\mathbf{r}_N, \tag{1.19}$$

where

$$\mathbf{x}_i \equiv (x_i, y_i, z_i, \omega_i), \tag{1.20}$$

in which Ψ is an antisymmetric many-electron wave function and where the first three variables (x_i, y_i, z_i) refer to the Cartesian space coordinates of the i^{th} electron and the spin of which is specified by a "spin coordinate" ω_i which is the argument of either an α or β spin function, and where the superscripted $(^*)$ implies complex conjugation.

Given eq. (1.19), clearly the arrows of relation (1.18) are invertible, that is, given the many-electron wave function we can obtain the electron density. This electron density is indirectly determined by solving the phase problem using the set of experimental X-ray diffraction structure factors collectively referred to as the set $\{F(\mathbf{H})\}$. Hence, the electron density, the principal object studied by the field of crystallography, is accessible from both ends:

$$\left[\begin{array}{c}\textbf{theory}\\(\text{quantum mechanics})\end{array}\right] \Psi \;\rightarrow\; \rho(\mathbf{r}) \;\leftarrow\; \{F(\mathbf{H})\} \left[\begin{array}{c}\textbf{experiment}\\(\text{crystallography})\end{array}\right]. \tag{1.21}$$

Relation (1.21) embodies the spirit of the emerging field of QCr as the intersection of quantum mechanics (theory) and crystallography (experiment).

On a final note, it is important to recall that the (total) charge density, $\rho_{\text{total}}(\mathbf{r})$, that is, the sum of a negative term due to the distribution of the electronic charge density and a positive term reflecting the nuclear charge density, is given in atomic units (where $e = 1$) by

$$\rho_{\text{total}}(\mathbf{r}) = -\rho(\mathbf{r}) + Z_A\delta(\mathbf{R}_A - \mathbf{r}), \tag{1.22}$$

where Z_A and $\mathbf{R}_A$ are the charge and position of the Ath nucleus, and $\delta(\mathbf{R_A}-\mathbf{r})$ is a Dirac delta function that represents the discrete distribution of point nuclear charges.

The total charge density and the electron density are interdetermined. They provide two equivalent descriptions of the same physical situation. This is due to the well-known Kato cusp condition [49]. Kato has shown that the derivative of the spherically averaged charge density with respect to the radial distance from a point-like nucleus and the atomic number Z_A are related by [49]

$$Z_A = -\frac{1}{2n(r_A = 0)}\frac{dn(r_A)}{dr_A}\bigg|_{r_A = 0}, \tag{1.23}$$

where n is the spherically averaged electron density around the nuclear cusp of the Ath nucleus. Eq. 1.23 is also given in atomic units (see pages 28–29).

In closing this chapter, it is important to mention another approach to recover the electron density within a crystal by maximizing the entropy of the electron density distribution in the unit cell over voxels subject to the constraint of reproducing the experimentally derived structure factors. This method is termed the maximum entropy method (MEM) of crystallography (see review [50] and literature cited therein). While it appears to be less generally used, this method has the advantage of not being biased by an underlying assumed atom centered model (whether spherical or multipolar). Hence, at times, MEM refinement can yield accurate representations of regions with small changes in the electron density as, for example, occurs in nonnuclear attractors, which are also known as nonnuclear maxima [51]. MEM is particularly suited for

highly disordered systems, which makes it an ideal choice to obtain electron densities from powder diffraction experiments [50].

1.5 Conclusion

Crystallography is a science of structure. It started with the study of the macroscopic structures and symmetries of crystals. With the discovery of X-rays, the meaning of the term crystallography has been extended to include the determination of the structure, that is, the atomic arrangement within the unit cell of the crystal, by X-ray diffraction experiments. Importantly, one of crystallography's end goals is relating macroscopic properties of matter with its underlying atomic structure. One can take this line of attack one step further by inquiring whether one can make a statement about the *electronic structure* of the atoms composing the crystals. In this sense [1],

> *X-Ray experiments provide the data, and quantum theory the language, ideas and mathematics required to expose the detailed structure associated with electronic orbitals.*

The electron density filling the crystal's space is accessible from theory and experiment. By virtue of the HK-1 theorem, the ground-state electron density determines all the properties of matter in its ground and excited states. The development of DFT in the 1960–1980s coincided with the advent of multipolar methods of refining of high-quality X-ray diffraction experimental data.

Of course what is missed in the classical crystallography, which in its own right is of profound scientific importance, is one thing. That is the quantum mechanics of the molecular electron density and that can be extracted from exactly the same data as used classically, so long as the formalism for interpretation of the data is inherently quantum mechanical.

References

[1] Massa, L. Quantum model of coherent X-ray diffraction. *Chem. Script.* 26, 469–472 (1986).
[2] Wikipedia *Quantum Crystallography:* https://en.wikipedia.org/wiki/Quantum_crystallography (2022).
[3] Massa, L, Huang, L, Karle, J. Quantum crystallography and the use of kernel projector matrices. *Int. J. Quantum. Chem.* 56, 371–384 (1995).
[4] Huang, L, Massa, L, Karle, J. Quantum crystallography. *J. Mol. Struct.* 474, 9–12 (1999).
[5] Huang, L, Massa, L, Karle, J. Quantum crystallography applied to crystalline maleic anhydride. *Int. J. Quantum Chem.* 73, 439–450 (1999).
[6] Huang, L, Massa, L, Karle, J. Quantum crystallography, a developing area of computational chemistry extending to macromolecules. *IBM J. Res. & Dev.* 45, 409–415 (2001).

[7] Jayatilaka, D, Grimwood, DJ. Tonto: A Fortran based object-oriented system for quantum chemistry and crystallography. *International Conference on Computational Science ICCS 2003: Computational Science – Conference proceedings, Part IV (Springer-Verlag)* (2003**)**, 142–151.
[8] Huang, L, Massa, L, Karle, J. Quantum kernels and quantum crystallography: Applications in biochemistry. Chapter 1 in: *Quantum Biochemistry: Electronic Structure and Biological Activity (Vol. 1)*; Matta, CF (Ed.), Wiley-VCH, Weinheim (2010), 3–60.
[9] Gatti, C, Macchi, P. *Modern Charge-Density Analysis*. Springer, Berlin, (2012).
[10] Matta, CF (Guest Editor). Honoring Professor Lou Massa: A Path through Quantum Crystallography. *Struct. Chem. (Special Issue)* **2017**, *28*, 1277–1606.
[11] Grabowsky, S, Genoni, A, Bürgi, H-B. Quantum crystallography. *Chem. Sci.* 8, 4159–4176 (2017).
[12] Massa, L. A zigzag path through quantum crystallography. *Struct. Chem.* 28, 1293–1296 (2017).
[13] Matta, CF. A path through quantum crystallography: A short tribute to Professor Lou Massa. *Struct. Chem.* 28, 1279–1283 (2017).
[14] Matta, CF. Quantum Crystallography: From the intersection to the union of crystallography and quantum mechanics. *J. Comput. Chem.* 39, 1019–1020 (2018).
[15] Genoni, A, Bučinský, L, Claiser, N, Contreras-García, J, Dittrich, B, Dominiak, PM, Espinosa, E, Gatti, C, Giannozzi, P, Gillet, J-M, Jayatilaka, D, Macchi, P, Anders AØ, Massa, L, Matta, CF, Merz, KM, Jr., Nakashima, P, Ott, H, Ryde, U, Scherer, W, Schwarz, K, Sierka, M, Grabowsky, S. Quantum crystallography: Current developments and future perspectives. *Chem. Eur. J.* 24, 10881–10905 (2018).
[16] Massa, L, Matta, CF. Exploiting the full quantum crystallography. *Can. J. Chem.* 96, 599–605 (2018).
[17] Tsirelson, V. Early days of quantum crystallography: A personal account. *J. Comput. Chem.* 39, 1029–1037 (2018).
[18] Macchi, P. The connubium between crystallography and quantum mechanics. *Crystallogr. Rev.* 26, 209–268 (2020).
[19] Stout, GH, Jensen, LH. *X-Ray Structure Determination: A Practical Guide, (Second Edition)*. John-Wiley and Sons, New York, (1989).
[20] Rhodes, G. *Crystallography Made Crystal Clear: A Guide for Users of Macromolecular Models (Third Edition)*. Elsevier, Inc. and Academic Press, Inc., San Diego, (2006).
[21] Sands, DE. *Introduction to Crystallography*. Dover Publications, Inc., New York, (1975).
[22] Sivia, DS. *Elementary Scattering Theory: For X-Ray and Neutron Users*. Oxford University Press, Oxford, (2011).
[23] James, JF. *A Student Guide to Fourier Transforms: With Applications in Physics and Engineering*. Cambridge University Press, Cambridge, UK, (1995).
[24] Champeney, DC. *Fourier Transforms in Physics*. Wiley Eastern, Ltd., New Delhi, (1985).
[25] Aubert, E, Lecomte, C. Illustrated Fourier transforms for crystallography. *J. Applied Cryst.* 40, 1153–1165 (2007).
[26] Hirshfeld, FL. Bonded-atom fragments for describing molecular charge densities. *Theor. Chim. Acta* 44, 129–138 (1977).
[27] Spackman, MA, Maslen, EN. Chemical properties from the promolecule. *J. Phys. Chem.* 90, 2020–2027 (1986).
[28] *International Tables for Crystallography (Vols. A-G), International Union of Crystallography (*http://it.iucr.org*)* (2016).
[29] Coppens, P. Comparative X-ray and neutron diffraction study of bonding effects in *s*-triazine. *Science* 158, 1577–1579 (1967).
[30] Coppens, P. *X-Ray Charge Densities and Chemical Bonding*. Oxford University Press, Inc., New York, (1997).

[31] Stewart, RF, Bentley, J, Goodman, B. Generalized X-ray scattering factors in diatomic molecules. *J. Chem. Phys.* 63, 3786–3793 (1975).
[32] Stewart, RF. One-electron density functions and many-centered finite multipole expansions. *Isr. J. Chem.* 16, 124–131 (1977).
[33] Hansen, NK, Coppens, P. Testing aspherical atom refinement on small molecules data sets. *Acta Cryst. A* 34, 909–921 (1978).
[34] Tsirelson, VG, Ozerov, RP. *Electron Density and Bonding in Crystals: Principles, Theory and X-ray Diffraction Experiments in Solid State Physics and Chemistry*. Institute of Physics Publishing, New York, (1996).
[35] Koritsanszky, TS, Coppens, P. Chemical applications of X-ray charge-density analysis. *Chem. Rev.* 101, 1583–1628 (2001).
[36] Coppens, P. The old and the new: My participation in the development of chemical crystallography during 50+ years. *Phys. Script.* 90, Article # 058001, 1–6 (2015).
[37] Stewart, RF. Electron population analysis with rigid pseudoatoms. *Acta Cryst.* A32, 565–574 (1976).
[38] Guillot, B, Viry, L, Guillot, R, Lecomte, C, Jelsch, CJ. Refinement of proteins at subatomic resolution with MOPRO. *J. App. Cryst.* 34, 214–223 (2001).
[39] Pichon-Pesme, V, Lecomte, C, Lachekar, H. On building a data bank of transferable experimental density parameters: Application to polypeptides. *J. Phys. Chem. 99*, 6242–6250 (1995).
[40] Jelsch, C, Pichon-Pesme, V, Lecomte, C, Aubry, A. Transferability of multipole charge-density parameters: Application to very high resolution oligopeptide and protein structures. *Acta Cryst. D* 54, 1306–1318 (1998).
[41] Jelsch, C, Teeter, MM, Lamzin, V, Pichon-Pesme, V, Blessing, RH, Lecomte, C. Accurate protein crystallography at ultra-high resolution: Valence electron distribution in crambin. *Proc. Natl. Acad. Sci. USA* 97, 3171–3176 (2000)
[42] Matta, CF, Huang, L, Massa, L. Quantum crystallography: *N*-representability big and small. *Isr. J. Chem.* 62, Article # e202100108, 1–14 (2022).
[43] Hohenberg, P, Kohn, W. Inhomogeneous electron gas. *Phys. Rev. B* 136, 864–871 (1964).
[44] Parr, RG, Yang, W. *Density-Functional Theory of Atoms and Molecules*. Oxford University Press, Oxford, (1989).
[45] Bright Wilson, E Jr. DFT explained. In: *Structural Chemistry and Molecular Biology: A Volume Dedicated to Linus Pauling by his Students, Colleagues, and Friends*; Rich, A, Davidson, N (Eds.), W. H. Freeman and Company, San Fransisco (1968), 753–760.
[46] Löwdin, P-O. Twenty-five years of Sanibel Symposia: A brief historic and scientific survey. *Int. J. Quantum Chem.* 28, 19–37 (1985).
[47] Anderson, JSM, Massa, L, Matta, CF. Non-nuclear maxima and the universality of Bright Wilson's justification of the first Hohenberg Kohn theorem revisited. *Chem. Phys. Lett.* 780, Article # 138940, 1–6 (2021).
[48] Gaudoin, R, Burke, K. Lack of Hohenberg-Kohn theorem for excited states. *Phys. Rev. Lett.* 93, 173001, 1–4 (2004).
[49] Kato, WA. On the eigenfunctions of many-particle systems in quantum mechanics. *Commun. Pure Appl. Math.* 10, 151–177 (1957).
[50] Magdysyuk, OV, van Smaalen, S, Dinnebier, RE. Application of the maximum-entropy method to powder-diffraction data. *Int. Tables Crystallogr.* vol. H, Chapter 4.8, 473–488 (2019).
[51] Iversen, BB, Larsen, FK, Souhassou, M, Takata, M. Experimental evidence for the existence of non-nuclear maxima in the electron-density distribution of metallic beryllium. A comparative study of the maximum entropy method and the multipole refinement method. *Acta Cryst. B* 51, 580–591 (1995).

Chapter 2
Some basic concepts of quantum chemistry

Quantum theory has had a two-fold impact on chemistry. The first is conceptual, for there is now hardly an area of chemistry left in which we do not use language and ideas that come from quantum mechanics, ideas which must in large part be formulated in later chapters. The second has to do with the possibility, which with present-day computers is fast becoming a reality, of actually calculating from first principles many of the things we wish to know about molecules. Roy McWeeny (1979)

(*Coulson's Valence*. The English Language Book Society and Oxford University Press, Oxford, (1979), p. 9).

The fundamental equation of motion describing the quantum properties of a molecule is the Schrödinger equation. We are concerned here with the time-independent Schrödinger equation as it applies to many-electron systems. The solution of this equation for fermions is an antisymmetric many-particle function of the coordinates of all *N* particles that make up the system. An obviously complicated function, its essentials can be extracted from it by integration over all particles' coordinates except those for either one particle or two particles resulting, respectively, in the one- or two-particle density matrix. These are sufficient to calculate all one- and two-particle position and momentum properties of a molecular system. Thus, the complicated *N*-particle wave function may be eschewed in favor of the simpler density matrices with no loss of one- and two-particle information. The one-particle density matrix is single determinant *N*-representable on condition that it is represented as a Hermitian normalized projector. The corresponding two-particle density matrix is a known functional of the one-particle case. Both Hartree–Fock and density functional theory (DFT) Kohn–Sham "wave functions" are single determinants and encompass the Pauli principle.

2.1 Introduction

Quantum mechanics is the fundamental theory describing the microworld, a world that includes atoms, molecules, and elementary particles. It describes the interactions of microscopic particles and gives expression to the quantum ideas of particle/wave duality, discrete energy levels, and the Heisenberg uncertainty principle. The science of crystallography has been moving from a classical study of the relative atomic geometrical structure toward the quantum study of the electronic structure of the components of the unit cell. To grasp this movement, we discuss, here, the basic ideas of quantum mechanics which apply to atoms and molecules and which will be related to interpretation of the X-ray coherent scattering experiment.

We concluded the previous chapter by underscoring that the missing element of classical crystallography is quantum mechanics of the molecular electron density. This chapter attempts to provide the basics of quantum mechanics necessary to follow the remainder of the chapters of this book. This chapter is not a review or

https://doi.org/10.1515/9783110566673-003

even an introduction to the topic, just a highlight of the key concepts used in later chapters. The focus is primarily on molecular quantum mechanics. What will be briefly touched upon is nonrelativistic molecular quantum mechanics within the Born–Oppenheimer approximation (BO approximation). The latter approximation separates the motion of the electrons from the much slower motion of the nuclei. No attempt will be made to cover any advanced features of quantum chemistry since this is well covered in the standard literature [1–8]. In this book, the state is expressed as an analytical "wave function" in direct space, where the operators are algebraic operators on the wave function space. In latter chapters, use will also be made of the abstract vector formulation of quantum mechanics, where the quantum state is represented by a vector in a dual Hilbert space and the operators by matrices. The state vector, represented by the ket $|\psi\rangle$, is related to the wave function representation (in one direct space dimension) through

$$|\psi\rangle = \int_{x=-\infty}^{x=+\infty} \psi(x)|x\rangle dx, \tag{2.1}$$

where $\psi(x)$ is the projection of ψ along the basis vector $|x\rangle$, and the complex conjugate transpose of $|\psi\rangle$ is the bra $\langle\psi|$ in the well-known Dirac bra–ket notation.

2.2 The Schrödinger equation

The equation of motion describing a quantum system is the time-dependent Schrödinger equation:

$$\hat{H}\Psi(\mathbf{r},t) = i\hbar\frac{\partial\Psi(\mathbf{r},t)}{\partial t}. \tag{2.2}$$

If the Hamiltonian, $\hat{H}$, is time-independent, and if the wave function $\Psi(\mathbf{r},t)$ can be factorized as a product of a time-dependent and a time-independent functions, that is, $\Psi(\mathbf{r},t) = \theta(t)\psi(\mathbf{r})$, then one can separate out the time-independent Schrödinger equation:

$$\hat{H}\psi(\mathbf{r}) = E\psi(\mathbf{r}), \tag{2.3}$$

where the time-independent Hamiltonian $\hat{H}$ is an operator that represents the energy of the system, ψ is the wave function of the system, E is an eigenvalue of the system (energy), and $\hbar = h/2\pi$ is the reduced Planck's constant.

The electronic structure of crystallography is most obviously related to solutions of the time-independent eigenvalue equation, that is, eq. (2.3), which is the case often relevant to the coherent X-ray scattering experiments.

The wave function of a single particle in the direct space representation is a probability amplitude for particle's position. The wave function must conform to

certain mathematical conditions in order to apply to physical reality. According to Max Born's interpretation, given the wave function for a particle, the probability $P(\mathbf{r})$ for finding the particle at position $\mathbf{r} \equiv (x, y, x)$ is proportional to the square of the wave function, that is:

$$P(\mathbf{r}) \propto \psi^* \psi \, dx \, dy \, dz. \tag{2.4}$$

In order for the particle to be found somewhere in space, and to maintain the probabilistic interpretation, the wave function must be normalizable, that is, one must be able to ensure that:

$$\int_{-\infty}^{+\infty} \int_{-\infty}^{+\infty} \int_{-\infty}^{+\infty} \psi^* \psi \, dx \, dy \, dz \; = 1. \tag{2.5}$$

Every observable, as in classical mechanics, is a function of position ($\mathbf{r} = x\mathbf{e}_x + y\mathbf{e}_y + z\mathbf{e}_z \equiv \{x, y, z\}$, where $\mathbf{e}_x$, $\mathbf{e}_y$, and $\mathbf{e}_z$ are the unit vectors in the Cartesian representation) and momentum ($\mathbf{p}$). In quantum mechanics, these variables become mathematical operators, defined according to the correspondence rules of Paul Ehrenfest, namely, $\mathbf{r}$ is replaced by the quantum operator $\hat{\mathbf{r}}$, which operates on a wave function as in $\hat{\mathbf{r}}\psi$, and $\mathbf{p}$ becomes a quantum operator $\hat{\mathbf{p}}$, which applies a derivative operation to a wave function, as in

$$\hat{\mathbf{p}} \equiv -i\hbar \left(\mathbf{e}_x \frac{\partial}{\partial x} + \mathbf{e}_y \frac{\partial}{\partial y} + \mathbf{e}_z \frac{\partial}{\partial z} \right) \equiv -i\hbar \nabla. \tag{2.6}$$

In addition, physical reality requires of the wave function that it be single-valued, continuous, and finite. The expectation value of an observable A is determined by the wave function, in accordance with its probability interpretation by evaluation of the integral:

$$\langle A \rangle = \int_{-\infty}^{+\infty} \int_{-\infty}^{+\infty} \int_{-\infty}^{+\infty} \psi^* \hat{A} \, \psi \, dx \, dy \, dz, \tag{2.7}$$

where the angular brackets in $\langle A \rangle$ indicate averaging, and the wave function is (from now on) assumed normalized.

A measurement of an observable represented by a linear Hermitian operator $\hat{A}$ yields an experimental result that is one of the real eigenvalues of that operator a_i that corresponds to the eigenfunction ψ_i:

$$\hat{A}\psi_i = a_i \psi_i. \tag{2.8}$$

Any arbitrary quantum state in the space of $\hat{A}$ spanned by its complete set of eigenfunctions can be expanded as a linear combination of these eigenfunctions:

$$\psi = \sum_{i=1}^{n} c_i \psi_i, \tag{2.9}$$

where c_i are the expansion coefficients, and the square of which represents the probability of observing the eigenvalue a_i associated with the corresponding state ψ_i.

2.3 Atomic units (au)

In this book, results are often quoted in the conventional *Système International* (SI) units and sometimes in other convenient units such as kcal/mol or ångström (Å). In addition to these systems, frequently, the equations and the results are in a dimensionless (relative) system of units used in atomic and quantum physics called the system of *atomic units* (abbreviated as "au") [1].

The system of au takes as its measuring gauge several of the fundamental properties of the electron. Thus, the electron's rest mass m_e is taken as the unit of mass (instead of the kilogram), the Bohr radius a_0 is taken as the unit of length (instead of the meter), the elementary charge (the magnitude of the charge of one electron, e) as the unit of charge (instead of the coulomb), and the reduced Planck's constant ($\hbar = h/2\pi$) as the unit of action or angular momentum (instead of the joule.second). Note that the au of mass, that is, the mass of an electron, *is different from, and not to be confused with, the "atomic mass unit" (amu), also known as "the dalton."* One dalton is $(1/12)$th of the mass of an atom of the carbon 12 isotope (^{12}C), and 1 amu $\approx$ 1,822.9 au.

In this system of units, the energy is expressed in hartrees, the energy of an electron in the first Bohr orbit, E_{hartree}, or E_h for short, instead of the joule. The time in this system is measured in units of $\hbar/E_h$. Finally, the speed of light ($c = 1/\alpha \approx 137$) is the reciprocal of the fine structure constant in this system of units. The latter is a dimensionless constant with the approximate value $\alpha \approx 1/137.036$ – to three decimals, which is often taken approximately as 1/137.[1] In the au system, the electric constant $k = (1/(4\pi\varepsilon_0))$ is set equal to 1.

1 It is interesting that Feynmanium ^{137}Fy (element 137) is a hypothetical element that cannot exist even in principle. Fy sets the limit on the periodic table as the first *impossible* element, since with an atomic number of 137, the classical speed of the electron becomes $v = \frac{Zc}{n}\underbrace{\left[\frac{e^2}{2\varepsilon_0 hc}\right]}_{\alpha \approx \frac{1}{137.036}} \equiv \frac{Zc}{n}\alpha \approx \frac{Zc}{137n}$ (within the simple Bohr atomic model). In this case, for element $Z = 137$, the speed of an electron in the first shell ($n = 1$) reaches the speed of light. This limits the periodic table due to the impossibility of the motion of the electrons and has nothing to do with the structure of the nucleus or with the fast decay of the strong nuclear force (visit https://www.chemedx.org/blog/search-final-element for further elaboration).

The adoption of the au system simplifies and compactifies the appearance of the equations at the cost of hiding several of the fundamental constants. For example, the Schrödinger equation for the hydrogen atom is written explicitly as follows:

$$\left[-\frac{\hbar^2}{2m_e}\nabla^2 - \frac{e^2}{4\pi\varepsilon_0 r} \right] \Psi = E\Psi. \tag{2.10}$$

When this is transformed to the au system, the coordinates are scaled by a_0, the electric constant is set to 1, the wave function is expressed in terms of the scaled coordinates, and E is now given relative to E_h; hence, the same symbols used further have different meanings than in eq. (2.10), which now becomes [1]

$$\left[-\frac{1}{2}\nabla^2 - \frac{1}{r} \right] \Psi = E\Psi. \tag{2.11}$$

Some common conversion factors include 1 au of length = $a_0 \approx 5.29 \times 10^{-9}$ cm = 0.529 Å; 1 au of charge = $e \approx 1.602 \times 10^{-19}$ C = 4.803×10^{-10} esu (electrostatic units); 1 au of charge density = $e/{a_0}^3 \approx 6.748$ eÅ^{-3} = 1.081×10^{12} Cm^{-3}; 1 au of Laplacian of the electron density = $e/{a_0}^5 \approx 24.099$ eÅ^{-5}; 1 au of dipole moment = $ea_0 \approx 2.5418$ debyes; 1 au of energy = $e^2/a_0 \approx 627.51$ kcal/mol ≈ 2.6255×10^3 kJ/mol ≈ 27.212 eV.

2.4 The molecular Hamiltonian

Most of the applications in this monograph are concerned with crystals made up of ground-state closed-shell (large biological) molecules. The following discussion will hence be focused on closed-shell molecular – rather than periodic – calculations.

The Hamiltonian operator of a molecule as expressed in au:

$$\hat{H} \equiv -\frac{1}{2}\sum_{i=1}^{N}\nabla_i^2 - \sum_{A=1}^{M}\frac{1}{2m_A}\nabla_A^2 - \sum_{i=1}^{N}\sum_{A=1}^{M}\frac{Z_A}{r_{iA}} + \sum_{i=1}^{N}\sum_{j>i}^{N}\frac{1}{r_{ij}} + \sum_{A=1}^{M}\sum_{B>A}^{M}\frac{Z_A Z_B}{R_{AB}}, \tag{2.12}$$

where N and M are the numbers of electrons and nuclei in the system, respectively; m_A is the mass of the Ath nucleus; Z_A is the atomic number (which equals the nuclear charge in au) of the Ath nucleus; $r_{iA} = |\mathbf{r}_i - \mathbf{R}_A|$, $r_{ij} = |\mathbf{r}_i - \mathbf{r}_j|$, and $R_{AB} = |\mathbf{R}_A - \mathbf{R}_B|$, where the capitalized "**R**" refers to the position vectors of the nuclei and the lowercase "**r**" refers to electronic coordinates.

The above Hamiltonian does not include spin–orbit effects nor other relativistic corrections which are important mainly in systems with heavy atoms [9]. It also does not take the finite size of the nucleus into consideration, and the nuclei are considered as mathematical points. Since the Hamiltonian considers nuclei as point charges without a finite size or internal structure, the potential, the wave function, and the electron density all exhibit cusps (singularities) at the positions of the

nuclei [10, 11]. Further, this Hamiltonian – as written earlier – is insensitive to spin which must be injected "by hand" into the wave function itself according to Pauli's antisymmetry principle for Fermionic particles such as a system of electrons.

Hamiltonian (2.12) contains both nuclear and electronic coordinates. The quantum mechanical operator for the kinetic energy of a particle, written explicitly as $\hat{T} \equiv -(\hbar^2/2m)\nabla^2$, has mass of the particle m in its denominator. Hence, the contribution of this term due to nuclear motion is negligible compared to the analogous contribution of the electrons. This allows one to omit, in a first (but good) approximation, the second term in the Hamiltonian written in eq. (2.12). In fact, electronic motion occurs at an attosecond timescale (1 as = 10^{-18} s) compared to a nanosecond (1 ns = 10^{-9} s) timescale of the nuclear motion [12, 13]. This approximation enables to decouple the electronic and nuclear motion which can, thus, be separated into two Hamiltonians accounting for the two motion: one electronic and one nuclear. This separation of motions based on their respective timescales allows one to approximately factorize the total wave function as a product of a purely electronic wave function and a purely nuclear one ($\Psi_{\text{total}}(\mathbf{r},\mathbf{R}) = \Psi_{\text{e}}(\mathbf{r};\mathbf{R})\Psi_{\text{n}}(\mathbf{R})$). This is the essence of the so-called BO approximation [14]. This timescale difference allows us to ignore the kinetic energy of the nuclei when examining the motion of the electrons, that is, the nuclei are "clamped" or "frozen" in their positions in the three-dimensional space. One can then solve an electronic Schrödinger equation in which the nuclear positions are frozen. The splitting of the problem into two separate Schrödinger equations yields one for the electrons with electronic coordinates treated as variables but the nuclear coordinates are constant parameters. Once this is solved, the nuclear coordinates may then be altered and, with this new set of parameters, the electronic Schrödinger equation solved anew, and so on. What results is a "potential energy (hyper)surface (PES)," a term that dates back to Henry Eyring and Michael Polanyi [15], as the geometry of this (semiclassical) system is varied.

There are of course situations where this approximation is invalid and the concept of a PES breaks down [16, 17]. Examples of these situations include conical intersections, whereby a low-lying excited state surface is close to a point on the ground state surface, or in the cases where we have exotic systems such as muonic atoms and the like [18].

Thus, within the BO approximation, the electronic Schrödinger equation for a set of fixed nuclei, in standard notation and in au (the convention adopted henceforth unless otherwise stated), is

$$\hat{H}_{\text{e}}\Psi_{\text{e}}(\mathbf{r};\mathbf{R}) \equiv \left(-\frac{1}{2}\sum_{i=1}^{N}\nabla_i^2 - \sum_{i=1}^{N}\sum_{A=1}^{M}\frac{Z_A}{r_{iA}} + \sum_{i=1}^{N}\sum_{j>i}^{N}\frac{1}{r_{ij}} \right)\Psi_{\text{e}}(\mathbf{r};\mathbf{R}) = E_{\text{e}}(\mathbf{R})\Psi_{\text{e}}(\mathbf{r};\mathbf{R}), \quad (2.13)$$

where the semicolon indicates parametric dependence, N is the total number of electrons in the system, and $E_{\text{e}}(\mathbf{R})$ is the *purely electronic energy* that includes the kinetic energies of all electrons (first term in $\hat{H}_{\text{e}}$), their total attraction to all nuclei

in the system (second term), and their total mutual repulsion (the last term). Note that Eq. (2.13) does not include the nuclear–nuclear repulsion term. The *total electronic energy* $E_{\text{total}}(\mathbf{R})$ is then obtained by adding the nuclear–nuclear repulsion (last term in the Hamiltonian given by eq. (2.12)), a classical term which is constant for a given nuclear skeleton geometry, to $E_{\text{e}}(\text{R})$ after solving the electronic problem. Thus, $E_{\text{total}}(\mathbf{R})$ is defined as follows:

$$\hat{H}_{\text{total}}\Psi_{\text{e}}(\mathbf{r};\mathbf{R}) \equiv \left(E_e(\mathbf{R}) + \sum_{A=1}^{M}\sum_{B>A}^{M}\frac{Z_A Z_B}{R_{AB}}\right)\Psi_{\text{e}}(\mathbf{r};\mathbf{R}) = E_{\text{total}}(\mathbf{R})\Psi_{\text{e}}(\mathbf{r};\mathbf{R}). \tag{2.14}$$

The Hamiltonian appearing in eq. (2.14) is identical to Hamiltonian expressed in eq. (2.13) except that it includes the addition of the nuclear–nuclear repulsion energy. The addition of the constant nuclear–nuclear repulsion does not alter the eigenfunctions of the ground and excited states and only adds a constant to the eigenvalues (the energies). From here on, the subscript "total" will be dropped if it is clear from the context that $E_{\text{total}}(\mathbf{R}) \equiv E(\mathbf{R})$.

The nuclear Schrödinger equation is written as follows:

$$\hat{H}_{\text{nuc.}}\Psi_{\text{nuc.}}(\mathbf{R}) \equiv \left(-\sum_{A=1}^{M}\frac{1}{2m_A}\nabla_A^2 + \sum_{A=1}^{M}\sum_{B>A}^{M}\frac{Z_A Z_B}{R_{AB}} + E_e(\mathbf{R})\right)\Psi_{\text{nuc.}}(\mathbf{R}) = E_{\text{nuc.}}\Psi_{\text{nuc.}}(\mathbf{R}), \tag{2.15}$$

where M is the total number of nuclei, m_A is the mass of the Ath nucleus, and $E_{\text{nuc.}}$ is the total energy of the nuclei in the potential created by the electronic system $E_{\text{e}}(\mathbf{R})$. This energy, $E_{\text{nuc.}}$, includes contributions from the kinetic energies of all nuclei (first term in $\hat{H}_{\text{n}}$), the total nuclear–nuclear repulsion of all nuclei in the system (second term), and the electronic energy $E_{\text{e}}(\mathbf{R})$ defined in eq. (2.13). Notice that, as mentioned already, the nuclei move in an electronic potential. We shall see in later chapters the importance attached to the BO approximation in the quantum crystallographic treatment of large molecules.

2.5 The variational principle

The search for an optimal approximate wave function includes (i) variational methods epitomized by the Hartree–Fock method and post-Hartree–Fock methods that build on it, and (ii) perturbational methods such as any one of the nth-order Møller–Plesset perturbation theoretic methods named MPn, with $n = 2, 4$ typically.

Variational methods get their name from the underlying mathematical apparatus rooted in the calculus of variations. The result in this case is that the energy is a functional of the wave function, and this functional dependence is symbolized by square brackets. This principle states that *the ground state energy* E_0 *obtained*

from the exact wave function Ψ_0 is always lower than that obtained using an approximate wave function Ψ_{approx}. A straightforward mathematical proof of this theorem can be found in Ref. [19], while the final result is expressed as follows:

$$E[\Psi_{\text{approx.}}] = \frac{\int \Psi^*_{\text{approx.}} \hat{H} \Psi_{\text{approx.}}\, d\tau}{\int \Psi^*_{\text{approx.}} \Psi_{\text{approx.}} d\tau} \geq E_0[\Psi_0], \tag{2.16}$$

where $d\tau$ is a volume element that has, in general, $3N$ space and N spin coordinates.

The theorem prescribes a definitive pathway to improve the wave function, that is, through the systematic minimization of the energy functional with respect to all parameters in the wave function while maintaining the normalization condition. In the variational method, a trial function is first employed and is subsequently improved systematically through an iterative procedure until no further minimization of the energy is possible. The latter point is when the calculation is stopped, no further improvement is possible, and it is considered to have converged.

2.6 The Pauli exclusion principle

Variational solutions to the electronic problem without any arbitrary parameters (save the fundamental constants and the core approximations outlined at the beginning of this chapter) are known as *ab initio* methods. The Hartree–Fock theory is the foundation of all such *ab initio* methods for many-electron systems.

A crucial approximation central to all these methods of solution is the well-known "*orbital approximation*." According to this approximation, the many-electron wave function $\Psi(\mathbf{x}_1, \mathbf{x}_2, \ldots, \mathbf{x}_N)$ is factorized into a product of one-electron functions known as "*orbitals*" ($\psi_i(\mathbf{x}_i)$, $i = 1, 2, \ldots, N$). This factorization, in essence, reduces an insolvable many-body N-electron problem into N-tractable one-electron problems.

Douglas Hartree has first proposed a simple product of one-electron functions, $\psi_1(\mathbf{x}_1)\psi_2(\mathbf{x}_2)\ldots\psi_N(\mathbf{x}_N)$, now known as the "Hartree product." The Hartree product, however, turned out not to be satisfactory in describing fermionic systems since it ignores electron indistinguishability (it assigns specific electrons to specific orbitals) and violates the Pauli principle [20]. This latter principle states that for fermions (particles with the magnitude of the spin angular momentum (in units of $\hbar$) $S = i + \frac{1}{2}$, $i = 0, 1, 2, 3, \ldots$) such as electrons, *the many-particle wave function of an ensemble of strongly interacting indistinguishable fermions must be antisymmetric to the interchange of the spatial and spin coordinates, $\mathbf{x} \equiv \{x, y, z, \omega\}$, of any pair of particles*:

$$\Psi(\mathbf{x}_1, \ldots, \mathbf{x}_i, \ldots, \mathbf{x}_j, \ldots, \mathbf{x}_N) = -\Psi(\mathbf{x}_1, \ldots, \mathbf{x}_j, \ldots, \mathbf{x}_i, \ldots, \mathbf{x}_N), \tag{2.17}$$

where the coordinates of the ith and jth particles have been interchanged. For bosons (particles with the magnitude of the spin angular momentum (in units of $\hbar$)

$S = i$, where $i = 0, 1, 2, 3, \ldots$) such as photons or α-particles, the Pauli exclusion principle does not apply since now the many-particle wave function is symmetric with respect to the exchange of particles. In other words, in the latter case, the wave function does not change its sign upon the interchange of two identical particles, manifested, for example, in Einstein–Bose condensation. This symmetry/antisymmetry principle has been introduced in the theory as a postulate that correctly predicts corresponding statistics of the two families of particles.

A direct consequence of the Pauli principle is what is known in chemistry as the "exclusion principle," that is, the impossibility of electrons to be described by the same four quantum numbers in isolated atoms, for example. This principle, is what allows elements to exist and form the system in the periodic table, prevents material objects from occupying the same space at the same time, and is the physical mechanism preventing neutron stars from collapsing under their own enormous gravitational central pull. A many-boson system such as photons, in contrast to one made of fermions, tends to populate the same quantum state as occurs, for example, in the generation of lasers. Reviews of the origin and meaning of the principle can be found in Massimi's book [20] and in chapter 20 (pp. 427–447) of Henry Margenau's book [21].

The incorporation of both indistinguishability and the Pauli principle into nonrelativistic *ab initio* calculations is done "by hand," since the symmetry properties of the wave function emerge naturally only through a relativistic treatment [9]. To simultaneously incorporate indistinguishability and antisymmetry into the *N*-electron wave function, one can form the so-called antisymmetrized product of spin orbitals. A "spin orbital," χ_i, is defined as the product of a spatial orbital and a spin function:

$$\chi_i(\mathbf{x}) = \phi_i(\mathbf{r})\sigma_i(\omega) = \phi_i(x, y, z)\sigma_i(\omega), \tag{2.18}$$

where ϕ_i is the spatial one-electron function factor of χ_i, and σ_i refers to either α or β and each of which is a function of the spin coordinate ω such that

$$\hat{S}\alpha = +\frac{1}{2}\hbar\alpha, \tag{2.19}$$

and that

$$\hat{S}\beta = -\frac{1}{2}\hbar\beta, \tag{2.20}$$

where $\hat{S}$ is the spin angular momentum operator and α and β are the eigenfunctions of this operator with eigenvalues of $\pm(1/2)\hbar$. These eigenfunctions are orthonormal, that is:

$$\langle\sigma|\sigma'\rangle = \int d\omega\, \sigma^*(\omega)\sigma'(\omega) = \delta_{\sigma\sigma'} = \begin{cases} 1 & \text{if } \sigma = \sigma' \\ 0 & \text{if } \sigma \neq \sigma' \end{cases}, \tag{2.21}$$

where $\delta_{\sigma\sigma'}$ is the so-called Kronecker delta function that equals 1 or 0 depending on whether its indices are equal or not.

John C. Slater proposed to satisfy the Pauli principle within the orbital model by expressing the many-electron wave function as an antisymmetrized sum of products named after him as the "*Slater determinant*" (det) [22]:

$$\Psi_0 \approx \Psi_{\text{det}} \equiv \frac{1}{\sqrt{N!}} \begin{vmatrix} \chi_1(\mathbf{x}_1) & \chi_2(\mathbf{x}_1) & \cdots & \chi_N(\mathbf{x}_1) \\ \chi_1(\mathbf{x}_2) & \chi_2(\mathbf{x}_2) & \cdots & \chi_N(\mathbf{x}_2) \\ \vdots & \vdots & & \vdots \\ \chi_1(\mathbf{x}_N) & \chi_2(\mathbf{x}_N) & \cdots & \chi_N(\mathbf{x}_N) \end{vmatrix}, \tag{2.22}$$

where the factor before the determinant ensures the normalization of the N-electron wave function, and the spin orbitals are usually chosen to be orthonormal:

$$\langle \chi_i \,|\, \chi_j \rangle = \int \chi_i^* \chi_j d\mathbf{x} = \delta_{ij}, \tag{2.23}$$

and the space orbitals are also chosen to be orthonormal, that is,

$$\langle \phi_i \,|\, \phi_j \rangle = \int \phi_i^* \phi_j d\mathbf{r} = \delta_{ij}, \tag{2.24}$$

where in both eqs. (2.23) and (2.24), δ_{ij} is a Kronecker delta function.

It is common to refer to this determinant in quantum chemistry textbooks in an abbreviated form listing only this determinant's diagonal elements as follows:

$$\Psi_{\text{det}} = |\chi_1(\mathbf{x}_1)\, \chi_2(\mathbf{x}_2)\, \cdots\, \chi_N(\mathbf{x}_N)|. \tag{2.25}$$

A Slater determinant, by construction, *allows every electron to occupy every spin orbital*. In this manner, the electrons are made indistinguishable. Furthermore, from the elementary properties of determinants, the interchange of any pair of rows or any pair of columns changes the sign of the determinant. This interchange is equivalent to interchanging the labels in eq. (2.17). Thus, in one stroke, the Slater determinant has lifted the artificial distinguishability of a strongly interacting system of electrons and satisfied the Pauli antisymmetry principle for this ensemble of fermions. It is important to note that the Pauli antisymmetry principle is physically manifested as the "Pauli exclusion principle." In this sense, the Slater determinant correlates the motion of same-spin electrons, a correlation that tends to keep same-spin electrons apart.

Slater determinants enjoy a special role within quantum crystallography. One of the driving motivations of quantum crystallography is to extract from X-ray scattering the full quantum mechanics in a way that allows calculation of all quantum properties. That is not doable with the information obtained from classical crystallography, no matter how accurate may be the electron density so measured. For example, any property

which depends upon *momentum* is inherently not obtainable from classical crystallographic electron density determinations because the momentum operator contains a derivative which requires the wave function or an *N*-representable antisymmetric density matrix to evaluate its expectation value. Thus, to extract quantum properties from the X-ray scattering experiment, a procedure to obtain antisymmetric wave functions, or *N*-representable density matrices, is required to describe the scattering.

As mentioned earlier, the Hartree–Fock theory is the point of departure to all electronic structure methods. To keep this monograph self-contained, it is useful, hence, to review very briefly the formalism of this theory, that of post-Hartree–Fock methods, and of density functional theory (DFT).

2.7 The Hartree–Fock method

The so-called linear combination of atomic orbitals (LCAO) has long been the basis of an efficient variational approach for an approximate solution of the Schrödinger equation. Naturally, the larger the set of "atomic orbitals (AOs)" (the number of basis functions, b) used to expand the ith molecular spin orbital χ_i, the better its description and the better the solution of the Schrödinger equation (the lower the energy). Naturally, the best possible description is when the number of basis functions is infinite, a clearly unachievable ideal limit. The LCAO formalism is

$$\phi_i = \sum_{\mu=1}^{b} c_{i\mu}\psi_\mu, \tag{2.26}$$

where $c_{i\mu}$ are the expansion coefficients and the ψ_μ are the atomic-centered basis functions (AOs). There is no requirement for centering the basis functions (the AOs) at the positions of the nuclei, since they are strictly *not* AOs but just a convenient set of functions used to expand the MOs. Centering the AOs at the position of the respective nuclei is, however, a common choice in computational chemistry.

Written as an expectation value of the Hamiltonian in eq. (2.14), whereby we change the notation from here on for simplicity $\hat{H}_{\text{total}} \rightarrow \hat{H}$, the Hartree–Fock energy is given by

$$E_{\text{HF}} = \langle \Psi_{\text{det}} | \hat{H} | \Psi_{\text{det}} \rangle \tag{2.27}$$

For a closed-shell system with N electrons occupying $N/2$ space orbitals, and upon writing the explicit form of the Hamiltonian operator, and inserting the Slater determinant form of the total wave function (eq. (2.22)), we get [1]

$$E_{\mathrm{HF}} = 2\sum_{i=1}^{N/2}\int \phi_i^*(1)\left[-\frac{1}{2}\nabla^2 - \sum_{A}^{M}\frac{Z_A}{r_{1A}}\right]\phi_i(1)\, d\mathbf{r}_1 + \sum_{i=1}^{N/2}\sum_{j=1}^{N/2}\left\{2\left[\int\int |\phi_i(1)|^2\left(\frac{1}{r_{12}}\right)|\phi_j(2)|^2 d\mathbf{r}_1 d\mathbf{r}_2\right] - \left[\int\int \phi_i(1)\,\phi_j^*(1)\left(\frac{1}{r_{12}}\right)\phi_j(2)\,\phi_i^*(2)\, d\mathbf{r}_1 d\mathbf{r}_2\right]\right\} + V_{nn}, \tag{2.28}$$

which is written in atomic units, and where the integrals are over space coordinates (spin coordinates are already integrated out since the Hamiltonian is spinless), and V_{nn} represents the nuclear-nuclear repulsion energy. Note the simplification of the notation that is used subsequently whereby a functional dependence on "(1), (2), etc." is to be read as on the coordinates of electron 1, that is, as equivalent to a functional dependence on "($\mathbf{r}_1$), ($\mathbf{r}_2$), . . .". is The latter equation can be expressed in a more compact notation as:

$$E_{\mathrm{HF}} = 2\sum_{i=1}^{N/2} H_i + \sum_{i=1}^{N/2}\sum_{j=1}^{N/2}(2J_{ij} - K_{ij}) + V_{nn}. \tag{2.29}$$

In this expression, J_{ij} and K_{ij} are known as the *Coulomb* and *exchange integrals*, respectively, and both involve averaging over two electron operators. The average over one-electron operators (H_i) yields the energy of an electron in orbital i in the bare nuclear potential of all nuclei. It is the average of the kinetic energy of a single electron in addition to its interaction with the nuclear potential (the external potential).[2]

The lead factor of 2 in the first summation is necessary to account for the double occupation of any given occupied space orbital for a closed-shell system. The average energy of electrostatic repulsion between the electron density in two orbitals ϕ_i and ϕ_j is then given by the corresponding Coulomb integral. In this manner, the instantaneous electron–electron repulsion experienced by every electron due to the motion of every other electron is hugely simplified by considering only the motion of a given electron in the *average field* of the remaining electrons. Meanwhile, the exchange integrals (K_{ij}) account for the correlation of the motions of electrons of parallel spins and account for the exchange part of the total correlation of electronic motion. An elaboration on the physical meaning of this energy term can be found in the third volume of Richard Feynman's classic [23] (Chapter 4, pp. 4–1 to 4–15) and in Henry Margenau's book (chapter 20, pp. 427–447) [21].

2 The word "external" in "external potential" indicates a potential associated with any source except that of the system of electrons itself. The bare nuclear potential is an example of an external potential. The potential associated with an externally imposed electromagnetic field is another example of an external potential.

Exchange energy between same-spin electrons is a quantum mechanical energy term that has no classical analogues. Since J_{ij} and K_{ij} appear in eq. (2.29) with opposite signs, exchange energy corrects for the nonphysical self-repulsion ($J_{kk} = J_{(\text{self})} = -K_{kk} = -K_{(\text{self})}$).

According to Margenau's interpretation, the negative gradient of this "exchange energy" behaves as a pseudo-force. This pseudo-force has all the hallmarks of a repulsive force between same-spin electrons except that it is *not mediated by the exchange of bosons* as "normal" field-mediated forces, but it rather originates from the antisymmetry of the wave function. As a result, this pseudo-force, by tending to keep same-spin electrons apart, lowers the energy of the system and leads, for instance, to the first Hund's rule. This rule states that the electronic configuration with the highest possible multiplicity is the most stable when everything else is equal. The highest multiplicity maximizes the number of same-spin electrons while this exchange pseudo-force keeps them apart, hence reducing the energy of the system compared to configurations with lower multiplicities.

The Hartree–Fock theory determines the set of molecular orbitals (MOs) that minimize the energy subject to the constraint that they are orthonormal. These orbitals are eigenfunctions of the so-called Fock operator $\hat{F}$. The eigenvalues of this operator, ε_i, are the energies of these orbitals. The corresponding one-electron eigenvalue equation is [1]

$$\hat{F}(1)\,\phi_i(1) = \varepsilon_i\,\phi_i(1), \tag{2.30}$$

where, in the case of a closed-shell system,

$$\hat{F}(1) = \hat{H}(1) + \sum_{j=1}^{N/2}\left[2\hat{J}_j(1) - \hat{K}_j(1)\right], \tag{2.31}$$

in which

$$\hat{H}(1) \equiv -\frac{1}{2}\nabla^2 - \sum_{A}^{M}\frac{Z_A}{r_{1A}}, \tag{2.32}$$

$$\hat{J}_j(1)\,\phi_i(1) = \left[\int \phi_j^*(2)\left(\frac{1}{r_{12}}\right)\phi_j(2)\,d\mathbf{r}_2\right]\phi_i(1), \tag{2.33}$$

and

$$\hat{K}_j(1)\,\phi_i(1) = \left[\int \phi_j^*(2)\left(\frac{1}{r_{12}}\right)\phi_i(2)\,d\mathbf{r}_2\right]\phi_j(1), \tag{2.34}$$

where all integrations are carried out over all space, and operators $\hat{J}_j$ and $\hat{K}_j$ are called the "Coulomb" and the "exchange" operators, respectively. It is worth noting here that the exchange operator is a *nonlocal operator* rendering the entire Fock operator to be nonlocal. This is to be contrasted with the Kohn–Sham (KS) operator of

DFT (*vide infra*). A "*local*" operator is one which operates on a function at a point entirely independent of other point(s) of space. In this sense, the Coulomb operator is local because the result of its operation on the *i*th orbital, $\hat{J}_j(1)\,\phi_i(1)$, only depends on the value of this orbital at the point of evaluation. The exchange operator, however, when it operates on the *i*th orbital, $\hat{K}_j(1)\,\phi_i(1)$, requires the knowledge of this orbital at all other points in three-dimensional space. This is manifested by the appearance of ϕ_i within the integral in eq. (2.34).

If we now substitute eq. (2.26) into eq. (2.30) we get

$$\sum_{\mu=1}^{b} c_{i\mu}\hat{F}\psi_\mu = \varepsilon_i \sum_{\mu=1}^{b} c_{i\mu}\psi_\mu. \tag{2.35}$$

Pre-multiplication of this last equation by ψ_ν followed by integration over all space gives

$$\sum_{\mu=1}^{b} c_{i\mu}(F_{\nu\mu} - \varepsilon_i S_{\nu\mu}) = 0, \tag{2.36}$$

where $\nu = 1,\ 2,\ \ldots,\ b$

$$F_{\nu\mu} \equiv \langle\psi_\nu|\hat{F}|\psi_\mu\rangle, \tag{2.37}$$

and

$$S_{\nu\mu} \equiv \langle\psi_\nu|\psi_\mu\rangle. \tag{2.38}$$

Equation (2.36) is known as the Roothaan equation [1, 24].

A nontrivial solution of these *b* simultaneous linear homogeneous equations with *b* unknowns $\{c_{i\mu}\}$ is found by setting the secular determinant equal to zero, that is:

$$\det\,(F_{\nu\mu} - \varepsilon_i S_{\nu\mu}) = 0, \tag{2.39}$$

which yields *b* orbital energies (ε_i) as its roots.

By inspection, one realizes that the Hartree–Fock equations are coupled integrodifferential equations. The coupling arises because the potential in the Fock operator depends on the very orbitals we are trying to determine. Such a system does not have an analytical solution and must instead be solved iteratively starting from a guessed solution (a set of guessed MOs). These guessed orbitals are then used to construct the operators to obtain a new set of improved orbitals, and the process is repeated until convergence. The procedure is said to have converged when a set of orbitals generate a field that, when inserted in the operators, regenerates the same orbitals within a given precision. Since the field is, in a sense, self-regenerating, this procedure is also known in the literature as the *self-consistent field* (SCF) approach.

A set of guessed occupied MOs is first expanded according to the LCAO model in the chosen set of basis functions (basis set). The choice of a basis set is particularly adapted to the operation of digital computers since it transforms an analytical problem (that of optimizing the form of a three-dimensional function) into a linear algebra problem (optimizing a set of coefficients that change the relative weights of a set of given functions). As mentioned earlier, usually these basis functions (AOs) are centered on the atomic nuclei, but this is by no means a fundamental requirement. One can place these basis functions anywhere or even use plane wave functions, the latter choice being particularly common in periodic solid-state calculations.

In molecular-type SCF calculations, each (*i*th) MO of the set of occupied MOs is guessed by specifying the initial expansion coefficients $\{c_{i\mu}\}$. With this initial guessed set of occupied MOs, the algorithm constructs the Fock operator which is used to evaluate the matrix elements (eqs. (2.37) and (2.38)). The matrix elements are then inserted into the secular determinant (eq. (2.39)) which yields the first set of eigenvalues (the set of orbital energies $\{\varepsilon_i\}$). This set of eigenvalues are then inserted into eq. (2.36) to get the next improved set of coefficients. The new coefficients are used to construct the next set of improved occupied MOs and Fock operator. The same procedure is repeated until the set of occupied MOs within the Fock operator yields the same ones as a solution of the secular equations. This is when the calculation has reached self-consistency and we now have the "best" possible set of MOs that yield the minimum energy within the chosen basis set as required by the variational principle. A final Slater determinant can then be constructed using the SCF MOs.

With the orbitals that result from the SCF procedure, one can then calculate any of the desired properties of the system. An important example is the electron density, which is defined as follows:

$$\rho(\mathbf{r}) = N \sum_{\omega} \int \cdots \int \Psi^* (\mathbf{x}_1, \ldots, \mathbf{x}_N) \Psi(\mathbf{x}_1, \ldots, \mathbf{x}_N) \, d\mathbf{r}_2, \ldots, d\mathbf{r}_N, \tag{2.40}$$

where

$$\mathbf{x}_i \equiv (x_i, y_i, z_i, \omega_i), \tag{2.41}$$

in which Ψ is the antisymmetric many-electron wave function and x_i, y_i, z_i are the space coordinates of electron i with spin coordinate ω_i which is the argument of either an α or a β spin function. The mode of integration in eq. (2.40), whereby the space integration is effected over the three-dimensional coordinates of all electrons in the system except one followed by the discrete summation over both spins, is often written in short-hand notation as the integral:

$$\int d\tau' \equiv \sum_{\omega} \int \cdots \int d\mathbf{r}_2, \ldots, d\mathbf{r}_N. \tag{2.42}$$

In this manner, the electron density expression (eq. (2.40)) is written as follows:

$$\rho(\mathbf{r}) = N \int \Psi^* \Psi d\tau'. \tag{2.43}$$

The electron density written in an abstract manner in eq. (2.40) can be calculated from the sum of the square of all doubly occupied MOs (in a closed-shell system), which in the single determinant scheme is expressed as follows:

$$\rho(\mathbf{r}) = N \int d\tau' \; \Psi^*_{\text{det}} \Psi_{\text{det}} \tag{2.44}$$

$$= 2 \sum_{j=1}^{N/2} \phi_j^* \phi_j \tag{2.45}$$

$$= 2 \sum_{\nu=1}^{b} \sum_{\mu=1}^{b} \sum_{j=1}^{N/2} c_{\nu j} c_{\mu j} \psi_\nu^* \psi_\mu \tag{2.46}$$

$$= 2 \sum_{\nu=1}^{b} \sum_{\mu=1}^{b} P_{\nu\mu} \psi_\nu^* \psi_\mu, \tag{2.47}$$

where the coefficients are taken to be real and where

$$P_{\nu\mu} = \sum_{j=1}^{N/2} c_{\nu j} c_{\mu j} \tag{2.48}$$

are the elements of the *density matrix* (**P**) for a closed-shell molecule. Since **P** determines the MOs in the chosen basis set, it determines the (reduced) one- and two-electron density matrices (1-RDM, 2-RDM) and every other property of the system within the Hartree–Fock theory.

In matrix notation, and for a single determinantal wave function, one can express eq. (2.48) as

$$\mathbf{P} = \mathbf{C}^\dagger \mathbf{C}, \tag{2.49}$$

where **P** is a $b \times b$ matrix, b is the number of basis functions in the chosen basis set, **C** is a matrix of row vectors of b coefficients, and the superscripted dagger "†" implies complex conjugate transposition. (In general, the coefficients are complex, but can always be chosen to be real in the absence of external magnetic fields.)

It is worth noting at this point a type of shortage of nomenclature by virtue of which the terms "density matrix" are used to indicate the matrix of the coefficients, while the 1- and 2-RDMs are defined, respectively, as follows:

$$\rho_1(\mathbf{r}_1, \mathbf{r}_1') = N \sum_{\omega} \int \cdots \int \Psi^* (\mathbf{r}_1 \omega_1, \ldots, \mathbf{r}_N \omega_N) \, \Psi(\mathbf{r}_1' \omega_1, \ldots, \mathbf{r}_N \omega_N) \, d\mathbf{r}_2, \ldots, d\mathbf{r}_N, \tag{2.50a}$$

$$\equiv N \int \Psi^* (\mathbf{r}_1 \omega_1, \ldots, \mathbf{r}_N \omega_N) \Psi(\mathbf{r}_1' \omega_1, \ldots, \mathbf{r}_N \omega_N) d\tau' \tag{2.50b}$$

and

$$\rho_2(\mathbf{r}_1, \mathbf{r}_2|\mathbf{r}_1', \mathbf{r}_2') = \frac{N(N-1)}{2}\sum_{\omega_i}\int\cdots\int\Psi^*(\mathbf{r}_1\omega_1, \mathbf{r}_2\omega_2, \ldots, \mathbf{r}_N\omega_N) \Psi(\mathbf{r}_1'\omega_1, \mathbf{r}_2'\omega_2, \ldots, \mathbf{r}_N\omega_N)\, d\mathbf{r}_3, \ldots, d\mathbf{r}_N. \quad (2.51)$$

For a single determinantal wave function, these reduced density matrices can be expressed in linear algebraic form (where $\boldsymbol{\psi}$ is a column vector of basis functions) as:

$$\rho_1(\mathbf{r}_1, \mathbf{r}_1') = 2\,\mathrm{tr}\,\mathbf{P}\boldsymbol{\psi}(\mathbf{r}_1)\otimes\boldsymbol{\psi}^\dagger(\mathbf{r}_1'), \quad (2.52)$$

$$\rho_2(\mathbf{r}_1, \mathbf{r}_2|\mathbf{r}_1', \mathbf{r}_2') = \begin{vmatrix} \rho_1(\mathbf{r}_1, \mathbf{r}_1') & \frac{1}{2}\rho_1(\mathbf{r}_1, \mathbf{r}_2') \\ \rho_1(\mathbf{r}_2, \mathbf{r}_1') & \rho_1(\mathbf{r}_2, \mathbf{r}_2') \end{vmatrix}. \quad (2.53)$$

In this notation, the electron density is itself obtained by dropping the distinction (primed *vs*. unprimed) between the coordinates in the arguments, including the omission of the subscript "1," of the basis functions whereby eq. (2.52) becomes

$$\rho(\mathbf{r}) = 2\mathrm{tr}\,\mathbf{P}\boldsymbol{\psi}(\mathbf{r})\otimes\boldsymbol{\psi}^\dagger(\mathbf{r}). \quad (2.54)$$

Thus, the diagonal elements of the 1-RDM are obtained if we remove the prime, which yields the electron density as defined in eq. (2.40). Meanwhile, if we remove the primes from the 2-RDM we obtain the electron *pair density*, a function of six spatial coordinates of a pair of electrons, which is written as follows

$$\rho(\mathbf{r}_1, \mathbf{r}_2) = \frac{N(N-1)}{2}\sum_{\omega_i}\int\cdots\int\Psi^*(\mathbf{r}_1\omega_1, \mathbf{r}_2\omega_2, \ldots, \mathbf{r}_N\omega_N) \Psi(\mathbf{r}_1\omega_1, \mathbf{r}_2\omega_2, \ldots, \mathbf{r}_N\omega_N)d\mathbf{r}_3, \ldots, d\mathbf{r}_N. \quad (2.55)$$

The pair density is the conditional probability to find an electron in volume element $d\mathbf{r}_1$ centered at $\mathbf{r}_1$ while another one is located in volume element $d\mathbf{r}_2$ centered at $\mathbf{r}_2$ weighted by the total number of distinct pairs (the factor $N(N-1)/2$). While the electron density is accessible via crystallography, the pair density can be obtained from inelastic scattering experiment whether using X-ray or electron beams [25–27].

We now return to the "density matrix" defined above. This matrix, $\mathbf{P}$, has the important mathematical properties of *idempotency* and *hermiticity*, which are expressed,

$$\mathbf{P}^n = \mathbf{P} \text{ and } \mathbf{P} = \mathbf{P}^\dagger, \quad (2.56)$$

respectively, and where n is any nonzero integer and $\mathbf{P}^\dagger$ is the complex conjugate transpose of $\mathbf{P}$ [28, 29]. A special case of idempotency is

$$\mathbf{P}^2 = \mathbf{P}. \quad (2.57)$$

Those functions $\rho_1(\mathbf{r}_1,\mathbf{r}_1')$ which are idempotent (also known as projectors) map back to antisymmetric N-body wave functions. It is that property of idempotency which defines the N-representability of the one-body density matrix [30].

An N-representable one-body reduced density matrix has restrictions on its eigenvalues, that is, the orbitals' occupation numbers. By virtue of the Pauli principle, no spin orbital can be the locus of more than one electron. When these occupation numbers (eigenvalues) are either 0 or 1, the one-body RDM maps into a single Slater determinant. In this case, the corresponding $\mathbf{P}$ matrix represents an idempotent Hermitian operator (Eq. (2.56)) which is also normalized, that is,

$$\operatorname{tr}\mathbf{P} = N. \tag{2.58}$$

A single determinant accounts for Fermi correlation that governs the motion of same-spin electrons but fails to account for the Coulombic correlation between all electrons [31]. As for any approximate wave function, the Hartree–Fock energy (E_{HF}) is greater than the exact energy (E_0) of the ground state. The difference between the exact nonrelativistic energy and the Hartree–Fock limit (i.e., the SCF energy that would be obtained with an infinitely large basis set) has been termed by Per-Olov Löwdin as the "correlation energy" ($E_{\mathrm{C}}^{\mathrm{HF}}$) [32]:

$$E_{\mathrm{C}}^{\mathrm{HF}} = E_0 - E_{\mathrm{HF}}. \tag{2.59}$$

How to account for this Coulombic correlation energy has been, and continues to be, a central problem of computational quantum chemistry. It provided a main impetus to develop DFT as well as post-Hartree–Fock methods such as *configuration interaction* (CI) methods and perturbational approaches such as Møller–Plesset's.

In a typical (single reference) CI calculation, a set of MOs (occupied and virtual) is obtained from an initial SCF calculation. The SCF MOs are then used to construct sets of different electronic configurations, ground and excited ($^0\Psi_{\mathrm{det}}$ (ground state), $\{^1\Psi_{\mathrm{det}}\}$ (a set of singly excited configurations), $\{^2\Psi_{\mathrm{det}}\}$ (a set of doubly excited configurations), etc.). Each configuration in every set is represented by a single Slater determinant, and the many-electron wave function representing the state is expressed as a linear combination of configurations [1]:

$$\Psi_{\mathrm{CI}} = C_0\,{}^0\Psi_{\mathrm{det}} + \left\{C_1\,{}^1\Psi_{\mathrm{det}}\right\} + \left\{C_2\,{}^2\Psi_{\mathrm{det}}\right\} + \cdots \tag{2.60}$$

where the unknown expansion coefficients $\{C_i\}$ are obtained variationally.

In general, there exists more than one configuration of each type except for the ground state, which is why we have written $\{C_i^i\Psi_{\mathrm{det}}\}$ as a set (indicated by the braces). An example in use is the CI with single and double excitations (CISD). This CISD approximation expands the state in terms of all the configurations differing from the ground state by one- and two-electronic excitations. Clearly, the CISD is a truncated CI since, in principle, the calculation can include all possible configurations of proper

symmetry within the set of available MOs. In this latter case, the calculation is known as "full-CI," highly accurate but highly expensive as well.

According to the theorem known as "*Brillouin's theorem*" [33], the matrix elements of the ground electronic state's SCF determinant with any of the determinants produced by a single excitation vanish. This is expressed, as in the following example, between the ground state and one of the singly excited states as follows:

$$\left\langle {}^{0}\Psi_{\text{det}} \left| \hat{H} \right| {}^{1}\Psi_{\text{det}} \right\rangle = 0. \tag{2.61}$$

Since the first-order corrections vanish as a consequence of Brillouin's theorem, Hartree–Fock calculations deliver all one-electron properties (e.g., electron density, dipole moment, and higher electric multipoles) that are correct to second-order. This theorem implies that any single determinant calculation of the ground state is already equivalent to the one that includes configuration with all singly excited states. CI calculations, to differ from SCF, must include higher orders in the expansion given by eq. (2.60).

2.8 Some essentials of density functional theory (DFT)

An elegant approach to incorporate Coulombic correlation effects within a single determinant scheme is DFT which is faster than CI calculations given the same system and basis set [30, 34, 35]. Resting on the first Hohenberg–Kohn theorem (HK-1 theorem) [36], discussed in Chapter 1 of this book, DFT was soon thereafter converted from an abstract "existence" theorem into a practical computational scheme by Kohn and Sham [37].

To briefly recap, the HK-1 theorem says that the external potential (V) is fixed by the nondegenerate ground-state electron density ($\rho(\mathbf{r})$), and so is the total number of electrons (N). These two determinations completely specify the system's Hamiltonian. It follows that the electron density determines all of the system's wave functions and energies of ground and excited states. Since all of the system's wave functions are fixed, the ground-state electron density also fixes all properties of the system, ground and excited. This is expressed symbolically:

$$\rho(\mathbf{r}) \rightarrow \left\{ \begin{matrix} V[\rho(\mathbf{r})] \\ N[\rho(\mathbf{r})] \end{matrix} \right\} \rightarrow \hat{H} \rightarrow \{\Psi_i\}, \tag{2.62}$$

where $i = 0, 1, 2, \ldots, \infty$, and the square brackets indicate a functional dependence on the ground-state electron density.

The external potential operator acting on electron i, where the caret above $\hat{V}$ (informally referred to as "hat") which has been added to emphasize its role as a

quantum mechanical operator, is defined (in au – as is the remainder of this chapter) as follows:

$$\hat{V}(\mathbf{r}_i) = -\sum_{A=1}^{M} \frac{Z_A}{r_{iA}}. \tag{2.63}$$

The electronic Hamiltonian, eq. (2.13), expresses the total electronic energy of the ground electronic state as the sum of the electronic kinetic energy, the nuclear–electronic potential energy, and the electron–electron repulsion energy. These three energy terms can be written as

$$E_0[\rho_0] = \langle T_e[\rho_0] \rangle + \langle V_{ne}[\rho_0] \rangle + \langle V_{ee}[\rho_0] \rangle, \tag{2.64}$$

where averaging is symbolized by the angular brackets, functional dependence by the square brackets, T refers to kinetic energy, V refers to a potential energy, and the subscripts "e" and "n" refer to electrons and nuclei, and ρ_0 is the electron density of the ground electronic state.

From eqs. (2.63) and (2.64), we have

$$\hat{V}_{ne} = \sum_{i=1}^{N} \hat{V}(\mathbf{r}_i) = -\sum_{i=1}^{N} \sum_{A=1}^{M} \frac{Z_A}{r_{iA}}. \tag{2.65}$$

The average of nuclear–electron attraction energy is obtained from

$$\langle V_{ne} \rangle = \langle \Psi_0 | \sum_{i=1}^{N} \hat{V}(\mathbf{r}_i) | \Psi_0 \rangle, \tag{2.66a}$$

where Ψ_0 is the many-electron ground-state wave function, thus:

$$\langle V_{ne} \rangle = \int\int \Psi_0^* \left[\sum_{i=1}^{N} \hat{V}(\mathbf{r}_i) \right] \Psi_0 \, d\tau' \, d\mathbf{r} = \int\int \Psi_0^* \left[N \hat{V}(\mathbf{r}) \right] \Psi_0 \, d\tau' d\mathbf{r} \tag{2.66b}$$

$$= \int \underbrace{N \int \Psi_0^* \Psi_0 \, d\tau'}_{\rho_0(\mathbf{r})} \hat{V}(\mathbf{r}) d\mathbf{r} = \int \rho_0(\mathbf{r}) \, V(\mathbf{r}) \, d\mathbf{r} \tag{2.66c}$$

$$= \langle V_{ne}[\rho_0] \rangle, \tag{2.66d}$$

where $V(\mathbf{r})$ represents the nuclear attraction potential acting on an electron, any electron, at a point given by the position vector $\mathbf{r}$, and the final result of eq. (2.66) is *the only explicitly known functional* ($\langle V_{ne}[\rho_0] \rangle$) that appears in eq. (2.64). The two other functionals in eq. (2.64) are unknown.

If we now include the explicit form of the only known functional (of the nuclear–electronic potential energy) into eq. (2.64) followed by combining the remaining two other unknown functionals into one functional ($F[\rho_0]$), we get:

$$E_0[\rho_0] = \int \rho_0(\mathbf{r})\ V(\mathbf{r})\ d\mathbf{r} + \langle T_e[\rho_0]\rangle + \langle V_{ee}[\rho_0]\rangle \tag{2.67a}$$

$$= \int \rho_0(\mathbf{r})\ V(\mathbf{r})\ d\mathbf{r} + F[\rho_0], \tag{2.67b}$$

where

$$F[\rho_0] \equiv \langle T_e[\rho_0]\rangle + \langle V_{ee}[\rho_0]\rangle. \tag{2.68}$$

This result, eq. (2.68), is not actionable because it contains the unknown functional $F[\rho_0]$.

A second Hohenberg and Kohn theorem (HK-2 theorem) states that the true ground-state density is the one that minimizes the energy [36]:

$$E_0[\rho_{\text{trial}}] \geq E_0[\rho_0]. \tag{2.69}$$

We would have, hence, a variational theorem that affords a clear path in search for an optimal ground-state electron density. The computational implementation of the HK-2 theorem has been introduced in a 1965 paper by Kohn and Sham (KS) [37]. This DFT variational theorem holds only if the exact energy functional $F[\rho_0]$ is known, in which case one could start with an approximate density and iterate variationally to improve it by lowering the energy. The exact functional is, however, unknown and is approximated by the plethora of existing functionals in the literature [2, 34, 35, 38, 39]. For any approximation to $F[\rho_0]$, the method is nonvariational and one may obtain energies that are lower than the true ground-state energy, unlike in the (post) Hartree-Fock methods where the true ground state energy is a lower bound to the energy.

In DFT, one examines a fictitious noninteracting (NI) N-electron system that defines an electron density ρ_{NI} which is identical to the exact fully interacting real system ρ_0. The NI fictitious system of electrons is governed by $\hat{H}_{\text{NI}}$, a Hamiltonian operator consisting of a sum of one-electron KS Hamiltonians $\hat{h}_i^{\text{KS}}$:

$$\hat{H}_{\text{NI}} = \sum_{i=1}^{N} \left[-\frac{1}{2}\nabla_i^2 + V_{\text{NI}}(\mathbf{r}_i) \right] \equiv \sum_{i=1}^{N} \hat{h}_i^{\text{KS}}. \tag{2.70}$$

where the one-electron NI Hamiltonian is defined as follows:

$$\hat{h}^{\text{KS}} \equiv -\frac{1}{2}\nabla^2 + V_{\text{NI}}(\mathbf{r}). \tag{2.71}$$

The ground-state wave function describing a system of NI electrons (fermions) can be exactly written as a Slater determinant (eq. (2.22)) constructed from occupied KS

spin orbitals u_i^{KS}. The spatial parts of these KS orbitals, θ_i^{KS}, are eigenfunctions of $\hat{h}^{\mathrm{KS}}$, that is:

$$\hat{h}^{\mathrm{KS}}\theta_i^{\mathrm{KS}} = \varepsilon_i^{\mathrm{KS}}\theta_i^{\mathrm{KS}}, \tag{2.72}$$

where $\varepsilon_i^{\mathrm{KS}}$ are known as the KS orbital energies, and eq. (2.72) are the KS equation.

The following substitutions are now introduced to render eq. (2.64) calculable:

$$\langle \Delta T[\rho] \rangle \equiv \langle T[\rho] \rangle - \langle T_{\mathrm{NI}}[\rho] \rangle, \tag{2.73}$$

and

$$\langle \Delta V_{\mathrm{ee}}[\rho] \rangle \equiv \langle V_{\mathrm{ee}}[\rho] \rangle - \frac{1}{2}\int\int \frac{\rho(\mathbf{r}_1)\rho(\mathbf{r}_2)}{r_{12}} d\mathbf{r}_1 d\mathbf{r}_2, \tag{2.74}$$

where the naught has been dropped from the symbol of the ground-state electron density, the difference between the expectation value of the kinetic energy of the real and the NI system is $\langle \Delta T[\rho] \rangle$, and the separation between $\mathbf{r}_1$ and $\mathbf{r}_2$ is r_{12}. In eq. (2.74), the double integral on the right-hand side is the Hartree potential giving the classical energy of repulsion between two charge clouds, while $\langle V_{\mathrm{ee}}[\rho] \rangle$ is the average energy of repulsion in the real interacting density. The Hartree potential represents the *average* electrostatic repulsion between the electrons in a classical system that neither exhibits Coulombic correlation nor exchange-symmetry correlation. Finally, $\langle \Delta V_{\mathrm{ee}}[\rho] \rangle$ is the potential energy portion to the correlation energy. The factor (½) in front of the Hartree potential ensures counting every interaction only once.

Now as we have all the explicitly known terms well-defined, the two unknown functionals, $\langle \Delta T[\rho] \rangle$ and $\langle \Delta V_{\mathrm{ee}}[\rho] \rangle$, are collected into the so-called *exchange–correlation functional*, defined as

$$E_{\mathrm{xc}}[\rho] \equiv \langle \Delta T[\rho] \rangle + \langle \Delta V_{\mathrm{ee}}[\rho] \rangle. \tag{2.75}$$

From eqs. (2.73)–(2.75), and (2.67) and (2.68), one can write:

$$E_0[\rho] = \int \rho(\mathbf{r})\ V(\mathbf{r})\ d\mathbf{r} + \langle T_{\mathrm{NI}}[\rho] \rangle + \frac{1}{2}\int\int \frac{\rho(\mathbf{r}_1)\rho(\mathbf{r}_2)}{r_{12}} d\mathbf{r}_1 d\mathbf{r}_2 + E_{\mathrm{xc}}[\rho], \tag{2.76}$$

which upon substitution of the explicit forms of the operators and quantum mechanical averaging yields:

$$\begin{aligned} E_0 = &- \sum_{A=1}^{M} Z_A \int \frac{\rho(\mathbf{r}_1)}{r_{1A}} d\mathbf{r}_1 - 2\sum_{i=1}^{N/2} \langle \theta_i^{\mathrm{KS}}(1) \,|\, \frac{1}{2}\nabla_1^2 | \theta_i^{\mathrm{KS}}(1) \rangle \\ &+ \frac{1}{2}\int\int \frac{\rho(\mathbf{r}_1)\rho(\mathbf{r}_2)}{r_{12}} d\mathbf{r}_1 d\mathbf{r}_2 + E_{\mathrm{xc}}[\rho(\mathbf{r})], \end{aligned} \tag{2.77}$$

where the "(1)" in $\theta_i^{\mathrm{KS}}(1)$ as well as the subscripted "1" in ∇_1^2 refer to electron 1, any single electron in the system. This leaves KS orbitals (θ_i^{KS}) and the exchange–correlation functional as the remaining unknowns to be determined.

The electron density of the ground state can be expressed in terms of the KS orbitals, again for a closed-shell system where all space orbitals are doubly occupied, as follows:

$$\rho = 2\sum_{i=1}^{N/2} \left|\theta_i^{\mathrm{KS}}\right|^2, \tag{2.78}$$

the integration of which satisfies the normalization condition:

$$\int \rho(\mathbf{r})\, d\mathbf{r} = N. \tag{2.79}$$

The minimization of the energy expression (eq. (2.77)) subject to the normalization constraint, along with imposing the constraints of orthonormality on KS orbitals, is achieved by the Lagrange undetermined multiplier technique. This yields a set of Fock-like one-electron, but *local*, equations known as KS equations [30]:

$$\left[-\frac{1}{2}\nabla_1^2 - \sum_{A=1}^{M}\frac{Z_A}{r_{1A}} + \int\frac{\rho(\mathbf{r}_2)}{r_{12}}d\mathbf{r}_2 + v_{\mathrm{xc}}(1)\right]\theta_i^{\mathrm{KS}}(1) = \varepsilon_i^{\mathrm{KS}}\theta_i^{\mathrm{KS}}(1), \tag{2.80}$$

where the effective (one-electron) KS Hamiltonian, the lead square bracket ($\hat{h}^{\mathrm{KS}}$), includes an "*exchange–correlation potential*," $v_{\mathrm{xc}}(\mathbf{r})$. The KS equations, eq. (2.80), can be written in a short-hand form as in eq. (2.72) above.

The exchange–correlation potential in the KS equations is taken as the functional derivative of the exchange–correlation energy E_{xc}:

$$v_{\mathrm{xc}}(\mathbf{r}) = \frac{\delta E_{\mathrm{xc}}[\rho(\mathbf{r})]}{\delta\rho(\mathbf{r})}. \tag{2.81}$$

Given an explicit form of functional $E_{\mathrm{xc}}[\rho(\mathbf{r})]$, the exchange–correlation potential is obtained (eq. (2.81)) which, when inserted into the KS equations, would be what is needed for an iterative solution. The functional is, however, unknown and remains one of the principal frontier problems of modern DFT.

While formally and superficially similar, Hartree–Fock and KS theories differ in significant ways. First, and as emphasized already, the $\hat{h}^{\mathrm{KS}}$ is a *local operator*, as can be seen from eqs. (2.71) and (2.80) since the result of its operation on a function depends on that function's value only at the point of evaluation. Further, Coulombic correlation, unaccounted for in Hartree–Fock theory, is accounted for by $\hat{h}^{\mathrm{KS}}$ via v_{xc}. Hartree–Fock theory, on the other hand, incorporates exchange (Fermi) correlation between same-spin electrons (eq. (2.34)) but ignores Coulombic correlation between all electrons. Finally, the exchange and correlation contributions to the energy, both quantum mechanical in nature, are merged into E_{xc}. KS exchange–correlation energy implicitly incorporates also a kinetic energy contribution to the correlation. At the present, the exchange–correlation potential is only known approximately.

The quality of a DFT calculation rests in large part on how well the exchange–correlation functional is approximated. An exact v_{xc} would deliver the exact fully correlated ground-state electron density, but this requires knowing the exact E_{xc}. There appears to be no systematic way to approach the exact E_{xc}. In practice, empiricism is adopted through comparison of the results obtained from educated guesses at the form of E_{xc} with experimentally known thermodynamic, kinetic, and geometric results.

An approximation to the form of $E_{xc}[\rho(\mathbf{r})]$ functional is the so-called *local density approximation* (LDA) [37]:

$$E_{xc}^{LDA}[\rho(\mathbf{r})] = \int \rho(\mathbf{r})\ \varepsilon_{xc}[\rho(\mathbf{r})]\ d\mathbf{r}. \tag{2.82}$$

The symbol ε_{xc} stands for the sum of the exchange and correlation energies per electron in a uniform electron gas that has the same electron density, locally, as the density of interest. This approximation assumes that the electron density in the system of interest changes slowly with position and hence does not depend on the gradient of the electron density. The assumption of slow-changing density renders LDA generally inaccurate when it exhibits large gradients as typically encountered in molecular calculations.

A more accurate class of approximations than LDA constitute what is known as "*gradient corrected*" functionals. These functionals are developed within the scheme commonly known as the "*generalized gradient approximation*" or GGA. The GGA includes terms that depend explicitly on the gradient of the electron density of each spin:

$$E_{xc}^{GGA}[\rho^{\alpha}(\mathbf{r}),\rho^{\beta}(\mathbf{r})] = \int f\left(\rho^{\alpha}(\mathbf{r}),\rho^{\beta}(\mathbf{r}),\nabla\rho^{\alpha}(\mathbf{r}),\nabla\rho^{\beta}(\mathbf{r})\right)d\mathbf{r}, \tag{2.83}$$

where the energy functional is partitioned into separate exchange and correlation contributions:

$$E_{xc}^{GGA} = E_{x}^{GGA} + E_{c}^{GGA}, \tag{2.84}$$

and each of the two contributions is modeled independently.

According to this scheme, one can mix any desired exchange functional with any correlation functional. An example of this mixing is that of Becke 1988 exchange functional with Lee–Yang–Parr correlation functional denoted as BLYP [40]. Finally, a *hybrid functional* is one in which the proportions of exchange functional and correlation functional in the mix are empirically adjusted to fit experimental data such as atomization energies. A well-known and popular hybrid functional is B3LYP [40–42].

A Hartree–Fock SCF calculation requires an initial guess of the orbitals because they are used to construct the Fock operator; hence, this problem must be solved

iteratively. Not dissimilarly, the operator in the KS equations (eq. (2.80)) is constructed using the very unknown to be sought, that is, the electron density. Thus, in this case as well, an iterative solution and an initial guess of the electron density is required.

The initial guess of the electron density used to start the iterative solution of the KS equations is often the promolecule. The promolecular density is defined as a superposition of spherical atomic densities centered at the assumed initial positions of the nuclei. To obtain this guess, spherically averaged precalculated atomic densities are placed at their respective initial guessed positions and are allowed to overlap:

$$\rho^{\text{pro}} = \sum_{i=1}^{M} \rho_i, \tag{2.85}$$

where ρ_i is the isolated atomic electron densities and ρ^{pro} is the initial promolecular guessed density.

The promolecular density is then used to obtain E_{xc} from the explicit functional form assumed within the given approximation. The functional derivative of this energy with respect to the density (eq. (2.81)) then delivers an initial guess for v_{xc}. With the promolecular density and the initial v_{xc}, the KS equations can now be constructed since the KS Hamiltonian is fully specified (eq. (2.80)). The iterative procedure starts by delivering the initial set of KS orbitals expressed in terms of the chosen basis set:

$$\theta_i^{\text{KS}} = \sum_{\mu=1}^{b} c_{i\mu}\, \psi_\mu. \tag{2.86}$$

The reader is to note the formal identity of eqs. (2.26) and (2.86). This identity suggests the adoption by DFT of the same solution algorithm, from this point onward, as the one used to solve the Hartree–Fock–Roothaan equations (eqs. (2.36)–(2.39)), hence:

$$\sum_{\mu=1}^{b} c_{i\mu}(h_{\nu\mu}^{\text{KS}} - \varepsilon_i^{\text{KS}} S_{\nu\mu}) = 0, \tag{2.87}$$

where $\nu = 1,\ 2,\ \ldots,\ b$,

$$h_{\nu\mu}^{\text{KS}} \equiv \langle \psi_\nu | \hat{h}^{\text{KS}} | \psi_\mu \rangle, \tag{2.88}$$

and

$$S_{\nu\mu} \equiv \langle \psi_\nu | \psi_\mu \rangle. \tag{2.89}$$

Solving the KS equations using the promolecular density as an initial guess to determine the KS Hamiltonian yields an initial set of KS orbitals. These orbitals are then used to construct an improved electron density which, in turn, is used to

obtain a correspondingly improved KS Hamiltonian, and the process is repeated until convergence.

In closing this section, it is important to note that, while the KS equations deliver orbitals that can be used to form a Slater determinant (eq. (2.22)), this is *not* the "many-electron wave function" of the real interacting system. This determinant is the wave function of the non-interacting (fictitious) system of N-electrons. This, however, does not prevent the "practical" utilization of the Slater determinant made up of KS orbitals. This is justified since occupied KS orbitals usually exhibit shapes that closely resemble Hartree–Fock orbitals [2].

2.9 Level of theory in molecular calculations

A level of theory of an *ab initio* quantum chemical calculation is the conjunction of a type of underlying electronic structure theory and a given basis set. In periodic solid-state calculations, for example those implemented in programs such as VASP (*Vienna Ab initio Simulation Package*), one uses plain-wave basis sets, while in programs such as CRYSTAL or in GAUSSIAN (which is mainly used for isolated molecular system but has also capabilities to run periodic calculations), an atom-centered basis set is used. In software such as ADF (Amsterdam Density Functional), atom-centered Slater basis sets are used.

Since here we are focused primarily on molecular systems, the atom-centered bases will briefly be reviewed along with the notation convention commonly used in quantum chemistry to denote the level of theory of a given calculation with a focus on the popular Pople basis set notation (more comprehensive discussions on basis stets can be found elsewhere [5–8]).

A given level of theory is denoted as follows:

$$\text{Theory}\,//\,\text{Basis Set}\,(1)\,/\,\text{Basis Set}\,(2),$$

or

$$\text{Theory}\,1//\text{Basis Set}\,(1)\,/\,\text{Theory}\,2//\text{Basis Set}\,(2)$$

where "Theory" is the theoretical method such as DFT-B3LYP or Hartree–Fock. Prefix R, U, or RO before the "Theory" designation indicates, respectively, that the calculation is a restricted (all MOs are doubly occupied), unrestricted open-shell where the space parts of MOs for α- and β-electrons are optimized separately (generally used for systems with unpaired electrons), and restricted open-shell where the MOs are obtained as in R calculations except that some levels may be singly occupied as required for open-shell systems. As an example, B3LYP//6-311++G**/6-31+G* indicates a DFT-B3LYP single-point calculation using a 6-311++G** basis set at the geometry optimized with the smaller basis set 6-31+G*. (Lack of prefix usually implies "R").

In denoting atom-centered basis sets, a "G" signifies that Gaussian basis functions are used. Such a basis set has an artificial maximum at the position of the nuclei, which – in the zero-finite size of the atomic nucleus approximation – should exhibit cusps, that is, singularities, rather than true maxima given the singularity of the Coulomb potential in this case. In contrast with Gaussian basis functions, Slater-type orbitals (STOs) exhibit cusps at nuclear positions. STOs have the form $\exp[-(\xi r/a_0)]$, where a_0 is the Bohr radius, r is the distance from the nucleus, and ξ is the orbital exponent. The STOs are computationally expensive in general. The cusp behavior (as well as the long-range behavior) of the electron density exhibited by STOs can be approached using a linear combinations of Gaussian-type orbitals (GTOs). GTOs have the form $\exp\left[-\left(\alpha r^2/{a_0}^2\right)\right]$where α is referred to as the Gaussian exponent of the GTO. GTOs are more expedient computationally than STOs since the product of two Gaussian functions is another Gaussian. This mathematical fact simplifies many-center integrals (e.g., two-center overlap integrals) leading to considerable reduction of computational time compared with the STO counterparts.

Basis sets are denoted with the Pople notation such as n_1-$n_2n_3n_4$++G**. This implies that what comes after the dash and before the pluses (or the G, depending on the case) is a "split valence" basis set. In the given example, the basis set flexibility has been enhanced by augmenting it with diffuse functions (plus signs) and polarization functions (here denoted by the stars). Finally, the lead digit (n_1) is the number of Gaussian primitive functions used to construct the atomic cores in linear combination. A 3-21G basis set, thus, uses three Gaussians to represent the 1*s* orbital. One, in this case, says that the 1*s* basis function is contracted from three primitive Gaussians. Following the dash, the digits $n_2n_3n_4$ denote the particular split of the valence shell. If there are three digits, this means that the valence shell is triply split, while the presence of only two digits as in 3-21G indicates that the valence shell is doubly split. The splitting of the valence basis means that more than one size of contracted functions for each orbital type is used to represent the valence shell.

Let us look at a concrete example in some detail, say the case of the 6-31G basis set. In this case, the core is contracted from six Gaussian primitives. Meanwhile, the valence shell is split into two differently sized basis functions: One with a smaller size is contracted from three primitive Gaussians and an outer larger one consists of a single Gaussian primitive in this example. The basis functions centered on a hydrogen and on a carbon atom are

$$\text{H:}\quad \underbrace{1s}_{3\,\text{GTO}},\ \underbrace{1s'}_{1\,\text{GTO}}$$

$$\text{C:}\quad \underbrace{1s}_{6\,\text{GTO}},\ \underbrace{2s,\ 2p_x,\ 2p_y,\ 2p_z,}_{3\,\text{GTO}}\ \underbrace{2_s{}',\ 2p_x{}',\ 2p_y{}',\ 2p_z{}'}_{1\,\text{GTO}}$$

The splitting of the valence basis functions allows more radial flexibility but does not have any effect on improving the angular flexibility of a given basis set. To also

allow for angular flexibility, the basis set is enlarged by the addition of basis functions with angular momenta that exceed the minimum required for a given atom in its isolated ground state. These added functions are known as "polarization functions" and are indicated by a bracket after the G (or in their simplest cases by stars after the G). A first star refers to polarization function added to non-hydrogen atoms while a second star (or a basis function placed after a comma) indicates that polarization functions were also added to hydrogens. For example, the basis set 6-311G(2*df*,2*p*) indicates that the 6-311G basis set has been augmented with 2*d* functions and 1*f* function on non-hydrogen atoms (before the comma) and with two sets of *p* functions on the hydrogens (after the comma). Since the stars (**) denote one set of *d* function on heavy atoms and one set of *p* functions on hydrogens, this augmentation scheme may equally be denoted by (*d*,*p*), for example, 6-31G** = 6-31G(*d*,*p*).

Anions, hydrogen-bonded systems, π-stacked system, weakly bonded van der Waals complexes, and the like have electron densities that extend further from nuclei than usual. This necessitates the use of augmented basis sets with *s* and *p* basis functions that have particularly larger radial extensions. These "diffuse functions" are indicated by "+" signs immediately before G. A 6-31+G* basis set, for instance, is a 6-31G(*d*) basis set augmented with diffuse function centered on non-hydrogen atoms. Meanwhile, a 6-31++G(*d*) basis set includes diffuse functions on all atoms including the hydrogens (the second plus).

Dunning *et al.* have developed widely the used "correlation-consistent basis sets" [43–46] which have the virtue of converging to the limit of "complete basis set" in *ab initio* calculations that account for Coulombic correlation. The notation for these basis sets start with either "cc-p" meaning "correlation-consistent polarized" or "aug-cc-p" which means "augmented correlation-consistent polarized" basis set. The second part of the designation, VNZ (where N = D, T, Q, S, . . .), implies that the valence is split into double (D), triple (T), quadruple (Q), quintuple (5), sextuple (6), . . ., zeta. The reader is referred to the original papers for an in-depth discussion of these basis functions [43–46].

For large systems, it is more and more common nowadays to use a multilayered approach, whereby the center of interest is treated at the highest level of theory and the surroundings at lower levels. This approach incorporates the effect of the electronic environment in an approximate way with a corresponding payoff in the form of a considerable speeding up of the calculations. A comprehensive review of multilayered approach can be found elsewhere [47].

References

[1] Szabo, A, Ostlund, NS. *Modern Quantum Chemistry: Introduction to Advanced Electronic Structure Theory*. Dover Publications, Inc, New York, (1989).

[2] Levine, IN. *Quantum Chemistry, (Seventh Edition)*. Pearson Prentice Hall, New York, (2014).

[3] Pilar, FL. *Elementary Quantum Chemistry, (Second Edition)*. Dover Publications, New York, (1990).
[4] McWeeny, R, Sutcliffe, BT. *Methods of Molecular Quantum Mechanics*. Academic Press, New York, (1969).
[5] Cook, DB. *Handbook of Computational Quantum Chemistry*. Dover Publications, Inc, Mineola, New York, (2005).
[6] Jensen, F. *Introduction to Computational Chemistry*. John Wiley and Sons, Ltd, New York, NY, (1999).
[7] Springborg, M. *Methods of Electronic-Structure Calculations: From Molecules to Solids*. John Wiley & Sons, Ltd, New York, (2000).
[8] McQuarrie, DA. *Quantum Chemistry (Second Edition)*. University Science Books, Sausalito, California, (2008).
[9] Reiher, M, Wolf, A. *Relativistic Quantum Chemistry: The Fundamental Theory of Molecular Science*. Wiley-VCH, Weinheim, (2009).
[10] Kato, WA. On the eigenfunctions of many-particle systems in quantum mechanics. *Commun. Pure Appl. Math.* 10, 151–177 (1957).
[11] Steiner, E. Charge densities in atoms. *J. Chem. Phys.* 39, 2365–2366 (1963).
[12] Yuan, K-J, Bandrauk, AD. Ultrafast X-ray photoelectron diffraction in triatomic molecules by circularly polarized attosecond light pulses. *Phys. Chem. Chem. Phys. (PCCP)* 22, 325–336 (2020).
[13] Matta, CF, Bandrauk, AD. An introduction to laser-fields effects on chemical reactivity. Chapter 11 in: *Effects of Electric Fields on Structure and Reactivity: New Horizons in Chemistry*; Shaik, S, Stuyver, T (Eds.), Royal Society of Chemistry, London (2021), 394–419.
[14] Born, M, Oppenheimer, R. Zur quantentheorie der moleküle. *Ann. Phys.* 84, 457–484 (1927).
[15] Eyring, H, Polanyi, M. On simple gas reaction. *Z. Physik. Chem. B* 12, 279–311 (1931).
[16] Goli, M, Shahbazian, S. Atoms in molecules: Beyond Born-Oppenheimer paradigm. *Theor. Chem. Acc.* 129, 235–245 (2011).
[17] Pisana, S, Lazzeri, M, Casiraghi, C, Novoselov, KS, Geim, AK, Ferrari, AC, Mauri, F. Breakdown of the adiabatic Born–Oppenheimer approximation in graphene. *Nat. Mater.* 6, 198–201 (2007).
[18] Waluck, J. *Conformational Analysis of Molecules in Excited States*. Wiley-VCH, Inc, New York, (2000).
[19] Smith, VH, Absar, I. Basic concepts of quantum chemistry for electron density studies. *Isr. J. Chem.* 16, 87–102 (1977).
[20] Massimi, M. *Pauli's Exclusion Principle: The Origin and Validation of a Scientific Principle*. Cambridge University Press, Cambridge, UK, (2005).
[21] Margenau, H. *The Nature of Physical Reality: A Philosophy of Modern Physics*. McGraw-Hill Book Company, New York, (1950).
[22] Slater, JC. Note on Hartree's method. *Phys. Rev.* 35, 210–211 (1930).
[23] Feynman, RP, Leighton, RB, Sands, M. *The Feynman Lectures on Physics. (Volume III)*. Addison-Wesley Publishing Co., Inc, Reading, MA, (1964).
[24] Roothaan, CCJ. New developments in molecular orbital theory. *Rev. Mod. Phys.* 23, 69–89 (1951).
[25] Watanabe, N, Kamata, Y, Yamauchi, K, Udagawa, Y. Calculation of X-ray scattering intensities by means of coupled cluster singles and doubles model. *J. Comput. Chem.* 22, 1315–1320 (2001).
[26] Stewart, RF. Total X-ray scattering and two-electron density functions. *Isr. J. Chem.* 16, 111–114 (1977).
[27] Bartel, LS, Gavin, RM, Jr. Effect of electron correlation in X-ray and electron diffraction. *J. Am. Chem. Soc.* 86, 3493–3498 (1964).

[28] Coleman, AJ, Yukalov, VI. *Reduced Density Matrices: Coulson's Challenge*. Springer, Berlin, (2000).
[29] Davidson, ER. *Reduced Density Matrices in Quantum Chemistry*. Academic Press, Inc, New York, (1976).
[30] Parr, RG, Yang, W. *Density-Functional Theory of Atoms and Molecules*. Oxford University Press, Oxford, (1989).
[31] McWeeny, R. The nature of electron correlation in molecules. *Int. J. Quantum Chem.* 1 (Supplement 1), 351–359 (1967).
[32] Löwdin, P-O. Correlation problem in many-electron quantum mechanics I. Review of different approaches and discussion of some current ideas. *Adv. Chem. Phys.* 2, 207–322 (1959).
[33] Brillouin, L. *Les Champs 'self-consistents' de Hartree et de Fock*. Hermann et Cie, Paris, (1934).
[34] Scholl, DS, Steckel, JA. *Density Functional Theory: A Practical Introduction*. Wiley, Hoboken, New Jersey, (2009).
[35] Koch, W, Holthausen, MC. *A Chemist's Guide to Density Functional Theory, (Second Edition)*. Wiley-VCH, New York, (2001).
[36] Hohenberg, P, Kohn, W. Inhomogeneous electron gas. *Phys. Rev. B* 136, 864–871 (1964).
[37] Kohn, W, Sham, LJ. Self consistent equations including exchange and correlation effects. *Phys. Rev. A* 140, 1133–1138 (1965).
[38] Sahni, V. *Quantal Density Functional Theory (Second Edition)*. Springer-Verlag, Berlin, (2016).
[39] Cramer, CJ. *Essentials of Computational Chemistry: Theories and Models*. John Wiley & Sons, Ltd, New York, (2002).
[40] Becke, AD. A new mixing of Hartree-Fock and local density-functional theories. *J. Chem. Phys.* 98, 1372–1377 (1993).
[41] Becke, AD. Density-functional thermochemistry.3. The role of exact exchange. *J. Chem. Phys.* 98, 5648–5652 (1993).
[42] Lee, C, Yang, W, Parr, R. Development of the Colle-Salvetti correlation-energy formula into a functional of the electron-density. *Phys. Rev. B* 37, 785–789 (1988).
[43] Dunning, TH. Gaussian basis sets for use in correlated molecular calculations. I. The atoms boron through neon and hydrogen. *J. Chem. Phys.* 90, 1007–1023 (1989).
[44] Kendall, RA, Dunning, TH, Jr, Harrison, RJ. Electron affinities of the first-row atoms revisited. Systematic basis sets and wave functions. *J. Chem. Phys.* 96, 6796–6806 (1992).
[45] Dunning, TH, Peterson, KA, Wilson, AK. Gaussian basis sets for use in correlated molecular calculations. X. The atoms aluminum through argon revisited. *J. Chem. Phys.* 114, 9244–9253 (2001).
[46] Prascher, B, Woon, D, Peterson, K, Dunning, T, Wilson, A. Gaussian basis sets for use in correlated molecular calculations. VII. Valence, core-valence, and scalar relativistic basis sets for Li, Be, Na, and Mg. *Theoret. Chim. Acta* 128, 69–82 (2011).
[47] Clemente, FR, Vreven, T, Frisch, MJ. Getting the most out of ONIOM: Guidelines and pitfalls. Chapter 2 in: *Quantum Biochemistry: Electronic Structure and Biological Activity (Vol. 1)*; Matta, CF (Ed.), Wiley-VCH, Weinheim (2010), 61–83.

Chapter 3
Quantum crystallography: an introduction

The obvious is that which is never seen until someone expresses it simply. Khalil Gibran (1927) (*Sand and Foam*. William Heinemann, Ltd., Melbourne, (1954)).

N-representability, a concept that is fundamental and defining the nature of quantum crystallography, is defined and discussed. A numerical methodology for the implementation of *N*-representability in connection to extraction of quantum mechanical information from X-ray scattering data is required. This is the purpose for derivation of the Clinton equations. Using theoretical data of Stewart, Davidson, and Simpson, it is shown that an accurate least squares fit to data is not mandated to be *N*-representable, whereas the analogous fit to the same data using the Clinton equations is *N*-representable.

3.1 *N*-representability

The idea of *N*-representability as foundation of what we named quantum crystallography goes back to the laboratory of Professor William Clinton of Georgetown university [1–7]. *N*-representability (Fig. 3.1) had been much discussed [8–16] independently of crystallography. The physical indistinguishability of electrons requires that valid solutions of the Schrödinger equation must be antisymmetric. The definition of quantum mechanically valid reduced density matrices [8] follows from such antisymmetric wave functions Ψ:

$$\rho_p(\mathbf{r}_1 \ldots \mathbf{r}_p \,|\, \mathbf{r}_1' \ldots \mathbf{r}_p') = \frac{N(N-1)\ldots(N-p+1)}{p!} \sum_{\omega} \int \ldots \int \Psi^* \Psi d\mathbf{r}_{p+1} \ldots d\mathbf{r}_N. \tag{3.1}$$

N-representability is the problem of stating those conditions which allow recognition of such functions as can be mapped back to valid wave functions Ψ consistent with eq. (3.1).

The most important density matrices occur for $p = 2$ or $p = 1$, that is, the 2-reduced density matrix and 1-reduced density matrix, because most physical properties are determined by them. They are expressed, respectively as (see Chapter 2):

$$\begin{aligned} \rho_2(\mathbf{r}_1, \mathbf{r}_2 \,|\, \mathbf{r}_1', \mathbf{r}_2') = \frac{N(N-1)}{2} \sum_{\omega} \int \ldots \int \Psi^*(\mathbf{r}_1\omega_1,\ \mathbf{r}_2\omega_2,\ \ldots,\ \mathbf{r}_N\omega_N) \\ \Psi(\mathbf{r}_1'\omega_1,\ \mathbf{r}_2'\omega_2,\ \ldots,\ \mathbf{r}_N\omega_N)\, d\mathbf{r}_3,\ \ldots,\ d\mathbf{r}_N \end{aligned} \tag{3.2}$$

https://doi.org/10.1515/9783110566673-004

and

$$\rho_1(\mathbf{r}_1 \mid \mathbf{r}_1{}') = N \sum_{\omega} \int \ldots \int \Psi^*(\mathbf{r}_1\omega_1, \ldots, \mathbf{r}_N\omega_N)\, \Psi(\mathbf{r}_1'\omega_1, \ldots, \mathbf{r}_N\omega_N)\, d\mathbf{r}_2, \ldots, d\mathbf{r}_N. \quad (3.3)$$

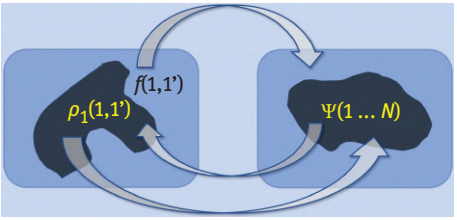

Fig. 3.1: An illustration of the concept of *N*-representability: the map between density matrices and wave functions. Given a wave function, through integration of its modulus squared over of the space coordinates of all particles but one (maintaining the distinction between the coordinates 1 and 1') followed by summation over all spin variables, one obtains the one-particle density matrix $\rho_1(1,1')$. Only these density matrices which are *N*-representable are guaranteed to map back to an antisymmetric wave function Ψ. In general a function *f* of the coordinates of one electron does not map to an antisymmetric wavefunction and therefore is not *N*-representable.

It is helpful to simplify the notation. Hence, the above two expressions are rewritten in a more compact form, where summation over spins is implied:

$$\rho_2(12, 1'2') = \frac{N(N-1)}{2} \int \Psi^* \Psi d3 \ldots dN \quad (3.4)$$

and

$$\rho_1(1, 1') = N \int \Psi^* \Psi d2 \ldots dN. \quad (3.5)$$

A comparison of the corresponding pairs of equations (eqs. (3.2) and (3.4), and (3.3) and (3.5)) gives the new symbols their meaning.

One may notice immediately that the reduced density matrices are simpler than the wave functions from which they derive. Knowledge of *N*-representable density matrices would allow dispensing with the use of the more complicated wave functions. In particular, calculation of the energy using *N*-representable ρ_2 would satisfy the variational principle guaranteeing an upper bound to the exact ground-state energy. In fact, the entire molecular quantum mechanics can be framed in terms of *N*-representable density matrices free of their more complicated corresponding wave functions.

Importantly, the *N*-representability of ρ_1, useful to describe X-ray scattering, is defined by its properties of idempotency, Hermiticity, and normalization. Moreover, ρ_2 is a known functional of ρ_1 in the case of a single determinant [8]. Independent particle models, such as Hartree–Fock and density functional theory, are characterized by their normalized projector density matrix ρ_1 [13]. Gilbert [14] has shown that

every well-behaved density is single determinant *N*-representable. Many numerical examples [17] have shown the plausibility of representing an exact density with a single determinant of realistic molecular orbitals.

A single Slater determinant, which is antisymmetric with respect to the interchange of particles and which represents electron indistinguishability, may be constructed from a set of singly occupied spin orbitals $\{\chi_i\}$ as,

$$\Psi_{\text{det}}(1\ldots N) = \frac{1}{\sqrt{N!}}\begin{vmatrix} \chi_1(1) & \chi_2(1) & \cdots & \chi_N(1) \\ \chi_1(2) & \chi_2(2) & \cdots & \chi_N(2) \\ \vdots & \vdots & & \vdots \\ \chi_1(N) & \chi_2(N) & \cdots & \chi_N(N) \end{vmatrix} \tag{3.6}$$

where

$$\chi_i(1) = \phi_i(\mathbf{r}_1)\sigma_i(\omega_1) = \phi_i(x_1, y_1, z_1)\sigma_i(\omega_1). \tag{3.7}$$

The Slater determinant has already been introduced in Chapter 2 (eq. (2.22)) and is now re-written in a more compact notation adopted here.

The normalization condition imposed on the Slater determinantal wave function introduced above is, in the new notation:

$$\int \Psi^*_{\text{det}}\Psi_{\text{det}}d1\ldots\, dN = 1. \tag{3.8}$$

Expressed in terms of a Slater determinental wave function, the reduced spinless density matrices of arbitrary, second, and first orders are written as follows, respectively:

$$\rho_{N\,\text{det}} = N!\ \Psi^*_{\text{det}}\Psi_{\text{det}} = \begin{vmatrix} \rho_1(1,1') & \cdots & \rho_1(1,N') \\ \vdots & & \vdots \\ \rho_1(N,1') & \cdots & \rho_1(N,N') \end{vmatrix}, \tag{3.9}$$

$$\rho_{2\,\text{det}} = \frac{N(N-1)}{2}\int \Psi^*_{\text{det}}\Psi_{\text{det}}d3\ldots dN = \begin{vmatrix} \rho_1(1,1') & \rho_1(1,2') \\ \rho_1(2,1') & \rho_1(2,2') \end{vmatrix}, \tag{3.10}$$

and

$$\rho_{1\,\text{det}} = N\int \Psi^*_{\text{det}}\Psi_{\text{det}}d2\ldots dN = \rho_1(1,1'), \tag{3.11}$$

where the numerical labels refer to spatial coordinates since the spins have been integrated out.

The conditions necessary and sufficient for *N*-representability of $\rho_{1\,\text{det}}$ are [8]

$$\rho_1^2 = \rho_1, \qquad \int \rho_1 d1 = N, \qquad \rho_1^\dagger = \rho_1, \tag{3.12}$$

that is, the one-body density matrix is idempotent, normalized, and Hermitian.

McWeeny [12] discusses the properties of ρ_1 displaying iterative equations satisfying the conditions given by eq. (3.12), and indicating that idempotency allows ρ_1 to be factored into a sum of squares of orbitals.

The full two-body Hamiltonian, which contains one- and two-body terms, is written in its general form as follows:

$$\hat{H} = \sum \hat{h}_i + \sum \hat{h}_{ij}, \tag{3.13}$$

an example of which is written explicitly in atomic units as

$$\hat{H} \equiv \underbrace{-\frac{1}{2}\sum_{i=1}^{N} \nabla_i^2 - \sum_{i=1}^{N}\sum_{A=1}^{M} \frac{Z_A}{r_{iA}}}_{\text{One-body } (\hat{h}_i)} + \underbrace{\sum_{i=1}^{N}\sum_{j>i}^{N} \frac{1}{r_{ij}}}_{\text{Two-body } (\hat{h}_{ij})}. \tag{3.14}$$

Using such a generalized Hamiltonian, the energy is expressed as

$$E = \int \hat{h}_1 \rho_{1\,\mathrm{det}}(1,1')\Big|_{1'\to 1} d1 + \int \hat{h}_{12} \rho_{2\,\mathrm{det}}(1,2) d1 d2 \geq E_0, \tag{3.15}$$

which satisfies the variational theorem. In eq. (3.15), the Löwdin notation, $\int \hat{h}_1 \rho_{1\,\mathrm{det}}(1,1')\big|_{1'\to 1} d1$ has been adopted, and this implies that the operator operates first on the density matrix coordinate 1′ and then coordinate 1′ is set equal to 1 before integrating.

Clinton's equations [1–7] are a modification of McWeeny's purification to idempotency [12] in order to include constraints such as satisfaction of X-ray scattering, thus,

$$\mathbf{P}_{n+1} = 3\mathbf{P}_n^2 - 2\mathbf{P}_n^3 + \sum\nolimits_k \lambda_k^{(n)} \mathbf{O}_k + \lambda_N^{(n)} \mathbf{1}. \tag{3.16}$$

where $\mathbf{P}$ is the representative of the density matrix in an orthonormal basis $\boldsymbol{\psi}$, n is an index indicating the value obtained at the nth iteration, λ_k is a Lagrangian multiplier to enforce the kth constraint (e.g., constraints to reproduce the X-ray data), λ_N is a Lagrangian multiplier to enforce the normalization constraint, $\mathbf{O}_k$ is the matrix representative of an operator of the kth constraint, and $\mathbf{1}$ is the unit (identity) matrix. The equations of constraint are

$$\langle \hat{\mathbf{O}}_k \rangle = \mathrm{tr}\, \mathbf{P}\mathbf{O}_k, \tag{3.17}$$

and

$$N = \mathrm{tr}\, \mathbf{P}\mathbf{1}. \tag{3.18}$$

The conditions of constraint in such case are

$$F(\mathbf{K}) = \int e^{i\mathbf{K}.\mathbf{r}} \rho(\mathbf{r}) d^3\mathbf{r} \tag{3.19}$$

Where $\mathbf{K} = (2\pi/\lambda)\hat{\mathbf{k}}$ is the wave vector in the direction of the unit vector $\hat{\mathbf{k}}$, and where

$$\rho(\mathbf{r}) = \rho_1(\mathbf{r}, \mathbf{r}')|_{r' \to r}. \tag{3.20}$$

Thus, the satisfaction of the experimental constraint equations allows the extraction of an *N*-representable density matrix from an X-ray scattering experiment. This is the heart of quantum crystallography. The Clinton equations allow this and are discussed next. Applied to the X-ray scattering experiment, the Clinton equations can deliver the"exact" density.

3.2 Derivation of the Clinton equations

We call the representative of ρ_1 in the basis $\boldsymbol{\psi}$ by the name $\mathbf{P}$ so that for the case of doubly occupied orbitals,

$$\rho_1(1, 1') = 2 \,\mathrm{tr}\, \mathbf{P}\boldsymbol{\psi}(1) \otimes \boldsymbol{\psi}^{\dagger}(1'), \tag{3.21}$$

where $\boldsymbol{\psi}$ is a column vector, $\boldsymbol{\psi}^{\dagger}$ is its complex conjugate transpose, and $\otimes$ indicates a direct product.

Following McWeeny's procedure [12], we can purify $\mathbf{P}$ to idempotency by

$$\delta \,\mathrm{tr}\, (\mathbf{P}^2 - \mathbf{P})^2 = 2 \,\mathrm{tr}\, (\mathbf{P}^2 - \mathbf{P})\, \delta(\mathbf{P}^2 - \mathbf{P}) = 0, \tag{3.22}$$

where δ is the symbol for variation.

As the variation in eq. (3.22) is arbitrary, this implies [1]

$$\mathbf{P}^2 - \mathbf{P} = 0. \tag{3.23}$$

To enforce this last property of $\mathbf{P}$, we impose the condition that

$$\delta \mathrm{tr}\, (\mathbf{P}^2 - \mathbf{P})^2 = 2 \,\mathrm{tr}\, (2\mathbf{P}^3 - 3\mathbf{P}^2 + \mathbf{P})\, \delta\mathbf{P} = 0. \tag{3.24}$$

Again, as $\delta\mathbf{P}$ is arbitrary, it must be that

$$2\mathbf{P}^3 - 3\mathbf{P}^2 + \mathbf{P} = 0. \tag{3.25}$$

Rearrangement to solve this last equation iteratively gives us

$$\mathbf{P}_{n+1} = 3\mathbf{P}_n^2 - 2\mathbf{P}_n^3, \tag{3.26}$$

which is the result of McWeeny [12].

Proceeding toward the Clinton equations, we require $\mathbf{P}$ to satisfy the constraints

$$\mathrm{tr}\,\mathbf{P}\mathbf{O}_k = \langle \hat{\mathbf{O}}_k \rangle, \tag{3.27}$$

with $\langle \hat{\mathbf{O}}_k \rangle$ a general expectation value and $\mathbf{O}_k$ the matrix representative of the operator $\hat{\mathbf{O}}_k$. In our case, $\langle \hat{\mathbf{O}}_k \rangle$will be an experimentally derived structure factor.

The requirements of eqs. (3.24) and (3.27) can be imposed by using Lagrangian multipliers $2\lambda_k$. In that way, the problem may be re-formulated as:

$$\delta\,\mathrm{tr}\left[(\mathbf{P}^2 - \mathbf{P})^2 - \sum\nolimits_k 2\lambda_k \mathbf{P}\mathbf{O}_k\right] = 0, \tag{3.28}$$

in which the summation runs over all experimental constraints.

Imposing the variation of $\mathbf{P}$, we have

$$\mathrm{tr}\,(2\mathbf{P}^3 - 3\mathbf{P}^2 + \mathbf{P} - \sum\nolimits_k \lambda_k \mathbf{O}_k)\,\delta\mathbf{P} = 0, \tag{3.29}$$

and recognizing, again, the arbitrariness of $\delta\mathbf{P}$ yields,

$$2\mathbf{P}^3 - 3\mathbf{P}^2 + \mathbf{P} - \sum\nolimits_k \lambda_k \mathbf{O}_k = 0. \tag{3.30}$$

Solving for $\mathbf{P}$ iteratively gives us the Clinton equations (eq. (3.16)), rewritten further with the normalization constraint absorbed within the last summation for conciseness,

$$\mathbf{P}_{n+1} = 3\mathbf{P}_n^2 - 2\mathbf{P}_n^3 + \sum\nolimits_k \lambda_k^{(n)} \mathbf{O}_k. \tag{3.31}$$

The Lagrangian multipliers $\lambda_k^{(n)}$ for the nth iteration are determined from the equations of constraint $\mathrm{tr}\,\mathbf{P}_{n+1}\mathbf{O}_k = \langle \hat{\mathbf{O}}_k \rangle$ yielding a set of linear equations,

$$\underbrace{\begin{pmatrix} \mathrm{tr}\,\mathbf{O}_1^2 & \cdots & \mathrm{tr}\,\mathbf{O}_1\mathbf{O}_k \\ \vdots & & \vdots \\ \mathrm{tr}\,\mathbf{O}_k\mathbf{O}_1 & \cdots & \mathrm{tr}\,\mathbf{O}_k^2 \end{pmatrix}}_{\boldsymbol{\tau}} \underbrace{\begin{pmatrix} \lambda_1^{(n)} \\ \vdots \\ \lambda_k^{(n)} \end{pmatrix}}_{\boldsymbol{\lambda}^{(n)}} = \underbrace{\begin{pmatrix} \langle \hat{\mathbf{O}}_1 \rangle - \mathrm{tr}\,(3\mathbf{P}_n^2 - 2\mathbf{P}_n^3)\mathbf{O}_1 \\ \vdots \\ \langle \hat{\mathbf{O}}_k \rangle - \mathrm{tr}\,(3\mathbf{P}_n^2 - 2\mathbf{P}_n^3)\mathbf{O}_k \end{pmatrix}}_{\boldsymbol{\Delta}^{(n)}}. \tag{3.32}$$

The appearance of these last equations is simplified if we define the matrix of traces on the left as $\boldsymbol{\tau}$ and the column matrix from the right side as $\boldsymbol{\Delta}^{(n)}$, obtaining

$$\boldsymbol{\lambda}^{(n)} = \boldsymbol{\tau}^{-1}\boldsymbol{\Delta}^{(n)}. \tag{3.33}$$

The importance of the Clinton equations is that they define a density matrix $\mathbf{P}$ which is guaranteed to be both N-representable and satisfying equations of constraint, for example, X-ray scattering and normalization constraints.

Given the form of the Clinton equations which deliver projector matrices $\mathbf{P}$, a question arises regarding how many constraints are required to fix the elements of $\mathbf{P}$. With too few constraints, there will occur an infinite number of projectors which satisfy these constraints. To calculate the number of independent complex elements in a projector, one may recall that it may be factored into its orbital LCAO coefficients

$\mathbf{P} = \mathbf{C}^{\dagger}\mathbf{C}$. The matrix $\mathbf{C}$ is of dimension $m \times N$ (where m is the number of basis functions and N is the number of molecular orbitals) and $\mathbf{C}^{\dagger}\mathbf{C} = \mathbf{1}_N$.

The number of elements in $\mathbf{C}$ defining the orbitals is [18,19]

$$\kappa(m, N) = m \times N - N^2 = N(m - N), \tag{3.34}$$

which accounts for the number of elements defining the N orbitals reduced by the number of their normalization and orthogonality requirements [1]. A detailed and clarifying exposition of all considerations that have been proposed relating to the number of constraints needed to fix the elements of the density matrix has been led by Arnaud Soirat [18,19]. The previous equation implies that $\kappa(m,N)$ X-ray density constraints will determine the projector matrix consistent with that density *via* the Clinton equations. One obtains thereby from the X-ray scattering data, an N-representable one-body density matrix, its corresponding electron density, and molecular orbitals.

A simple example from the literature [3] illustrates the importance of N-representability, which is always guaranteed by using the Clinton equations to satisfy X-ray scattering constraints. Stewart, Davidson, and Simpson (SDS) [20] present a sum of two spherical atomic densities as a best fit to the electron density of H_2 obtained from highly accurate wave functions calculated by Kolos–Roothaan [21,22]. Using a basis of 1*s* and 2*s* orbitals, one may represent the electron density matrix in the usual way as in eq. (3.21). The $\mathbf{P}$ matrix in eq. (3.21) was fit by a least squares procedure to the density of SDS in two different ways: either imposing idempotency, $\mathbf{P}_{\text{Idem.}}$, or not, $\mathbf{P}_{\text{Not Idem.}}$ The results are listed in Tab 3.1.

Tab. 3.1: Eigenvalues N_1 and N_2 of $\mathbf{P}_{\text{Not Idem.}}$ and $\mathbf{P}_{\text{Idem.}}$, respectively, for various values of basis orbital exponents, ξ (after Ref. [3]).

	$\mathbf{P}_{\text{Not Idem.}}$		$\mathbf{P}_{\text{Idem.}}$	
ξ	N_1	N_2	N_1	N_2
0.98	1.0935	−0.0935	1.0000	0.0000
1.00	1.0407	−0.0407	1.0000	0.0000
1.02	1.0063	−0.0063	1.0000	0.0000
1.04	0.9909	0.0090	1.0000	0.0000

Table 3.1 lists the changes of the eigenvalues of the density matrix as a function of changes in the basis orbitals' exponent (ξ). What results is as follows. The idempotent matrices (projectors) have the constant eigenvalues of 1 and 0. But the non-idempotent matrices have varying eigenvalues, and in every case the values lie outside the strict Coleman requirement that for N-representability to be possible they must lie in the range bounded by 1 and 0. It can be concluded from this example that a least squares fit to X-ray data is *insufficient* to ensure N-representability of a density matrix. Of

course, any quantum mechanical density matrix is valid only on condition of its *N*-representability, and that is guaranteed by the projector property of **P**.

3.3 Conclusion

Because electrons are physically indistinguishable fermions, the *N*-particle wave function which represents them must be antisymmetric with respect to the interchange of spin and spatial coordinates of any pair of electrons in the system. Slater's determinant representation of the orbitals implements automatically the Pauli principle through the properties of determinants, that is, the interchange of any pair of rows or columns changes the sign of the determinant and the presence of any two equal rows or columns result in that the determinant vanishes.

For each single-determinant of doubly-occupied orbitals there exists a corresponding set of one- and two-electron density matrices as emphasized in Chapter 2. The existence of a mapping between the density matrices mathematical space and that of antisymmetric wave functions is termed "*N*-representability". In other words, not every mathematical function of the same variables as those of the reduced density matrices can be derived from an antisymmetric wave function, and the subset that *does* includes what are referred to as *N*-representable density matrices.

Within the single determinant approximation, the one-electron density matrix, which is a projector, contains the information that needs to be extracted from the wave function. Crystallographic X-ray scattering data may be used to define the elements of such a one-electron density matrix. The mathematical procedure to fit the projector density matrix to the experimental data is that expressed by the Clinton matrix equations. Here they have been derived and used to show that their numerical solutions are indeed *N*-representable. The energy calculated from such density matrices obey the variational principle.

References

[1] Clinton, WL, Galli, AJ, Massa, LJ. Direct determination of pure-state density matrices. II. Construction of constrained idempotent one-body densities. *Phys. Rev.* 177, 7–12 (1969).
[2] Clinton, WL, Galli, AJ, Henderson, GA, Lamers, GB, Massa, LJ, Zarur, J. Direct determination of pure-state matrices. V. Constrained eigenvalue problems. *Phys. Rev.* 177, 27–33 (1969).
[3] Clinton, WL, Massa, LJ. Determination of the electron density matrix from X-ray diffraction data. *Phys. Rev. Lett.* 29, 1363–1366 (1972).
[4] Massa, LJ, Clinton, WL. Antisymmetric wavefunction densities from coherent diffraction data. *Trans. Am. Cryst. Assoc.* 8, 149–153 (1972).
[5] Clinton, WJ, Massa, LJ. The cusp condition: Constraint on the electron density matrix. *Int. J. Quantum Chem.* 6, 519–523 (1972).

[6] Clinton, WL, Frishberg, CA, Massa, LJ, Oldfield, PA. Methods for obtaining an electron-density matrix from X-ray data. *Int. J. Quantum Chem.* 7, 505–514 (1973).
[7] Clinton, WL, Frishberg, CA, Goldberg, MJ, Massa, LJ, Oldfield, PA. Density matrix model for coherent X-ray diffraction: Study of experimental factors related to idempotency. *Int. J. Quantum Chem.* 24, 517–525 (1983).
[8] Löwdin, P-O. Quantum theory of many-particle systems. I. Physical interpretations by means of density matrices, natural spin-orbitals, and convergence problems in the method of configurational interaction. *Phys. Rev.* 97, 1474–1489 (1955).
[9] Mayer, JE. Electron correlation. *Phys. Rev.* 100, 1579–1586 (1955).
[10] Fano, U. Description of states in quantum mechanics by density matrix and operator techniques. *Rev. Mod. Phys.* 29, 74–93 (1957).
[11] Tredgold, RH. Density matrix and the many-body problem. *Phys. Rev.* 105, 1421–1423 (1957).
[12] McWeeny, R. Some recent advances in density matrix theory. *Rev. Mod. Phys.* 32, 335–369 (1960).
[13] Coleman, AJ. Structure of fermion density matrices. *Rev. Mod. Phys.* 35, 668–686 (1963).
[14] Gilbert, TL. Hohenberg-Kohn theorem for nonlocal external potentials. *Phys. Rev. B* 12, 2111–2120 (1975).
[15] Davidson, ER. *Reduced Density Matrices in Quantum Chemistry*. Academic Press, Inc., New York, (1976).
[16] Coleman, AJ, Yukalov, VI. *Reduced Density Matrices: Coulson's Challenge*. Springer, Berlin, (2000).
[17] Frishberg, C, Massa, LJ. Idempotent density matrices for correlated systems from X-ray-diffraction structure factors. *Phys. Rev. B* 24, 7018–7024 (1981).
[18] Soirat, AJA, Massa, L. Number of independent parameters needed to define a projector. *Phys. Rev. B* 50, 3392 (1994).
[19] Soirat, AJA, Massa, L. The number of independent parameters defining a projector: Proof in matrix representation and resolution of previously conflicting arguments. Chapter 8 in: *Electron, Spin and Momentum Densities and Chemical Reactivity*; Mezey, PG, Robertson, BE (Eds.), London (2000), 127–145.
[20] Stewart, RF, Davidson, ER, Simpson, WT. Coherent X-ray scattering for the hydrogen atom in the hydrogen molecule. *J. Chem. Phys.* 42, 3175–3187 (1965).
[21] Kolos, W, Roothaan, CCJ. Correlated orbitals for the ground state of the hydrogen molecule. *Rev. Mod. Phys.* 32, 205–210 (1960).
[22] Kolos, W, Roothaan, CCJ. Accurate electronic wave functions for the H_2 molecule. *Rev. Mod. Phys.* 32, 219–232 (1960).

Chapter 4
Example applications of the Clinton equations

To have applied science we must have science to apply. John C. Polanyi (*ca*. 2003)

(*C. F. Matta, personal verbal communication recalled from memory (2022)*).

At a time when a beryllium crystal experiment of Larsen and Hansen produced the most accurate X-ray diffractometer data in the crystallographic literature, these data were used to test the utility of extracting quantum information from X-ray scattering. The results, a proof of the value of the Clinton equations for imposing *N*-representability upon the fit to X-ray scattering data, appeared in *Phys. Rev. Lett.* in 1985. The experimental electron density closely matched the best available theoretical densities. The structure factor errors were distributed randomly over the entire range of scattering angle, yielding an *R*-factor of small magnitude, $R = 0.0018$.

In a subsequent work the Clinton equations were applied to a typical small organic molecule, that is, maleic anhydride. In this work, X-ray data obtained by Louis Todaro in the Laboratory for Quantum Crystallography at Hunter College (City University of New York) was used to fit a projector density matrix to the scattering structure factors resulting in an *R*-factor of about 1%. Subsequently the computer program XD was used to represent the data with multipoles, which resulted in a chemically pleasing representation of the bonding density and lone pairs, very much in accordance with the previous experience of Philip Coppens alluded to in Chapter 1. But how about large organic molecules? The use of multipoles in the case of maleic anhydride gave rise to the idea that the problem of quantum crystallography for large molecules can be broken into two parts. (1) The classical geometrical structure can be determined with accuracy using multipolar refinement. Then, (2) the quantum electronic structure is obtained using quantum chemical calculations based upon the determined classical structure. In this way the problem of data, too few in numbers to fix the elements of the density matrix for a large molecule, may be overcome.

4.1 First application: the beryllium crystal

Clinton's equations were tested against theoretically simulated X-ray data. Examples of this include H (atomic hydrogen), H_2, N_2, and CH_4 [1]. However, in this section the focus will be on experimentally derived data for a metallic crystal (beryllium) and, in the following section, on a small organic molecule (maleic anhydride).

The first example of the use of the Clinton equations with real experimental data occurs with beryllium crystal data, as reported in [2, 3]. The data used is the highly accurate single crystal diffraction results of Larsen and Hansen [2]. The experimental constraints within the Clinton equations use all the experimental data and yields a small *R*-factor = 0.0018 [3]. The experimental density matrix corresponds to a charge redistribution due to crystal bonding in agreement with Hartree–Fock calculations of Dovesi *et al.* [4] and local density functional DFT calculations by Cohen *et al.* [5].

https://doi.org/10.1515/9783110566673-005

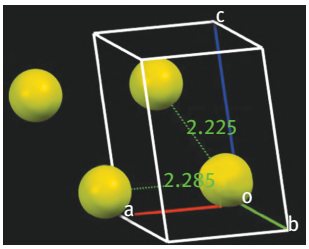

Fig. 4.1: Two adjacent unit cells of metallic beryllium crystal (space group: $P6_3/mmc$), showing two characteristic interatomic distances, with one cell labeled with the conventional crystallographic axes, where $a = b = 2.2853(2)$ Å, $c = 3.5842(3)$ Å, the cell volume = 16.211 Å^3, and $Z = 2$. (The display has been generated with the Mercury Programme using the *crystallographic information file* (cif) deposited by Larsen and Hansen [2]).

Importantly, the experimental density matrix projector $\rho_{1\text{det}}$ allows, within the single determinant approximation, the quantum mechanical calculation of all physical properties (see Chapter 3). This includes such properties that are described by operators that include derivatives of the wave function (or density matrices) such as the kinetic energy or the Compton momentum profile. The significance of this is underlined by noting that such calculations are not obtainable from the density alone, no matter how accurately obtained by methods of classical crystallography. The orbital expansion of $\rho_{1\text{det}}$ gives the electron density matrix in a form representing the components which are responsible for bonding. These ideas are illustrated with an early example of application of quantum crystallography using the X-ray scattering data of Larsen and Hansen – see Fig. 4.1.

The Clinton equations formalism can be applied to X-ray scattering data to extract therefrom an N-representable density matrix $\rho_{1\text{det}}$ and a corresponding Slater determinant characteristic of the molecular density. Here, the Clinton equations are applied to obtain a density matrix and a Slater determinant characteristic of D_3h-hybridized Be atoms placed at experimental lattice positions delivering the electron density of the Be crystal. This is a model of a crystal-field sort representing the crystal but not the Bloch-wave vector-dependent extended system [6].

The population matrix $\mathbf{P}$ has elements determined by a fit to the X-ray scattering factors in a least-squares sense. To ensure N-representability, as mentioned in Chapter 2, it is required that the $\mathbf{P}^2 = \mathbf{P}$, $\mathbf{P} = \mathbf{P}^\dagger$, and tr $\mathbf{P} = N$. The X-ray atomic scattering (form) factor of Be is taken from the *International Tables of Crystallography* [7], but after ridding it from its spherical symmetry in favor of $2\text{tr}\mathbf{Pf}_{\text{Be}}$. The matrix $\mathbf{f}_{\text{Be}}$ is constructed from the Fourier transforms of products of basis functions, each having core and valence parts.

Huzinaga has calculated a Be 1*s* core for the free Be atom [8]. These were adopted in the calculation and held fixed on the assumption that they are unperturbed by the crystal field. A 2*s* orbital augmented with one floating spherical Gaussian orbital were taken to represent the valence shell. (A floating orbital is one whose center is not constrained to be

coinciding with the position of the nucleus.) The valence basis functions were then made orthogonal with respect to the core bases and then constrained to be normalized. A 2×2 density matrix **P** results from these two valence basis functions.

The **P** matrix is determined by imposing normalization and hermiticity, as required for a proper quantum projector, by a least-squares minimization of the *R*-factor with respect to its elements. Thus, experimental parameters include, in addition to the traditional overall X-ray scale factor, the maximum extinction correction, thermal parameters, the elements of the **P** matrix, the position of the floating spherical Gaussian orbital, and the exponent of that Gaussian. The latter three are, thus, added parameters that emerge from the refinement and are responsible for connecting the experiment with the underlying electronic structure theory. In this work, all the experimental scattering data have been used for determination of all of the parameters of the quantum model. The experimental magnitude of these parameters and the technical details can be found in the original report [3].

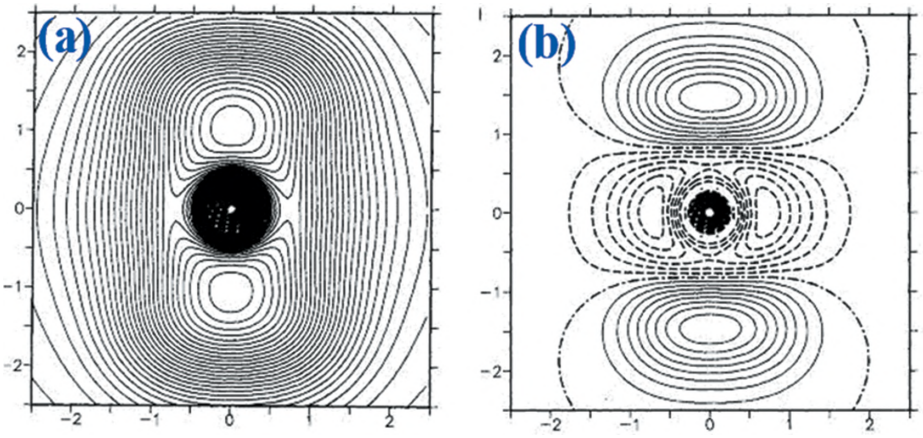

Fig. 4.2: (a) A contour representation of the valence wave function of the Be atom with contours separated by 0.01 $Å^{-3/2}$. (b) The corresponding deformation density with contours separated by 0.01 $e/Å^3$ and where solid and dashed contours represent, respectively, positive and negative values of the deformation density. Both plots are in the crystallographic (110) plane where distances along the *x*- and *y*-axes are in Å units. Reproduced with permission from Ref. [3] © 1985 American Physical Society.

Figure 4.2(a) displays the quantum crystallographic contours of the Be valence orbital in the 110 plane, while Fig. 4.2(b) shows a deformation density on the same plane and for the same field of view. The deformation density is defined as the difference between the quantum crystallographic model and that of a promolecular model. Notice that the quantum model projector matrix allows for the orbitals to be recovered from the X-ray scattering data. Of course, the electron density of the projector **P** cannot be negative since it equals a sum of squares of such orbitals.

Figure 4.2 indicates that the valence orbital peaks at the beryllium nucleus and that the vertical direction in the plot exhibits the expected aspherical aspects of the valence orbital due to the formation of chemical bonding interaction between neighboring Be atoms. Quantum expectation values of the nonspherical atom fragments, within a crystal field approximation, were calculated from their orbitals within a single determinant wave function approximation [3]. Stated differently, given the set of orbitals describing a Be atom in its crystalline environment, all of its expectation values are calculable, in contrast with the density alone. Even an accurate diffraction experiment that delivers the density alone, as is commonly practiced, cannot deliver the entire set of quantum properties of the system. The latter goal is the raison d'être of quantum crystallography developed in this monograph. Consider, for example, the kinetic energy represented by a quantum mechanical operator containing derivatives and, hence, is not simply multiplicative. A general diagonal matrix element representative of this operator, in atomic units (as in all subsequent equations), is:

$$\left\langle \varphi_i(\mathbf{r}) \right| -\frac{1}{2}\nabla^2 \left| \varphi_i(\mathbf{r}) \right\rangle = \int \varphi_i^*(\mathbf{r}) \left(-\frac{1}{2}\nabla^2 \right) \varphi_i(\mathbf{r})\, d^3\mathbf{r} \tag{4.1a}$$

$$= \int \left(-\frac{1}{2}\nabla^2 \right) \left\{ \left[\rho_{1\,\det}(\mathbf{r}, \mathbf{r}') \right]_{ii} \right\} \Big|_{\mathbf{r}\to\mathbf{r}'} d^3\mathbf{r}, \tag{4.1b}$$

written in Löwdin's notation [9] implying the operation of ∇^2 on the primed coordinates, then the primes are eliminated before integration. In contrast, the density $\rho(\mathbf{r})$ alone cannot be used to deliver the expectation value of the kinetic energy operator appearing in in eq. (4.1) above. Only multiplicative operators' expectation values can be evaluated with the electron density alone. Hence, the general form of operators that can be used to extract an expectation value from the density alone is exemplified when it is *multiplied* by the position operator, $\hat{\mathbf{r}} = \mathbf{r}\times$, to obtain the expectation value of the magnitude of the electronic contribution to the dipole moment:

$$\langle \mathbf{r} \rangle = \int \mathbf{r}\rho(\mathbf{r}) d\mathbf{r}. \tag{4.2}$$

From the valence orbital (displayed in Fig. 4.2(a)) and the 1*s* core of the Be atom, the density matrix consistent with the structure factors is determined. This density matrix is then used to calculate expectation values of (*a*) the electron–nuclear attraction energy, (*b*) the average distance of electrons from the nucleus, (*c*) the average squared electron–nuclear distance, and (*d*) the electronic kinetic energy. In atomic units, the calculated expectation values within the crystal contrasted with those calculated for the free Be atom – the latter in brackets, are, respectively [3]:

(a). $$\left\langle -\frac{Z}{r} \right\rangle = -31.6608\ (-33.2340),$$

(b). $\langle r \rangle = 7.8409\ (6.1259),$

(c). $\langle r^2 \rangle = 19.1857\ (17.2820),$

(d). $\left\langle -\frac{1}{2}\nabla^2 \right\rangle = 13.6911\ (14.5720).$

The key point in listing the above experimentally-derived expectation values is to illustrate numerically how quantum crystallography allows one to evaluate the expectation values of nonmultiplicative operators, including, say, the kinetic energy. This is so since this procedure delivers a density matrix, in contrast with traditional diffraction analysis designed to deliver the electron density alone.

These results follow chemical intuition. For example, the electronic cloud stretched into the bonding regions between the Be atoms in the crystal would be expected to have a lesser kinetic energy than their counterpart in the free atom, which is what is observed in point (*d*) above [3]. This appears to be the first *experimental* verification of Ruedenberg's theoretical conclusion that bonding lowers the kinetic energy of the electronic system [10].

The deformation density, Fig. 4.2(b), visualizes the nonsphericity of the Be atom in its crystal environment due to the flow of electronic charge accompanying chemical bonding. Electronic charge is redistributed to impoverish the region near the nucleus of the Be atom (at the center of the plot) in favor of the bonding region at the top and bottom extremities of the plot. The increase in the density accompanying the bond formation along the crystallographic *c*-axis is further reflected in the contraction of the c/a ratio from the ideal value of a perfect hexagonal close packing of spheres to the actual value in this crystal which is 1.568, 3% lower than the ideal value of 1.633 [11].

The deformation density of the crystal can be obtained from the superposition of its composing atomic deformation densities of Be atoms in the crystal field. This superposition has been implemented for a crystal fragment consisting of 125 orthohexagonal unit cells (hexagonal orthorhombic C-centered unit cells) made up of 500 atoms. The resulting deformation map is in close agreement with those determined by Larsen and Hansen [2]. The deformation maps all exhibit a depletion of electron density at the vicinity of the nuclei and octahedral channels while exhibiting a build-up in the tetrahedral hole regions – along which the bonding is directed.

Figure 4.3 displays the quantum crystallographic hybrid model valence-density map in the (x, y, ¼) crystal plane (middle panel). The figure also displays maps obtained from two sets of *ab initio* theoretical calculations: those of Dovesi *et al.* [4] (left panel) and those of Cohen *et al.* [5] (right panel). The first set of calculations, displayed in the left panel of the figure, are obtained at the Hartee–Fock level, while those appearing in the right panel are the result of local density DFT calculations. In the three maps appearing in the figure, the essential features are reproduced across the board. The visual resemblance between the map of Dovesi *et al.* bears

particularly striking resemblance to the quantum crystallographic map. Further, the quantum crystallographic map is in agreement with the experimental deformation map of Larsen and Hansen [2] qualitatively, where there is a perfect mapping of the regions that are depleted and those that are enriched in electron density upon crystal formation [3]. The best quantitative agreement occurs between the quantum crystallographic map and the experimental map of Larsen and Hansen, both of which fall numerically mid-way between the calculated maps of Dovesi *et al.* and Cohen *et al.*

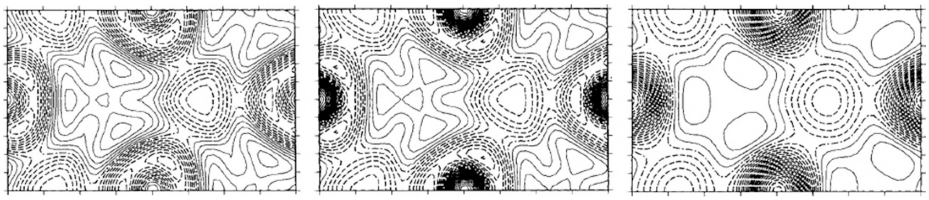

Fig. 4.3: The valence electron density calculated theoretically by (*left*) Dovesi *et al.* [4], (*middle*) the quantum crystallographic map obtained by Massa *et al.* [3], and, finally (*right*) the map calculated by Cohen *et al.* [5]. The adjacent contours differ by 0.01 $e/Å^3$, where solid and dashed contours represent, respectively, positive and negative values of the deformation density. The beryllium nuclei are the darker features with a depleted density, the tetrahedral holes are the features showing positive buildup are the features appearing at the the centroid of the three beryllium nuclei triangle to the left of the plots, and finally the electron-depleted octahedral holes (at the centroid of the three beryllium nuclei triangle to the right of the plots). The three maps are qualitatively consistent in the relative disposition of these features. Reproduced with permission from Ref. [3] © 1985 American Physical Society.

Figure 4.4 is a plot of the relative error (in units of standard deviation σ) in the quantum crystallographic prediction of the structure factors as a function of $(\sin\theta)/\lambda$. An error analysis readily demonstrates that the errors as a function of the scattering angle are normally distributed indicating no systematic error introduced by the model. The weighted *R*-factor (*wR*-factor) using the quantum crystallographic structure factors is 0.0018 with a goodness of fit of 1.33 indicating good agreement with experiment.

The main result of the application of the Clinton equations to the Be data is that it shows that valid quantum mechanical information *can be* extracted from highly accurate X-ray scattering data. This argument is illustrated graphically in Figs. 4.2–4.4. In this case, the quantum model is restricted to a hybrid orbital representation on the Be atom. But the accuracy of the quantum representation is guaranteed by the small magnitude of the *wR*-factor, and by the similarity of its electron density maps to the *ab initio* calculated maps, which are considered to be accurate, and to the experimentally determined maps of Larsen and Hansen.

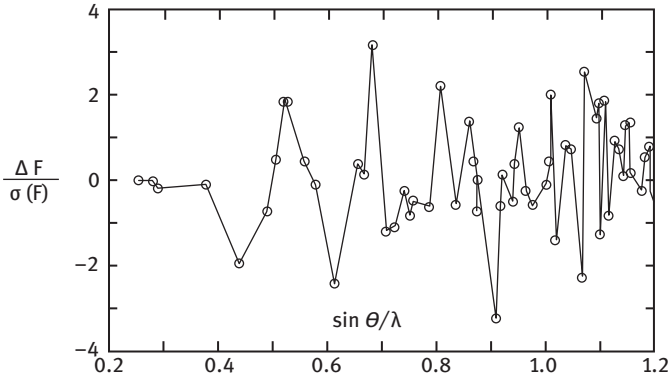

Fig. 4.4: The distribution of errors (in units of standard deviation) in predicted versus experimentally derived structure factors as a function of (sin θ)/λ. The scatter of the errors follows approximately a normal distribution indicating no systematic error inherent in the quantum crystallographic method. Reproduced with permission from Ref. [3] © 1985 American Physical Society.

4.2 Second application: maleic anhydride crystal

In the previous section we have seen how a projector matrix of size 2×2 with two independent matrix elements can be extracted from experimental structure factors and deliver the entire panoply of desired quantum mechanical properties. That was the case of a metallic system, that is, beryllium. In this section we move to a small organic molecule (maleic anhydride) for which the same ideas are extended to a system whereby the projector matrix has, not two independent elements, but 2,250 independent elements. Therefore, it will be of interest to see that the Clinton equations work perfectly well to extract the quantum mechanics from the crystallography scattering data even with so many unknown matrix elements.

The experience to be described here with maleic anhydride [12], and with many others, for example see Refs. [13–17], make clear that the Clinton equations are useful to determine the *N*-representable single-determinant density matrix of small organic molecules. Considerations of this molecule also led to a new idea for how one could approach the problem of large molecules in which inevitably there would exist too few X-ray data to determine all the elements of the *N*-representable single-determinant density matrix for the problem. These considerations are taken up in sequence.

Maleic anhydride (*cis*-butenedioc anhydride, molecular formula: $C_4H_2O_3$) is a widely used chemical in the polymer industry. This molecule has been chosen as a typical small organic molecule with well-formed crystals that can be used as a test case for quantum crystallography. Scheme 4.1 displays the chemical structure of

the maleic anhydride molecule along with the numbering scheme adopted in the crystallographic determination discussed below.

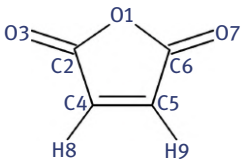

Scheme 4.1: Chemical structural formula of maleic anhydride ($C_4H_2O_3$).

In this discussion, the quantum mechanics associated with the structure of maleic anhydride is extracted from the X-ray scattering data of this crystal which was obtained by Dr. Louis Todaro [18] in 1999 in the Laboratory for Quantum Crystallography at Hunter College [12]. The crystal structure re-determined in 1999 is similar in all respects to the one obtained in 1962 by Marsh *et al.* [19]. Maleic anhydride crystallizes in the space group $P2_1P2_1P2_1$ with four molecules per unit cell (two displays of the unit cell can be seen in Fig. 4.5). The crystal structure of maleic anhydride was solved using a spherical atom model to obtain the atomic coordinates and the thermal parameters [17,18]. The procedure followed to obtain the projector density matrix from the experimental scattering was similar to that discussed earlier in the case of the beryllium crystal (discussed in detail in refs. [12,20]).

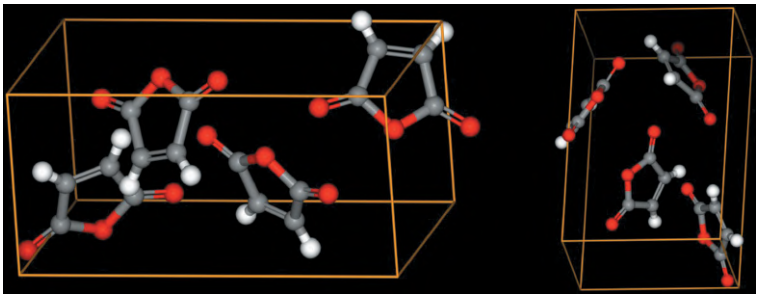

Fig. 4.5: Two views of a ball and stick model of the unit cell of the maleic anhydride crystal. The space group is $P2_1P2_1P2_1$ with $Z = 4$, and $a = 5.322(3)$ Å, $b = 7.009(1)$ Å, and $c = 10.987(1)$ Å [12,18].

Our primary interest in the present discussion concerning maleic anhydride is the question of whether or not the Clinton equations are suitable for determining a large number of projector matrix elements. In other words, are the Clinton equations suitable for the quantum crystallography of organic molecules, in general? Another way of asking this is as follows: Given suitable experimental scattering data for an organic molecule, do the Clinton equations converge and deliver thereby a good quantum crystallographic result?

The procedure of putting the experimental structure factor data into a useful form for Clinton equation application requires several modifications. For the details of these experimental adjustments to the measured structure factors, the reader is referred to the original paper [12]. A summary of these steps is sketched in the flowchart displayed in Fig. 4.6.

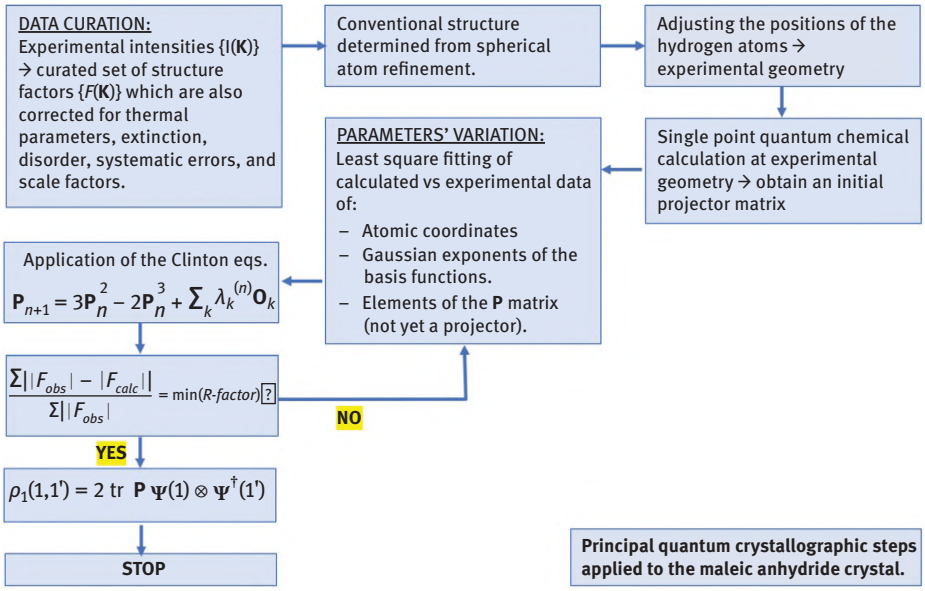

Fig. 4.6: A flowchart describing the principal steps taken in the quantum crystallographic study of maleic anhydride.

The collection of structure factors is corrected for thermal motion and for systematic errors. Subsequently the data is subjected to a minimization of the crystallographic *R*-factor by variation of the parameters affecting the quantum mechanical results. These include the atomic coordinates, exponents of the Gaussian basis functions, and the elements of the density matrix, which is the great concern of the Clinton equations which renders it *N*-representable.

It occurs that in the case of maleic anhydride, the number of curated structure factors (507 symmetry-unique structure factors), when all eight scattering octants are accounted for, is 4,056. Using the cc-pVTZ Gaussian basis set (which stands for correlation-consistent polarized basis set with valence triple zeta split [21]) for the expansion of the density matrix, the number of independent elements to be determined are 2,250. Thus, the ratio of data/unknowns is ~1.8.

As shown in Fig. 4.6, directly-obtained experimentally-derived structure factors are readied for analysis by the parameters' adjustment alluded to above. The procedure is

an iterative one. In this procedure, the variation of the different types of parameters follows one another until self-consistency is reached. In this particular case, it was found convenient to apply a least squares minimization – first – to only the diagonal elements of the projector **P** matrix. Then iterations of the Clinton equations generated the corresponding off-diagonal elements. Importantly, the procedure converged to a minimized *R*-factor. At this point, an experimental *N*-representable quantum crystallographic representation of the electronic structure of the maleic anhydride molecule has been obtained [12]. The best *R*-factor achieved within this study obtained from the quantum crystallographic refinement is $R = 1.14\%$ whereas the best *R*-factor obtained from a simple spherical atom refinement at the same geometry is $R = 3.22\%$.

An additional result of this calculation was that it gave rise to a new idea for an efficient way to treat quantum crystallography of large molecules. Using the program XD [22] we calculated the deformation density of maleic anhydride placing multipoles at the atomic positions obtained from experimental structure factors. The deformation density is displayed in Fig. 4.7. The deformation density suggests that the crystal has rearranged the spherical density of the free atoms so that it flows into the bonding regions between atoms and into the lone pairs of the oxygen atoms. This suggested a solution to the problem which arises in the application of quantum crystallography to biological molecules of large size as measured in numbers of atoms. For such molecules, one can have fewer experimental data than independent elements in the projector matrix **P** to be determined. But the accuracy of multipole representations of the structure, as suggested by the deformation density map (Fig. 4.7), implies that one may break the quantum crystallography problem into two parts: (1) the multipole representation to solve for an accurate structure and (2) a quantum chemical calculation of the density matrix using that structure as input data.

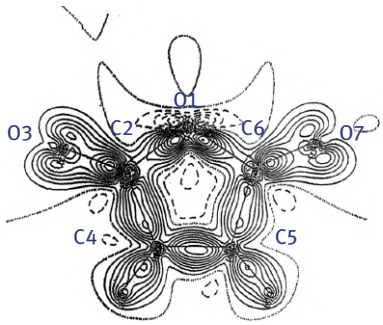

Fig. 4.7: Maleic anhydride's electron density difference map (deformation map). Positive regions (of electron density buildup) are represented by continuous lines, those with electron impoverishment are dashed, and the nodal surface's intersection with the plane of the figure are indicated by dotted lines. Neighboring contours are in steps of 0.1 $e/Å^3$. Adapted with modification with permission from Ref. [12] © 1999 Wiley Periodicals, LLC.

As explicitly stated in the original paper on maleic anhydride [12]: "This experience led us to conclude that the objectives of quantum crystallography could perhaps be best fulfilled [for very large molecules] by using the coordinates obtained from crystal structure determination".

4.3 Conclusion

It is clear from the contrast of the beryllium and the maleic anhydride examples that the number of independent elements grow very fast with the size of the employed basis set. The growth of these independent elements will cross and supersede, at a given point, the number of experimental data-points and hence leads to an under-determined system of equations. In these cases, these results suggest to use the experimentally determined structure as a skeleton upon which the quantum mechanics is to be applied. That is what led to the idea that quantum crystallography, for very large molecules, could be broken into two problems: (1) classical crystallography to determine structure based on multipolar refinement, and (2) the quantum chemical calculation of the density matrices (and hence of all one- and two-particle properties). The adequacy of this approach is judged by the magnitude of the *R*-factor obtained from the comparison of the experimental structure factors with those obtained from the electron density that ensues from the theoretical calculations. In order to perform the quantum chemistry on the envisaged large systems one has to simplify these calculations to avoid the notorious scaling with the size of the calculation. A method that proved capable of achieving soft-scaling with size while preserving accuracy is termed the kernel energy method (KEM) which is the subject of the next chapter.

References

[1] Huang, LS. *X-Ray Orthonormal Orbital Model of Crystallography*, *PhD Thesis*; Graduate Center, City University of New York (CUNY), New York, NY, (1993).
[2] Larsen, FK, Hansen, NK. Diffraction study of the electron density distribution in beryllium metal. *Acta Cryst. B* 40, 169–179 (1984).
[3] Massa, L, Goldberg, M, Frishberg, C, Boehme, R, LaPlaca, S. Wave functions derived by quantum modeling of the electron density from coherent X-Ray diffraction: Beryllium metal. *Phys. Rev. Lett.* 55, 622–625 (1985).
[4] Dovesi, R, Pisani, C, Ricca, F, Roetti, C. *Ab initio* study of metallic beryllium. *Phys. Rev. B* 25, 3731–3739 (1982).
[5] Chou, MY, Lam, PK, Cohen, ML. *Ab initio* study of structural and electronic properties of beryllium. *Phys. Rev. B* 28, 4179–4185 (1983).
[6] Goldberg, MJ, Massa, LJ. Quantum model of coherent X-ray diffraction: Extension to Bloch orbitals. *Int. J. Quantum Chem.* 24, 113–126 (1983).

[7] *International Tables for Crystallography (Vols. A-G), International Union of Crystallography* (http://it.iucr.org/) (2016).
[8] Huzinaga, S. Gaussian-type functions for polyatomic systems. *J. Chem. Phys.* 42, 1293–1302 (1965).
[9] Löwdin, P-O. Quantum theory of many-particle systems. I. Physical interpretations by means of density matrices, natural spin-orbitals, and convergence problems in the method of configurational interaction. *Phys. Rev.* 97, 1474–1489 (1955).
[10] Ruedenberg, K. The physical nature of the chemical bond. *Rev. Mod. Phys.* 34, 326–376 (1962).
[11] Kittel, C. *Introduction to Solid State Physics, (Eighth Edition)*. John Wiley & Sons, Hoboken, NJ, (2005).
[12] Huang, L, Massa, L, Karle, J. Quantum crystallography applied to crystalline maleic anhydride. *Int. J. Quantum Chem.* 73, 439–450 (1999).
[13] Hernández-Trujillo, J, Bader, RFW. Properties of atoms in molecules: Construction of one-density matrix from functional group densities. *J. Chem. Phys.* 115, 10595–10607 (2001).
[14] Snyder, JA, Stevens, ED. A wavefunction and energy of the azide ion in potassium azide obtained by a quantum-mechanically constrained fit to X-ray diffraction data. *Chem. Phys. Lett.* 313, 293–298 (1999).
[15] Howard, ST, Huke, JP, Mallinson, PR, Frampton, CS. Density-matrix refinement for molecular crystals. *Phys. Rev. B* 49, 7124–7136 (1994).
[16] Boehme, RF, La Placa, SJ. Empirical molecular hydrogen wave function modeled from theoretically derived X-ray diffraction data. *Phys. Rev. Lett.* 59, 985–987 (1987).
[17] Henderson, GA, Zimmerman, RK, Jr. One electron properties as variational parameters. *J. Chem. Phys.* 65, 619–622 (1976).
[18] Todaro, L. *Private communication* (1999).
[19] Marsh, RE, Ubell, E, Wilcox, HE. The crystal structure of maleic anhydride. *Acta Cryst.* 15, 35–41 (1962).
[20] Huang, L, Massa, L, Karle, J. Quantum kernels and quantum crystallography: Applications to biochemistry. Chapter 1 in: *Quantum Biochemistry: Electronic Structure and Biological Activity (Vol. 1)*; Matta, CF (Ed.), Wiley-VCH, Weinheim (2010), 3–60.
[21] Dunning, TH. Gaussian basis sets for use in correlated molecular calculations. I. The atoms boron through neon and hydrogen. *J. Chem. Phys.* 90, 1007–1023 (1989).
[22] Koritsanszky, TS, Howard, S, Macchi, P, Gatti, C, Farrugia, LJ, Mallinson, PR, Volkov, A, Su, Z, Richter, T, Hansen, NK, XD (version 4.10, July 2003) (Free University of Berlin, Germany; University of Wales, Cardiff, U.K.; Universita di Milano, U.K.; CNR-ISTM, Milano, U.K.; University of Glasgow, U.K.; State University of New York, Buffalo, U.S.A.; University of Nancy, France, 2003).

Chapter 5
The kernel energy method: a computational approach to large systems

From what has already been demonstrated, you can plainly see the impossibility of increasing the size of structures to vast dimensions either in art or in nature; likewise the impossibility of building ships, palaces, or temples of enormous size in such a way that their oars, yards, beams, iron bolts, and, in short, all their other parts will hold together; nor can nature produce trees of extraordinary size because the branches would break down under their own weight, so also it would be impossible to build up the bony structures of men, horses, or other animals so as to hold together and perform their normal functions if these animals were to be increased enormously in height; for this increase in height can be accomplished only by employing a material which is harder and stronger than usual, or by enlarging the size of the bones, thus changing their shape until the form and appearance of the animals suggest a monstrosity. This is perhaps what our wise Poet had in mind, when he says, in describing a huge giant:

Impossible it is to reckon his height
So beyond measure is his size
Galileo Galilei (b. 1564 – d. 1642)

(*Quoted through: J. B. S. Haldane, in: The World of Mathematics, Vol 2 – J. R. Newman (Ed.), Simon & Schuster, New York 1956, p. 952*).

This chapter briefly reviews a workaround the computational size bottleneck of *ab initio* computational methods. This solution is in fragmenting the system in single and double kernel fragments, possibly capped with hydrogen atoms when necessary if covalent bonds are severed in the fragmentation, followed by the reconstruction of the full system from these fragments. The method reviewed is termed the "kernel energy method" with an emphasis on its theoretical foundations in physics. The temporal scaling of CPU utilization compared to direct calculation is explored and shown to decrease dramatically with molecular size and with the scaling coefficient of the electronic structure method (the model chemistry) itself.

5.1 The computational scaling bottleneck of quantum calculations

In this chapter, we are concerned with molecular calculations and no attempt will be made to discuss periodic systems. This emphasis is so since most of the examples we

Note: This chapter is reproduced with modification and adaptation with permission from: Massa, L., Fahimi, P., Castanedo, L. A. M., Matta, C. F. (2023) "In silico approaches and challenges for quantum chemical calculations on macromolecules", Chapter 6 in: In-silico *Approaches to Macromolecular Chemistry*, Thomas, J., Thomas, S.; Kornweitz, H., Thomas, M. (Eds.), Elsevier, The Netherlands (pp. 185–197).

https://doi.org/10.1515/9783110566673-006

will explore in the next chapter (Chapter 6) are on calculations performed on isolated molecules such as peptides, proteins, and nucleic acids.

In this context, large molecular size is a well-known limitation when it comes to performing quantum chemical calculations especially at the *ab initio* (non-semiempirical) level. The cost of solving the molecular Schrödinger equation increases fast with the number of atoms or basis functions. The approximate scaling of calculation with N (the number of atoms) is N^4 for single determinant methods such as Hartree–Fock or density functional theory calculations, N^5 for second-order perturbational approaches such as Møller–Plesset (MP2) which reaches N^7 if this approximation is taken to the fourth order (MP4), N^6 for configuration interaction (CI) involving single and double excitations, *etc*. This long-standing scaling problem has numerous solutions, one of which will be briefly reviewed in this chapter, a solution that is particularly tuned to biological macromolecules.

5.2 The KEM method as a solution to the computational scaling bottleneck

There are several approaches described in the literature to bypass the above-mentioned computational bottleneck [1–46], a review of which is beyond the scope of this chapter. Instead, this chapter is focused on a method developed by the authors and Jerome Karle (Chemistry Nobel Laureate, 1985) and which is termed the kernel energy method (KEM). The method has been shown to deliver excellent approximations for many properties of large systems in record times. A built-in advantage of KEM is the availability of a clear pathway to constrain it to be N-representable to deliver variational energies as we shall see later in this chapter.

KEM shares the philosophy of splitting a large system into manageable parts with several other methods, but differs from these methods in significant ways. The driving concept is to reassemble the small fragments to reconstruct the large target system. The divide and conquer approach [1–3], the fragment molecular orbitals approach [4, 5], and the adjustable density matrix assembler [31] are of particular note. A difference with the previously mentioned methods is that, in KEM, use is made of hydrogen atoms to saturate dangling bonds that result from the splitting of the large target system, and N-representability is imposed.

5.3 The lead-up to the KEM formalism

The electron density obtained from a quantum mechanical calculation can be obtained from the antisymmetrized many electron wave fuction, $\Psi(\mathbf{x}_1, \ldots, \mathbf{x}_N)$, as usual:

$$\rho(\mathbf{r}) = N \sum_{\omega} \int \ldots \int \Psi^*(\mathbf{x}_1, \ldots, \mathbf{x}_N)\, \Psi(\mathbf{x}_1, \ldots, \mathbf{x}_N)\, d\mathbf{x}_2, \ldots, d\mathbf{x}_N, \tag{5.1}$$

where

$$\mathbf{x}_i \equiv (x_i, y_i, z_i, \omega_i), \tag{5.2}$$

is the set of space coordinates (x_i, y_i, z_i) and spin coordinate ω_i of electron i. In eq. (5.1) the star refers to complex conjugation as customary.[1]

An operational expression of eq. (5.1) in terms of the (squared) doubly occupied MOs (ϕ_j), assuming a closed-shell system of electrons, and assuming – for simplicity – a single determinant many electron wave fuction, is written:

$$\rho(\mathbf{r}) = N \int d\tau'\, \Psi^*_{\text{det}} \Psi_{\text{det}}, \tag{5.3}$$

where $\int d\tau'$ denotes the mode of integration explicitly shown in eq. (5.1), that is, the integration over the space coordinates of all electrons but one followed by summation over spins. The density can be expressed in terms of the MOs as:

$$\rho(\mathbf{r}) = 2 \sum_{j=1}^{N/2} \phi_j^* \phi_j, \tag{5.4}$$

which in terms of atomic orbitals (atomic-centered basis functions) becomes:

$$\rho(\mathbf{r}) = 2 \sum_{\nu=1}^{b} \sum_{\mu=1}^{b} \sum_{j=1}^{N/2} c_{\nu j} c_{\mu j} \chi_\nu^* \chi_\mu \tag{5.5}$$

$$= 2 \sum_{\nu=1}^{b} \sum_{\mu=1}^{b} R_{\nu\mu} \chi_\nu^* \chi_\mu. \tag{5.6}$$

In eq. (5.6), the elements of the *density matrix* (**P**) are expressed as:

$$R_{\nu\mu} \equiv \sum_{j=1}^{N/2} c_{\nu j} c_{\mu j}, \tag{5.7}$$

which in matrix notation, and again in the single determinantal case, is written compactly as a $b \times b$ matrix (b is the number of orthonormal basis functions (the set $\{\chi\}$) composing the basis set of the selected chemical model):

1 **Bold** typeface is reserved to indicate vectors and matrices, a direct (tensor) product is indicated by the symbol $\otimes$, while regular inner or matrix product is understood when two such quantities are written in immediate succession (e.g. **ab**). A star indicates complex conjugation of a generally complex quantity and a superscripted dagger symbol "†" denotes complex conjugate transposition of a vector or a matrix.

$$\mathbf{R} = \mathbf{C}^{\dagger}\mathbf{C}, \tag{5.8}$$

where $\mathbf{C}^{\dagger}$ and $\mathbf{C}$ are, respectively, column and row vectors listing the coefficients of the b basis functions that enter in the expansion of each MO.

There is a basis set transformation which connects the density matrices written in terms of an orthonormal basis $\{\boldsymbol{\psi}\}$ and an atomic orbital basis $\{\boldsymbol{\chi}\}$. This transformation in matrix notation [47]:

$$\boldsymbol{\psi} = \mathbf{S}^{-1/2}\boldsymbol{\chi}, \tag{5.9}$$

where

$$\mathbf{S} = \int \boldsymbol{\chi}^{\dagger} \otimes \boldsymbol{\chi}\, d\mathbf{r}, \tag{5.10}$$

in which $\boldsymbol{\chi}^{\dagger}$is a column whose elements are the original (nonorthonormalized) atomic-centered basis functions.

Given the transformation between basis functions (eq. (5.9)), the corresponding relationship between the density matrix $\mathbf{R}$ written in terms of the $\{\boldsymbol{\chi}\}$ set and $\mathbf{P}$ written in terms of the $\{\boldsymbol{\psi}\}$ set becomes:

$$\mathbf{R} = \mathbf{S}^{-1/2}\mathbf{P}\mathbf{S}^{-1/2}. \tag{5.11}$$

$\mathbf{R}$ is essentially a matrix of the linear combination of atomic orbitals coefficient products which weight the relative importance of atomic basis functions products.

The matrix $\mathbf{P}$ is endowed with what is known as "idempotency", meaning [48]:

$$\mathbf{P}^{n} = \mathbf{P}, \tag{5.12}$$

where $n = 1, 2, 3, \ldots$, of which a particularly important special case is:

$$\mathbf{P}^{2} = \mathbf{P}. \tag{5.13}$$

There is a sort of overbooking of terms in this domain. This is so since the phrase "*density matrix*" which above was used to mean the *matrix of the coefficients* is also used to designate different mathematical objects, namely, 1- and 2-"*reduced density matrices*" (1- and 2-RDMs).

Either the $\mathbf{P}$ or the $\mathbf{R}$ matrix determines the 1-RDM in the basis set to which they correspond. Furthermore, in the single determinant case, the 1-RDM determines the 2-RDM. These two RDMs in terms of the molecular wave function are defined as:

$$\rho_1(\mathbf{r}_1, \mathbf{r}_1{}') = N \sum_{\omega} \int \ldots \int \Psi^{*}(\mathbf{r}_1\omega_1,\ \ldots,\ \mathbf{r}_N\omega_N)\, \Psi(\mathbf{r}_1{}'\omega_1,\ \ldots,\ \mathbf{r}_N\omega_N)\, d\mathbf{r}_2,\ \ldots,\ d\mathbf{r}_N, \tag{5.14}$$

and

$$\rho_2(\mathbf{r}_1, \mathbf{r}_2, \mathbf{r}_1', \mathbf{r}_2') = \frac{N(N-1)}{2} \sum_{\omega} \int \cdots \int \Psi^*(\mathbf{r}_1\omega_1,\ \mathbf{r}_2\omega_2,\ \ldots,\ \mathbf{r}_N\omega_N) \Psi(\mathbf{r}_1'\omega_1,\ \mathbf{r}_2'\omega_2,\ \ldots,\ \mathbf{r}_N\omega_N)\, d\mathbf{r}_3,\ \ldots,\ d\mathbf{r}_N, \tag{5.15}$$

which can be expressed in matrix format in terms of the basis functions, respectively, as:

$$\rho_1(\mathbf{r}_1, \mathbf{r}_1') = 2 \operatorname{tr} \mathbf{P}\boldsymbol{\psi}(\mathbf{r}_1) \otimes \boldsymbol{\psi}^{\dagger}(\mathbf{r}_1'), \tag{5.16}$$

and within the single determinant representation, the 2-RDM can be obtained from the 1-RDM as follows:

$$\begin{aligned} \rho_2(\mathbf{r}_1, \mathbf{r}_2, \mathbf{r}_1', \mathbf{r}_2') &= \begin{vmatrix} \rho_1(\mathbf{r}_1, \mathbf{r}_1') & \frac{1}{2}\rho_1(\mathbf{r}_1, \mathbf{r}_2') \\ \rho_1(\mathbf{r}_2, \mathbf{r}_1') & \rho_1(\mathbf{r}_2, \mathbf{r}_2') \end{vmatrix} \\ &= \rho_1(\mathbf{r}_1, \mathbf{r}_1')\rho_1(\mathbf{r}_2, \mathbf{r}_2') - \tfrac{1}{2}\rho_1(\mathbf{r}_1, \mathbf{r}_2')\rho_1(\mathbf{r}_2, \mathbf{r}_1'). \end{aligned} \tag{5.17}$$

If now we rid eq. (5.16) of the distinction between the two sets of coordinates by setting $\mathbf{r}' = \mathbf{r}$, this leads to the diagonal element of this expression which is the electron density:

$$\rho_1(\mathbf{r}, \mathbf{r}) = 2 \operatorname{tr} \mathbf{P}\boldsymbol{\psi}(\mathbf{r}) \otimes \boldsymbol{\psi}^{\dagger}(\mathbf{r}). \tag{5.18}$$

Correspondingly, the omission of the prime in eq. (5.14) is tantamount to preserving only the diagonal elements of the 1-RDM, that is, the electron density. A similar removal of the coordinates' distinction in eq. (5.15) yields the *electron pair density*:

$$\rho(\mathbf{r}_1, \mathbf{r}_2) = \frac{N(N-1)}{2} \sum_{\omega} \int \cdots \int \Psi^*(\mathbf{r}_1\omega_1,\ \mathbf{r}_2\omega_2,\ \ldots,\ \mathbf{r}_N\omega_N) \Psi(\mathbf{r}_1\omega_1,\ \mathbf{r}_2\omega_2,\ \ldots,\ \mathbf{r}_N\omega_N) d\mathbf{r}_3,\ \ldots,\ d\mathbf{r}_N. \tag{5.19}$$

This pair density is the conditional probability of the presence of one electron in an infinitesimal volume element at $\mathbf{r}_1$ while a second electron is present in an infinitesimal volume element at $\mathbf{r}_2$, multiplied by the number of distinct pairs ($N(N-1)/2$). Since Ψ is assumed to be normalized, an integral of this pair density over the remaining two coordinates gives the total number of distinct electron pairs in the system.

Although all double kernels may be included in KEM calculations, Huang, Massa, and Karle have reasoned that one can speedup calculations on large systems by setting to zero all the elements of the **R** matrix that represent the weights of products of basis functions centered on distant atoms [34, 35, 41]. This idea is consistent with the known "*short sightedness*" of the density matrix [49, 50].

As an illustration of implementation of these ideas, take a tri-hydrated cyclic hexapeptide, c[Gly-Gly-D-Ala-D-Ala-Gly-Gly].3H_2O [51], that can be conceptually broken down into, say, six amino acid residues "fragments" whereby the two flanking amino acids and any water of hydration represent the "neighborhood" [34, 41]. From the known atomic coordinates, the threshold is set beyond which the atoms are considered not to interact.

The shortsightedness is implemented by calculating the overlap matrix of the atomic orbitals. Where the overlap is small enough according to a preset threshold the element of the overlap matrix is set to exactly zero. The pattern of zeros in the overlap matrix is then superimposed in the same way within the density matrix **R**. In this way, a density matrix is constructed for each of the kernels. Then these kernel density matrices are summed (as a direct sum $\oplus$) to reconstruct an approximate representation of the density matrix of the full system,

$$\mathbf{R}(0) = \bigoplus_{j=1}^{6} \mathbf{R}_j(0), \tag{5.20}$$

where the "(0)" indicates the patterns of zeros imposed upon the **R** matrix as explained above. Equation (5.20) can be expressed more explicitly as:

$$\mathbf{R}(0) = \begin{pmatrix} \mathbf{R_{11}} & \mathbf{R_{12}} & \mathbf{0} & \mathbf{0} & \mathbf{0} & \mathbf{R_{16}} \\ \mathbf{R_{21}} & \mathbf{R_{22}} & \mathbf{R_{23}} & \mathbf{0} & \mathbf{0} & \mathbf{0} \\ \mathbf{0} & \mathbf{R_{32}} & \mathbf{R_{33}} & \mathbf{R_{34}} & \mathbf{0} & \mathbf{0} \\ \mathbf{0} & \mathbf{0} & \mathbf{R_{43}} & \mathbf{R_{44}} & \mathbf{R_{45}} & \mathbf{0} \\ \mathbf{0} & \mathbf{0} & \mathbf{0} & \mathbf{R_{54}} & \mathbf{R_{55}} & \mathbf{R_{56}} \\ \mathbf{R_{61}} & \mathbf{0} & \mathbf{0} & \mathbf{0} & \mathbf{R_{65}} & \mathbf{R_{66}} \end{pmatrix}. \tag{5.21}$$

An approximate one-body reduced electron density matrix (1-RDM) of the full system can, thus, be written as:

$$\rho_1(\mathbf{r}_1, \mathbf{r}_1')(0) = 2\,\mathrm{tr}\,\mathbf{R}(0)\left(\boldsymbol{\psi}(\mathbf{r}_1) \otimes \boldsymbol{\psi}^{\dagger}(\mathbf{r}_1')\right)(0), \tag{5.22}$$

with a corresponding electron density of the form:

$$\rho(\mathbf{r})(0) = 2\,\mathrm{tr}\,\mathbf{R}(0)\left(\boldsymbol{\psi}(\mathbf{r}) \otimes \boldsymbol{\psi}^{\dagger}(\mathbf{r})\right)(0). \tag{5.23}$$

In eq. (5.22), the pattern of zeros in $\left(\boldsymbol{\psi} \otimes \boldsymbol{\psi}^{\dagger}\right)(0)$ is the same as in $\mathbf{S}(0)$ and $\mathbf{R}(0)$. This is an elegant and fast approach to reconstruct a good approximation to the density matrices of a large system from the corresponding smaller kernel matrices. Such density matrices would have *N*-representability imposed by their insertion into the Clinton equations [52]:

$$\mathbf{R}_{i+1} = 3(\mathbf{R}_i\mathbf{S}\mathbf{R}_i)^2 - 2(\mathbf{R}_i\mathbf{S}\mathbf{R}_i\mathbf{S}\mathbf{R}_i)^3 + \lambda^{(i)}\mathbf{1}, \tag{5.24}$$

and purifying it iteratively (where i, here, is the index of iteration) and subject to the normalization constraint, that is:

$$\mathrm{tr}\,\mathbf{R}\mathbf{S} = \frac{N}{2}, \tag{5.25}$$

the number of doubly occupied molecular orbitals.

Electron density maps calculated from this approximation and those calculated directly at the Hartree–Fock level using the same basis set are visually indistinguishable (see Refs. [34, 41]).

To sum-up the philosophy of this approach, the interaction between distant kernels is completely neglected (equated to zero) which leads to a great simplification of the formalism. That simplification is what has come to be called the KEM, which we describe next.

KEM is a simpler implementation of this strategy, without the burden of having to keep track of what atoms belong to what kernel. Furthermore, KEM also has the advantage of taking account of the interactions between different kernels explicitly and is inherently parallelizable. These are some of the motivations that led to the development of the KEM. In this sense, *KEM can be thought of as extending the concept of the near sightedness of the density matrix to its limit.*

5.4 The kernel energy method

In the KEM, a large molecule, which contains so many atoms that it cannot be easily subjected to *ab initio* calculations as a whole molecule, is simply cut into entirely separate fragments called kernels (Fig. 5.1). Such a severance into parts will leave dangling bonds which are healed by the attachment of capping hydrogen atoms in the place previously occupied by heavier atoms. The kernels are chosen small enough that they can be calculated by *ab initio* methods. Experience shows that the results of this approximation are quite accurate which is a consequence of the shortsightedness of the density matrix alluded to above. In what follows the KEM formalism is briefly reviewed and justified.

The philosophy of KEM is to break the large target molecule into computationally manageable small pieces (the kernels). The choice of kernels is not unique, but experience has been accumulating that provide guidelines as to how they are chosen [41]. Importantly, the quality of the results does not, in general, depend on the particular choice of kernels. Any dangling bond resulting from the fragmentation is then capped with hydrogen atoms. Such capping is *not always* required, an example being when a kernel is, itself, a closed-shell molecule. Thus, only if covalent bonds are cut one has to cap with hydrogens. As can be inferred from the formulas

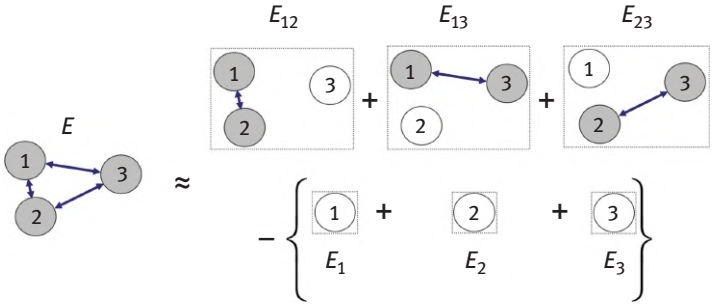

Fig. 5.1: A conceptual diagram illustrating the kernel energy method (KEM). The many- (here three-) body energy is approximated as the sum of the individual pair-wise interacting subsystems (gray) energies minus the overcounted single subsystems' "self" energies. In this manner, a large molecule is mathematically cut into kernels with the dangling bonds saturated with hydrogen atoms as needed.

described next, it can be inferred that the contributions of the capping hydrogens cancel (to near perfection).

A general expression for the energy of interaction (E_{int}) of an n-body system is expressed as:

$$E_{\text{total}} \approx \sum_{c=1}^{n} E_c + \sum_{a=1}^{n-1} \sum_{b=a+1}^{n} (E_{ab} - E_a - E_b) \equiv \sum_{c=1}^{n} E_c + \sum_{a=1}^{n-1} \sum_{b=a+1}^{n} \Delta E_{ab} \tag{5.26}$$

where E_{total} refers to the total energy of the fully-interacting system, E_i (where $i = a, b, c$) refers to the energy of the ith body in isolation, and E_{ij} is a two-body energy. Clearly, the two-body interaction energy is, then, the difference between E_{ij} and the sum ($E_i + E_j$). Eq. (5.26) implicitly involves the approximation of neglecting higher-order interactions. This is justified in the observation that perturbations of higher orders, that is, third, fourth, etc., are negligible compared to the pair-wise interactions. With this understanding, from now on, the approximate symbol will be converted to an equality symbol.

If we now gather the terms in an alternative manner, Eq. (5.26) simplifies to:

$$E_{\substack{\text{total} \\ (\text{KEM})}} = \sum_{a=1}^{n-1} \sum_{b=a+1}^{n} E_{ab} - (n-2) \sum_{c=1}^{n} E_c \tag{5.27}$$

where the first term on the right-hand-side, the double sum, is the total energy of all double kernels (ab) in the system. This total energy includes all pair energies (E_{ab}) and, in addition, the sum of all single kernels (E_c) counted ($n - 2$) times. This inclusion of (over-counted) self-energies is corrected by the factor ($n - 2$) in front of the second summation. This factor when multiplied by the sum over all single

kernels self-energies reduces the pair energy term by the number of times the self-energies of single kernels are over-counted in the pair energy terms.

As a simple example, consider a system broken into $n = 4$ single kernels: *A, B, C,* and *D*. In this case, the double sum of Eq. (5.27), written explicitly, reads:

$$\sum_{a=1}^{n-1}\sum_{b=a+1}^{n} E_{ab} = E_{\mathrm{AB}} + E_{\mathrm{AC}} + E_{\mathrm{AD}} + E_{\mathrm{BC}} + E_{\mathrm{BD}} + E_{\mathrm{CD}}, \tag{5.28}$$

which counts each single kernel "A, ..., D" three times, that is, $(n - 1)$ times, noticing that the special way the sums are defined avoid counting the same interaction twice since, for example, $E_{\mathrm{AB}} = E_{\mathrm{BA}}$. From this sum (Eq. 5.28), one must subtract the weighted sum of the one-body term in Eq. (5.27), a correction that reads explicitly:

$$(n-2)\sum_{c=1}^{n} E_c = (4-2)(E_A + E_B + E_C + E_D) \tag{5.29}$$

which, when subtracted from the sum of the doubles energies as specified in Eq. (5.27) yields the KEM approximation to the total energy of this four-kernel system. (For an illustration of the simpler 3 kernels example, please see Fig. 5.1).

If we rearrange and group terms, and solve for the approximate (KEM) total energy, we get:

$$E_{\substack{\mathrm{total}\\(\mathrm{KEM})}} = E_{AB} + E_{AC} + E_{AD} + E_{BC} + E_{BD} + E_{CD} - 2E_A - 2E_B - 2E_C - 2E_D \tag{5.30}$$

which is an explicit expansion of Eq. (5.27) for this particular example with $n = 4$.

As noted earlier, from eq. (5.30) it should be clear that, if hydrogen caps are used to satisfy any dangling bonds that result from the fragmentation, the *number* of hydrogen caps on double kernels is equal to the number of such caps on single kernels. Since these two sets of hydrogen cap contributions appear in eq. (5.30) with opposite signs, they essentially cancel save for the small error introduced by the slightly different electronic environments of these sets of caps. This cancellation of the caps' contribution renders KEM a method of general utility whether kernels are obtained by severing chemical covalent bonds, fissioning aromatic bonds, splitting hydrogen bonds, or by choosing separate closed-shell molecular entities within a molecular complex as kernels.

5.5 The scaling of the KEM

The whole point of KEM is to avoid the computational scaling bottleneck that plagues *ab initio* quantum chemical calculations. The scaling exponent α, to which the size of the atomic basis set is to be raised, is generally greater than 3 or 4. In order to give the reader some sense of how much computational resources savings

can be affected by the use of the KEM approach, we can consider an ideal back-of-an-envelope calculation that can give an order of magnitude estimate.

Say that we have a macromolecule described by M basis functions and that we can split it into m kernels of equal size. Suppose each of these kernels is described by a basis set made up of μ atomic-like functions. In this case, the relative time (t_{rel}) taken by a KEM calculation with respect to the intact/full molecular calculation follows from the KEM partitioning that splits the system into m single kernels and $\frac{m^2-m}{2}$ double kernels. The relative CPU/GPU time is then:

$$t_{\text{rel}} = \frac{t_{\text{KEM}}}{t_{\text{direct}}} = \frac{m\mu^{\alpha} + \frac{m^2-m}{2}(2\mu)^{\alpha}}{M^{\alpha}} \tag{5.31}$$

This equation can be further simplified by realizing that $M = m\mu$, then we have:

$$t_{\text{rel}} = \frac{m\mu^{\alpha} + (m^2-m)(2^{\alpha-1}\mu^{\alpha})}{(m\mu)^{\alpha}}, \tag{5.32}$$

$$t_{\text{rel}} = \frac{2^{\alpha-1}(m-1)+1}{m^{\alpha-1}}. \tag{5.33}$$

As can be seen from eq. (5.33), the relative time is independent of the size of the basis set. The equation shows that one must break the system into at least three kernels to affect CPU (and/or GPU) time-saving – anything less is meaningless (which is also reflected in the equation). In fact, it can be shown that, for the idealized system for which eq. (5.33) has been derived, to achieve saving, the conditions are that $m > 3$ kernels and $\alpha > 3$.

Equation (5.33) has been used to generate the entries in Tab. 5.1 showing that within a model chemistry that scales cubically, and if the system is broken into 10 kernels, one saves less than an order of magnitude in time. However, with a splitting into 1,000 kernels, the saving in time jumps to $O(10^3)$. The savings are magnified dramatically with steeper scalings as can be gleaned from the table. For $\alpha = 5$, a split into 1,000 kernels speeds up the calculation by 100 million times compared to a full molecular calculation.

Finally and importantly, KEM can be further sped-up by several orders of magnitude by heavily parallelized computations. A 1,000 core cluster, commonly available nowadays, would speed the calculation by $O(10^3)$ over an above the savings outlined above. Specific examples of such savings will be revisited in the next chapter of this book.

On the top of the considerable scaling economies inherent in the KEM itself due to the conversion of the power of a large number to the sum of smaller numbers raised to the same power, an added advantage of the method is that it is ideally suited for massively parallel computing. As a graphical illustration of this parallelization, Fig. 5.3 shows how this concept may be implemented in practice using a tripeptide as an

Tab. 5.1: Relative times (t_{rel}) of KEM relative to full molecular calculations as a function of the number of single kernels (m) and the scaling parameter (α) predicted from eq. (5.33).

	$t_{rel}\,(m,\alpha)$		
m	$\alpha = 3$	$\alpha = 4$	$\alpha = 5$
10	4×10^{-1}	7×10^{-2}	1×10^{-2}
50	8×10^{-2}	3×10^{-3}	1×10^{-4}
200	2×10^{-2}	2×10^{-4}	2×10^{-6}
1,000	4×10^{-3}	8×10^{-6}	2×10^{-8}
5,000	8×10^{-4}	3×10^{-7}	1×10^{-10}

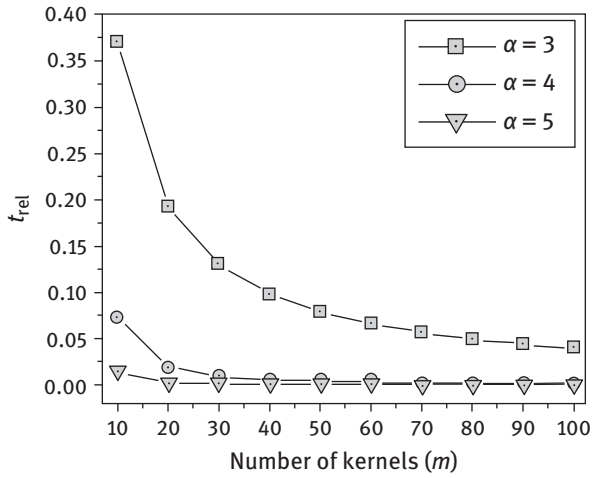

Fig. 5.2: Relative times according to eq. (5.33) as a function of the number of single kernels and scaling exponents.

example. Such parallel implementation of the KEM algorithm may further enhance the savings in computing times by a further two to four orders of magnitudes.

5.6 Closing remarks

We have briefly outlined the context, history, and intellectual antecedents of the KEM. This chapter is concerned with the theoretical foundations of the method and its context within the larger scheme of computational quantum chemistry, while the next chapter reviews some examples of its applications.

The KEM method takes advantage of nature's short-sightedness reflected in its representation by density matrices. The method takes this shortsightedness to its

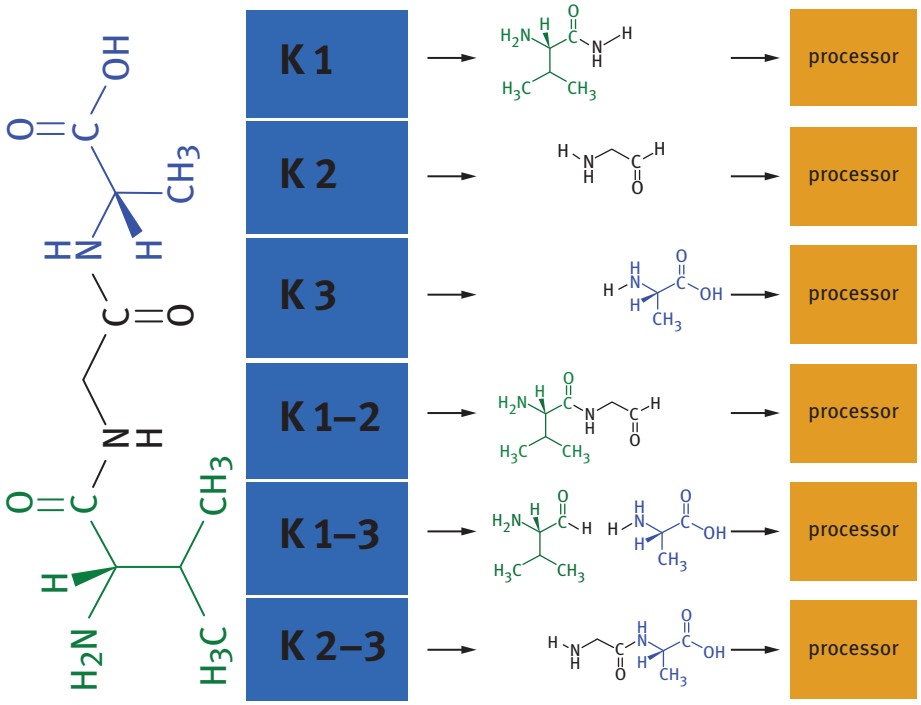

Fig. 5.3: Parallelization of a calculation on the non-zwitter-ionic form of the tripeptide Val-Gly-Ala showing how the calculation on each separate single- or double-kernel can be run on a separate core in a CPU or GPU reducing by another few orders of magnitude the inherent time of a KEM calculation compared to the full-system calculation.

limits. Simple considerations show the CPU (and/or GPU) time savings that this method can bring to *ab initio* calculations. As the scaling factor gets bigger the computational advantage of KEM gets magnified. Given the result indicated in Fig. 5.2, we may conclude that a molecular system of practically any size including even, perhaps, millions of atoms can be described by accurate *ab initio*-quality calculations using KEM.

References

[1] Yang, W. Electron density as the basic variable: A divide-and-conquer approach to the *ab initio* computation of large molecules. *J. Mol. Struct. (Theochem)* 255, 461–479 (1992).

[2] Yang, W, Lee, T-S. A density-matrix divide-and-conquer approach for the electronic structure calculations of large molecules. *J. Chem. Phys.* 103, 5674–5678 (1995).

[3] Lee, T-S, Lewis, JP, Yang, W. Linear-scaling quantum mechanical calculations of biological molecules: The divide-and-conquer approach. *Comput. Mater. Sci.* 12, 259–277 (1998).

[4] Kitaura, K, Ikeo, E, Asada, T, Nakano, T, Uebayasi, M. Fragment molecular orbital method: An approximate computational method for large molecules. *Chem. Phys. Lett.* 313, 701–706 (1999).
[5] Fedorov, D, Kitaura, K. *The Fragment Molecular Orbital Method: Practical Applications to Large Molecular Systems*. CRC Press, Boca Raton, Florida, (2009).
[6] Zhang, DW, Zhang, JZH. Molecular fractionation with conjugate caps for full quantum mechanical calculation of protein-molecule interaction enegry. *J. Chem. Phys.* 119, 3599–3605 (2003).
[7] Zhang, DW, Xiang, Y, Zhang, JZH. New advance in computational chemistry: Full quantum mechanical *ab initio* computation of streptavidin-biotin interaction energy. *J. Phys. Chem B* 107, 12039–12041 (2003).
[8] Chen, XH, Zhang, DW, Zhang, JZH. Fractionation of peptide with disulfide bond for quantum mechanical calculation of interaction energy with molecules. *J. Chem. Phys.* 120, 839–844 (2004).
[9] Mei, Y, Zhang, DW, Zhang, JZH. New method for direct linear-scaling calculation of electron density of proteins. *J. Phys. Chem. A* 109, 2–5 (2005).
[10] He, X, Zhang, JZH. A new method for direct calculation of total energy of protein. *J. Chem. Phys.* 122, 031103 (2005).
[11] Mei, Y, Ji, C, Zhang, JZH. A new quantum method for electrostatic solvation energy of protein. *J. Chem. Phys.* 125, 094906 (2006).
[12] Li, S, Li, W, Fang, T. An efficient fragment-based approach for predicting the ground-state energies and structrues of large molecules. *J. Am. Chem. Soc.* 127, 7215–7226 (2005).
[13] Li, W, Fang, T, Li, S. A fragment energy assembler method for Hartree-Fock calculations of large molecules. *J. Chem. Phys.* 124, 154102 (2006).
[14] Jiang, N, Ma, J, Jiang, Y. Electrostatic field-adapted molecular fractionation with conjugated caps for energy calculations of charged biomolecules. *J. Chem. Phys.* 124, 114112 (2006).
[15] Li, W, Li, S, Jiang, Y. Generalized energy-based fragmentation approach for computing the ground-state energies and properties of large molecules. *J. Phys. Chem. A* 111, 2193–2199 (2007).
[16] Hua, S, Hua, W, Li, S. An efficient implementation of the generalized energy-based fragmentation approach for general large molecules. *J. Phys. Chem. A* 114, 8126–8134 (2010).
[17] Deev, V, Collins, MA. Approximate *ab initio* energies by systematic molecular fragmentation. *J. Chem. Phys.* 122, 154102 (2005).
[18] Collins, MA, Deev, VA. Accuracy and efficiency of electronic energies from systematic molecular fragmentation. *J. Chem. Phys.* 125, 104104 (2006).
[19] Netzloff, HM, Collins, MA. *Ab initio* energies of nonconducting crystals by systematic fragmentation. *J. Chem. Phys.* 127, 134113 (2007).
[20] Addicoat, MA, Collins, MA. Accurate treatment of nonbonded interactions within systematic molecular fragmentation. *J. Chem. Phys.* 131, 104103 (2009).
[21] Bettens, RPA, Lee, AM. A new algorithm for molecular fragmentation in quantum chemical calculations. *J. Phys. Chem. A* 110, 8777–8785 (2006).
[22] Lee, AM, Bettens, RPA. First principles NMR calculations by fragmentation. *J. Phys. Chem. A* 111, 5111–5115 (2007).
[23] Le, H-A, Lee, AM, Bettens, RPA. Accurately reproducing *ab initio* electrostatic potentials with multipoles and fragmentation. *J. Phys. Chem. A* 113, 10527–10533 (2009).
[24] Ganesh, V, Dongare, RK, Balanarayan, P, Gadre, SR. Molecular tailoring approach for geometry optimization of large molecules: Energy evaluation and parallelization strategies. *J. Chem. Phys.* 125, 104109 (2006).

[25] Hung, L, Carter, EA. Accurate simulations of metals at the mesoscale: Explicit treatment of 1 million atoms with quantum mechanics. *Chem. Phys. Lett.* 475, 163–170 (2009).
[26] Chang, C, Bader, RFW. Theoretical construction of a polypeptide. *J. Phys. Chem.* 96, 1654–1662 (1992).
[27] Breneman, CM, Weber, LW. Transferable Atom Equivalents. Molecular Electrostatic Potentials from the Electric Multipoles of PROAIMS Atomic Basins. In: *NATO ASI Series: The Application of Charge Density Research to Chemistry and Drug Design*. Plenum Press, New York, (1991), 357–358.
[28] Breneman, CM, Thompson, TR, Rhem, M, Dung, M. Electron density modeling of large systems using the transferable atom equivalent method. *J. Comput. Chem.* 19, 161–179 (1995).
[29] Breneman, CM, Rhem, M. QSPR Analysis of HPLC column capacity factors for a set of high-energy materials using electronic van der Waals surface property descriptors computed by transferable atom equivalent method. *J. Comput. Chem.* 18, 182–197 (1997).
[30] Sukumar, N, Breneman, CM. QTAIM in drug discovery and protein modeling. In: *The Quantum Theory of Atoms in Molecules: From Solid State to DNA and Drug Design*; Matta, CF, Boyd, RJ (Eds.), Wiley-VCH, Weinheim (2007), 473–498.
[31] Exner, TE, Mezey, PG. *Ab initio* quality properties for macromolecules using ADMA approach. *J. Comput. Chem.* 24, 1980–1986 (2003).
[32] Matta, CF. Theoretical reconstruction of the electron density of large molecules from fragments determined as proper open quantum systems: The properties of the oripavine PEO, enkephalins, and morphine. *J. Phys. Chem. A* 105, 11088–11101 (2001).
[33] Bader, RFW, Matta, CF, Martín, FJ. Atoms in medicinal chemistry. In: *Medicinal Quantum Chemistry*; Carloni, P, Alber, F (Eds.), Wiley-VCH, Weinheim (2003), 201–231.
[34] Massa, L, Huang, L, Karle, J. Quantum crystallography and the use of kernel projector matrices. *Int. J. Quantum. Chem.* 56, 371–384 (1995).
[35] Huang, L, Massa, L, Karle, J. Kernel projector matrices for Leu^1-zervamicin. *Int. J. Quantum. Chem.* 60, 1691–1700 (1996).
[36] Huang, L, Massa, L, Karle, J. Kernel energy method illustrated with peptides. *Int. J. Quantum Chem.* 103, 808–817 (2005).
[37] Huang, L, Massa, L, Karle, J. Kernel energy method: Application to DNA. *Biochemistry* 44, 16747–16752 (2005).
[38] Huang, L, Massa, L, Karle, J. Kernel energy method: Application to insulin. *Proc. Natl. Acad. Sci. USA* 102, 12690–12693 (2005).
[39] Huang, L, Massa, L, Karle, J. The kernel energy method: Application to a tRNA. *Proc. Natl. Acad. Sci. USA* 103, 1233–1237 (2006).
[40] Huang, L, Massa, L, Karle, J. Kernel energy method applied to vesicular stomatitis virus nucleoprotein. *Proc. Natl. Acad. Sci. USA* 106, 1731–1736 (2009).
[41] Huang, L, Massa, L, Karle, J. Quantum kernels and quantum crystallography: Applications in biochemistry. In: *Quantum Biochemistry: Electronic Structure and Biological Activity, Vol. 1*; Matta, CF (Ed.), Wiley-VCH, Weinheim (2010), 3–60.
[42] Huang, L, Bohórquez, H, Matta, CF, Massa, L. The kernel energy method: Application to graphene and extended aromatics. *Int. J. Quantum Chem.* 111, 4150–4157 (2011).
[43] Huang, L, Massa, L, Matta, CF. A graphene flake under external electric fields reconstructed from field-perturbed kernels. *Carbon* 76, 310–320 (2014).
[44] Huang, L, Matta, CF, Massa, L. The kernel energy method (KEM) delivers fast and accurate QTAIM electrostatic charge for atoms in large molecules. *Struct. Chem.* 26, 1433–1442 (2015).
[45] Polkosnik, W, Matta, CF, Huang, L, Massa, L. Fast quantum crystallography. *Int. J. Quantum Chem.* 119, e26095 (2019).

[46] Massa, L, Keith, T, Cheng, Y, Matta, CF. The kernel energy method applied to quantum theory of atoms in molecules – Energies of interacting quantum atoms. *Chem. Phys. Lett.* 734, 136650 (2019).
[47] Löwdin, P-O. On the nonorthogonality problem. *Adv. Quantum Chem.* 5, 185–199 (1970).
[48] Davidson, ER. *Reduced Density Matrices in Quantum Chemistry*. Academic Press, Inc., New York, (1976).
[49] Prodan, E, Kohn, W. Nearsightedness of electronic matter. *Proc. Natl. Acad. Sci. USA* 102, 11635–11638 (2005).
[50] Bader, RFW. Chemistry and the near-sighted nature of the one-electron density matrix. *Int. J. Quantum Chem.* 56, 409–419 (1995).
[51] Karle, IL, Gibson, JW, Karle, J. Conformation and crystal structure of the cyclic polypeptide [Gly-Gly-D-Ala-D-Ala-Gly-Gly].$3H_2O$. *J. Am. Chem. Soc.* 92, 3755–3760 (1970).
[52] Clinton, WL, Galli, AJ, Massa, LJ. Direct determination of pure-state density matrices. II. Construction of constrained idempotent one-body densities. *Phys. Rev.* 177, 7–12 (1969).

Chapter 6
The kernel energy method: accurate and fast calculations on large systems by example

The proof of the pudding is in the eating. Proverb

(*E. M. Knowles, Little Oxford Dictionary of Proverbs, Oxford University Press, Oxford, 2016*)

The kernel energy method (KEM) is a fragmentation method applicable to very large molecular systems, for example, large protein and nucleic acid molecules. The previous chapter describes the manner in which fragmentation may be realized and how the full molecular system is reconstructed from the fragments in such fashion that it is reasonable to expect that accurate *ab initio* accuracy is to be maintained. It has been emphasized that dealing with fragments allows overcoming the computational difficulty which grows with a high power of the number of atoms (and therefore of the number of basis functions) involved in the calculation. Moreover, fragmentation can be accompanied by an inherent parallel implementation of the calculations which is an important factor in the possible speed-up of calculations above and beyond that brought up by the reduction in the size of quantum calculations.

This chapter is concerned with examples of KEM calculations related to its accuracy and speed of calculation. Illustrations of KEM calculations considered here include biological molecules and materials of technological importance. KEM, in *N*-representable form, can deliver all one- and two-body properties in a quantum mechanically valid form. These would include energies, response properties, and the electron density. KEM reconstruction of some of the Bader's quantum theory of atoms in molecules (QTAIM) properties is also discussed which showcases how KEM recovers one-electron and two-electron properties accurately and fast.

6.1 An approach to quantum calculations on large systems: the kernel energy method

The theoretical underpinnings of the kernel energy method (KEM) has been introduced in the previous chapter (Chapter 5). The present chapter switches the focus to applications. In terms of types of systems used here to illustrate how KEM can deliver useful information, these systems span biological macromolecules and technologically promising materials such as graphene nanoribbons. Perhaps more importantly is the *type* of information that can be delivered by the method. In principle, quantum

Note: This chapter is reproduced with modification and adaptation with permission from: Massa, L., Castanedo, L. A. M., Fahimi, P., and Matta, C. F. (2023) "Applications of in-silico quantum chemical calculations to large systems: The kernel energy method", Chapter 7 in: In-silico *Approaches to Macromolecular Chemistry*, Thomas, J., Thomas, S., Kornweitz, H., and Thomas, M. (Eds.), Elsevier, The Netherlands (pp. 199–215), © 2023 Elsevier.

https://doi.org/10.1515/9783110566673-007

mechanical properties can be predicted from KEM since it can deliver approximate N-representable density matrices of the full system. In practice, we will show the viability of this approach to deliver, not only energies, but, equally importantly, other properties such as those defined within the quantum theory of atoms in molecules (QTAIM) including two-electron properties such as the localization and delocalization indices (LIs and DIs). Moreover, the ability of the method to predict field-induced response quantities will also be briefly reviewed. It may be helpful to first summarize the principal points and tenets of the KEM approach (details can be found in Chapter 5 and the references therein).

As mentioned in the previous chapter, the cost of quantum chemical computations grows quickly as M^{α} where M is the number of basis functions necessary to describe the system and α is the scaling of the given chemical model. There exists a panoply of methods to attack this problem (see literature cited in Chapter 5). KEM is one of these approaches.

KEM involves the fragmentation of the large system into smaller parts saturated, if necessary, with hydrogen atoms to saturate dangling bonds that may result from this partitioning. Given the general expression for the energy of interaction of n-bodies [1]:

$$E_{\text{total}} = \sum_{a=1}^{n-1} \sum_{b=a+1}^{n} \Delta E_{ab} + \sum_{c=1}^{n} E_c \tag{6.1}$$

where E_{total} is the total energy of the system, ΔE_{ab} is the interaction energy of a double kernel (the abth), and E_c is the energy of the cth isolated body ignoring all perturbations of higher orders than the second [2] where the interaction energy is defined:

$$\Delta E_{ab} \equiv E_{ab} - E_a - E_b \tag{6.2}$$

which upon simplification and rearranging leads to

$$E_{\substack{\text{total} \\ (\text{KEM})}} = \sum_{a=1}^{n-1} \sum_{b=a+1}^{n} E_{ab} - (n-2) \sum_{c=1}^{n} E_c. \tag{6.3}$$

As was shown in Chapter 5, to get an order-of-magnitude sense of the time savings of the KEM method, suppose a macromolecule described by a basis set of size M is broken into m equal kernels each described by a basis set of size μ. The ratio of the time of a KEM calculation with respect to that of the direct (full molecule) calculation, t_{rel}, is:

$$t_{\text{rel}} = \frac{t_{\text{KEM}}}{t_{\text{direct}}} = \frac{m\mu^{\alpha} + \frac{m^2 - m}{2}(2\mu)^{\alpha}}{M^{\alpha}}. \tag{6.4}$$

Remembering that $M = m\mu$, one can simplify this equation to:

$$t_{\text{rel}} = \frac{2^{\alpha-1}(m-1)+1}{m^{\alpha-1}}. \tag{6.5}$$

Equation (6.5) shows that the relative time savings of KEM increases quickly with the *number of kernels* and with the *scaling of the method* (α), but is quite independent of the size of the basis set itself (see Tab. 5.1 and Fig. 5.2 of Chapter 5). To illustrate, splitting a 200 amino acid peptide into single amino acid residue kernels, the saving for a single determinant method is $O(10^2)$, but for a more accurate method with $\alpha = 5$ the saving is of the order of a million. So, the time savings of KEM are more important for larger system that could be broken into more fragments but also for the more accurate methods, for example configuration interaction or Møller–Plesset (MP*n*) perturbation method at various orders (*n*). Parallelization can multiply these time savings by the number of available cores, each devoted to a single or double kernel calculation separately. (The reader may also refer to Fig. 5.3 of Chapter 5 for an illustration).

6.2 The kernel energy method applied to large biomolecules

The first introduction of KEM was accompanied by testing how fast it could recover the energies of 16 different oligopeptides of known X-ray crystallographic structures. The studied oligopeptides range from 5 amino acid residues (80 atoms) to 19 amino acids (327 atoms) [3]. In this paper, Lulu Huang, Lou Massa, and Jerome Karle (HMK) compare the savings in time brought about by the KEM calculations. These savings are substantial and in line with the order of magnitudes predicted by eq. (6.5). Further, since this 2005 paper is the first wherein the KEM approach is introduced [3], the authors have tried to increase the time saving by retaining in the calculations only those double kernels that are chemically bonded to one another and ignoring the contributions of all other double kernels. This last approximation did not turn out to be very accurate though, hence it is concluded that, for high accuracy work, *all double kernels* must be retained into the calculation [3]. For very large systems, a distance criterion cutoff can eliminate the contribution of any double kernel in which its single kernels are separated by a very large distance, but this is to be explored in the future. Jerome Karle gave a lecture in 2006 at the 56th Lindau Nobel Laureate Meeting concerning the topic of Ref. [3]; the lecture is available online [4].

Soon after the appearance of this 2005 paper [3], the accuracy and speed of the KEM approximation has been vetted by its application to biological macromolecules. This vetting begins with relatively small peptides such as insulin [5] made-up of two peptide chains (A and B), altogether made-up of 51 amino acids and 777 atoms, and ending up with a calculation on an entire asymmetric unit of a virus capsid (*vesicular stomatitis* virus) [6].

With regards to insulin, HMK calculated the Hartree–Fock energies for each of the two chains separately and combined [5]. The KEM single-point energies of the gas-phase calculations differ by *ca*. 0.3 kcal/mol from the full calculation [5]. If now we take the solvent molecules as an additional kernel, the calculated KEM total energy of the fully solvated insulin differs from the energy obtained directly for the full insulin-solvent system by *ca*. 3.8 kcal/mol [5]. Given the size of the system, it is clear that the KEM approximation delivers energies within the order of magnitude of chemical accuracy.

Turning to nucleic acids, HMK showed that KEM, when applied to the three forms of DNA (B, A, and Z), yields results of similar accuracy [7]. In these calculations, a kernel is taken as a nucleotide. The KEM approximation has also proved accurate when applied to RNA, specifically to a tRNA with known X-ray crystallographic structure, that of tRNA of methionine in yeast (yeast initiator tRNA, Protein Databank Code: 1YFG). This tRNA consists of 2,565 atoms (Fig. 6.1) within 75 nucleotides [8]. Except for one trinucleotide single kernel, all single kernels in this KEM calculation consist of 4 nucleotides giving a total of 19 single kernels. The total energy of the full molecule differs from the KEM approximate energy by 4.6 kcal/mol [8]. Moreover, KEM has also been shown to deliver good estimates of interaction energies associated with hydrogen-bonding pairs. These interaction energies were obtained by calculating the energies of a hydrogen-bonded double kernel minus the sum of the energies of the two (separate) single kernels defining the double kernel [8].

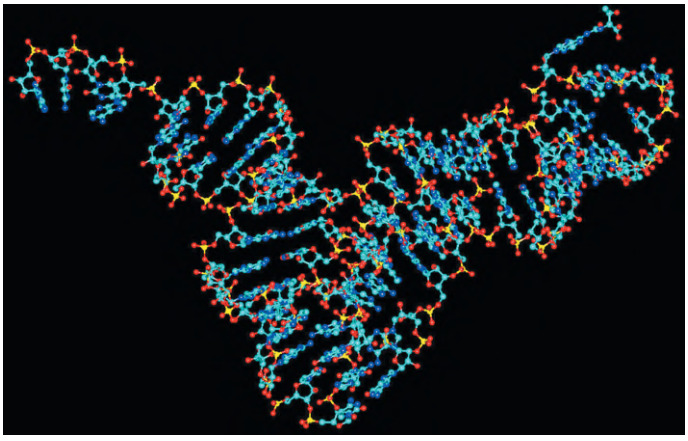

Fig. 6.1: Ball-and-stick representation of the crystallographic structure yeast initiator tRNA, Protein Databank Code 1YFG. The molecule, consisting of 2,565 atoms and 75 nucleotides, is broken into 18 single kernels made of 4 nucleotides and one kernel made of 3 nucleotides [8].

The KEM approximation has also been used to elucidate the electronic structure of the so-called proto-ribosome [9, 10]. As is well-known, the ribosome is the protein manufacturing plant of all living cells where the genetic code is translated into proteins. The protoribosome, in its turn, is believed to be the prebiotic ancestor of present-day ribosome – in line with what is known as the RNA-World hypothesis [11, 12]. The protoribosome, in order to exercise its function, must possess the ability to catalyze the formation of peptide bonds – just as contemporary ribosomes do, and is believed to be the active center of the modern ribosome without most of its present-day surroundings. In fact, the protoribosome is a miniscule part of the contemporary ribosome. Crystal coordinates taken from the modern ribosome were used to build a model of the protoribosome [9, 10]. KEM in conjunction with density functional theory DFT–B3LYP/3–21G* has been used to demonstrate the structural stability and the favorable attachment of the protoribosome to its substrates. These findings reinforce the idea that certain necessary conditions for the formation of the peptide bond are satisfied by the protoribosome [9, 10].

This section is concluded with a quantum mechanical study of the *vesicular stomatitis* virus capsid asymmetric unit [6], shown in Fig. 6.2. The asymmetric unit of this viral protein is composed of 5 peptide chains, each of which consists of 421 amino acid residues made-up of 6,635 atoms. This brings the total number of atoms to $5 \times 6{,}635 = 33{,}175$ atoms. HMK, have obtained an estimate of this protein's total energy at an *ab initio* level of theory. The authors could not compare this case with the full molecule calculation due to the size of the system. However, a comparison has been done between KEM calculations at the Hartree–Fock level (that does not account for dynamic electron correlation) with calculations that take this correlation into account (at the MP2 level of theory) [6]. HMK conclude that dynamic correlation is *crucial* in understanding how the different peptide chains bind to one another through interchain hydrogen bonding [6].

6.3 The kernel energy method and the calculation of response properties

Graphene's technological promise was such that, only a few years after its discovery by Andre Geim and Konstantin Novoselov [13, 14] these workers were awarded the Nobel Prize in Physics in 2010. Graphene is an infinite two-dimensional system of fused benzene rings with extraordinary optical, electrical, and mechanical properties. Such infinite systems are tackled by either periodic calculations or finite cluster calculations in quantum chemistry [15]. Usually finite cluster representations of infinite systems are used to represent nonperiodic features and/or defects. However, here, the KEM method is tested on a finite pristine graphene cluster to establish its applicability to a delocalized electronic system which is subjected to the imposition of external intense electric fields.

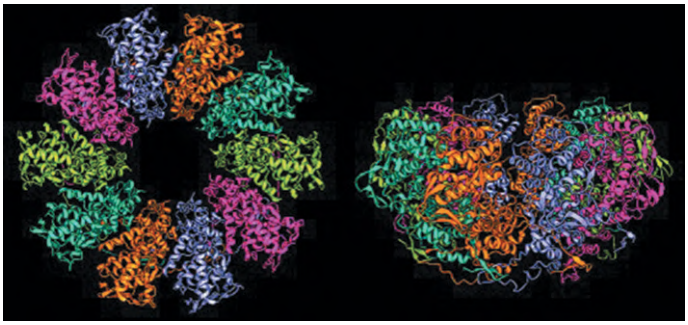

Fig. 6.2: Two views of a ribbon representation of the crystallographic structure of vesicular stomatitis virus nucleoprotein, Protein Databank Code 2QVJ. The molecule is a dimer of 2 symmetry-related halves, each made up of 33,175 atoms in 5 × 421 = 2,105 amino acid residues. In the KEM, each one of the 5 chains is divided into 66 single kernels [6].

The first problem in the application of KEM to this type of system is in the manner in which the system is split into kernels, since in this case there are no clear single bonds that represent a natural choice where the system is to be fragmented. Sivaramakrishnan et al. devised a DFT-based fissioning scheme of polycyclic aromatic hydrocarbons (PAHs) that proved accurate in empirically predicting their heats of formation [16]. The work of these authors shows that it is important not to sever aromatic rings but rather to fission the extended system in a zigzag fashion along the chosen fragmentation lines followed by the saturation of the created dangling bonds as needed [16].

The energy of a finite hydrogen-terminated graphene nanoribbon ($C_{78}H_{26}$) consisting of 27 benzenoid rings and 104 atoms was calculated directly, and also using the KEM approximation at the Hartree–Fock/3-21G and at the MP2/3-21G levels of theory [17]. The KEM total energies of the nanoribbon at the two levels of theory are in both cases within *ca.* 1 kcal/mol – that is, of chemical accuracy – with a relative error $O(10^{-5}\%)$ [17].

Taking this work one more step, a question is now whether the *response* of this graphene nanoribbon to an external electric field is itself recoverable from the KEM approximation? This is an important question for two reasons: (i) Technological and nanoscience experimental procedures are expected to have situations in which the nanoribbon is exposed to strong external fields (as for example in the gap of a scanning tunneling microscope (STM) or nanoelectrical junctions), and (ii) if the field is imposed within the aromatic plane, this will be a challenging case for the KEM approximation since there will be a field-induced polarization of the electron density within each fragment as well as a net charge transfer between the fragments.

To test KEM against these challenges, the response of the total energy and of the molecular dipole moment of a finite hydrogen-terminated zigzag graphene flake ($C_{46}H_{20}$), in 2×7 benzenoid rings, has been investigated with a variety of imposed external fields [18]. The study involves comparing the response to the field calculated with KEM against the response calculated exactly (directly). Uniform parallel-plate capacitor electric fields were applied along the long molecular axis (Fig. 6.3), reaching a maximum strength of 5×10^9 V/m [= 0.01 atomic units (au)]. This field strength is commonplace in nanoelectronics and in, say, the gap of an STM [19, 20].

When one imposes strong external fields on molecular or atomic systems, the precaution of not inducing tunnel ionization must be observed. This is done by inserting the ionization potential in the Keldysh equation [21, 22] to determine the rate of tunnel ionization (see Ref. [23] for an example of how this is done). The Keldysh equation predicts a characteristic time of tunneling ionization for this nanoribbon of the order of a millisecond at the strongest studied field which can be neglected since the timescale of a C–C bending, the vibration with the smallest frequency occurs at the picosecond timescale [24].

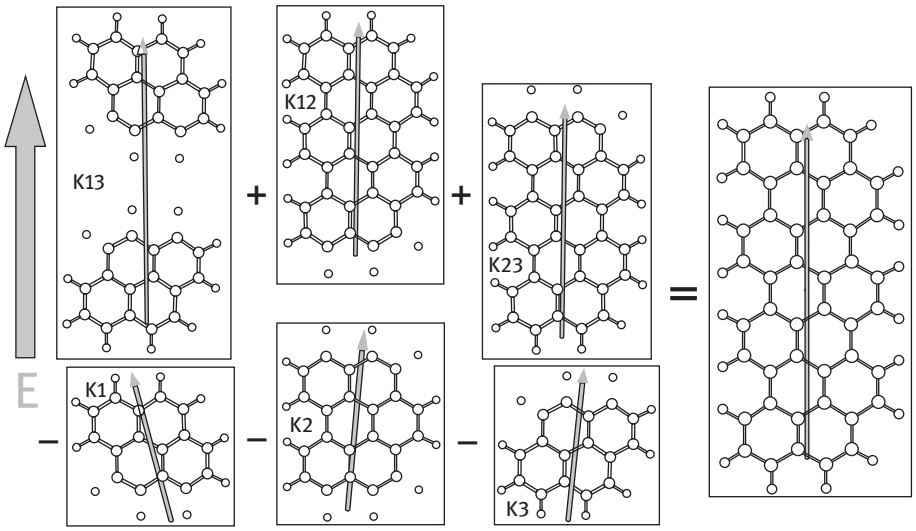

Fig. 6.3: The KEM fissioning of the hydrogen saturated zigzag armchair graphene nanoribbon ($C_{46}H_{20}$ in 14 (2 × 7) rings with C_{2v} symmetry, far-right) into double kernels (top row before the equal sign) and single kernels (bottom row before the equal sign). The arrow at the far left depicts the direction of the external electric field. The diagram mimics eq. (6.3) as it applies to the fissioning of this nanoribbon [18]. The arrows on the molecular structures indicate the direction of the field-induced dipole moment, while an arrow length is proportional to the total dipole moment magnitude [18]. The convention used in depicting the dipoles is the "physicist" convention, meaning that the head of the arrow points to the positive pole of the dipole [25, 26].

The dipole moment (a vector quantity) is reconstructed within the KEM approximation in an analogous manner as the total energy (eq. (6.3)), where every component of the dipole moment vector is treated with a separate equation just as a scalar. Hence, the *i*th component (x, y, or z) of the dipole moment is approximated as [18]:

$$\mu_{i\,(\mathrm{KEM})} = \sum_{a=1}^{n-1} \sum_{b=a+1}^{n} \mu_{ab} - (n-2) \sum_{c=1}^{n} \mu_c. \tag{6.6}$$

The field-induced responses of the total energy ΔE(eV) and of the dipole moment μ(debye) are displayed in Fig. 6.4. Calculations at three different model chemistries MP2/6-311G(2*d*,2*p*), DFT-B3LYP/6-311G(2*d*,2*p*), and Hartree–Fock/6-311G(2*d*,2*p*), all yield similar field responses, both in absolute values and in trends and for both the KEM and the direct calculations (see also Supplementary Information that accompany Ref. [18]). These two sets of calculations (KEM and full-molecular direct calculations), agree remarkably at all field strengths, for all studied properties, and with all three model chemistries tested (Fig. 6.4).

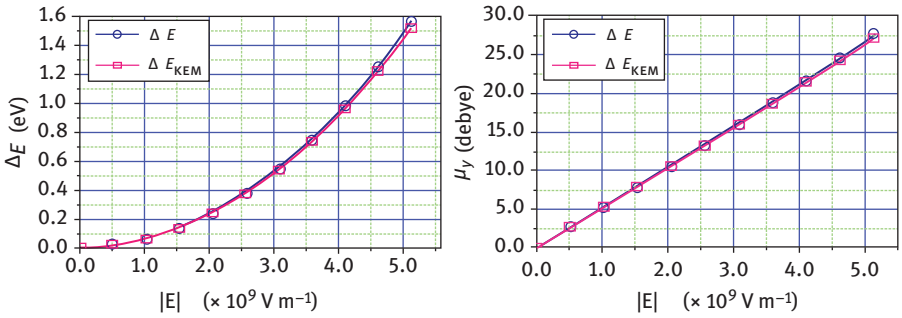

Fig. 6.4: A graphical comparison of the change in the total energy (ΔE) and the dominant (induced) dipole moment component μ_y as a function of the field strength along the *y*-direction (the long axis of the graphene nanoribbon) calculated directly versus those calculated from KEM. The changes in the KEM energies are obtained from differences between eq. (6.3) obtained from the field-free case and that in a given field, while a similar procedure has been implemented to compute the values in the plot for the dipole moment, this time using eq. (6.6) (results of calculations at the MP2/6-311G (2*d*, 2*p*) level of theory). See Ref. [18] for details.

6.4 The kernel energy method and the calculation of properties of atoms in molecules

Richard F. W. Bader developed a theory of chemistry on the basis of a topological and topographical analysis of electron density known as the quantum theory of atoms in molecules (QTAIM) [27–31]. This theory starts by analyzing the gradient

vector field associated with the electron density ($\nabla\rho$) and, in doing so, the various critical points are located (where the gradient of the density vanishes, $\nabla\rho = \mathbf{0}$) as well as the separatrices that split the molecular density into mono-nuclear atomic regions. Stable critical points that can be found in an isolated molecule must satisfy the Poincaré–Hopf relation (an adaptation of Euler's topological identity) [27]:

$$n_{\mathrm{NCP}} - n_{\mathrm{BCP}} + n_{\mathrm{RCP}} - n_{\mathrm{CCP}} = 1, \tag{6.7}$$

where, n refers to the "number" of a given type of critical point and where NCP refers to *nuclear critical points* (local maxima in the electron density, each NCP exhibits three negative curvatures), BCP refers to *bond critical points* (a maximum in two orthogonal directions but a minimum along the third, two negative curvatures); RCP refers to *ring critical points* (a minimum in two orthogonal directions but a maximum along the third, two positive curvatures), and finally CCP which refers to *cage critical points* (local minimum, exhibiting three positive curvatures).

It is noteworthy that the pair of NCPs of two chemically bonded atoms exhibits a bond path linking them, that is, a line of locally maximal electron density linking these two nuclei [32, 33]. The bond path usually corresponds to the known "chemical bond", however, it exhibits no bond multiplicity *per se* save for the values determined at the associated bond critical point which numerically give away the nature and strength of the chemical bonding.

The separatrices between the bonded atoms are surfaces of local zero-flux in the gradient of the electron density, that is, satisfying the following boundary condition at every point belonging to the surface [27]:

$$\nabla\rho(\mathbf{r}) \cdot \mathbf{n}(\mathbf{r}) = 0, \tag{6.8}$$

where $\mathbf{n}(\mathbf{r})$ is the normal unit vector on the surface at the point specified by the position vector $\mathbf{r}$ which is, in Cartesian coordinates, $\mathbf{r} \equiv \hat{e}_x x + \hat{e}_y y + \hat{e}_z z$. The union of several of these surfaces is usually bounding an atom in a molecule, in addition to an external isodensity envelope (for atoms exposed to the exterior) [29]. As for that isodensity, the envelope with $\rho = 0.001$ au usually encloses >99% of the molecular electron population in the vacuum phase and, because of that, it is taken as the outer molecular surface up to which numerical integrals are evaluated [27]. In the condensed or solvated phase, this isodensity is higher and equals 0.002 au.

Mononuclear regions surrounded by zero-flux surfaces are identified as the atoms-in-the-molecule (AIMs) and they have been shown to behave as open quantum sub-systems with well-defined properties including at least two forms of the kinetic

energy.[1] Since the average electronic kinetic energy is well-defined for an AIM (in at least two of its most used forms), and by virtue of an atomic expression of the virial theorem, postulated [34] and then demonstrated [27, 35–37], any region bounded by a zero-flux surface has a well-defined (atomic) energy. These atomic energies have the desirable property of being additive yielding the total molecular energy when summed over all the atoms composing the molecule.

Furthermore, once the atomic basins are defined on the basis of the electron density, any property density can be integrated over these spatial domains to obtain the corresponding quantum average over the atom of interest. This is no longer limited to one-electron properties even though the electron density that led to the spatial partitioning is itself a one-electron property. Hence, one can obtain energies (which include electron–electron terms) and electron localization and delocalization indices (LIs and DIs) which involve integrals of the Fermi (and Coulomb) holes over one or a pair of atomic basins, respectively.

The DIs, $\delta(\Omega_i,\Omega_j)$, count the number of electrons delocalized (or shared) between pairs of basins (Ω_i and Ω_j) which, for a closed-shell molecule at a single determinant level, is written [38]:

$$\delta(\Omega_i,\Omega_j) = 2\left|F^{\alpha}(\Omega_i,\Omega_j)\right| + 2\left|F^{\beta}(\Omega_i,\Omega_j)\right|, \tag{6.9}$$

in which the Fermi correlation is obtained by integrating the product $\varphi_k^*(\mathbf{r}_1)\varphi_l(\mathbf{r}_1)$ $\varphi_l^*(\mathbf{r}_2)\varphi_k(\mathbf{r}_2)$ sweeping $\mathbf{r}_1$ over the volume of Ω_i and $\mathbf{r}_2$ over the volume of Ω_j and summing over all occupied spin orbitals φ_k and φ_l:

$$F^{\sigma}(\Omega_i,\Omega_j) = -\sum_{k}^{occ}\sum_{l}^{occ}\int_{\Omega_i}\int_{\Omega_j}\varphi_k^*(\mathbf{r}_1)\varphi_l(\mathbf{r}_1)\varphi_l^*(\mathbf{r}_2)\varphi_k(\mathbf{r}_2)d\mathbf{r}_1 d\mathbf{r}_2 \tag{6.10}$$

$$= -\sum_{k}^{occ}\sum_{l}^{occ} S_{kl}(\Omega_i)\ S_{lk}(\Omega_j), \tag{6.11}$$

where $S_{kl}(\Omega_i) = S_{lk}(\Omega_i)$ represents the overlap integral of the given pair of spin orbitals over basin Ω_i. In the above equations, σ refers to a given spin, α or β.

For methods of calculation involving a single determinant, the first order reduced density matrix determines all the properties of the system. Except when dynamical correlation is important, the Müller approximation [39] has been shown to

1 Occasionally one encounters maxima in the electron density at positions other than at the nuclei. These maxima are termed nonnuclear attractors (NNAs) or nonnuclear maxima (NNM). They behave as pseudo-atoms in a molecule and can be characterized with all the properties normally assigned to atoms except the nuclear charge/mass since there are no nuclei. These entities define a pseudo-atomic basin surrounded by zero-flux surface(s) as any "real" atom. See Ref. [51] and literature cited within.

be relatively accurate in obtaining a second-order density matrix from the first order density matrix [40].

Setting $i = j$ in eqs. (6.10) and (6.11), that is, when the two integrals are over one and the same basin, the product $S_{kl}(\Omega_i)S_{lk}(\Omega_j)$ collapses to $[S_{kl}(\Omega_i)]^2$ which measures the Fermi correlation of the electrons in that basin. In this case, we have defined the localization index (LI) written as [38]:

$$\Lambda(\Omega_i, \Omega_i) = |F^{\alpha}(\Omega_i, \Omega_i)| + \left|F^{\beta}(\Omega_i, \Omega_i)\right|. \tag{6.12}$$

The LIs and DIs are not independent since an atom's electron population is, in part, residing within that atom and, in part, shared with every other atom in the molecule. The population of atom i can be written in terms of the following bookkeeping formula [38]:

$$N(\Omega_i) = \Lambda(\Omega_i) + \frac{1}{2}\sum_{j\neq i}^{n} \delta\left(\Omega_i, \Omega_j\right) = \int_{\Omega_i} \rho(\mathbf{r}) d\mathbf{r}. \tag{6.13}$$

In this manner, the population of Ω_i can be obtained either from the middle equality (which we call the "Bader summation") given the LI and all the DIs involving that atom. The population can also be accessed from the last equality by integration of the electron density over the ith atomic basin. With the atomic population $N(\Omega_i)$ and the atomic number Z_{Ω_i}, one finds the net atomic charge ($q(\Omega_i)$ in au) from:

$$q(\Omega_i) = Z_{\Omega_i} - N(\Omega_i). \tag{6.14}$$

Finally, given the Bader summation relating the LI and the DIs of a given atom to its total electron population, the full set of LIs and DIs characterizing a molecule can be cast in an electron localization–delocalization matrix (LDM) [41–46]:

$$\begin{array}{l} \\ \text{LDM} \equiv \\ \\ \\ \\ \sum\limits_{\text{column}} \end{array} \begin{array}{c} \\ \left[\begin{array}{cccc} \Lambda(\Omega_1) & \delta(\Omega_1,\Omega_2)/2 & \cdots & \delta(\Omega_1,\Omega_n)/2 \\ \delta(\Omega_2,\Omega_1)/2 & \Lambda(\Omega_2) & \cdots & \delta(\Omega_2,\Omega_n)/2 \\ \vdots & \vdots & \ddots & \vdots \\ \delta(\Omega_n,\Omega_1)/2 & \delta(\Omega_n,\Omega_2)/2 & \cdots & \Lambda(\Omega_n) \end{array}\right]_{n\times n} \\ \\ \underbrace{\qquad\qquad\qquad\qquad\qquad\qquad\qquad\qquad}_{\sum\limits_{i=1}^{n} N(\Omega_i) = N} \end{array} \begin{array}{l} \sum\limits_{\text{row}} \\ \\ = N(\Omega_1) \\ = N(\Omega_2) \\ \vdots \\ = N(\Omega_n) \\ \\ \text{tr(LDM)} = N_{\text{loc}} \end{array} \begin{array}{l} \\ \\ \\ \\ \left.\begin{array}{l} \\ \\ \\ \\ \end{array}\right\} \sum\limits_{i=1}^{n} N(\Omega_i) = N. \\ \\ \\ \\ \end{array} \tag{6.15}$$

The sum over the matrix elements in any row or column of an LDM is, by Bader summation, the population $N(\Omega_i)$ of the atom represented by that row or column. The sum of all atomic populations is the total molecular electron population N. Finally, the trace of the LDM represents the number of all electrons that are localized within basins over the entire molecule (N_{loc}) and, by difference; the delocalized population can be obtained.

In the work about to be described, formulae analogous to eq. (6.3) were used to predict the localization and delocalization indices, and have been shown to work with high accuracy. The formula for the DIs is [43]:

$$\delta_{KEM}(\Omega_i,\Omega_j)=\sum_{a=1}^{n-1}\sum_{b=a+1}^{n}\left[\delta_{ab}(\Omega_i,\Omega_j)\right]_{\Omega_i\wedge\Omega_j\in K_{ab}}-(n-2)\sum_{c=1}^{n}\left[\delta_c(\Omega_i,\Omega_j)\right]_{\Omega_i\wedge\Omega_j\in K_c}, \quad (6.16)$$

while the LIs are approximated as:

$$\Lambda_{KEM}(\Omega_i)=\sum_{a=1}^{n-1}\sum_{b=a+1}^{n}\left[\Lambda_{ab}(\Omega_i)\right]_{\Omega_i\in K_{ab}}-(n-2)\sum_{c=1}^{n}\left[\Lambda_{ab}(\Omega_i)\right]_{\Omega_i\in K_c}. \quad (6.17)$$

Finally, a similar equation has been used to approximate the value of the electron density at the various critical points [43]:

$$\begin{aligned}\rho_{KEM}(\mathbf{r}_{BCP(\Omega_i|\Omega_j)})=&\sum_{a=1}^{n-1}\sum_{b=a+1}^{n}\left[\rho_{ab}(\mathbf{r}_{BCP(\Omega_i|\Omega_j)})\right]_{\Omega_i\wedge\Omega_j\in K_{ab}}\\&-(n-2)\sum_{c=1}^{n}\left[\rho_c(\mathbf{r}_{BCP(\Omega_i|\Omega_j)})\right]_{\Omega_i\wedge\Omega_j\in K_c},\end{aligned} \quad (6.18)$$

where $\rho_{KEM}(\mathbf{r}_{BCP(\Omega_i|\Omega_j)})$ is the KEM approximation to density at a bond critical point between the nuclei of the *i*th and *j*th atoms, and where the vertical bar "|" symbolizes the separatrix separating these two basins. The same form of eq. (6.18) is also used to estimate the densities at the ring critical points. In eq. (6.18) and in analogy with eq. (6.3), ρ_{ab} and ρ_c are the densities at the BCPs of the *ab*th (double) and the *c*th (single) kernel. An additional condition for the inclusion of a kernel's contributions into the sum is the existence of the BCP in the kernel in question (which contrasts such a local property at a specific point in space with a global property such as the energy to which *all* of the kernels do contribute.

Figure 6.5 (*top*) provides an example of how well electron densities at bond and ring critical points are recovered (all values in the figure are identical, up to the adopted precision, whether calculated directly or approximated from KEM). This shows that the electron density is well reproduced on a point-by-point basis from the KEM approximation.

These latter findings amplify earlier work where KEM has been shown to approximate QTAIM charges to a similar accuracy on a number of small peptides [47]. If one can recover the electron density on a point-by-point basis, it is perhaps not

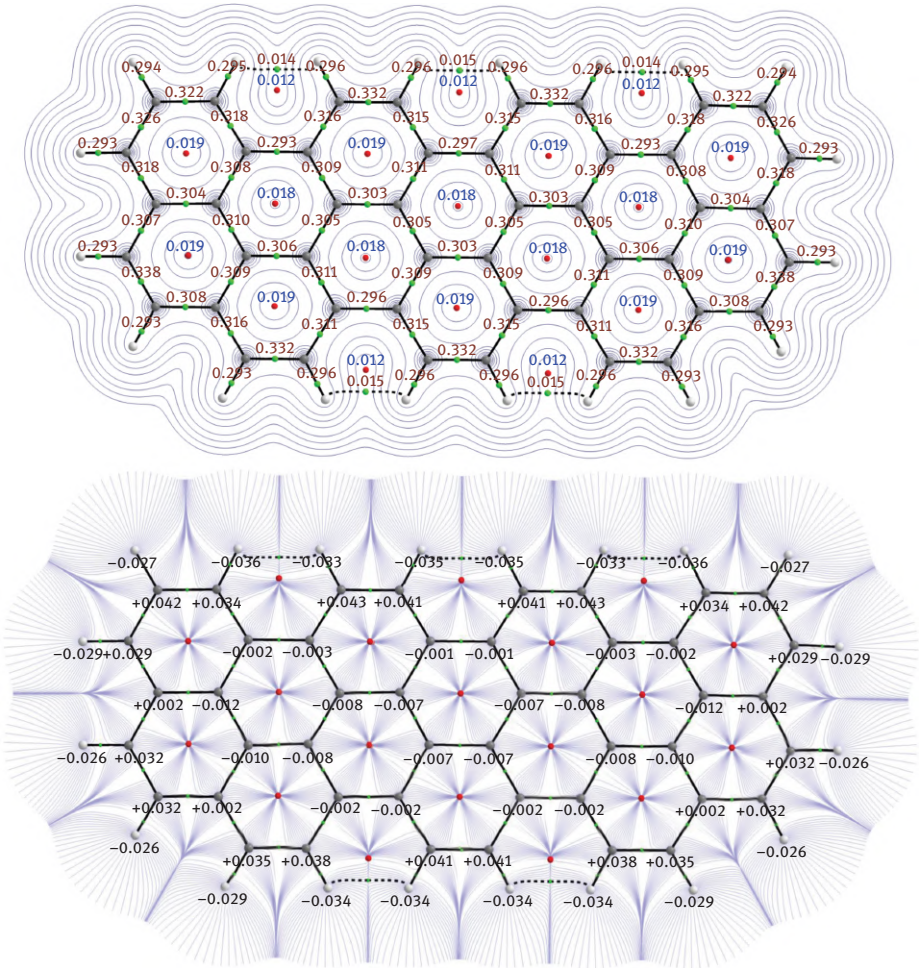

Fig. 6.5: *Top*: A contour map representation of the electron density in the σ_v' symmetry plane of a $C_{46}H_{20}$ hydrogen-terminated graphene nanoribbon. The contours from the outside inward are in au: 0.001, 0.002, 0.004, 0.008, 0.02, 0.04, 0.08, 0.2, 0.4, and 0.8. Superimposed on the figure is the molecular graph, that is, the lines of maximal electron density linking bonded nuclei. The bond paths include those between van der Waals bonded neighboring hydrogen atoms in "bay" regions (known as H . . . H bonding [48–50]) – represented by broken lines. The dots on the bond paths represent the bond critical points while those within rings are the ring critical points. The label near a critical point is the magnitude of the electron density at this point (in au). *Bottom:* The molecular graph with the superimposition of the gradient vector field of the electron density. The interatomic surfaces of zero-flux (separatrices) between bonded atoms delimit them from one another as nonoverlapping regions of space [29]. Each basin is labeled by its QTAIM atomic charge $q(\Omega)$ (eq. (6.14)). All quoted values are identical whether from the direct calculation or from the KEM reconstruction up to and including the given decimal precision. The calculations were performed at the HF/6–31+G(d,p) level of theory. (Reprinted from Ref. [43] with permission of the copyright holder © 2014 *The American Chemical Society*).

totally surprising that the integral of the density is also recovered accurately. The novelty in the case of the graphene nanoribbon is the added challenge of representing this delocalized fused benzenoid ring system within the KEM approximation, including but not limited to challenges as to how to split the system into kernels [43].

Using 14-aromatic ring/66 atom hydrogen-terminated graphene nanoribbon ($C_{46}H_{20}$), depicted in Fig. 6.3 along with the KEM fragmentation, Timm et al. have shown that its 66 × 66 LDM can be reconstructed from eqs. (6.16) and (6.17) with accuracy [43]. The LDM of $C_{46}H_{20}$ consists of 66 LIs along its diagonal and 4,290 DIs/2 (only half of which are unique since $\delta_{ij} = \delta_{ji}$).

The overall average % error in the LIs and the DIs/2 introduced by the KEM approximation in the case of a carbon atom is 0.02 ± 0.03%, and 0.01 ± 0.01% for an average hydrogen atom. Meanwhile, the cumulative integration errors in the total electron population of this 296-electron molecule are +0.0003 e^- for the direct calculation (+0.0001%) and +0.0022 e^- for the KEM (+0.0007%). Finally, the full sets of electron densities at the 84 bond critical points and 19 ring critical points calculated from the KEM approach are identical, within and including three decimals (in au), to the directly calculated results.

6.5 Closing remarks

In Chapter 5, we outlined the foundation and formalism of the KEM. The present chapter illustrates some of its applications. These start with the accurate and fast estimation of the total and interaction energies of a variety of large biological macromolecules from insulin to an entire viral capsid protein with more than 33,000 atoms. The versatility of KEM is also demonstrated in that it can be applied to virtually any large system including nucleic acids such as double stranded DNA and RNA whether in the protoribosome or in tRNA.

The next leap is in the application of KEM to nanotechnological materials. A relevant example of the latter class is graphene especially under the perturbation of a relatively intense external electric field. The problem is challenging since (i) the system is delocalized with an infinity of fused benzenoid rings in a planar arrangement raising the question as to how to fragment this system into kernels, and (ii) the imposed field induces charge transfers across the boundaries of neighboring kernels in the intact molecule, so how can this flow of charge be represented in the fragmented system? It is shown that KEM can be used to predict the global/molecular-field-induced response properties.

Another question is whether KEM can recover properties such as the electron density at specified points and properties of atoms-in-molecules (AIMs) - as defined within QTAIM - including two-electron properties such as the complete set of LIs and DIs? The answer appears to be “yes,” at least for the studied graphene system.

KEM-like formulae have been used to predict the electron density and electron pair density-derived properties. Nevertheless, a more fundamentally founded approach would be to, first, calculate the one-body and two-body reduced density matrices, and then use these density matrices to compute two electron properties. This is work relegated to the future. Here, the postulate that the form of eq. (6.3), when applied to other properties, is empirically demonstrated to work.

Many problems remain to be solved for a universal applicability of the KEM approach. Among them is the inclusion in KEM's formulation the ability to treat systems carrying net charges, open-shell systems, excited electronic states, crystal unit cells including the adaptation to periodic calculations. Also, remaining to be solved is the calculation of vibrational frequencies, geometry optimizations, and the estimation of UV/Vis spectra within this approximation.

References

[1] Huang, L, Massa, L, Karle, J. Quantum kernels and quantum crystallography: Applications in biochemistry. Chapter 1 in: *Quantum Biochemistry: Electronic Structure and Biological Activity (Vol. 1)*; Matta, CF (Ed.), Wiley-VCH, Weinheim (2010), 3–60.

[2] Huang, L, Massa, L, Karle, J. The kernel energy method of quantum mechanical approximation carried to fourth-order terms. *Proc. Natl. Acad. Sci. USA* 105, 1849–1854 (2008).

[3] Huang, L, Massa, L, Karle, J. Kernel energy method illustrated with peptides. *Int. J. Quantum Chem.* 103, 808–817 (2005).

[4] Karle, J. Kernel energy method illustrated with peptides. *56th Lindau Nobel Laureate Meeting (https://www.mediatheque.lindau-nobel.org/videos/31296/kernel-energy-method-illustrated-with-peptides-2006)* (2006).

[5] Huang, L, Massa, L, Karle, J. Kernel energy method: Application to insulin. *Proc. Natl. Acad. Sci. USA* 102, 12690–12693 (2005).

[6] Huang, L, Massa, L, Karle, J. Kernel energy method applied to vesicular stomatitis virus nucleoprotein. *Proc. Natl. Acad. Sci. USA* 106, 1731–1736 (2009).

[7] Huang, L, Massa, L, Karle, J. Kernel energy method: Application to DNA. *Biochemistry* 44, 16747–16752 (2005).

[8] Huang, L, Massa, L, Karle, J. The kernel energy method: Application to a tRNA. *Proc. Natl. Acad. Sci. USA* 103, 1233–1237 (2006).

[9] Huang, L, Krupkin, M, Bashan, A, Yonath, A, Massa, L. Protoribosome by quantum kernel energy method. *Proc. Natl. Acad. Sci. USA* 110, 14900–14905 (2013).

[10] Yonath, A. Quantum mechanic glimpse into peptide bond formation within the ribosome shed light on origin of life. *Struct. Chem.* 28, 1285–1291 (2017).

[11] Cech, TR. The RNA worlds in context. *Cold Spring Harb. Perspect. Biol.* 4, a006742 (2012).

[12] Neveu, M, Kim, HJ, Benner, SA. The "strong" RNA world hypothesis: Fifty years old. *Astrobiol* 13, 391–403 (2013).

[13] Novoselov, KS, Geim, AK, Morozov, SV, Jiang, D, Zhang, Y, Dubonos, SV, Grigorieva, IV, Firsov, AA. Electric field effect in atomically thin carbon films. *Science* 306, 666–669 (2004).

[14] Novoselov, KS, Jiang, D, Schedin, F, Booth, TJ, Khotkevich, VV, Morozov, SV, Geim, AK. Two-dimensional atomic crystals. *Proc. Natl. Acad. Sci. USA* 102, 10451–10453 (2005).

[15] Springborg, M. *Methods of Electronic-Structure Calculations: From Molecules to Solids*. John Wiley & Sons, Ltd., New York, (2000).
[16] Sivaramakrishnan, R, Tranter, RS, Brezinsky, K. Ring conserved isodesmic reactions: A new method for estimating the heats of formation of aromatics and PAHs. *J. Phys. Chem. A* 109, 1621–1628 (2005).
[17] Huang, L, Bohórquez, H, Matta, CF, Massa, L. The kernel energy method: Application to graphene and extended aromatics. *Int. J. Quantum Chem.* 111, 4150–4157 (2011).
[18] Huang, L, Massa, L, Matta, CF. A graphene flake under external electric fields reconstructed from field-perturbed kernels. *Carbon* 76, 310–320 (2014).
[19] Bai, C. *Scanning Tunneling Microscopy and its Applications (Second Edition)*. Springer, Berlin, (1992).
[20] Stroscio, JA, Kaiser, WJ. *Scanning Tunneling Microscopy*. Academic Press, New York, (1993).
[21] Keldysh, LV. Ionization in the field of a strong electromagnetic wave. *Sov. Phys. JETP* 20, 1307–1314 (1965).
[22] Long, ZJ, Liua, W-K. Keldysh theory of strong-field ionization. *Can. J. Phys.* 88, 227–245 (2010).
[23] Sowlati-Hashjin, S, Matta, CF. The chemical bond is external electric fields: Energies, geometries, and vibrational Stark shifts of diatomic molecules. *J. Chem. Phys.* 139, 144101 (2013).
[24] Turro, NJ. *Modern Molecular Photochemistry*. University Science Books, Sausalito, CA, (1991).
[25] Hovick, JW, Poler, JC. Misconceptions in sign conventions: Flipping the electric dipole moment. *J. Chem. Edu.* 82, 889 (2005).
[26] Coulson, CA. *Electricity*. Oliver and Boyd, London, (1961).
[27] Bader, RFW. *Atoms in Molecules: A Quantum Theory*. Oxford University Press, Oxford, U.K., (1990).
[28] Matta, CF. On the connections between the quantum theory of atoms in molecules (QTAIM) and density functional theory (DFT): A letter from Richard F. W. Bader to Lou Massa. *Struct. Chem.* 28, 1591–1597 (2017).
[29] Bader, RFW, Matta, CF. Atoms in molecules as non-overlapping, bounded, space-filling open quantum systems. *Found. Chem.* 15, 253–276 (2013).
[30] Popelier, PLA. *Atoms in Molecules: An Introduction*. Prentice Hall, London, (2000).
[31] Matta, CF, Boyd, RJ (Eds.). *The Quantum Theory of Atoms in Molecules: From Solid State to DNA and Drug Design*. Wiley-VCH, Weinheim, (2007).
[32] Bader, RFW. A bond path: A universal indicator of bonded interactions. *J. Phys. Chem. A* 102, 7314–7323 (1998).
[33] Runtz, GR, Bader, RFW, Messer, RR. Definition of bond paths and bond directions in terms of the molecular charge distribution. *Can. J. Chem.* 55, 3040–3045 (1977).
[34] Bader, RFW, Beddall, PM. Virial field relationship for molecular charge distributions and the spatial partitioning of molecular properties. *J. Chem. Phys.* 56, 3320–3329 (1972).
[35] Bader, RFW, Beddall, PM, Peslak, J. Theoretical development of a virial relationship for spatially defined fragments of molecular systems. *J. Chem. Phys.* 58, 557–566 (1973).
[36] Srebrenik, S, Bader, RFW. Towards the development of the quantum mechanics of a subspace. *J. Chem. Phys.* 63, 3945–3961 (1975).
[37] Srebrenik, S, Bader, RFW, Nguyen-Dang, TT. Subspace quantum mechanics and the variational principle. *J. Chem. Phys.* 68, 3667–3679 (1978).
[38] Fradera, X, Austen, MA, Bader, RFW. The Lewis model and beyond. *J. Phys. Chem. A* 103, 304–314 (1999).
[39] Müller, AMK. Explicit approximate relation between reduced two- and one-particle density matrices. *Phys. Lett. A* 105, 446–452 (1984).

[40] Outeiral, C, Vincent, MA, Martín-Pendás, Á, Popelier, PLA. Revitalizing the concept of bond order through delocalization measures in real space. *Chem. Sci.* 9, 5517–5529 (2018).
[41] Matta, CF. Modeling biophysical and biological properties from the characteristics of the molecular electron density, electron localization and delocalization matrices, and the electrostatic potential. *J. Comput. Chem.* 35, 1165–1198 (2014).
[42] Sumar, I, Ayers, PW, Matta, CF. Electron localization and delocalization matrices in the prediction of pK_a's and UV-wavelengths of maximum absorbance of *p*-benzoic acids and the definition of super-atoms in molecules. *Chem. Phys. Lett.* 612, 190–197 (2014).
[43] Timm, MJ, Matta, CF, Massa, L, Huang, L. The localization-delocalization matrix and the electron density-weighted connectivity matrix of a finite graphene nanoribbon reconstructed from kernel fragments. *J. Phys. Chem. A* 118, 11304–11316 (2014).
[44] Matta, CF. Localization-delocalization matrices and electron density-weighted adjacency matrices: New electronic fingerprinting tools for medicinal computational chemistry. *Future Med. Chem.* 6, 1475–1479 (2014).
[45] Dittrich, B, Matta, CF. Contributions of charge-density research to medicinal chemistry. *Int. U. Cryst. J. (IUCrJ)* 1, 457–469 (2014).
[46] Sumar, I, Cook, R, Ayers, PW, Matta, CF. AIMLDM: A program to generate and analyze electron localization-delocalization matrices (LDMs). *Comput. Theor. Chem.* 1070, 55–67 (2015).
[47] Huang, L, Matta, CF, Massa, L. The kernel energy method (KEM) delivers fast and accurate QTAIM electrostatic charge for atoms in large molecules. *Struct. Chem.* 26, 1433–1442 (2015).
[48] Matta, CF, Hernández-Trujillo, J, Tang, TH, Bader, RFW. Hydrogen-hydrogen bonding: A stabilizing interaction in molecules and crystals. *Chem. Eur. J.* 9, 1940–1951 (2003).
[49] Matta, CF. Hydrogen-hydrogen bonding: The non-electrostatic limit of closed-shell interaction between two hydrogen atoms. A critical review. Chapter 9 in: *Hydrogen Bonding – New Insight*; Grabowski, S (Ed.), Springer (2006), 337–376.
[50] Hernández-Trujillo, J, Matta, CF. Hydrogen-hydrogen bonding in biphenyl revisited. *Struct. Chem.* 18, 849–857 (2007).
[51] Anderson, JSM, Massa, L, Matta, CF. Non-nuclear maxima and the universality of Bright Wilson's justification of the first Hohenberg Kohn theorem revisited. *Chem. Phys. Lett.* 780, Article # 138940, 1–6 (2021).

Chapter 7
The quantum theory of atoms in molecules

Like all other stars, the Sun is believed to have condensed from a large diffuse gas cloud. . . . [I]t can be easily shown that there is a balance between the total gravitational energy V, which is negative, and the kinetic energy T of the stellar material, such that

$$2T + V = 0.$$

This is the virial theorem of Poincaré and Eddington and is valid provided no other forces, such as electromagnetic forces, play a significant role in the hydrostatic balance. . . . The total energy of the star is

$$E = T + V$$

which, by the virial theorem, is simply −T. As energy is radiated from the surface of a star, E decreases and, consequently, T rises. This is perhaps the most important property of a self-gravitating body, and leads to a natural accentuation of the temperature difference between the body and its surroundings.[1] Douglas Gough (1977)

(*In: The Encyclopaedia of Ignorance: Everything you ever wanted to Know about the Unknown, Ronald Duncan and Miranda Weston-Smith (Editors), Pergamon Press, Oxford, 1977*)

The electron density determined by crystallography and its associated density matrices (or the corresponding wave functions) are frequently analyzed in the crystallographic literature using Richard F. W. Bader's quantum theory of atoms in molecules (QTAIM). The physical foundations of the theory are best described in Bader's 1990 book on the subject. In this chapter, a short summary distilled from that book is presented aiming at showing the founding of QTAIM in the physics of open systems. The chapter starts by reviewing the observational bases of QTAIM, in particular, the definition of the bonded topology through an examination of the topography of the entire scalar field of the electron density. Concepts such as Bader's zero-flux boundary between chemically bonded atoms and its associated bond path are reviewed. The development of the quantum mechanics for such open subsystems as atoms-within-a-molecule is shown to coincide with the partitioning suggested by the shape of the gradient vector field associated with the electron density.

7.1 From topography to topology

Boundaries are inextricably associated with form and with the idea of space filling matter. Atoms and groups of atoms, whether in a molecule or in a crystal, are real space-filling objects endowed with a form dictated by their bounding surfaces. Bounded atoms contrast with the widely shared view that atoms overlap. A common-sense argument that appears in one of Bertrand Russell books states:

1 In the original text, the symbol for the potential energy is Ω, but was replaced here with V to align the symbols with their counterparts in this chapter.

https://doi.org/10.1515/9783110566673-008

> Or, to take Aristotle's examples, if a man makes a bronze sphere, bronze is the matter, and sphericity is the form; while in the case of a calm sea, water is the matter and smoothness is the form. So far, all is simple.
>
> He goes on to say that it is in virtue of the form that the matter is some one definite thing, and this is the substance of the thing. *What Aristotle means seems to be plain common sense: a "thing" must be bounded, and the boundary constitutes its form. . . . We* should not naturally say that it is the form that confers substantiality, but that is because the atomic hypothesis is ingrained in our imagination. *Each atom, however, if it is a "thing," is so in virtue of its being delimited from other atoms, and so having, in some sense, a "form."*[2] Bertrand Russell [[1], p.165]

The quantum theory of atoms in molecules (QTAIM) developed by Richard F. W. Bader [2–7] defines atoms in real space by specifying their bounding surface and hence determines their form. From this idea, the theory follows taking the electron density as its object of analysis. A year before the birth of modern density functional theory with the appearance in 1964 of the well-known paper of Pierre Hohenberg and Walter Kohn [8], Bader and Glenys A. Jones make, in 1963, the following remark [9]:

> The manner in which the electron density is disposed in a molecule has not received the attention its importance would seem to merit. Unlike the energy of a molecular system which requires a knowledge of the second-order density matrix for its evaluation [10] many of the observable properties of a molecule are determined in whole or in part by the simple three-dimensional electron-density distribution. In fact, these properties provide a direct measure of a wide spectrum of different moments averaged directly over the density distribution. Thus the diamagnetic susceptibility, the dipole moment, the diamagnetic contribution to the nuclear screening constant, the electric field, and the electric field gradient (as obtained from nuclear quadrupole coupling constants) provide a measure of (aside from any angular dependencies) $\langle r_i^2 \rangle$, $\langle r_i \rangle$, $\langle r_i^{-1} \rangle$, $\langle r_i^{-2} \rangle$, and $\langle r_i^{-3} \rangle$, respectively. The electric field at a nucleus due to the electron density distribution is of particular interest due to the theorem derived by Hellmann [11] and Feynman [12]. They have demonstrated that the force acting on a nucleus in a molecule is determined by the electric field at that nucleus due to the other nuclei and to the electron-density distribution. Richard F. W. Bader and Glenys A. Jones (1963).

The electron density, as it turns out, determines all the properties of the system's ground and excited states by virtue of the first Hohenberg–Kohn (HK-1) theorem [8] discussed in Chapter 2. Restated symbolically here, the HK-1 theorem implies the following relations:

$$\rho(\mathbf{r}) \rightarrow \left\{ \begin{array}{c} V[\rho(\mathbf{r})] \\ N[\rho(\mathbf{r})] \end{array} \right\} \rightarrow \hat{H} \rightarrow \{\Psi_i\}, \tag{7.1}$$

where $i = 0, 1, 2 \ldots \infty$ refers to the electronic states, which tells us that $\rho(\mathbf{r})$, the nondegenerate ground-state electron density, fixes the external potential (V) and the total number of electrons (N), and hence determines the Hamiltonian uniquely. Given a particular Hamiltonian, dictated by $\rho(x, y, z)$, all the eigenfunctions and eigenvalues of the ground- and excited states are fixed. As remarked by Bader and Jones [9], the electron density determines *many of the observable properties of a*

2 Second and last sentences of the second paragraph are italicized by the present authors.

molecule. We now know, by virtue of HK-1 theorem, that the electron density determines *all* the properties of the system despite that the exact mapping relation of the density to some of these properties remains unknown.

The electron density is defined as [2]:

$$\rho(\mathbf{r}) = N \sum_{\omega_i} \int \ldots \int \Psi^*(\mathbf{x}_1, \ldots, \mathbf{x}_N)\, \Psi(\mathbf{x}_1, \ldots, \mathbf{x}_N)\, d\mathbf{x}_2, \ldots, d\mathbf{x}_N, \tag{7.2}$$

where

$$\mathbf{x}_i \equiv (x_i, y_i, z_i, \omega_i), \ \mathbf{r} \equiv (x, y, z), \tag{7.3}$$

and where Ψ is an antisymmetric many-electron wave function, $\mathbf{r}$ is a position vector specifying a point in three-dimensional space ($\mathbf{r} = x\mathbf{e}_x + y\mathbf{e}_y + z\mathbf{e}_z \equiv \{x, y, z\}$, where $\mathbf{e}_x$, $\mathbf{e}_y$, and $\mathbf{e}_z$ are the unit vectors in the Cartesian representation), and $\mathbf{x}_i$ is the set of four space and spin coordinates of electron *i*. This mode of integration, that is, integrating over the coordinates of all electrons except one followed by summation over both spins, is often replaced by the following shorthand notation in the QTAIM literature:

$$\sum_{\omega_i} \int \ldots \int f(\mathbf{x}_1, \ldots, \mathbf{x}_N)\, d\mathbf{x}_2, \ldots, d\mathbf{x}_N \equiv \int f\, d\tau'. \tag{7.4}$$

In this notation, the electron density is expressed as:

$$\rho(\mathbf{r}) = N \int \Psi^* \Psi\, d\tau'. \tag{7.5}$$

As discussed in Chapter 1, the electron density, being a periodic function in the space of the crystal, can be expressed as a Fourier series [13–16]:

$$\rho(x, y, z) = \frac{1}{V} \sum_h \sum_k \sum_l F(hkl) \exp\left[-2\pi i(hx + ky + lz)\right], \tag{7.6}$$

where V is the volume of the unit cell and $F(hkl) \equiv F(\mathbf{H})$ are the Fourier coefficients (the *structure factors*) determined from the experimental data after the resolution of the phase problem.

Equations (7.2), (7.5), and (7.6) deliver the same object, that is, $\rho(x, y, z)$. Thus, the electron density can be approached from two directions: *Experiment* – using the set of phased experimental structure factors $\{F(\mathbf{H})\}$, and *theory* – using a properly antisymmetrized many-electron wave function $\Psi(\mathbf{x}_1, \ldots, \mathbf{x}_N)$. Symbolically, recalling relation (1.21) from Chapter 1, we may express these relations as:

$$\left[\begin{array}{c}\textbf{theory}\\(\text{quantum mechanics})\end{array}\right] \Psi(\mathbf{x}_1, \ldots, \mathbf{x}_N) \rightarrow \boxed{\rho(\mathbf{r})} \leftarrow \{F(\mathbf{H})\} \left[\begin{array}{c}\textbf{experiment}\\(\text{crystallography})\end{array}\right]. \tag{7.7}$$

The electron density, hence, plays the dual role as (*a*) an *intermediary between theory and experiment*, and (*b*) as a *carrier of all the quantum mechanical information* that can be known about the system (in principle). Further, the electron density is the embodiment of the form of matter itself as introduced above. In recent decades, the QTAIM has been developed on the foundation of this scalar field, the electron density, taking it as its point of departure for a complete theory of matter in its common physical states. QTAIM then analyzes either the density itself in terms of atomic or atom–atom interaction terms and/or analyzes the wave function over atoms or groupings of atoms to extract chemical information, as we shall see later in this chapter. QTAIM is not meant to replace or compete with molecular orbital theory (MO theory) [17–22] or valence bond theory (VB theory) [23–25], it complements both. This is so since at a final analysis, both MO or VB theories deliver the many-electron wave function of the system which can then be used to obtain the density (eq. (7.5)) after which the density and/or the wave function may be analyzed with QTAIM. Of course MO and VB models offer many useful ways to interpret and predict chemistry, one analyzes orbitals and their contributions (MO-models) while the latter analyzes VB structures and their contributions (VB-models). QTAIM offers an alternative approach, that is, it can analyze the density (accessible from both theory and experiment) and also wave functions/density matrices (which are normally accessible only from theory). In this manner, and since quantum crystallography offers an orbital description consistent with the experimental data, it may be followed by any one of these forms of analysis: QTAIM, MO models, or VB models.

The QTAIM, which has been reviewed extensively [2–7, 26–29], starts by defining atoms in real (direct) space as separate nonoverlapping three-dimensional blocks of electron density with a form dictated by an atom's electronic environment. The disjoint and exhaustive partitioning of space leads to: (i) The ability to define the interactions of this atomic space (an atom-in-a-molecule (AIM)) with other AIMs in the system, and (ii) allowing one to integrate property densities over that volume.

But how do we define the boundary of an AIM? To answer this question, we examine the topography and the topology of the electron density in three-dimensional space. The attractive force exerted by the positively charged nuclei on the electron density stamps it with its principal feature, that is, the presence of cusps at the positions of the nuclei. These cusps are singularities that reflect the neglect of the finite nuclear size in molecular Hamiltonians which are in common use (see Chapter 2). To incorporate the nuclear size would be complicated as it requires an explicit form of the potential seen by the electrons inside the nuclei and match the value of this potential at the surface of the nucleus, whether sharp or diffuse, with the potential seen by the electron beyond the nuclear radius. This is not done in the grand majority of cases, and hence we have nuclear cusps.

The Kato cusp condition provides a relation between the nuclear charge of nucleus α (which is equal to the atomic number Z_α times the elementary charge $|e|$)

and (i) the spherically averaged electron density $n(\mathbf{r})$ around the position $\mathbf{R}_\alpha$ of that nucleus and (ii) the derivative of the spherically-averaged electron density with respect to the radial distance, as stipulated by the Kato cusp condition [30–32]:

$$Z_\alpha|e| = -\left[\frac{a_0}{2n(r)}\frac{dn(r)}{dr}\right]_{r\to 0}, \tag{7.8}$$

where a_0 is the Bohr radius. (For a derivation of this condition, see Ref. [32].) The cusp condition delivers the atomic number directly from the properties of the electron density as eq. (7.8) specifies. Hence, the elemental identity of the atom is coded within the electron density itself.

An example of a calculated electron density distribution is displayed in Fig. 7.1. The figure depicts a relief map of the electron density in the plane of a guanine–cytosine Watson–Crick DNA base pair [33]. The dominance of the maxima of the electron density at the positions of the nuclei is clear from the figure. All cusps, except those at the positions of the hydrogen nuclei, are truncated being too high at the scale of the figure.

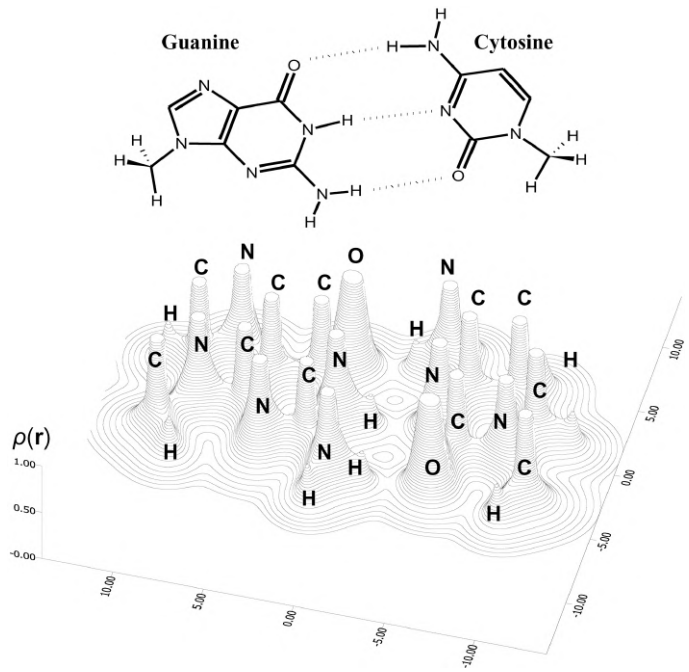

Fig. 7.1: The chemical structure of a guanine cytosine Watson–Crick (triply hydrogen bonded) base–pair and a relief representation of its electron density in the nuclear plane. All nuclear cusps are truncated except those associated with the hydrogen nuclei. Hence, the only cusps seen are those at the positions of the hydrogen nuclei. The ridges of density linking pairs of bonded nuclei trace the bond paths. These ridges in the *topography* of the density determine the *topology* of the density, that is, the connectivity of the various atoms (see also Figs. 7.2 and 7.3). Reproduced from Ref. [33] © 2002 C. F. Matta.

One can also realize from an examination of Fig. 7.1 that chemically bonded nuclei share a ridge along a line of locally maximum electron density linking them. This line is termed the *bond path* (BP) [34–37]. *The BP is the observable counterpart of the more abstract notion of "chemical bond,"* as emphasized by Bader [34]. BPs are now routinely determined in electron densities obtained from experiment and from theory. The first report on the BP appeared in a 1977 paper by Runtz, Bader, and Messer [34].

The BP is *a single line* (irrespective of the multiplicity of the bonding), traced in real space, of locally maximum electron density linking the pair of bonded nuclei. The BP detects chemical bonding whether weak, strong, closed-shell, open-shell, ionic, metallic, covalent, dative, hydrogen, and so on. The lowest point along a given BP in the relief representation (Fig. 7.1), the point with lowest density, is called the bond critical point (BCP).

A BCP is "critical" because all three derivatives of the electron density there are zero. The set of BPs characterizing a molecule or a unit cell constitutes its *molecular graph* which defines its *structure* unambiguously by defining the topology, in other words, the atoms' connectivity. In this manner, the topography of the density leads to the topology in a one-directional mapping. The topology then leads to the molecular graph, and the graph to the chemical structure, but these latter mappings are bijective. Hence, we may write:

$$\text{topography} \rightarrow \text{topology} \leftrightarrow \text{graph} \leftrightarrow \text{structure}. \tag{7.9}$$

The topography of the density can be analyzed by the application of the gradient operator, which converts the scalar field $\rho(\mathbf{r})$ to a vector field ($\nabla\rho(\mathbf{r})$), the gradient vector field of the electron density. The gradient field is "attracted" by the positively charged nuclei with each field line crossing the isodensity contour lines perpendicularly at all points until they reach the nucleus that dominates the region. Each atomic nucleus, and sometimes also certain points other than nuclei known as nonnuclear attractors (NNAs) (or non-nuclear maxima (NNM)), attract a bundle of gradient vector field lines. There is an entire physics of these bundles that relates them, and the properties integrated within volumes bounded by a subset of them, to material properties of the solid state (see, e.g., the work of Eberhart et al. [38–40]).

The gradient of the electron density vanishes at critical points (CPs) and is ill-defined at nuclear cusps (for Hamiltonians with point nuclei) since the value of the derivative, in this case, depends on the direction of approach. This is why the Kato condition takes the spherical average of this derivative (vide supra, and eq. (7.8)). In contrast, molecular and crystal electron densities occasionally exhibit maxima at positions not coinciding with any nucleus. These NNM and nuclear cusps are *topologically* indistinguishable, but in contrast with nuclear cusps, the gradient at an NNM is well-defined and is zero. They are true maxima and not cusps as sometimes described [41]. Clearly, NNM also constitute CPs in the electron density (see Ref. [31] and the literature cited therein).

Building on the example displayed in Fig. 7.1, the reader is referred to Fig. 7.2 where the relief map is converted to a contour map color-coded by element and also, simultaneously, by the values of the contours (given in the figure caption). The map shows a delineation of each atomic region by surfaces surrounding monoatomic regions in which the contained gradient vector field converges on one nucleus. The molecular graph also emerges from this map as can be seen when the background of the image is faded sufficiently to distinguish the BPs (Fig. 7.3).

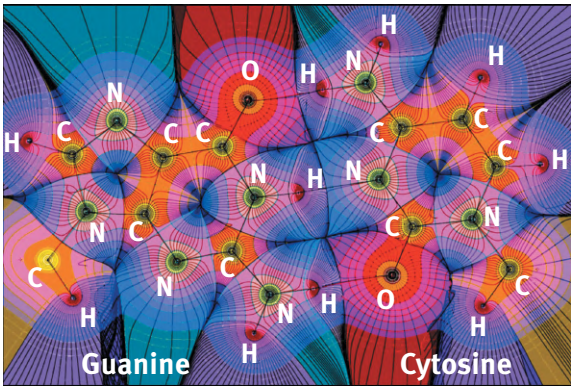

Fig. 7.2: An overlay of the electron density contour map and a representative sample of the gradient vector field lines of the density of a guanine–cytosine (GC) Watson–Crick triply hydrogen bonded base–pair corresponding to Fig. 7.1. The shape of the gradient vector field of the electron density suggests a partitioning of this density into distinct atomic basins. Each basin is dominated by one nucleus. Superimposed on the electron density map is the molecular graph consisting of the entire collection of bond paths defining the connectivity of this system (also see Fig. 7.3). The outermost contour has the isodensity value of 0.001 atomic unit (au) followed inwards by 2×10^n, 4×10^n and 8×10^n au with n starting at -3 and increasing in steps of unity. Reproduced from Refs. [33, 42] © 2002 C. F. Matta.

Bond paths have been found to favor electron exchange and were termed "exchange channels" [43], that is, a sort of intermolecular electronic highway system. Furthermore, to every BP graph, there exist a "shadow" graph, a *doppelgänger* graph, which is not necessarily coinciding spatially with the BP graph but which links the same nuclei. This shadow graph is that of a maximally stabilizing (maximally negative) potential energy density lines [44]. Stated differently, a line exists in space exhibiting maximally negative potential energy density that connects the very same nuclei bonded with a BP [44]. This line is the *virial path*, and the set of all virial paths define the *virial graph*, a graph shown to be homeomorphic with (i.e., exhibits the same topology as) the molecular graph [44]. On one hand, the BP as an exchange channel associates electron sharing with chemical bonding and, on the other hand, the existence of the virial path associates chemical bonding with energetic stability.

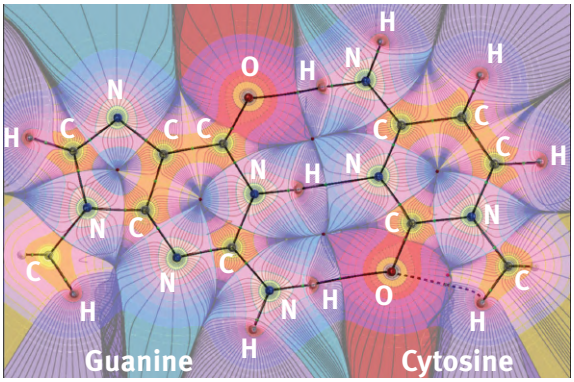

Fig. 7.3: The molecular graph of a guanine–cytosine base–pair corresponding to Figs. 7.1 and 7.2 as it emerges from the lines of gradients connecting the atomic nuclei. The lines connecting chemically bonded nuclei are the "bond paths" (BP). The background has been faded to bring-out the set of BPs that emerge from the electron density and which define the structure. The saddle point on each BP is where it crosses the the inter-atomic surface delimiting one atom from its bonded neighbor, these points are the bond critical points (BCPs). This set of BPs maps to the usual chemical structure (Fig. 7.1 (*top*)), but without visual distinction between covalent bonds of different bond orders or between covalent and hydrogen bonds, all bonds of all types being mapped to one corresponding BP. (The distinction between the type and strength of chemical bonding emerges from the "bond properties" obtained locally at the BCP, or through integration along the BP, or integration over the inter-atomic surface or over the volumes of the two atoms sharing the BP). Adopted from Refs. [33, 42] © 2002 C. F. Matta.

In most cases, the molecular graph is identical to the chemical structure graph based on the chemistry of the compound. The caveat in the last statement is that a single BP connects atoms bonded by any type of chemical bonding: Triple, double, single, ionic, hydrogen, and so on. The type and strength of the chemical bonding is reflected in locally determined properties at the BCP, or in those properties integrated over the BP, the inter-atomic surface, or the volume of the two atoms sharing a BP (as detailed later in this chapter).

Occasionally, however, BPs are found in unexpected positions or are absent where they would have been predicted based on chemical intuition. These "(un)expected" BPs are of much interest. It is occasionally stated that BPs are an artifact reflecting crowding and/or spatial proximity of pairs of atoms. While this is not an unreasonable working assumption, especially if calculations are to be undertaken on very large systems [45], BPs are *not* an automatic result of space proximity of atoms. To illustrate this point, an important example of the *lack* of a BP despite unusual geometric proximity will briefly be reviewed next [46].

An intriguing suggestion by Ernest et al. appeared in 1998 [47] claiming to report a first example in the literature of an agostic bond between saturated sp^3 carbon atoms to a transition metal atom. This suggestion has been made on the basis of the

unusually close proximity of two symmetry-unrelated carbon atoms to a titanium atom in an organo-titanium complex.

The organometallic complex in question along with the numbering scheme adopted in the experimental paper appears in Fig. 7.4. In the figure, and remarkably, atom C7 is slightly closer to the Ti than C4 which is formally bonded to the central transition metal atom (d(Ti–C4) = 2.299(6) Å), d(Ti–C7) = 2.293(7) Å). This Ti–C7 distance is even shorter (considerably) than the fluxional distance to any of the cyclopentadienyl ring carbons (a Ti–C distance averaging 2.333 Å). The latter value is well aligned with an average over 832 structures placing the Ti–C (of η^5-cyclopentadienyl) at 2.374 ± 0.031 Å [48]. The Ti–C2 distance of 2.579(7) Å is considerably smaller than the sum of the van der Waals radii of Ti (*ca*. 2.2 Å) and of C (*ca*. 1.7 Å) [49] which sum is commonly taken as an upper threshold indicator of bonding. Hence, both C2 and C7 appear to be bonded agostically to the central Ti atom, an extraordinary bonding situation that calls for a closer look at the electron density distribution and the underlying electronic structure [46].

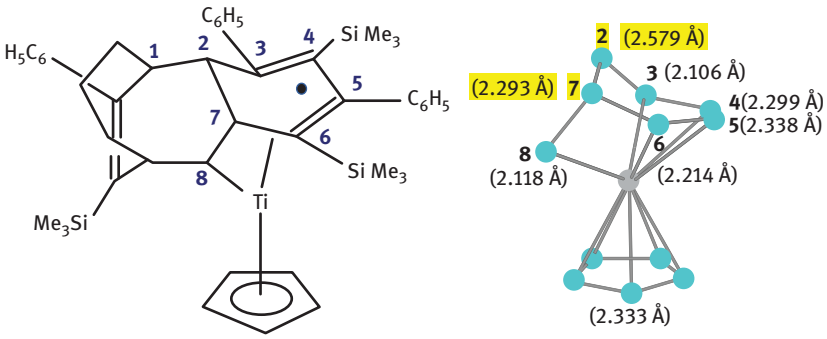

Fig. 7.4: (*Left*) The chemical structure deduced from X-ray crystallography by Ernst et al. [47] showing the numbering scheme adopted by these authors. (*Right*) A ball and stick representation of the Ti atom (grey sphere) surrounded by the carbon atoms (blue spheres) that can possibly be bonded according to a distance criterion at the experimental geometry (hydrogen atoms are omitted for clarity). Beside each carbon atom is its X-ray crystallographic distance from the central titanium in ångströms. The Ti–C2 and Ti–C7 distances have uncertainties of 0.007 Å while the remaining quoted Ti–C distances all have an experimental uncertainty of 0.006 Å. The two highlighted atoms (C2 and C7) are saturated sp^3 carbons with distances from the central Ti atom that are suggestive of a fifth (agostic) carbon-transition metal atom bond for each of these two carbons.

Bader and Matta performed Hartree–Fock and BLYP-DFT quasi-single point calculations (after optimizing only the positions of the hydrogen atoms but leaving all other geometrical parameters at their experimentally-derived values) [46]. The authors used a polarized basis set augmented with the necessary diffuse function for a proper description of long-range agostic interactions. The basis set used was a Pople 6–31+G* basis for the carbons and the hydrogens while the titanium atom was

described by a 14*s* 11*p* 6*d* contracted to [10*s* 8*p* 3*d*] triple-ζ valence basis set. The ensuing density and wave functions were analyzed within the framework of QTAIM.

The analysis produced a set of consistent results indicating the absence of bonding (or even incipient bonding) between C2 or C7 and the Ti atom. There are no BPs linking these two proximal carbons to the central Ti. Further, the delocalization indices (discussed below) indicate an almost complete absence of any electron sharing between these two particular carbon atoms and the Ti. Thus, for comparison, C3, 4, 5, 6, and 8 have delocalization indices (DIs) with Ti of 0.14, 0.14, 0.11, 0.24, and 0.33 electrons, respectively. Meanwhile, C2 and C7 exhibit DIs of 0.03 and 0.06 electrons. It is particularly striking to compare Ti–C4 ($d = 2.299(6)$ Å, and a DI of 0.14 e^-) and the slightly shorter (!) distanced Ti–C7 ($d = 2.293(7)$ Å, and a DI of 0.06 e^-). An analysis of the Laplacian of the electron density also shows no indication of distortion diagnostic of an incipient bonding interaction. There are more details skipped here for brevity, but the interested reader may consult Ref. [46].

The point of mentioning the example just discussed is that QTAIM is occasionally accused to place bonding where it "should not." QTAIM shows that, in this case, there is no unusual agostic bonding despite of the proximity of certain pairs of atoms. This negative result falsifies claims that whenever atoms within a molecule or a complex are sufficiently close a BP arises and that, because of that, the promolecule should have the same bonded structure as the full density.

Now, we turn to a counter example: That of a BP appearing where chemical intuition assumes a repulsive interaction. This is the case of the hydrogen–hydrogen (H . . . H) BP [50]. This BP appears between atoms that are "supposed to" experience a mutual "steric repulsion" such as pairs of closed-shell hydrogen atoms in a congested molecular system. These BPs were reported by Cioslowski and Mixon in 1992 and were considered by these authors as an indication of the existence of "non-bonded repulsive interactions" [51]. The evidence for the *stabilizing* nature of this closed-shell interaction has been reported in 2003 [50].

On closer inspection of these H . . . H BPs, it is found that the atomic (virial) energies of hydrogen atoms that participate in this interaction, which occur frequently in crowded systems, are found to be more negative (more stable) than comparable hydrogen atoms that are not linked by such H . . . H interactions. (*Vide infra* for the definition of "atomic virial energies.")

Figure 7.5 provides an example of such systems where an H . . . H BP is observed, which – in this case – occurs in the bay region of phenanthrene. The top panel of the figure displays the chemical structure, the molecular graph based on the BPs, and the virial graph. The bottom panel shows a contour map representation of the electron density (*left*) and the associated gradient vector field (*right*), with the molecular graph superimposed on both.

The gradient vector field suggests a partitioning of the electron density into atomic basins that span the entire space and which represent the atoms in the molecules. In the example displayed in Fig. 7.5, the molecular graph, the virial graph,

and the gradient vector field reproduce the chemical structure phenanthrene (*top left*). The figure also exhibits a BP between the crowded hydrogen atoms in the bay region. This BP reflects a hydrogen–hydrogen bonding interaction which stabilizes (locally) the system in which it exists.

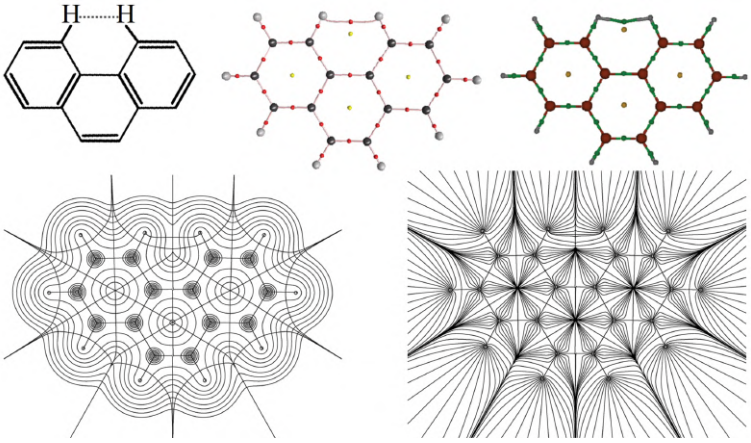

Fig. 7.5: (*Top-left):* The chemical structure of phenanthrene with the hydrogen–hydrogen interaction singled out as dotted line. (*Top-middle*)*:* The molecular graph showing the bond paths defining the structure and which corresponds to the chemical structure to the left. The red dots on the bond paths indicate the positions of the bond critical points. (*Top-right*)*:* The virial graph with identical topology as the molecular graph. (*Bottom-left*)*:* A contour representation of the electron density in the plane of the molecule along with a superimposition of the molecular graph and the interatomic surfaces of zero flux (see below). (*Bottom-right*)*:* The gradient vector field associated with the electron density showing the nuclei as attractors of the gradient field lines and suggesting a partitioning of the physical space into atoms-in-molecules.

The discovery of the hydrogen–hydrogen bonding sparked a debate about whether the H . . . H interaction stabilizes or destabilizes the system [52–56]. One often reads in the literature that this interaction is "repulsive," a relic of the concept of steric repulsion, but it is not clear how a fully optimized equilibrium geometry (with zero forces on the nuclei) exhibits any net repulsive or attractive interaction. In an optimized geometry, that is, at a critical point on the potential energy hyper-surface, the energy derivatives with respect to geometrical changes (the forces) vanish by definition. Thus, the discussion in such systems can be meaningfully couched in energy terms (stabilities) but not in terms of energy derivatives (repulsive or attractive forces) as we often see in the literature.

This is a good place to suggest the proper use of language in this context, since language is important in science. One can, by all means, talk about a locally stabilized region in a molecule at an optimized geometry (compared to other regions within the molecule or compared to the same region in a different geometry, say). However, *at an optimized geometry, whether a local/global minimum or a transition state structure, it is*

not meaningful to talk about attractive and/or net repulsive atom–atom interactions since the energy is stationary with respect to all geometric changes including atom–atom distances. Several authors refer to the H . . . H interaction as repulsive while others refer to it as attractive, that is, the interaction is described in terms of forces (i.e., implying an energy *derivative*). It seems more appropriate to recast such discussion in terms of stabilization or destabilization, that is, in energetic terms. Another point worth emphasizing is the *petitio principii* fallacy, more commonly known as the chicken-and-egg fallacy. We often read/hear about the presence of such and such interaction is the *cause* of stability or instability of a system. But the Hamiltonian recognizes no such "cause-and-effect" relation, they simply coexist: The system is at a minimum and at that minimum the wave function delivers a density such that a bonding interaction connects given atomic pairs. *Chemical bonding is associated with the particular state of the system and neither is the cause nor the effect of the other*. With these ideas in mind, we now proceed in the discussion about the H . . . H bonding interaction.

The debate sparked by the discovery of the H . . . H bonding appears to have now generally subsided in favor of the locally stabilizing nature of this interaction [57–68]. This debate may be rooted in the difficulty that some have in accepting that a *locally* stabilizing interaction may or may not be associated with a global stabilization of the system as a whole. Sometimes, the local stabilizing effect of H . . . H bonding is overwhelmed by the destabilization of other atoms in the molecule, and this is what occurs in planar biphenyl, for example. In that system, the four *ortho*-hydrogen atoms are bonded with BPs and have a considerably lower energy (more stable), by ~8 kcal/mol per atom, than the average energy of the remaining six hydrogen atoms. The total "local stabilizing" contribution of these *ortho*-hydrogen atoms is, hence, to the tune of 32 kcal/mol.

Further, in the planar (transition state) structure, the two *para*-carbon atoms are also more stable than their counterparts in the twisted geometry, each by ~3 kcal/mol. Hence, the main atoms that stabilize the planar transition state, that is, the four *ortho*-hydrogens and the two *para*-carbons, together lower the total energy of the system by ~38 kcal/mol compared to the twisted global minimum structure. Meanwhile, to accommodate the H . . . H bonded atoms in planar biphenyl, the bond between the two *ipso*-carbon atoms linking the two phenyl rings elongates. As a result of this elongation, the different contributions to the atomic energies are altered with respect to their corresponding values in the minimum twisted structure.

In the planar structure, there is a considerable loss of stabilizing interaction between the electrons in the basin of one *ipso*-carbon and the nucleus of the symmetry equivalent counterpart on the other ring (and vice versa). As a result, the virial energies of each of these two carbon atoms increases by 22 kcal/mol, leading to a total of 44 kcal/mol of energetic destabilization in the planar structure with respect to the twisted one. Ignoring the smaller changes in the virial energies of the rest of the atoms in biphenyl as it twists (differences that are all are less than 1 kcal/mol) and if we now account for the dominant stabilizing and destabilizing contributions we have $-38 + 44 \approx 6$ kcal/mol (the actual energy barrier is approximately 3 kcal/mol).

Thus the four *ortho*-hydrogens and the two *ipso*-carbons are the main contributor to the energy barrier of rotation in biphenyl, and – to a lesser extent – the two *para*-carbons atoms [50, 60, 61–62].

It may be simpler to teach freshmen students that biphenyl twists because of a repulsive steric interaction between two pairs of "sterically clashing" *ortho*-hydrogens in the planar transition state. An atom-by-atom energy analysis does not support this view. Instead the twisting of biphenyl is associated with the insufficiency of the local stability imparted by the two H . . . H bonding interactions in the planar structure to compensate the destabilization associated with the two *ispo*-carbon [50, 60, 61–69]. Albert Einstein is credited to have said [70]:

> *It can scarcely be denied that the supreme goal of all theory is to make the irreducible basic elements as simple and as few as possible without having to surrender the adequate representation of a single datum of experience.* Albert Einstein (date unknown)

This quotation is sometimes simplified as [*e*]*verything should be made as simple as possible, but not simpler*, and the H . . . H bonding is a case in point.

If the interaction of two-closed-shell hydrogen atoms can be placed on a linear scale, then the hydrogen . . . hydrogen bonding falls at one end opposite to the dihydrogen bonding [66, 71–76]: In the former, the pair of hydrogens involved in the bonding bear identical (or similar) net electrical charges – and could be close to electrical neutrality, while in the latter the bonding is between an acidic (positively charged) hydrogen atom and a hydridic (negatively charged) one.

7.2 Critical points in the electron density

The previous section reviews how the topography of the electron density scalar field dictates a bonded topology. The gradient vector field associated with the electron density can be used as a basis to delimit mono-atomic regions that can be associated with atoms-in-molecules (AIMs). The various AIMs are delimited from one another and do not overlap and they leave no gaps in the molecule that are unaccounted for. Their volumes cover all space, with the exception of systems with NNAs/NNMs in which case all space is covered upon taking the volumes of the NNAs' basins into account as well.

The three first derivatives of the electron density scalar field vanish at CPs. Thus, by definition, a CP is one where:

$$\nabla\rho = \mathbf{e}_x \frac{d\rho}{dx} + \mathbf{e}_y \frac{d\rho}{dy} + \mathbf{e}_z \frac{d\rho}{dz} = \vec{\mathbf{0}}, \tag{7.10}$$

where the zero vector implies that *every one of the three separate derivatives* in the above Cartesian expression of the gradient is identically zero and not just the sum of the three terms.

Local minima, local maxima, and saddle points can be distinguished by the second derivative. The nine second derivatives of the electron density, when cast into a matrix format, constitute the so-called the *Hessian matrix* ($\mathbf{A}(\mathbf{r}_c)$). At a CP ($\mathbf{r}_c$), the Hessian is:

$$\mathbf{A}(\mathbf{r}_c) = \begin{pmatrix} \frac{\partial^2\rho}{\partial x^2} & \frac{\partial^2\rho}{\partial x\partial y} & \frac{\partial^2\rho}{\partial x\partial z} \\ \frac{\partial^2\rho}{\partial y\partial x} & \frac{\partial^2\rho}{\partial y^2} & \frac{\partial^2\rho}{\partial y\partial z} \\ \frac{\partial^2\rho}{\partial z\partial x} & \frac{\partial^2\rho}{\partial z\partial y} & \frac{\partial^2\rho}{\partial z^2} \end{pmatrix}_{\mathbf{r}=\mathbf{r}_c} . \tag{7.11}$$

Since the Hessian matrix is real and symmetric, it is diagonalizable. Such diagonalization is equivalent to a coordinate rotation (in Cartesian expression: from $\mathbf{r} = (x, y, z)$ to $\mathbf{r'} = (x', y', z')$). The rotation is chosen to align x', y', z' with the three principal curvatures at the point of evaluation. The diagonalized Hessian ($\mathbf{\Lambda}$) is written (in Cartesian coordinates) as:

$$\mathbf{\Lambda} = \begin{pmatrix} \frac{\partial^2\rho}{\partial x'^2} & 0 & 0 \\ 0 & \frac{\partial^2\rho}{\partial y'^2} & 0 \\ 0 & 0 & \frac{\partial^2\rho}{\partial z'^2} \end{pmatrix}_{\mathbf{r}'=\mathbf{r}_c} , \tag{7.12}$$

where the diagonal elements represent the three pure second derivatives, each with respect one of the principal axes. These curvatures are given the symbol λ (with numerical subscripts defined below). In this way, the diagonalized Hessian can be expressed as:

$$\mathbf{\Lambda} \equiv \begin{pmatrix} \lambda_1 & 0 & 0 \\ 0 & \lambda_2 & 0 \\ 0 & 0 & \lambda_3 \end{pmatrix}. \tag{7.13}$$

The trace of Hermitian matrices is invariant to rotations of coordinates, and so is the trace of the Hessian introduced above. This trace coincides with the Laplacian of the electron density, which is written in its general form as:

$$\nabla^2\rho(\mathbf{r}) = \nabla \cdot \nabla\rho(\mathbf{r}), \tag{7.14}$$

or in Cartesian coordinates form as:

$$\nabla^2\rho(\mathbf{r}) = \frac{\partial^2\rho(\mathbf{r})}{\partial x^2} + \frac{\partial^2\rho(\mathbf{r})}{\partial y^2} + \frac{\partial^2\rho(\mathbf{r})}{\partial z^2}. \tag{7.15}$$

CPs can be classified using the three curvatures of the density. A CP is assigned a *rank* (ω) and a *signature* (σ). The number of nonzero curvatures of a given CP is its rank. CPs of lower rank than the dimensionality of space (ω < 3) are unstable and are rarely seen in electron density maps of equilibrium molecular structures. If present, such lower rank CPs are indicative of an imminent change in topology. In the majority of cases, thus, ω = 3. The signature counts the number of positive curvatures minus the number of negative ones. Given that the signature of a stable CP can only take the values −3, −1, +1, +3; we are left with four types of CPs:

- (3, −3): A local maximum (three negative curvatures).
- (3, −1): A saddle point (two negative curvatures and a positive one).
- (3, +1) A minimum in a given plane (two positive curvatures and a negative one).
- (3, +3) A local minimum (three positive curvatures).

Each type of critical point is identified with an element of chemical structure: (3,−3) *nuclear critical point* (NCP) (also *non-nuclear attractors critical poin*t (NNACP));[3] (3,−1) *bond critical point* (BCP); (3,+1) *ring critical point* (RCP); and (3,+3) *cage critical point* (CCP). The number *n* and type of critical points that can coexist in a molecule follow a topological relationship known as the *Poincaré-Hopf relationship* (PH) which states that [2]:

$$n_{\mathrm{NCP}} + n_{\mathrm{NNACP}} - n_{\mathrm{BCP}} + n_{\mathrm{RCP}} - n_{\mathrm{CCP}} = 1. \tag{7.16}$$

For an infinite crystalline lattice, the above equation is replaced by the Morse equation in which the equality is changed so that the right hand side is equal to zero, *i.e.* [77]:

$$n_{\mathrm{NCP}} + n_{\mathrm{NNACP}} - n_{\mathrm{BCP}} + n_{\mathrm{RCP}} - n_{\mathrm{CCP}} = 0. \tag{7.17}$$

The satisfaction the PH or the Morse relation is a necessary condition to ensure that no critical points in the system have been overlooked. The satisfaction of the relevant relation is, however, an insufficient condition since, in principle, one can add or omit the same number of oppositely-signed critical points and this would leave eqs. (7.16) or (7.17) unchanged [6]. For example, if a bond critical point *and* a ring critical point have both been missed, the Poincaré-Hopf relationship would still be valid, as in Eq. (7.18):

$$n_{\mathrm{NCP}} + n_{\mathrm{NNACP}} - (n_{\mathrm{BCP}} - 1) + (n_{\mathrm{RCP}} - 1) - n_{\mathrm{CCP}} = 1. \tag{7.18}$$

3 A nuclear critical point is not really a maximum since it is a cusp under the zero-nuclear size approximation. The derivative of the electron density at these cusps is, technically, ill-defined. However, the nuclear cusps are equivalent topologically and topographically to true maxima (where the derivative vanishes), and hence are treated as such. In contrast, a non-nuclear attractor critical point is a true maximum where the derivative vanishes.

Missing two CPs is unlikely with today's available software.

Normally, a CCP is enclosed by a polyhedron of ring surfaces from all sides, being literally located in a cage of ring surfaces. But this is not mathematically required as stated by Bader [2]: *while it is mathematically possible for a cage to be bounded by only two ring surfaces, the minimum number found in an actual molecule so far is three, as in bicyclo [1.1.1] pentane, for example*. This remained merely a mathematical possibility with a few exceptions as in the case of the derivative of the helical difluorinated polycyclic aromatic hydrocarbon 1,12-difluorobenzo[c]phenanthrene [78] and in the case of cyclooctatetraene [79] where, in both cases, a CCP is bounded by only two ring surfaces (instead of the minimum of three for a normal cage).

7.3 The zero-flux surface bounding proper open quantum systems

In the previous section, the zero-flux surface partitioning of the molecular space was introduced pictorially. The separatrix between an atom and its bonded neighbor is expressed as the so-called Bader zero-flux condition:

$$\nabla\rho(\mathbf{r}) \cdot \mathbf{n}(\mathbf{r}) = 0, \qquad \forall \ \mathbf{r} \in S(\Omega, \mathbf{r}), \tag{7.19}$$

where $\mathbf{n}(\mathbf{r})$ is the normal vector to the surface and Ω is an atomic basin bounded by the surface S. The condition expressed in eq. (7.19) is to be understood as a condition of *local* zero-flux. Generally, an atomic surface is the union of a number of zero-flux interatomic surfaces:

$$S(\Omega) = \bigcup_i S(\Omega|\Omega_i), \tag{7.20}$$

where the symbol Ω_i refers to the ith bonded neighbor of Ω and where the vertical bar denotes the zero-flux surface between atom Ω and Ω_i. We now turn to the question of the fundamental nature of the Bader condition as a prerequisite to define proper open quantum systems or, as more commonly known, AIMs.

An open quantum system is defined as a bounded volume contained within a total system such as an atom in a molecule or in a crystal. The total system, in this case, the molecule or the crystal in question, is the analogue of the thermodynamic "closed system" while the open quantum system is the analogue of the thermodynamic "open subsystem" within a larger closed system.

Suppose we mentally isolate a region within a total system, that is, a subsystem without any restriction on the choice of the form of its bounding surface. In this case, the kinetic energy due to the electronic motion cannot be defined uniquely as can be seen from what follows. We first start by applying the Leibniz identity for the divergence of a product of a vector function and a scalar function (where the vector

function is the gradient of an arbitrary but otherwise well-behaved complex scalar function of three-dimensional space ψ taken here to be a one-particle wave function):

$$\begin{aligned}\nabla^2(\psi^*\psi) &= \nabla\cdot[(\nabla\psi^*)\psi + \psi^*(\nabla\psi)] \\ &= (\nabla^2\psi^*)\psi + \psi^*(\nabla^2\psi) + 2\nabla\psi^*\nabla\psi,\end{aligned} \tag{7.21}$$

where the star denotes complex conjugation.

Rearranging eq. (7.21), and realizing that for a one particle system $\psi^*\psi = \rho$, this equation can be rewritten:

$$-\left[\psi\,\nabla^2\psi^* + \psi^*\nabla^2\psi\right] = 2\nabla\psi^*\cdot\nabla\psi - \nabla^2(\psi^*\psi). \tag{7.22}$$

Multiplying the above expression by constants that convert its dimensions to those of an energy density, and generalizing to an *N*-electron system described by an antisymmetrized many-electron wavefunction Ψ through the repeated action of a given operator with respect to the coordinates of each of the *N*-electrons, we get:

$$-\frac{\hbar^2}{4m}\sum_{i=1}^{N}\left[\Psi\,\nabla_i^2\Psi^* + \Psi^*\nabla_i^2\Psi\right] = \frac{\hbar^2}{2m}\sum_{i=1}^{N}\nabla_i\Psi^*\cdot\nabla_i\Psi - \frac{\hbar^2}{4m}\sum_{i=1}^{N}\nabla_i^2(\Psi^*\Psi), \tag{7.23}$$

where *m* is the rest mass of an electron.

Since electrons are indistinguishable and Ψ is antisymmetric, one can replace a given sum of *N* identical one-electron operators by *N* times the result of the corresponding operation in eq. (7.23) which gives:

$$-\frac{\hbar^2}{4m}N\left(\Psi\nabla^2\Psi^* + \Psi^*\nabla^2\Psi\right) = \frac{\hbar^2}{2m}N\nabla\Psi^*\cdot\nabla\Psi - \frac{\hbar^2}{4m}N\nabla^2(\Psi^*\Psi). \tag{7.24}$$

In eq. (7.24), the lead *N* has not been cancelled out in preparation for the following step. That step, which follows in eq. (7.25), converts the dimensions of three quantities in eq. (7.24) into those of one-electron energy densities. Thus, integrating the former expression over all space using the mode of integration introduced in eq. (7.4) leads to:

$$\underbrace{-\frac{\hbar^2}{4m}N\int d\tau'\left[\Psi\nabla^2\Psi^* + \Psi^*\nabla^2\Psi\right]}_{k(\mathbf{r})} = \underbrace{\frac{\hbar^2}{2m}N\int d\tau'\nabla\Psi^*\cdot\nabla\Psi}_{g(\mathbf{r})}\underbrace{-\frac{\hbar^2}{4m}\nabla^2\rho}_{l(\mathbf{r})}, \tag{7.25}$$

where $k(\mathbf{r})$ is termed the "Schrödinger kinetic energy density", $g(\mathbf{r})$ is known as the "gradient kinetic energy density", and $l(\mathbf{r})$ is the Laplacian distribution function of the electron density. The integration of the above terms over the remaining coordinate $\mathbf{r}$, together with their respective lead constants, yields the corresponding energies denoted as *K*, *G*, and *L*.

Because the gradient of the electron density vanishes at infinity ($\nabla\rho \to 0$, at $\mathbf{r} \to \infty$), the last term in eq. (7.25) also vanishes when integrated over all space (since $\nabla^2\rho = \nabla.\nabla\rho$). Thus, if the limits of the integration cover all space we have,

$$K = G = T, \tag{7.26}$$

where T is a well defined kinetic energy since now the integrals of the two distinct expressions of the kinetic energy density (k and g) converge to the same result when the integral is taken over all space.

In contrast, if the integral of eq. (7.25) over the remaining space coordinate $\mathbf{r}$ is taken over an arbitrary (open) subsystem Ω, the last integral will generally not vanish. This leads to the non-physical result whereby the two correct expressions of the kinetic energy density give different values for the kinetic energy of that subsystem. Stated differently, in general, the kinetic energy of an arbitrary subsystem is ill-defined.

To emphasize the inequality of K and G when evaluated over an arbitrary piece Ω of a total system, we rewrite eq. (7.25) after performing the integral over a subspace Ω (instead of over all space) and after using the identity $\nabla^2\rho = \nabla.\nabla\rho$:

$$K(\Omega) = G(\Omega) - \frac{\hbar^2}{4m}\int_{\Omega} d\mathbf{r}\ \nabla\cdot\nabla\rho, \tag{7.27}$$

where the last term (Laplacian function) is saved since it is generally non-vanishing in this case.

We next apply Gauss' divergence theorem to convert the volume integral of the divergence of the gradient of the electron density into a surface integral to obtain an expression for the net (total) flux of the gradient vector field of the density through the bounding surface. This procedure leads to:

$$K(\Omega) = G(\Omega) \underbrace{- \frac{\hbar^2}{4m}\oint dS(\Omega, \mathbf{r})\nabla\rho\cdot\mathbf{n}(\mathbf{r})}_{L(\Omega)}, \tag{7.28}$$

where $\mathbf{n}(\mathbf{r})$ is the normal vector to the closed surface S.

Equation (7.28) limits the equality expressed in eq. (7.26) to only those cases where the Laplacian function integral is zero when integrated over the surface S bounding Ω. Those cases where the Laplacian function integral vanishes when integrated over S (S not at infinity) are those in which S satisfies Bader's boundary condition (eq. (7.19)). Only then will the kinetic energy be well-defined and equality (7.26), $K = G = T$, is recovered this time for *a part* of the total system.

When used in conjunction with an atomic statement of the virial theorem, the kinetic energy of an atom-in-a-molecule is sufficient to determine the contribution of that atom to the total energy (a contribution that contains all the (intractable) atomic contributions to the potential energy terms). Thus, provided a virial theorem

(which will be proven later) can be stated for an atom-in-a-molecule Ω, that is, that the energy of that atom satisfies:

$$T(\Omega) = -\frac{1}{2}V(\Omega), \tag{7.29}$$

then the total energy of that atom-in-a-molecule is:

$$E(\Omega) = T(\Omega) + V(\Omega) = -T(\Omega)\cdot \tag{7.30}$$

The result expressed in eq. (7.30) is quite striking as it implies that the energy of atom Ω is simply the negative of its readily computable average kinetic energy (T(Ω)). As a consequence of this result, the total energy of a molecule (which includes the nuclear-nuclear repulsion energy) can be expressed as the sum of the energy contributions of its composing atoms, thus:

$$E = \sum_{\Omega} E(\Omega). \tag{7.31}$$

Bader often emphasized the observational basis of his theory and, that is, *when the electron density is transferable the kinetic energy density is also transferable and, by virtue of eqs. (7.30) and (7.31), so is the total energy of the molecule*. In this context, Bader used to say (as recalled by one of the authors (C.F.M.)) that *the form of an atom in a molecule determines that atom's contribution to the total energy* and that *atoms that "look" the same contribute equal amounts to the total energy*.

There exists families of functional forms that represent an infinity of valid expressions for the kinetic energy density such that their integrals over all space deliver the correct (unique) total kinetic energy of the system [80–82]. However, there appears to be a special role for the Schrödinger (k) and the gradient (g) kinetic energy densities as they are related, locally, by a term proportional to the Laplacian of the electron density as can be seen from eqs. (7.25) – (7.28).

7.4 Coincidence of the topological atom and the quantum atom

Quantum mechanical operators are Hermitian[4] when used in obtaining the corresponding quantum mechanical average over all space. In other words, Hermiticity is a property of operators averaged over the entire closed system and not over an open subsystem such that the same quantum mechanical operator when integrated over a subspace is no longer Hermitian. This is a consequence of, unlike the closed total

4 Hermiticity ensures that the eigenvalues of $\hat{O}$ are real as required for observables. An operator $\hat{O}$ is termed Hermitian if it is self-adjoint, that is, $\hat{O} = \hat{O}^{\dagger}$. The matrix representation of a Hermitian operator satisfies $\langle a|\hat{O}|b\rangle = \langle a|\hat{O}^{\dagger}|b\rangle = \langle b|\hat{O}|a\rangle^{*}$ where in this case the adjoint indicated by the superscripted dagger (†) implies complex conjugation and transposition of the matrix.

system, an open system experiences fluxes in property currents across its bounding surface. The development of the remainder of this (and the next) section(s) follows closely Bader's book [2].

The temporal evolution of an operator average $\langle \hat{A} \rangle$ is expressed by the Heisenberg equation of motion. This equation, written within the Schrödinger representation reads:

$$\frac{d\langle \hat{A} \rangle}{dt} = \frac{i}{\hbar} \langle \Psi | [\hat{H}, \hat{A}] | \Psi \rangle, \tag{7.32}$$

where $[\hat{H}, \hat{A}]$ is the commutator of the operator $\hat{A}$ with the Hamiltonian of the system, and the angular bracket (in Dirac notation) indicate quantum averaging such that:

$$\langle \Psi | [\hat{H}, \hat{A}] | \Psi \rangle = \langle \Psi | \hat{H}\hat{A} | \Psi \rangle - \langle \Psi | \hat{A}\hat{H} | \Psi \rangle. \tag{7.33}$$

Recalling Schrödinger equation written in Dirac notation:

$$\hat{H} | \Psi \rangle = E | \Psi \rangle, \tag{7.34}$$

and because of the Hermiticity of $\hat{A}$, eq. (7.33) yields:

$$\begin{aligned} \langle \Psi | [\hat{H}, \hat{A}] | \Psi \rangle &= \langle \hat{H}\Psi | \hat{A}\Psi \rangle - \langle \Psi | \hat{A}\ E | \Psi \rangle \\ &= E\langle \Psi | \hat{A} | \Psi \rangle - E\langle \Psi | \hat{A} | \Psi \rangle = 0, \end{aligned} \tag{7.35}$$

where Ψ is not necessarily an eigenfunction of $\hat{A}$, in other words:

$$\langle \Psi | [\hat{H}, \hat{A}] | \Psi \rangle = 0, \tag{7.36}$$

that is, the commutator of a Hermitian operator with the Hamiltonian vanishes. This is the well-known *hypervirial theorem* of quantum mechanics.

For an open system Ω, however, the Hermiticity of an otherwise Hermitian operator is no longer guaranteed. The averaging over the subsystem involves a special mode of integration whereby the integral is first taken over all space with respect to the coordinates of all electrons except one followed, as usual, by summation over all spins, and then a space integration over the remaining coordinates only over the open system's volume Ω. The non-Hermiticity is expressed symbolically as,

$$\langle \Psi | \hat{H}\hat{A}\Psi \rangle_{\Omega} \neq \langle \hat{H}\Psi | \hat{A}\Psi \rangle_{\Omega}, \tag{7.37}$$

in general, and, in this case:

$$\langle \Psi | [\hat{H}, \hat{A}] | \Psi \rangle_{\Omega} = \langle \Psi | \hat{H}\hat{A}\Psi \rangle_{\Omega} - \langle \Psi | \hat{A}\hat{H}\Psi \rangle_{\Omega} \neq 0. \tag{7.38}$$

Let us manipulate this result by adding and subtracting $\langle \hat{H}\Psi | \hat{A}\Psi \rangle_{\Omega}$ and using Schrödinger equation:

$$\langle\Psi|\left[\hat{H},\hat{A}\right]|\Psi\rangle_{\Omega} = \langle\Psi|\hat{H}\hat{A}\Psi\rangle_{\Omega} - \langle\hat{H}\Psi|\hat{A}\Psi\rangle_{\Omega} + \langle\hat{H}\Psi|\hat{A}\Psi\rangle_{\Omega} - \langle\Psi|\hat{A}\hat{H}\Psi\rangle_{\Omega} \tag{7.39a}$$

$$= \langle\Psi|\hat{H}\hat{A}\Psi\rangle_{\Omega} - \langle\hat{H}\Psi|\hat{A}\Psi\rangle_{\Omega} + E\langle\Psi|\hat{A}\Psi\rangle_{\Omega} - E\langle\Psi|\hat{A}\Psi\rangle_{\Omega} \tag{7.39b}$$

$$= \langle\Psi|\hat{H}\hat{A}\Psi\rangle_{\Omega} - \langle\hat{H}\Psi|\hat{A}\Psi\rangle_{\Omega}. \tag{7.39c}$$

In what follows, we consider the case of a single electron which can then be generalized to the many-electron system by the integral $\int d\tau'$ followed by multiplication by the total number of electrons N (as in eq. (7.5)).

The Hamiltonian of a single-electron atom is expressed as:

$$\left[-\frac{\hbar^2}{2m}\nabla^2 - \frac{e^2}{4\pi\varepsilon_0 r}\right]\Psi = E\Psi. \tag{7.40}$$

Now, since the potential energy operator in this Hamiltonian is additive, it will cancel if the explicit Hamiltonian is inserted into eq. (7.39c). With this cancellation, one gets:

$$\langle\Psi|\left[\hat{H},\hat{A}\right]|\Psi\rangle_{\Omega} = \frac{\hbar^2}{2m}\int_{\Omega} d\mathbf{r}\,\left[\left(\nabla^2\Psi^*\right)\hat{A}\,\Psi - \Psi^*\,\nabla^2\left(\hat{A}\Psi\right)\right] \tag{7.41a}$$

$$= \frac{\hbar^2}{2m}\int_{\Omega} d\mathbf{r}\,\boldsymbol{\nabla}\cdot\left[\left(\boldsymbol{\nabla}\Psi^*\right)\hat{A}\,\Psi - \Psi^*\,\boldsymbol{\nabla}\left(\hat{A}\Psi\right)\right]. \tag{7.41b}$$

Converting the volume integral in eq. (7.41b) into a surface integral using Gauss' theorem, we obtain:

$$\langle\Psi|\left[\hat{H},\hat{A}\right]|\Psi\rangle_{\Omega} = \oint dS(\Omega,\mathbf{r})\,\hbar\underbrace{\left\{\frac{\hbar}{2m}\left[\left(\boldsymbol{\nabla}\Psi^*\right)\hat{A}\,\Psi - \Psi^*\,\boldsymbol{\nabla}\left(\hat{A}\Psi\right)\right]\right\}}_{i\times(\text{negative of the current density of property } A)}\cdot\mathbf{n}(\mathbf{r}), \tag{7.42}$$

where the integrand is i times minus the current density vector of A through the surface, $-\mathbf{j}_A(\mathbf{r})$, where this current is expressed as:

$$\mathbf{j}_A(\mathbf{r}) \equiv \frac{\hbar}{2mi}\left[\Psi^*\boldsymbol{\nabla}(\hat{A}\,\Psi) - (\boldsymbol{\nabla}\,\Psi^*)\,(\hat{A}\Psi)\right]. \tag{7.43}$$

Equation (7.42) brings to the fore the difference between an open and a closed system. In the former, the commutator average of property A, $\langle\Psi|[\hat{H},\hat{A}]|\Psi\rangle_{\Omega}$ is equal to the flux in the density of A across the surface bounding the subsystem.

In order to guarantee that the result of the averaging is a "real" quantity, as required for an observable, one averages each term and its complex conjugate (cc) so that the imaginary part cancels in the process. Applying this averaging to eq. (7.42) along with the definition of the quantum mechanical current (eq. (7.43)) yields:

$$\frac{1}{2}\left\{\frac{i}{\hbar}\langle\Psi|\left[\hat{H},\hat{A}\right]|\Psi\rangle_{\Omega} + \text{cc}\right\} = \frac{1}{2}\left[\oint dS(\Omega,\mathbf{r})\ \mathbf{j}_A\cdot\mathbf{n}(\mathbf{r}) + \text{cc}\right]. \tag{7.44}$$

In short, there exists a net flux in the density of A through the bounding surface of the subsystem if $\hat{H}$ and $\hat{A}$ do not commute. That flux is given by the surface integral of this property current density through S given in the right-hand side of eq. (7.44).

To derive his famous equation, $\hat{H}\Psi = E\Psi$, Schrödinger imposed a stationarity condition on the energy functional $J[\Psi]$ with respect to first-order variations in the wave function ($\delta J[\Psi] = 0$) along with a normalization constraint [83]. The Schrödinger energy functional is:

$$J[\Psi] = \int d\tau\left[\left(\frac{\hbar^2}{2m}\right)\nabla\Psi^*\cdot\nabla\Psi + (\hat{V}+\lambda)\Psi^*\Psi\right], \tag{7.45}$$

where λ, the Lagrange multiplier for the constraint, is the negative of the total energy, that is, $E = -\lambda$), where the unprimed integration runs over the coordinates of all the electrons (without exception) followed by summation over all spins.

Following a similar line of development, Serbrenik and Bader applied Schrödinger's steps to a subsystem [84]. They proposed an analogue of the Schrödinger's energy functional expressed above but for an (open) subsystem, the constrained atomic energy functional ($\mathcal{G}_f$) [84]:

$$\mathcal{G}_f[\Psi,\Omega] = \int_{\Omega} d\tau\left[\left(\frac{\hbar^2}{2m}\right)\nabla\Psi^*\cdot\nabla\Psi + (\hat{V}-E)\Psi^*\Psi\right] \equiv \int_{\Omega} d\tau\ f(\Psi,\nabla\Psi), \tag{7.46}$$

where f, the integrand, is a function of both Ψ and $\nabla\Psi$.

The variation of $\mathcal{G}_f$ over the subspace Ω, that is, $\delta\mathcal{G}_f[\Psi,\Omega]$, consists of two contributions: One from the variation of the integrand while the surface is held constant and the second from the variation of the surface while the integrand is held constant. Further, if one considers Ψ and Ψ^* as two symmetric but independent variables, we get:

$$\delta\mathcal{G}_f[\Psi,\Omega] = \underbrace{\int_{\Omega} d\tau\left[\left(\frac{\partial f}{\partial\Psi}\right)\delta\Psi + \left(\frac{\partial f}{\partial\nabla\Psi}\right)\delta\nabla\Psi\right]}_{\text{variation of } f \text{ while the surface is constant}} + \underbrace{\oint dS(\Omega,\mathbf{r})\ f\ \times\ \delta S(\Omega,\mathbf{r})}_{\text{variation of the surface while } f \text{ is constant}} + \text{cc} \tag{7.47}$$

where the cc results from the variation of Ψ^*. This result yields (see [85]):

$$\delta\mathcal{G}[\Psi,\Omega] = \underbrace{\int_{\Omega} d\tau\,[\hat{H}\Psi^{*} - E\Psi^{*}]\,\delta\Psi}_{\substack{\text{variation of } f \\ \text{while the surface} \\ \text{is constant}}} + \oint dS(\Omega,\mathbf{r}) \left[\left(\frac{\hbar^2}{2m}\right) \nabla\Psi^{*}\cdot\mathbf{n}(\mathbf{r}) \underbrace{\delta\Psi}_{\substack{\text{variation} \\ \text{of } \Psi \text{ on} \\ \text{the surface}}} + f \times \underbrace{\delta S(\Omega,\mathbf{r})}_{\substack{\text{variation of the} \\ \text{surface through} \\ \text{the variation of } \Psi}} \right] + \text{cc.} \tag{7.48}$$

If the system extends to infinity, that is, when $\Omega = \mathbb{R}^3$ and coincides with the total closed system, its bounding system is, by definition, at infinity. Since the wave function vanishes when $\mathbf{r} = \infty$, hence, in this case $\delta\Psi = 0$ and the surface term also vanishes as a consequence. Alternatively, the surface term can be made to vanish through the imposition of what is known as the *natural boundary conditions*, that is:

$$\nabla\Psi\cdot\mathbf{n}(\mathbf{r}) = 0 \quad \text{and} \quad \nabla\Psi^{*}\cdot\mathbf{n}(\mathbf{r}) = 0 \qquad \forall\ \mathbf{r} = \infty. \tag{7.49}$$

The cancellation of the surface term when $\Omega = \mathbb{R}^3$ simplifies eq. (7.48) to:

$$\delta\mathcal{G}[\Psi,\Omega] = \int_{\Omega} d\tau\,[\hat{H}\Psi - E\Psi]\delta\Psi + \text{cc} = 0. \tag{7.50}$$

However, eq. (7.50) is true for arbitrary variations in Ψ which can only be true if the integrand itself vanishes leading us to Schrödinger equation and its complex conjugate:

$$\hat{H}\Psi = E\Psi \quad \text{and} \quad \hat{H}\Psi^{*} = E\Psi^{*}. \tag{7.51}$$

Thus, Schrödinger's equation applies at the point of variation of Ψ. Since this is the case, the first term in eq. (7.48) vanishes for a subsystem and for the total system. Ridding this equation from this term, we obtain:

$$\delta\mathcal{G}[\Psi,\Omega] = \oint dS(\Omega,\mathbf{r}) \left[\left(\frac{\hbar^2}{2m}\right) \nabla\Psi^{*}\cdot\mathbf{n}(\mathbf{r})\delta\Psi + f(\Psi,\nabla\Psi)\ \delta S(\Omega,\mathbf{r}) \right] + \text{cc.} \tag{7.52}$$

Since the surface term vanishes for the total system, we write:

$$\delta\mathcal{G}[\Psi,(\Omega = \mathbb{R}^3)] = 0. \tag{7.53}$$

In contrast, for a subsystem, $\delta\mathcal{G}[\Psi,\Omega] \neq 0$ in general. In this latter case, and as mentioned explicitly with regard to the second term of eq. (7.48), $\delta\mathcal{G}[\Psi,\Omega]$ as it appears in eq. (7.52) consists of a term proportional to the variation of Ψ at the surface of the subsystem in addition to another term proportional to the variation of the surface. The latter surface term in eq. (7.52) renders this equation nonoperational. To get rid

of this system, one may restrict the subsystem to a particular subclass of all possible open system.

To pursue this restriction, let's first write the integrand $f(\Psi, \nabla\Psi)$, defined in eq. (7.46) which incorporates the Hamiltonian operator, with its complex conjugate. Since $f = f^*$, including the complex conjugate effectively doubles f and we obtain:

$$2f(\Psi, \nabla\Psi) = \left[(\hat{H}\Psi)^*\Psi + \Psi^*\hat{H}\Psi\right] - 2E\Psi^*\Psi + 2\left(\frac{\hbar^2}{4m}\right)\nabla^2(\Psi^*\Psi). \tag{7.54}$$

Since Schrödinger equation and its complex conjugate are assumed to apply, all but the last term in eq. (7.54) vanish and we are left with:

$$f(\Psi, \nabla\Psi) = \left(\frac{\hbar^2}{4m}\right) \nabla^2\rho(\mathbf{r}). \tag{7.55}$$

This result implies that when Schrödinger equation applies the Schrödinger energy functional is proportional to the Laplacian of the electron density. Inserting eq. (7.55) into the expression for $\delta G[\Psi,\Omega]$, that is, eq. (7.52), we get:

$$\delta G[\Psi, \Omega] = \oint dS(\Omega, \mathbf{r}) \left[\left(\frac{\hbar^2}{4m}\right)\left(2\nabla\Psi^* \cdot \mathbf{n}(\mathbf{r})\delta\Psi + \delta S(\Omega, \mathbf{r})\ \nabla^2\rho\right)\right] + \text{cc}. \tag{7.56}$$

This last result leads to an "atomic statement" of the hypervirial theorem upon restricting the subsystem to one satisfying a variational constraint on its form imposed through a trial function Φ. We define subsystem $\Omega = \Omega(\Phi)$ delimited from the full system by a zero-flux surface (eq. (7.19)) that partitions the trial electron density corresponding to Φ, where this density is defined:

$$\rho_\Phi(\mathbf{r}) = \int d\tau'\ \Phi^*\Phi. \tag{7.57}$$

As $\Phi \to \Psi$, the region of space bounded by the zero-flux surface (that we will call an atom-in-a-molecule or a crystal (an AIM for short), henceforth) is continuously approaching the true AIM $\Omega(\Psi)$ as we impose the following variational constraint at all stages of the variation for an admissible trial function Φ:

$$\int\limits_{\Omega(\Phi\to\Psi)} d\mathbf{r}\, \nabla \cdot [\nabla\rho_\Phi] = \int\limits_{\Omega(\Phi\to\Psi)} d\mathbf{r}\, \nabla^2\rho_\Phi = 0, \tag{7.58}$$

which implies:

$$\delta\left[\int\limits_\Omega d\mathbf{r}\nabla^2\rho_\Phi(\mathbf{r})\right] = 0. \tag{7.59}$$

The variation in eq. (7.59) is, once again, a sum of a variation of the surface and the variation of the integrand. Written explicitly, we have:

$$\frac{\hbar^2}{4m}\oint dS(\Omega,\mathbf{r})\ \delta S(\Omega,\mathbf{r})\ \nabla^2\rho(\mathbf{r}) + \frac{\hbar^2}{4m}\int_{\Omega} d\mathbf{r}\ \delta\left[\nabla^2\rho(\mathbf{r})\right] = 0, \tag{7.60}$$

or

$$\frac{\hbar^2}{4m}\oint dS(\Omega,\mathbf{r})\ \delta S(\Omega,\mathbf{r})\ \nabla^2\rho(\mathbf{r}) = -\frac{\hbar^2}{4m}\int_{\Omega} d\mathbf{r}\ \delta\left[\nabla^2\rho(\mathbf{r})\right] \tag{7.61}$$

$$= -\frac{\hbar^2}{4m}\int_{\Omega} d\mathbf{r}\ \nabla\cdot[\nabla\Psi^*\delta\Psi + \Psi^*\nabla\delta\Psi], \tag{7.62}$$

and upon applying Gauss' theorem to convert the volume integral to a surface integral, we obtain:

$$\frac{\hbar^2}{4m}\oint dS(\Omega,\mathbf{r})\ \delta S(\Omega,\mathbf{r})\ \nabla^2\rho(\mathbf{r}) = -\frac{\hbar^2}{4m}\oint dS(\Omega,\mathbf{r})[\nabla\Psi^*\delta\Psi + \Psi^*\nabla\delta\Psi]\cdot\mathbf{n}(\mathbf{r}). \tag{7.63}$$

Inserting this last result into eq. (7.56), we obtain Schrödinger's energy functional for the subsystem expressed as a surface integral of electron current density:

$$\delta\mathcal{G}_{\mathcal{F}}[\Psi,\Omega] = \frac{\hbar^2}{4m}\oint dS(\Omega,\mathbf{r})[(\nabla\Psi^*)\,\delta\Psi - \Psi^*\delta(\nabla\Psi)]\cdot\mathbf{n}(\mathbf{r}) + \text{cc}, \tag{7.64}$$

by varying the expression for the current density (eq. (7.43)) after substituting $\hat{A} = \hat{1}$, we obtain:

$$\delta\mathbf{j}(\mathbf{r}) = \frac{\hbar}{2mi}\ [\Psi^*\delta(\nabla\Psi) - (\nabla\Psi^*)\delta\Psi], \tag{7.65}$$

which upon inserting into eq. (7.64) gives:

$$\delta\mathcal{G}_{\mathcal{F}}[\Psi,\Omega] = -\frac{i\hbar}{2}\oint dS(\Omega,\mathbf{r})\ \delta\mathbf{j}(\mathbf{r})\cdot\mathbf{n}(\mathbf{r}) + \text{cc}. \tag{7.66}$$

At this point, Bader applies Schwinger's infinitesimal unitary transformations [86] acting on the state function or observables. An infinitesimal unitary transformation is represented by the operator:

$$\hat{U} = \hat{1} - \frac{i\varepsilon}{\hbar}\hat{G} \tag{7.67}$$

and its Hermitian conjugate (which is also its inverse):

$$\hat{U}^{-1} = \hat{1} + \frac{i\varepsilon}{\hbar}\hat{G} \tag{7.68}$$

where ε is an infinitesimal and $\hat{G}$ is a linear Hermitian operator that *generates* the transformation. To first order, the variations in Ψ and in Ψ^* are expressed in terms of the generator $\hat{G}$:

$$\delta\Psi = -\frac{i\varepsilon}{\hbar}\hat{G}\Psi \tag{7.69}$$

and

$$\delta\Psi^* = \frac{i\varepsilon}{\hbar}\hat{G}\Psi^*. \tag{7.70}$$

If we now substitute $\delta\Psi$ and $\delta\Psi^*$ in eqs. (7.65) and (7.66) by their infinitesimal generators, we obtain [87]:

$$\delta\mathcal{G}[\Psi,\Omega] = -\frac{\varepsilon}{2}\left[\oint dS(\Omega,\mathbf{r})\ \mathbf{j}_G(\mathbf{r})\cdot\mathbf{n}(\mathbf{r}) + cc\right], \tag{7.71}$$

which is identical to the right-hand side of eq. (7.44) up to a sign and ε. Hence, we may write:

$$\delta\mathcal{G}[\Psi,\Omega] = -\frac{\varepsilon}{2}\left\{\frac{i}{\hbar}\ \langle\Psi|\left[\hat{H},\hat{G}\right]|\Psi\rangle_\Omega + \mathrm{cc}\right\}, \tag{7.72}$$

which is a mathematical expression for the principle of stationary action for a stationary state, whether for the total closed system when $\Omega = \mathbb{R}^3$ or for a subsystem when $\Omega < \mathbb{R}^3$.

The above development brings about the following important conclusion: *The topological and the quantum mechanical AIM are coinciding if the AIM is bounded by a zero-flux surface (*eq. (7.19)).

7.5 The atomic statement of the virial theorem

The atomic virial theorem expressed for an open system is central to QTAIM since it allows one to define the atomic contribution to the total energy uniquely and rigorously. It is also an excellent example of application of the generalized statement of the stationary action, developed in the previous section (expressed in eq. (7.72)), to an open subsystem.

If we now replace the generator $\hat{G}$ in eq. (7.72) by the virial operator $\hat{\mathbf{r}}\cdot\hat{\mathbf{p}}$, where $\hat{\mathbf{r}}$ and $\hat{\mathbf{p}}$ are the position and momentum operators, equating the right-hand side of both eqs. (7.72) and (7.71), and generalizing to an N-electron system, we have:

$$\frac{N}{2}\left\{\frac{i}{\hbar}\langle\Psi|\left[\hat{H},\hat{\mathbf{r}}\cdot\hat{\mathbf{p}}\right]|\Psi\rangle_{\Omega}+\text{cc}\right\}=\frac{N}{2}\left[\oint dS(\Omega,\mathbf{r})\;\mathbf{j}_{\hat{\mathbf{r}}\cdot\hat{\mathbf{p}}}(\mathbf{r})\cdot\mathbf{n}(\mathbf{r})+\text{cc}\right]. \tag{7.73}$$

Evaluating the explicit form of the commutator in the last equation, the L.H.S. gives:

$$\begin{aligned}\frac{N}{2}\left\{\frac{i}{\hbar}\langle\Psi|\left[\hat{H},\hat{\mathbf{r}}\cdot\hat{\mathbf{p}}\right]|\Psi\rangle_{\Omega}+\text{cc}\right\}&=2N\left(\frac{\hbar^2}{4m}\right)\int_{\Omega}d\mathbf{r}\int d\tau'\;\left[\Psi^*\nabla^2\Psi+(\nabla^2\Psi^*)\Psi\right]\\&\quad+N\int_{\Omega}d\mathbf{r}\int d\tau'\;\Psi^*(-\mathbf{r}\cdot\nabla\hat{V})\Psi,\end{aligned} \tag{7.74}$$

which defines the two resulting terms on the right side of eq. (7.74) by re-writing it in a condensed and more suggestive form as:

$$\frac{N}{2}\left\{\frac{i}{\hbar}\langle\Psi|\left[\hat{H},\hat{\mathbf{r}}\cdot\hat{\mathbf{p}}\right]|\Psi\rangle_{\Omega}+\text{cc}\right\}=2T(\Omega)+V_b(\Omega)\,, \tag{7.75}$$

where $V_b(\Omega)$ is the volume integral of the virial of the Ehrenfest force acting on an electron over the basin of atom Ω, and where $T(\Omega)$ is the volume integral of the kinetic energy density over the same AIM. The virial has dimensions of energy and $V_b(\Omega)$ represents the contribution of the virial of the Ehrenfest force integrated over the volume of the subsystem's basin to the potential energy of that atom in the molecule or crystal.

Turning to the right-hand side of eq. (7.73), if we substitute eq. (7.43), we obtain:

$$\begin{aligned}&\frac{N}{2}\left[\oint dS(\Omega,\mathbf{r})\;\mathbf{j}_{\hat{\mathbf{r}}\cdot\hat{\mathbf{p}}}(\mathbf{r})\cdot\mathbf{n}(\mathbf{r})+cc\right]=\\&-\frac{N\hbar^2}{4m}\left\{\oint dS(\Omega,\mathbf{r})\int d\tau'\left[\begin{array}{l}\Psi^*\boldsymbol{\nabla}(\mathbf{r}\cdot\nabla\Psi)-\nabla\Psi^*(\mathbf{r}\cdot\nabla\Psi)\\+\Psi\boldsymbol{\nabla}(\mathbf{r}\cdot\nabla\Psi^*)-\nabla\Psi(\mathbf{r}\cdot\nabla\Psi^*)\end{array}\right]\cdot\mathbf{n}(\mathbf{r})\right\},\end{aligned} \tag{7.76}$$

which is a result that, using the vector calculus identity

$$\boldsymbol{\nabla}(\mathbf{r}\cdot\nabla\Psi)=\nabla\Psi+\mathbf{r}\cdot\boldsymbol{\nabla}\nabla\Psi, \tag{7.77}$$

can be written more compactly as:

$$\begin{aligned}&\frac{N}{2}\left[\oint dS(\Omega,\mathbf{r})\;\mathbf{j}_{\hat{\mathbf{r}}\cdot\hat{\mathbf{p}}}(\mathbf{r})\cdot\mathbf{n}(\mathbf{r})+cc\right]=\\&\underbrace{-\oint dS(\Omega,\mathbf{r})\;\mathbf{r}\cdot\vec{\sigma}(\mathbf{r})\cdot\mathbf{n}(\mathbf{r})}_{-V_S(\Omega)}\;\underbrace{-\frac{\hbar^2}{4m}\oint dS(\Omega,\mathbf{r})\,\nabla\rho(\mathbf{r})\cdot\mathbf{n}(\mathbf{r})}_{L(\Omega)}\,,\end{aligned} \tag{7.78}$$

where the last term is nothing but the atomic integral of the Laplacian function as it appears in eq. (7.28), and where the one-electron quantum stress tensor $\overleftrightarrow{\boldsymbol{\sigma}}(\mathbf{r})$ is defined as:

$$\overleftrightarrow{\boldsymbol{\sigma}}(\mathbf{r}) = -\frac{\hbar^2}{4m}[\Psi^*\nabla(\nabla\Psi) + \nabla(\nabla\Psi^*)\Psi - \nabla\Psi^*\nabla\Psi - \nabla\Psi\nabla\Psi^*]. \tag{7.79}$$

The first term on the right-hand side of eq. (7.78) is the negative of the virial of the Ehrenfest forces acting on the surface of the atom ($\mathbf{r}\cdot\overleftrightarrow{\boldsymbol{\sigma}}(\mathbf{r})\cdot\mathbf{n}(\mathbf{r})$), where $\overleftrightarrow{\boldsymbol{\sigma}}(\mathbf{r})\cdot\mathbf{n}(\mathbf{r})$ has the dimension of force per unit area and is pointing to the outside of the subsystem. The virial itself has the dimension of energy. The contribution of the surface virial to the energy of an AIM is, thus, written as:

$$\mathcal{V}_S(\Omega) = \oint dS(\Omega,\mathbf{r})\ \mathbf{r}\cdot\overleftrightarrow{\boldsymbol{\sigma}}(\mathbf{r})\cdot\mathbf{n}(\mathbf{r}). \tag{7.80}$$

A comparison of eqs. (7.75) and (7.78) allows us to write:

$$2T(\Omega) + \mathcal{V}_b(\Omega) = -\mathcal{V}_S(\Omega) + L(\Omega), \tag{7.81}$$

which, upon realizing that the integral of the Laplacian function over an AIM (also known as the atomic Lagrangian) vanishes, that is, that:

$$\int_\Omega d\mathbf{r}\,\nabla^2\rho = 0, \tag{7.82}$$

simplifies to:

$$\mathcal{V}(\Omega) = -2T(\Omega), \tag{7.83}$$

where

$$\mathcal{V}(\Omega) \equiv \mathcal{V}_b(\Omega) + \mathcal{V}_S(\Omega), \tag{7.84}$$

is the total atomic virial stemming from two contributions: a basin and a surface term. The result in eq. (7.83) is Bader's expression of the virial theorem for an atom in a molecule.

Thus, in analogy to the molecular total energy, an AIM's energy is the sum of its virial and kinetic energy contributions. If there are no net forces exerted on the nuclei (i.e., in an optimized geometry) there are no additional terms due to the virial of these forces, and in this case the atom's electronic virial expressed in eq. (7.84) is identified as its potential energy $\mathcal{V}(\Omega) = V(\Omega)$. We have now proved the important result expressed above in eqs. (7.29) and (7.30).

Given the atomic statement of the virial theorem for an equilibrium geometry, whether a local or global minimum or a transition state on the potential energy surface, the total energy of the system can now be written as a sum of virial atomic energies (eq. (7.31)). This remarkable result is a quantum mechanical partitioning of all

the complicated interactions within a molecule into additive atomic energies each of which includes in it contributions from electron–nuclear, electron–electron, and nuclear–nuclear interactions that are difficult or impossible to split on an atom-by-atom basis individually otherwise.

7.6 The Laplacian of the electron density

From eqs. (7.14) and (7.15), the Laplacian can be either positive or negative in its overall sign and can be zero. If $\nabla^2\rho(\mathbf{r}) > 0$, this indicates a local depletion of electronic charge density relative to its average surroundings while if $\nabla^2\rho(\mathbf{r}) < 0$ then the density is locally concentrated. Such local charge concentrations and depletions have been found to play the role of Lewis basic/acidic centers, respectively. Generally (at least for the 3–4 first rows of the Periodic Table), the Laplacian reflects well the atomic shell structure in isolated atoms. In this sense, and unlike the monotonically declining electron density as a function of the distance from a give nucleus, the Laplacian captures the alternation of charge concentration and charge depletion that characterize an atomic shell [88, 89]. The outermost charge concentration shell, the so-called valence shell charge concentration (VSCC), is surrounded from the exterior by a sphere of charge depletion that goes to infinity. In a molecule or a crystal, the spherical symmetry of the VSCC can be broken and it can also be punctured. In these cases, and quoting Bader, a "lump" in the VSCC represents an electron donating region (a Lewis basic center) while a "hole" in the Laplacian plays the role of a Lewis acid center. In view of its depiction of regions of electronic charge concentration and depletion, the Laplacian has been shown to provide the physical basis for the Gillespie–Nyholm valence shell electron pair repulsion model (more commonly referred to in literature as the VSEPR model) of molecular geometry [90–97].

7.7 Examples of bond properties

This and the next section are far from a complete survey of all the bond properties. Only a few commonly used ones are cited briefly to keep this work self-contained.

7.7.1 The electron density at the BCP (ρ_b)

The electron density at the BCP provides a measure of the strength of the chemical bond especially in predominantly covalent type of bonding (with small or no charge transfer).

7.7.2 The Laplacian of the electron density at the BCP ($\nabla^2\rho_b$)

From eqs. (7.14) and (7.15), the Laplacian, evaluated at the BCP, is the sum of the three curvatures. By definition, the two curvatures that are perpendicular to the BP are listed first in decreasing order of their magnitudes ($|\lambda_1| > |\lambda_2|$) and both are negative, while the curvature parallel to the BP, the only positive one, is λ_3.

The magnitudes of the two negative curvatures quantify the degree to which density is concentrated along the bond path. The magnitude of the positive curvature measures the extent to which the electron density it is depleted at the point of intersection of the bond path and the interatomic surface and concentrated in the direction of the bonded atoms' nuclei.

In a primarily covalent interaction with significant electron sharing, the density is accumulated between the nuclei such that such bonding is characterized by a relatively large magnitude of ρ_b and by a negative Laplacian, an example is a C–H bond with $\rho_b = 0.29$ au and $\nabla^2\rho_b = -1.1$ au. Closed-shell interactions, on the other hand, are characterized by a removal of electron density from the contact region of the two bonded atoms and hence the magnitude of ρ_b is relatively small and the Laplacian is positive. An example of the latter is a typical hydrogen bond such as >C=O. . .H–N< with $\rho_b = 0.01$ au and $\nabla^2\rho_b = +0.03$ au. Finally, for significantly polar interactions, as in C=O, charge still accumulates between the nuclei as in shared interactions but the dominance of charge transfer is such that the BCP occurs where the valence density borders the core of the electropositive atom. In this case, the Laplacian rises steeply then changes sign and, hence, $\nabla^2\rho_b$ can be of either sign for such polar bonding.

7.7.3 The bond ellipticity (ε)

This is a gauge of the preferential accumulation of the electronic charge density within a given plane and is defined as:

$$\varepsilon = \frac{\lambda_1}{\lambda_2} - 1 \qquad (\text{where } |\lambda_1| \geq |\lambda_2|). \tag{7.85}$$

For cylindrically-symmetric bonds, for example, the carbon–carbon bond in ethane or the triple bond in acetylene, $\lambda_1 = \lambda_2$ and $\varepsilon = 0$. Contrast this with a π-bonding situation in ethylene where $\varepsilon \approx 0.45$ or with an aromatic ring such as benzene where $\varepsilon \approx 0.23$.

7.7.4 Energy densities at the BCP

The potential energy density (the virial field density), $V(\mathbf{r})$, is always negative. The integral of this density over all space delivers the potential energy of the molecule.

Bader has derived a local statement of the virial theorem which, for a stationary state, is [29, 87]:

$$\left(\frac{\hbar^2}{4m}\right)\nabla^2\rho(\mathbf{r}) = 2G(\mathbf{r}) + V(\mathbf{r}), \tag{7.86}$$

where the gradient kinetic energy density (which is always a positive quantity) is defined as:

$$G(\mathbf{r}) = \frac{\hbar^2}{2m}N\int d\tau'\ \nabla\Psi^*\cdot\nabla\Psi. \tag{7.87}$$

Since $G(\mathbf{r}) > 0$ and $V(\mathbf{r}) < 0$, and the sum is a term proportional to the Laplacian of the electron density, a bonding interaction where $\nabla^2\rho_b < 0$ is driven by a local lowering of the potential energy, while when $\nabla^2\rho_b > 0$ the bonding is driven by a local kinetic energy excess.

Cremer and Kraka proposed to evaluate the total energy density [$H(\mathbf{r}) = G(\mathbf{r}) + V(\mathbf{r})$] at the BCP [98]. From its name, the total energy density delivers the total energy of the system when integrated over all space. This density, $H(\mathbf{r})$, places the kinetic and potential energy densities on an equal footing (no factor 2 in front of $G(\mathbf{r})$). Generally, when $H_b < 0$, this indicates that the interaction is driven by electron sharing (i.e., can be described as predominantly covalent) while $|H_b|$ reflects the degree of "covalency" of the interaction [98].

7.8 Atomic contributions to molecular properties

The molecular expectation value of an operator, $\langle\hat{O}\rangle_{molecule}$, can be written as a sum of the corresponding expectation values averaged over the M atoms (or atoms and NNAs if these exist in the system) in the molecule:

$$\left\langle\hat{O}\right\rangle_{molecule} = \sum_{i=1}^{M}\left(N\int_{\Omega_i}\left\{\int\frac{1}{2}[\Psi^*\hat{O}\Psi + (\hat{O}\Psi)^*\Psi]d\tau'\right\}d\mathbf{r}\right), \tag{7.88}$$

$$= \sum_{i=1}^{M}\left(\int_{\Omega_i}\rho_O d\mathbf{r}\right) = \sum_{i=1}^{M}O(\Omega_i), \tag{7.89}$$

where $O(\Omega_i)$ is the operator averaged over the ith atom Ω_i. In this manner, as long as a physical quantity O is expressible as a real space density, $\rho_O(\mathbf{r})$, then it can be expressed in the form of a sum of atomic contributions.

7.9 Examples of atomic properties

Averaging an operator $\hat{O}$ over an AIM delivers that atom's contribution to the molecular counterpart of this property. Hence:

$$O(\Omega) = \left\langle \hat{O} \right\rangle_{\Omega} = \frac{N}{2} \int_{\Omega} d\mathbf{r} \int d\tau' \left[\Psi^* \hat{O} \Psi + (\hat{O}\Psi)^* \Psi \right]. \tag{7.90}$$

A few examples of explicit atomic properties commonly discussed in the literature are briefly outlined below.

7.9.1 Atomic population [$N(\Omega)$] and charge [$q(\Omega)$]

Setting $\hat{O} = \hat{1}$ in eq. (7.90) converts it into an equation to compute the electronic population of an atom as:

$$N(\Omega) = \int_{\Omega} \rho(\mathbf{r}) d\mathbf{r}, \tag{7.91}$$

which upon subtraction from the atomic number gives the QTAIM atomic charge (in atomic units):

$$q(\Omega) = Z_{\Omega} - N(\Omega), \tag{7.92}$$

7.9.2 Kinetic energy [$T(\Omega)$]

From eq. (7.25) we have the Schrödinger kinetic energy:

$$K(\Omega) = -\frac{\hbar^2}{4m} N \int_{\Omega} d\mathbf{r} \int d\tau' \left[\Psi \nabla^2 \Psi^* + \Psi^* \nabla^2 \Psi \right], \tag{7.93}$$

while the gradient kinetic energy is expressed as:

$$G(\Omega) = \frac{\hbar^2}{2m} N \int_{\Omega} d\mathbf{r} \int d\tau' \, \nabla \Psi^* \cdot \nabla \Psi. \tag{7.94}$$

For a subsystem bounded by a zero-flux surface, we have the analogue of the total system's eq. (7.26):

$$K(\Omega) = G(\Omega) = T(\Omega). \tag{7.95}$$

In practical calculations, the (small) deviations from this equality measured by the integral of the atomic Laplacian function is often taken as a measure of the accuracy of the numerical integration.

7.9.3 The atomic integrated Laplacian [$L(\Omega)$]

The Laplacian function (of dimensions of electrons × (length)$^{-5}$) vanishes when integrated over the total system or over the basin of an AIM:

$$L(\Omega) = K(\Omega) - G(\Omega) = -\frac{\hbar^2}{4m}\int_{\Omega} d\mathbf{r}\ \left[\nabla^2\rho(\mathbf{r})\right] = -\frac{\hbar}{4m}\int dS(\Omega,\mathbf{r})\,\nabla\rho(\mathbf{r})\cdot\mathbf{n}(\mathbf{r}) = 0. \qquad (7.96)$$

7.9.4 The (virial) atomic energy [$E(\Omega)$]

As already mentioned above, for a subsystem bounded by a zero-flux surface, eqs. (7.95) and (7.30) apply and the atomic energy $E(\Omega)$ is simply the negative of the unique kinetic energy $T(\Omega)$.

7.10 Back to experiment

The exposition in this chapter has, so far, briefly outlined some of the common tenets of QTAIM and some of its theoretical underpinnings. As explained earlier in this chapter, QTAIM starts from the topography of the electron density, using its associated gradient vector field to partition the system into separate atomic basins and to define bond paths and the separatrices (the zero-flux surfaces) between bonded atoms. The exposition outlined above should have demonstrated to the reader that the partitioning of the electron density space at the zero-flux surfaces has deep roots in quantum mechanical theory.

The electron density could be calculated from theory or derived from experiment as discussed in several parts of this book. Relation (7.7) summarizes conceptually the position of the electron density at the junction of theory and experiment. From this electron density one can get several, but – importantly – not all, the information that could be known about the system, the first Hohenberg–Kohn theorem notwithstanding. The analysis of experimentally-derived electron densities by QTAIM routinely includes discussions and displays of electron density maps, electron density deformation (difference) maps, atomic charges and higher electric multipoles, bond paths, bond ellipticities, and so on.

As seen above, QTAIM, however, does not stop at the analysis of the electron density alone. Rather it takes it as its starting point and once the system is divided into separate atoms in a molecule or a crystal, the wave function can then be analyzed and averaged over parts of the system as outlined above. This is how one obtains, for example, energy or electron pairing and/or (de)localization information. There are approximations that are widely used to obtain energy information from only the electron density. We cite two examples of particular importance.

The first is due to Abramov, who approximates the kinetic energy density $G(\mathbf{r})$ where both the electron density and its Laplacian have relatively small magnitudes [99]. This last requirement limits the validity of this approximation to within *ca.* 0.5–2.1 Å from an atomic nucleus. In atomic units (au) – as originally and often quoted – the Abramov expression reads [99]:

$$G(\mathbf{r}) = \left(\frac{3}{10}\right)\left(3\pi^2\right)^{2/3}\rho(\mathbf{r})^{5/3} + \left(\frac{1}{72}\right)\frac{|\nabla\rho(\mathbf{r})|}{\rho(\mathbf{r})} + \left(\frac{1}{6}\right)\nabla^2\rho(\mathbf{r}). \tag{7.97}$$

By the use of the local virial theorem, written again in au [100]:

$$\frac{1}{4}\nabla^2\rho(\mathbf{r}) = 2G(\mathbf{r}) + V(\mathbf{r}), \tag{7.98}$$

to obtain $V(\mathbf{r})$, one can also obtain an approximation to the total energy density $H(\mathbf{r}) = G(\mathbf{r}) + V(\mathbf{r})$ within the region of applicability of the Abramov expression from the electron density alone.

The second example is a study that examines the behavior of a large number of observed hydrogen bonding interactions in the crystallographic databases by Espinosa, Molins, and Lecomte [101]. These authors propose an empirical relation between a given hydrogen bond dissociation energy (D_e) in dimers and the potential energy density evaluated using Abramov's relation [101]:

$$E = -D_e = \frac{1}{2}V(\mathbf{r}_b). \tag{7.99}$$

The limitations of this relation have been discussed in a paper by Spackman [102].

The energy densities are recognizably of great interest but the use of expressions such as the ones quoted above have limitations of their applicability. The construction of experiment-consistent density matrices that are *N*-representable opens the door for the application of the full quantum mechanical mathematical apparatus of QTAIM starting from experimental diffraction data. For further discussion see Refs. [103, 104].

7.11 Conclusion

In this chapter, we have seen the central role of Bader's zero-flux condition which, when used in conjunction with the atomic statement of the virial theorem, provides a quantum mechanical partitioning of the real three-dimensional space into atomic basins. Each atomic basin contains one nucleus (or in less frequent cases a NNA). In all cases, a nucleus or an NNA is bonded to its neighbors via bond paths and virial paths. This is how the entire three-dimensional topography delivers the bonded topology of the system. Shahbazian and Goli have generalized QTAIM whereby protons are taken as quantum particles (and where the total wave function is expressed as a product of electronic and protonic wave functions) [105]. In doing so, the hydrogen atom basin splits and the highest density of the proton is split between the extremes of what would be classically the vibration amplitude about the equilibrium bond length [105]. Anderson and Ayers have shown that the zero-flux condition survives upon a scalar relativistic treatment [106], which is another important generalization of QTAIM.

The atomic virial theorem allows one to define additive atomic contributions to the total energy. This contribution is simply $-T(\Omega)$, an enormous simplification since it avoids the (impossible) explicit evaluation of the potential terms since the potential energy contribution of an atom in molecule must contain contributions from the nuclear-electronic attraction between the electron of the basin and all nuclei in the molecule, the electron–electron repulsion between the electrons in the basin and themselves and between them and the rest of the electrons in the molecules, and also a term due to the contribution of the nucleus of the atom in question to the overall nuclear–nuclear repulsion energy whereby we write:

$$V(\Omega) = V_{ne}(\Omega) + V_{ee}(\Omega) + V_{nn}(\Omega). \tag{7.100}$$

Equations (7.29) and (7.30) allow us to bypass the necessity for the explicit evaluation of the terms in eq. (7.100) and jump right to the final answer by averaging only a one-electron operator over the volume of the atom (or the pseudo-atom in case of an NNA), that is, the kinetic energy operator. Therein lies the importance of QTAIM in that it provides a coherent and complete decomposition of molecular properties into corresponding additive atomic properties. Such properties include one- and two-electron atomic contributions whether scalar, vector, or a higher-order tensor in nature.

References

[1] Russell, B. *A History of Western Philosophy*. Simon and Schuster, New York, (1945).
[2] Bader, RFW. *Atoms in Molecules: A Quantum Theory*. Oxford University Press, Oxford, U.K., (1990).

[3] Matta, CF. De la topographie de la densité électronique à une théorie quantique des atomes dans les molécules (From the topography of the electron density to a quantum theory of atoms in molecules). *Le BUP (Physique – Chimie)* 111, 825–845 (2017).
[4] Bader, RFW, Matta, CF. Atoms in molecules as non-overlapping, bounded, space-filling open quantum systems. *Found. Chem.* 15, 253–276 (2013).
[5] Matta, CF. On the connections between the quantum theory of atoms in molecules (QTAIM) and density functional theory (DFT): A letter from Richard F. W. Bader to Lou Massa. *Struct. Chem.* 28, 1591–1597 (2017).
[6] Popelier, PLA. *Atoms in Molecules: An Introduction*. Prentice Hall, London, (2000).
[7] Matta, CF, Boyd, RJ (Eds.). *The Quantum Theory of Atoms in Molecules: From Solid State to DNA and Drug Design*. Wiley-VCH, Weinheim, (2007).
[8] Hohenberg, P, Kohn, W. Inhomogeneous electron gas. *Phys. Rev. B* 136, 864–871 (1964).
[9] Bader, RFW, Jones, GA. The electron density distribution in hydride molecules. The ammonia molecule. *J. Chem. Phys.* 38, 2791–2802 (1963).
[10] Löwdin, P-O. Correlation problem in many-electron quantum mechanics I. Review of different approaches and discussion of some current ideas. *Adv. Chem. Phys.* 2, 207–322 (1959).
[11] Hellmann, H. *Einführung in Die Quantenchemie*. Deuticke, Leipzig and Vienna, (1937).
[12] Feynman, RP. Forces in molecules. *Phys. Rev.* 56, 340–343 (1939).
[13] Rhodes, G. *Crystallography Made Crystal Clear: A Guide for Users of Macromolecular Models (Third Edition)*. Elsevier, Inc. and Academic Press, Inc., San Diego, (2006).
[14] James, JF. *A Student Guide to Fourier Transforms: With Applications in Physics and Engineering*; Cambridge University Press: Cambridge, UK (1995).
[15] Champeney, DC. *Fourier Transforms in Physics*. Wiley Eastern, Ltd., New Delhi, (1985).
[16] Aubert, E, Lecomte, C. Illustrated Fourier transforms for crystallography. *J. Applied Cryst.* 40, 1153–1165 (2007).
[17] Mulliken, RS. Molecular orbital method and molecular ionization potential. *Phys. Rev.* 74, 736–738 (1948).
[18] Roothaan, CCJ. New developments in molecular orbital theory. *Rev. Mod. Phys.* 23, 69–89 (1951).
[19] Roberts, JD. *Notes on Molecular Orbital Calculations*. W. A. Benjamin, Inc., New York, (1962).
[20] Salem, L. *The Molecular Orbital Theory of Conjugated Systems*. W. A. Benjamin, Inc., New York, (1966).
[21] Pople, JA, Beveridge, DL. *Approximate Molecular Orbital Theory*. McGraw-Hill, Inc., New York, (1970).
[22] Hehre, WJ, Radom, L, Pople, JA, Schleyer, P. *Ab Initio Molecular Orbital Theory*. Wiley-Interscience, New York, (1986).
[23] Gallup, GA. *Valence Bond Methods*. Cambridge University Press, Cambridge, (2002).
[24] Shaik, S, Hiberty, PC. *A Chemist's Guide to Valence Bond Theory*. John Wiley and Sons, Inc., New Jersey, (2007).
[25] Hoffmann, R, Shaik, S, Hiberty, PC. A conversation on VB vs MO theory: A never-ending rivalry?. *Acc. Chem. Res.* 36, 750–756 (2003).
[26] Bader, RFW. Everyman's derivation of the theory of atoms in molecules. *J. Phys. Chem. A* 111, 7966–7972 (2007).
[27] Bader, RFW. The quantum mechanical basis of conceptual chemistry. *Monatsh. Chem.* 136, 819–854 (2005).
[28] Bader, RFW. A quantum theory of molecular structure and its applications. *Chem. Rev.* 91, 893–928 (1991).
[29] Bader, RFW, Nguyen-Dang, TT. Quantum theory of atoms in molecules – Dalton revisited. *Adv. Quantum Chem.* 14, 63–124 (1981).

[30] Kato, WA. On the eigenfunctions of many-particle systems in quantum mechanics. *Commun. Pure Appl. Math.* 10, 151–177 (1957).
[31] Anderson, JSM, Massa, L, Matta, CF. Non-nuclear maxima and the universality of Bright Wilson's justification of the first Hohenberg Kohn theorem revisited. *Chem. Phys. Lett.* 780, Article # 138940, 1–6 (2021).
[32] Mayer, I. *Simple Theorems, Proofs, and Derivations in Quantum Chemistry*. Kluwer Academic/Plenum Publishers, New York, (2003).
[33] Matta, CF. *Applications of the Quantum Theory of Atoms in Molecules to Chemical and Biochemical Problems; Ph.D. Thesis*. McMaster University, Hamilton, Canada, (2002).
[34] Runtz, GR, Bader, RFW, Messer, RR. Definition of bond paths and bond directions in terms of the molecular charge distribution. *Can. J. Chem.* 55, 3040–3045 (1977).
[35] Bader, RFW. Bond paths are not chemical bonds. *J. Phys. Chem. A* 113, 10391–10396 (2009).
[36] Bader, RFW. A bond path: A universal indicator of bonded interactions. *J. Phys. Chem. A* 102, 7314–7323 (1998).
[37] Bader, RFW, Matta, CF, Cortés-Guzmán, F. Where to draw the line in defining a molecular structure. *Organometallics* 23, 6253–6263 (2004).
[38] Jones, TE, Eberhart, ME, Imlay, S, Mackey, C, Olson, GB. Better alloys with quantum design. *Phys. Rev. Lett.* 109, 125506 (2012).
[39] Jones, TE, Eberhart, ME. The bond bundle in open systems. *Int. J. Quantum Chem.* 110, 1500–1505 (2010).
[40] Jones, TE, Eberhart, ME. The irreducible bundle: Further structure in the kinetic energy distribution. *J. Chem. Phys.* 130, 204108 (2009).
[41] Johansson, M. Summary: Total electron density cusps outside nuclei. *CCL: http://www.ccl.net/chemistry/resources/messages/2009/10/18.001-dir/index.html* (2009).
[42] Matta, CF (Ed.). *Quantum Biochemistry: Electronic Structure and Biological Activity (Vols. 1 And 2)*. Wiley-VCH, Weinheim, (2010).
[43] Martín-Pendás, Á, Francisco, E, Blanco, MA, Gatti, C. Bond paths as privileged exchange channels. *Chem. Eur. J.* 13, 9362–9371 (2007).
[44] Keith, TA, Bader, RFW, Aray, Y. Structural homeomorphism between the electron density and the virial field. *Int. J. Quantum Chem.* 57, 183–198 (1996).
[45] Contreras-García, J, Johnson, ER, Keinan, S, Chaudret, R, Piquemal, J-P, Beratan, D, Yang, W. NCIPLOT: A program for plotting non-covalent interaction regions. *J. Chem. Theory. Comput.* 7, 625–632 (2011).
[46] Bader, RFW, Matta, CF. Bonding to titanium. *Inorg. Chem.* 40, 5603–5611 (2001).
[47] Tomaszewski, R, Hyla-Kryspin, I, Mayne, CL, Arif, AM, Gleriter, R, Ernst, R. Shorter non-bonded than bonded contacts or nonclassical metal-to-saturated carbon atom interactions?. *J. Am. Chem. Soc.* 120, 2959–2960 (1998).
[48] Bürgi, H-B, Dunitz, JD. *Structure Correlation, Volume 1*. VCH, Weinheim, (1994).
[49] Batsanov, SS. Van der Waals radii of elements. *Inorg. Mater.* 37, 871–885 (2001).
[50] Matta, CF, Hernández-Trujillo, J, Tang, TH, Bader, RFW. Hydrogen-hydrogen bonding: A stabilizing interaction in molecules and crystals. *Chem. Eur. J.* 9, 1940–1951 (2003).
[51] Cioslowski, J, Mixon, ST. Universality among topological properties of electron density associated with the hydrogen-hydrogen nonbonding interactions. *Can. J. Chem.* 70, 443–449 (1992).
[52] Poater, J, Visser, R, Solà, M, Bickelhaupt, FM. Polycyclic benzenoids: Why kinked is more stable than straight. *J. Org. Chem.* 72, 1134–1142 (2007).
[53] Poater, J, Solà, M, Bickelhaupt, FM. Hydrogen-hydrogen bonding in planar biphenyl, predicted by atoms-in-molecules theory, does not exist. *Chem. Eur. J.* 12, 2889–2895 (2006).

[54] Poater, J, Solà, M, Bickelhaupt, FM. A model of the chemical bond must be rooted in quantum mechanics, provide insight, and possess predictive power. *Chem. Eur. J.* 12, 2902–2905 (2006).
[55] Bader, RFW. Definition of molecular structure: By choice or by appeal to observation?. *J. Phys. Chem. A* 114, 7431–7444 (2010).
[56] Bader, RFW. Pauli repulsions exist only in the eye of the beholder. *Chem. Eur. J.* 12, 2896–2901 (2006).
[57] Wolstenholme, D, Matta, CF, Cameron, TS. Experimental and theoretical electron density study of a highly twisted polycyclic aromatic hydrocarbon: 4 Methyl-[4]helicene. *J. Phys. Chem. A* 111, 8803–8813 (2007).
[58] Wolstenholme, DJ, Cameron, TS. Comparative study of weak interactions in molecular crystals: H-H bonds vs hydrogen bonds. *J. Phys. Chem. A* 110, 8970–8978 (2006).
[59] Robertson, KN, Knop, O. Cameron TS. C-H···H-C interactions in organoammonium tetraphenylborates: Another look at dihydrogen bonds. *Can. J. Chem.* 81, 727–743 (2003).
[60] García-Ramos, JC, Cortés-Guzmán, F, Matta, CF. Intermolecular interactions in molecular crystals: Fundamentals of crystal engineering. Chapter 16 in: *On the Nature of Hydrogen-Hydrogen Bonding*; Novoa, JJ (Ed.), Royal Society of Chemistry, London, UK (2018), 559–594.
[61] Hernández-Trujillo, J, Matta, CF. Hydrogen-hydrogen bonding in biphenyl revisited. *Struct. Chem.* 18, 849–857 (2007).
[62] Matta, CF. Hydrogen-hydrogen bonding: The non-electrostatic limit of closed-shell interaction between two hydrogen atoms. A critical review. Chapter 9 in: *Hydrogen Bonding – New Insight*, (Challenges and Advances in Computational Chemistry and Physics Series); Grabowski, S (Ed.), Springer (2006), 337–375.
[63] Cukrowski, I, Matta, CF. Hydrogen-hydrogen bonding: A stabilizing interaction in strained chelating rings of metal complexes in aqueous phase. *Chem. Phys. Lett.* 499, 66–69 (2010).
[64] Sabirov, D. A correlation between the mean polarizability of the "kinked" polycyclic aromatic hydrocarbons and the number of H…H bond critical points predicted by Atoms-in-Molecules theory. *Comput. Theor. Chem.* 1030, 81–86 (2014).
[65] Monteiro, NKV, Firme, CL. Hydrogen-hydrogen bonds in highly branched alkanes and in alkane complexes: A DFT, *ab initio*, QTAIM, and ELF study. *J. Phys. Chem. A* 118, 1730–1740 (2014).
[66] Bakhmutov, VI. *Dihydrogen Bonds: Principles, Experiments, and Applications*. Wiley-Interscience, New Jersey, (2008).
[67] Firme, CL. *Introductory Organic Chemistry and Hydrocarbons: A Physical Chemistry Approach*. CRC Press, New York, (2020).
[68] Gupta, VP. *Principles and Applications of Quantum Chemistry*. Elsevier, Academic Press, Amsterdam, (2016).
[69] Matta, CF, Sadjadi, S, Braden, DA, Frenking, G. The barrier to the methyl rotation in *cis*-2-butene and its isomerization energy to *trans*-2-butene revisited. *J. Comput. Chem.* 37, 143–154 (2016).
[70] Calaprice, A. *The Ultimate Quotable Einstein*. Princeton University Press and The Hebrew University of Jerusalem, Princeton, NJ, (2011).
[71] Echeverría, J, Aullón, G, Danovich, D, Shaik, S, Alvarez, S. Dihydrogen contacts in alkanes are subtle but not faint. *Nature Chem.* 3, 323–330 (2011).
[72] Grabowski, SJ. High-level *ab initio* calculations of dihydrogen-bonded complexes. *J. Phys. Chem. A* 104, 5551–5557 (2000).
[73] Calhorda, MJ. Weak hydrogen bonds: Theoretical studies. *Chem. Commun* 801–809 (2000).
[74] Popelier, PLA. Characterization of a dihydrogen bond on the basis of the electron density. *J. Phys. Chem. A* 102, 1873–1878 (1998).

[75] Alkorta, I, Rozas, I, Elguero, J. Non-conventional hydrogen bonds. *Chem. Soc. Rev.* 27, 163–170 (1998).
[76] Crabtree, RH. Dihydrogen complexes: Some structural and chemical studies. *Acc. Chem. Res.* 23, 95–101 (1990).
[77] Coppens, P. *X-ray Charge Densities and Chemical Bonding*. Oxford University Press, Inc., New York, (1997).
[78] Castillo, N, Matta, CF, Boyd, RJ. The first example of a cage critical point in a single ring: A novel twisted α-helical topology. *Chem. Phys. Lett.* 409, 265–269 (2005).
[79] Castanedo, LAM, Matta, CF, Ylijoki, KEO. The reaction path of cyclooctatetraene dimerization revisited. *Int. J. Quantum Chem.* 122, Article # e26866, 1–16 (2022).
[80] Cohen, L. Local kinetic energy in quantum mechanics. *J. Chem. Phys.* 70, 788–789 (1979).
[81] Cohen, L. Representable local kinetic-energy. *J. Chem. Phys.* 80, 4277–4279 (1984).
[82] Anderson, JSM, Ayers, PW, Rodriguez-Hernández, JI. How ambiguous is the local kinetic energy?. *J. Phys. Chem. A* 114, 8884–88895 (2010).
[83] Schrödinger, E. Quantisierung als eigenwertproblem. *Ann. D. Phys.* 79, 361–376 (1926).
[84] Srebrenik, S, Bader, RFW. Towards the development of the quantum mechanics of a subspace. *J. Chem. Phys.* 63, 3945–3961 (1975).
[85] Bader, RFW. Polanyi award lecture: Why are there atoms in chemistry? *Can. J. Chem.* 76, 973–988 (1998).
[86] Schwinger, J. The theory of quantized fields. I. *Phys. Rev.* 82, 914–927 (1951).
[87] Bader, RFW. Principle of stationary action and the definition of a proper open system. *Phys. Rev. B* 49, 13348–13356 (1994).
[88] Sagar RP, Ku ACT, Smith VH Jr, Simas AM. The Laplacian of the charge density and its relationship to the shell structure of atoms and ions. *J. Chem. Phys.* 88, 4367–4374 (1988).
[89] Shi, Z, Boyd, RJ. The shell structure of atoms and the Laplacian of the charge density. *J. Chem. Phys.* 88, 4375–4377 (1988).
[90] Gillespie, RJ, Nyholm, RS. *Quart. Rev. Chem. Soc.* 11, 339–380 (1957).
[91] Gillespie, RJ, Nyholm, RS. In: *Progress in Stereochemistry*; Butterworths, London (1958).
[92] Gillespie, RJ, Hargittai, I. *The VSEPR Model of Molecular Geometry*. Allyn and Bacon, Boston, (1991).
[93] Bader, RFW, MacDougall, PJ, Lau, CDH. Bonded and nonbonded charge concentrations and their relations to molecular geometry and reactivity. *J. Am. Chem. Soc.* 106, 1594–1605 (1984).
[94] Bader, RFW, Gillespie, RJ, MacDougall, PJ. A physical basis for the VSEPR model of molecular geometry. *J. Am. Chem. Soc.* 110, 7329–7336 (1988).
[95] Matta, CF, Gillespie, RJ. Understanding and interpreting electron density distributions. *J. Chem. Educ.* 79, 1141–1152 (2002).
[96] Carroll, MT, Chang, C, Bader, RFW. Prediction of the structures of hydrogen-bonded complexes using the Laplacian of the charge density. *Mol. Phys.* 63, 387–405 (1988).
[97] Carroll, MT, Cheeseman, JR, Osman, R, Weinstein, H. Nucleophilic addition to activated double bonds: Prediction of reactivity from the Laplacian of the charge density. *J. Phys. Chem.* 93, 5120–5123 (1989).
[98] Cremer, D, Kraka, E. Chemical bonds without bonding electron density – Does the difference electron-density analysis suffice for a description of the chemical bond? *Angew. Chem. Int. Ed. Engl.* 23, 627–628 (1984).
[99] Abramov, YA. On the possibility of kinetic energy density evaluation from the experimental electron-density distribution. *Acta Cryst. A* 53, 264–272 (1997).
[100] Bader, RFW. Quantum topology of molecular charge distributions. III. The mechanics of an atom in a molecule. *J. Chem. Phys.* 73, 2871–2883 (1980).

[101] Espinosa, E, Molins, E, Lecomte, C. Hydrogen bond strengths revealed by topological analyses of experimentally observed electron densities. *Chem. Phys. Lett.* 285, 170–173 (1998).
[102] Spackman, MA. How reliable are intermolecular interaction energies estimated from topological analysis of experimental electron densities?. *Cryst. Growth Des.* 15, 5624–5628 (2015).
[103] Massa, L, Matta, CF. Quantum cystallography: A perspective. *J. Comput. Chem.* 39, 1021–1028 (2018).
[104] Massa, L, Matta, CF. Exploiting the full quantum crystallography. *Can. J. Chem. 96*, 599–605 (2018).
[105] Goli, M, Shahbazian, S. Atoms in molecules: Beyond Born-Oppenheimer paradigm. *Theor. Chem. Acc.* 129, 235–245 (2011).
[106] Anderson, JSM, Ayers, PW. Quantum theory of atoms in molecules: Results for the SR-ZORA Hamiltonian. *J. Phys. Chem. A* 115, 13001–13006 (2011).

Chapter 8
The quantum theory of atoms in molecules and quantum crystallography: a symbiosis

If it is not measurable or not defined from physics I do not want to discuss it. Richard F. W. Bader (*ca*. 1995–2001)

(*C. F. Matta, personal verbal communication recalled from memory (2022)*)[1]

The kernel energy method (KEM) is shown as an efficient and accurate approximation for the fast evaluation of the quantum theory of atoms in molecules (QTAIM) atomic charges, and also of the interacting quantum atoms (IQA) energy components. A computational investigation using IQA energies reveals that the high accuracy of KEM stems from a cancellation of errors over groupings of several atoms, rather than from its ability to reproduce individual IQA components at an atomic resolution. One of the well-known characteristics of atoms-in-molecules defined within the QTAIM framework is their high degree of transferability. This transferability has provided the impetus for Hernández-Trujillo and Bader to use the Clinton equations to merge electron densities fragments obtained from computational "molds" at their interatomic surfaces. Hernández-Trujillo and Bader obtain excellent approximations to the electron density but the energies are not performing as well as the density. In contrast, Polkosnik and Massa, using an alternative approach (KEM), have recently shown that the imposition of the idempotency on the density matrix obtained from KEM (variational-KEM) is well-behaved physically. The chapter then discusses briefly a few examples of important properties that are not available from traditional X-ray diffraction crystallography. Such properties include (but are not limited to) density (matrices) in momentum space, total energies, QTAIM atomic virial energies and IQA energy components, and corresponding properties in excited states obtained by laser pump-probe X-ray diffraction experiments.

8.1 QTAIM charges for large molecules from KEM

The theoretical underpinnings of the kernel energy method (KEM) of quantum crystallography have been outlined in Chapter 5 followed by examples of application in Chapter 6. The examples discussed in Chapter 6 demonstrate how KEM is able to reproduce field-induced molecular properties [1] and also one- and two-electron properties obtained within the framework of the quantum theory of atoms (QTAIM) in molecules [2]. Here, a particularly useful QTAIM atomic property is shown to be reproduced accurately, that is, the atomic charge $q(\Omega)$.

1 Allegedly, there was also a sign on the door of Richard Bader's office at McMaster University with such a statement in the late 1980's.

https://doi.org/10.1515/9783110566673-009

Recalling that in QTAIM an atomic property is obtained by integrating a property density over the atomic basin (eq. (7.90)), it follows that upon setting $\hat{O} = \hat{1}$, the number operator, we get the electron population of an atom, $N(\Omega)$, (as given by eq. (7.91)). The subtraction from the atomic number Z_Ω of this electron population yields the QTAIM atomic charge which, expressed in atomic units (au), is given by $q(\Omega) = Z_\Omega - N(\Omega)$ – which we have seen in Chapter 7 (eq. (7.92)).

Since QTAIM atomic charges are expressed as quantum mechanical expectation values of a linear Hermitian operator (in this case $\hat{1}$) averaged over bounded atomic regions they *are* Dirac observables [3, 4]. From a utilitarian standpoint, these atomic charges have proven useful in the empirical modeling of physicochemical and biological properties of series of molecules [5–8] and, hence, are an important atomically-resolved molecular descriptor [9]. The calculation of QTAIM electron populations/atomic charges is an expensive procedure since it involves numerical integrations that also scale with the size of the basis set. This computational cost in term of CPU/GPU time is on the top of the rapid scaling with size of the underlying electronic structure calculation itself. In what follows, we will show how to cut such CPU time by the application of the KEM procedure to speed-up the calculation of QTAIM charges.

The CPU (and/or GPU) time savings are discussed in Chapter 5. To keep this chapter self-contained, we recap some salient points from Chapter 5.

The general expression for the energy of interaction (E_{int}) of an n-body system:

$$E_{\text{int}} = E_{\text{total}} - \sum_{c=1}^{n} E_c, \tag{8.1}$$

where E_{total} is the total energy and E_c is the energy of the isolated cth body. It is shown in Chapter 5 that starting from this expression, and ignoring interaction of orders higher than two, eq. (8.1) leads to:

$$E_{\substack{\text{total} \\ (\text{KEM})}} \approx \sum_{a=1}^{n-1} \sum_{b=a+1}^{n} E_{ab} - (n-2) \sum_{c=1}^{n} E_c, \tag{8.2}$$

where the double sum is the energy contributions of all double (pairwise) kernels ab, E_{ab}, and where E_c is the set of intrinsic energies of single kernels.

It is also shown in Chapter 5 that the time of a KEM calculation relative to the direct calculation is drastically reduced, an effect which is amplified the higher the scaling exponent of the model chemistry utilized and the larger the number of kernel fragments into which the system is broken. Thus, for a calculation using a basis set consisting of M basis functions split into m equal kernels, the relative CPU (and/or GPU) time is:

$$t_{\text{rel}} \approx \frac{2^{\alpha-1}(m-1)+1}{m^{\alpha-1}}, \tag{8.3}$$

which embodies a substantial reduction in CPU (and/or GPU) time as long as we break the molecule into three or more kernels. As an example, if one uses a model chemistry that scales as $\alpha = 5$ and by splitting the macromolecule into 1,000 kernels the saving in computational time is of the order of 100 million times, without considering parallelization on 1,000 CPUs (and/or GPUs).

In this section, the accuracy of QTAIM charges predicted from the much faster KEM approximation is gauged by numerical comparisons with full molecular calculations on three systems of increasing size and complexity of bonding environments [10]: (a) The explosive *N*,*N*'-dinitrourea ($C_3H_6N_4O_5$) a system with a total electron population $N = 92$ electrons (e^-), (b) the chelating agent pyridine-2-azo-*p*-phenyltetramethylguanidine (PAPT) ($C_{16}H_{20}N_6$, $N = 158$ e^-, and (c) acetyl-Cα,α-dipropylglycine (Ac-Dpg-7), a conformationally constrained synthetic heptapeptide ($C_{39}H_{71}N_7O_9$, $N = 426$ e^-). In all three examples, the KEM approximation approaches the directly calculated QTAIM charges with a minimum accuracy of 99.99% to two decimals, where $\%\,\text{error} \equiv (\sum q(\Omega)/N) \times 100$. The three studied systems are displayed in Fig. 8.1, while

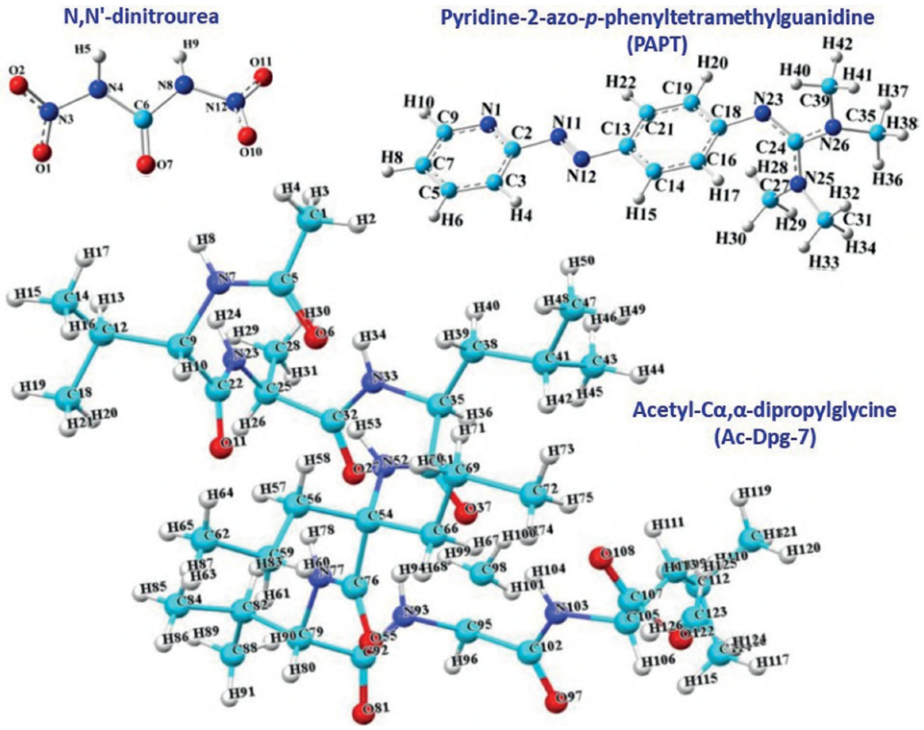

Fig. 8.1: The three molecules of increasing complexity used as test systems for the accuracy of KEM-QTAIM charges (clockwise from top-left corner): *N*,*N*'-dinitrourea ($C_3H_6N_4O_5$, $N = 92$ e^-), pyridine-2-azo-*p*-phenyltetramethylguanidine (PAPT) ($C_{16}H_{20}N_6$, $N = 158$ e^-), and acetyl-Cα,α-dipropylglycine (Ac-Dpg-7) ($C_{39}H_{71}N_7O_9$, $N = 426$ e^-).

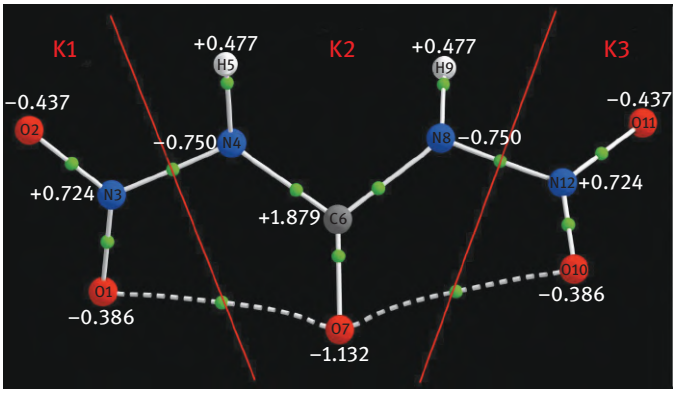

Fig. 8.2: The split into three KEM kernels shown for *N*,*N*'-dinitrourea along with the QTAIM charges (the charges are identical whether from the direct QTAIM calculation or the KEM-QTAIM approximation to the three decimals quoted in the figure). (Double kernels are not explicitly shown in this figure).

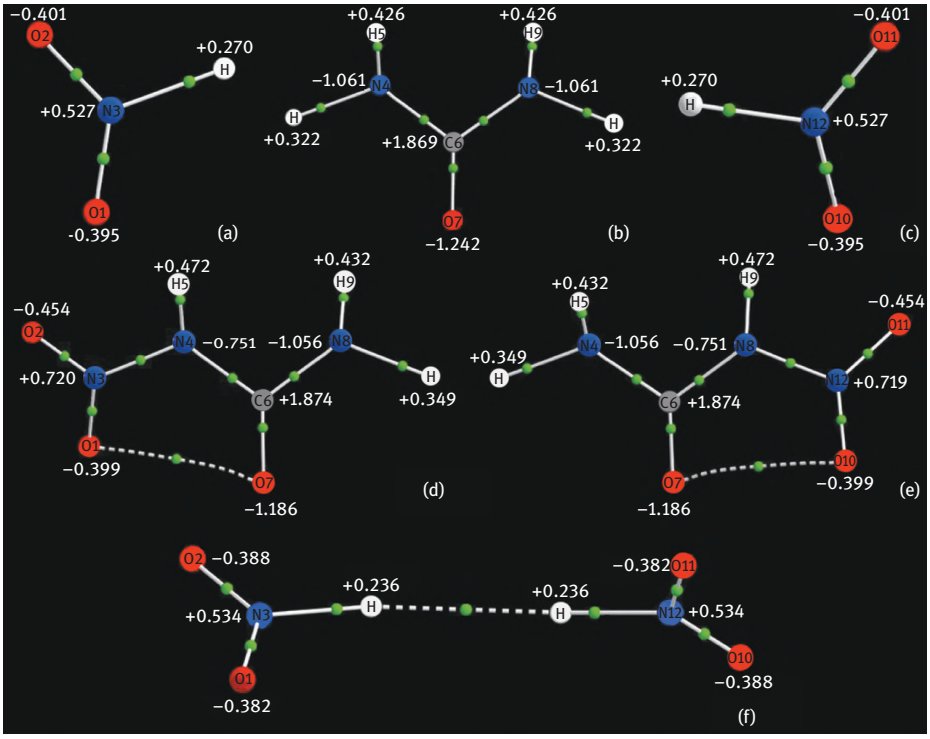

Fig. 8.3: The three single-kernels (a–c) and the three double-kernels (d–f) for pyridine-2-azo-*p*-phenyltetramethylguanidine (PAPT) along with the QTAIM charges (the charges are identical whether from the direct QTAIM calculation or the KEM-QTAIM approximation to the three decimals quoted in the figure).

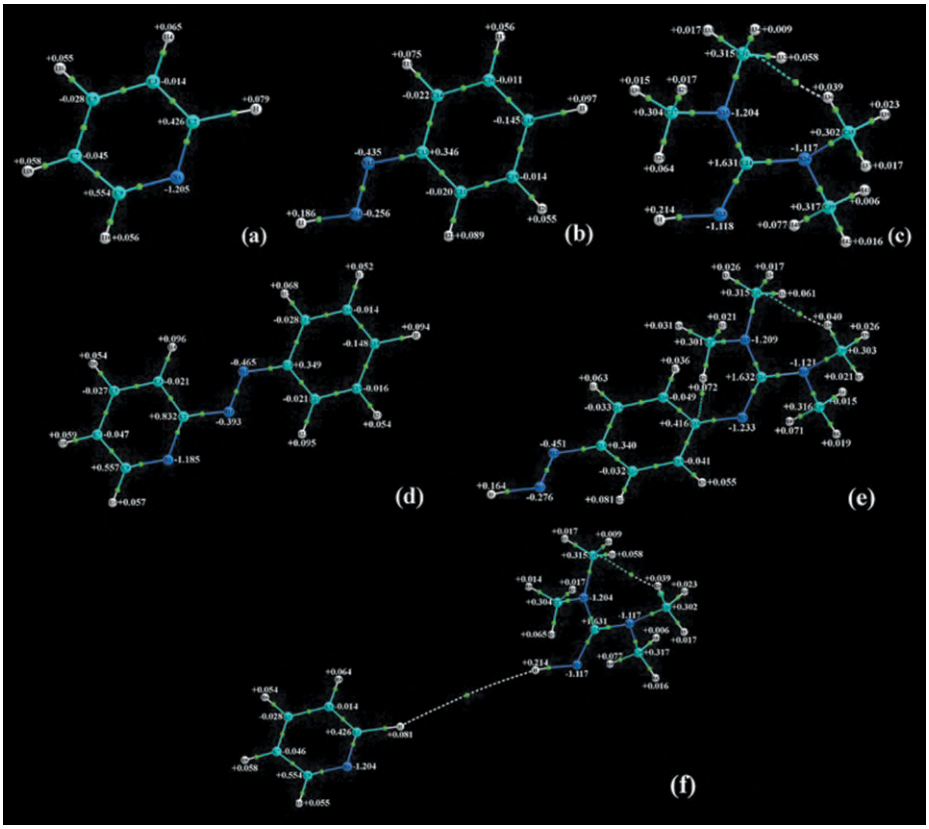

Fig. 8.4: (a) Single kernel-1, (b) single kernel-2, (c) single kernel-3, (d) double kernel-12, (e) double kernel-23, and (f) double kernel-13 for acetyl-Cα,α-dipropylglycine (Ac-Dpg-7) along with the QTAIM charges (the charges are identical whether from the direct QTAIM calculation or the KEM-QTAIM approximation to the three decimals quoted in the figure).

Figs. 8.2–8.4 display the splitting into kernel fragments along with the QTAIM atomic charges calculated for the given kernels.

To compute the QTAIM charges, the following conjecture is made: Atomic charges can be reconstructed from an analogous expression as eq. (8.2). Hence, we write the QTAIM atomic charges in terms of the KEM contributions as [10]:

$$q(\Omega_k) = \sum_{i=1}^{n-1} \sum_{j=i+1}^{n} q(\Omega_k)_{ij} - (n-2) \sum_{i=1}^{n} q(\Omega_k)_i, \tag{8.4}$$

where Ω_k is the kth atom in a molecule, $3 \le k \le K$ (total number of atoms), and n is number of single kernels. Then, the following algorithm is applied before insertion into eq. (8.4):

– if $\Omega_k \in \text{kernel}_{ij}$ or kernel_i, then calculate $q(\Omega_k)_{ij}$ & $q(\Omega_k)_i$, (8.5)

– if $\Omega_k \notin \text{kernel}_{ij}$ or kernel_i, $q(\Omega_k)_{ij}$ & $q(\Omega_k)_i = 0$. (8.6)

Calculations were conducted at the B3LYP/6-31+G(*d*) level of theory using the X-ray crystallographic geometries obtained from the Cambridge Structural Database (CSD) [10].

In the case of *N*,*N*'-dinitrourea, broken into three kernels, the average absolute deviations between the direct QTAIM calculation and the KEM-QTAIM approximation is $0.0022 \pm 0.0013\ e^-$ with a maximum unsigned error of $0.0037\ e^-$; that for PAPT, also broken into three kernels, is $0.0017 \pm 0.0020\ e^-$ and a maximum absolute deviation of $0.0068\ e^-$; and, finally, that of the largest system acetyl-Cα,α-dipropylglycine heptapeptide consisting of 126 atoms and 426 e^- and broken once into three kernels as in Fig. 8.4 and once into four kernels (not shown) and for which the average absolute deviation is $0.0013 \pm 0.0019\ e^-$ with a maximum deviation of magnitude $0.0160\ e^-$ [10].

8.2 Interacting quantum atoms energy components from from KEM

The molecular virial theorem states that, within the Born–Oppenheimer approximation, we have [11–14]:

$$2T + V = -\sum_{\alpha<\beta} R_{\alpha\beta}\left(\frac{\partial E}{\partial R_{\alpha\beta}}\right)_{R_{\gamma\delta}} \tag{8.7}$$

$$= -\sum_{\alpha} \mathbf{X}_\alpha \cdot \nabla_\alpha E \tag{8.8}$$

where T is the kinetic energy, V is the potential energy, E ($= T + V$) is the total energy, $R_{\alpha\beta}$ is the distance between the αth and the βth nucleus, the symbol subscripted at the right of the bracket involving the partial derivative means that this derivative is computed while keeping all other nuclear positions constant, and where $\mathbf{X}_\alpha$ is the position vector of the αth nucleus.

In eq. (8.7), the sum runs over *all* the elements of the inter-nuclear distance matrix while in eq. (8.8) the sum is over *all* nuclei, since a nucleus at $\mathbf{X}_\alpha$ is subjected to a force $\mathbf{F}_\alpha = -\nabla_\alpha E$. The virial of this force is $\mathbf{X}_\alpha \cdot \mathbf{F}_\alpha = -\mathbf{X}_\alpha \cdot \nabla_\alpha E$.

Since at any stationary point on the potential energy surface (PES) there are zero forces on the nuclei then, in this case, the right-hand sides of eqs. (8.7) and (8.8) vanish. These points include minima (stable equilibrium structure) and saddle points (unstable equilibrium transition state structures) since, at these critical points, every member of the set of the energy derivatives vanishes identically, that is:

$$\left\{\frac{\partial E}{\partial R_{\alpha\beta}}\right\} = \{\mathbf{X}_\alpha \cdot \nabla_\alpha E\} = 0, \qquad \forall \quad \alpha, \beta. \tag{8.9}$$

When this condition is satisfied, which occurs for geometry-optimized structures, eqs. (8.7) and (8.8) reduce to the familiar form of the virial theorem, that is:

$$2T + V = 0. \tag{8.10}$$

The virial theorem, in its simple form (eq. (8.10)) can, hence, only be applied to minima or transition state structures on the PES. For any other structure at an arbitrary point on the PES the sum $(2T + V)$ will equal to the sum of the virial of the forces on the nuclei. While the sum of these virials is unique, the individual contributions are origin dependent. Hence, that creates an ambiguity in the definition of the (virial) atomic energy except when the virial of the forces on all nuclei vanish (see Ref. [15]).

A solution to the non-uniqueness of atomic energies at arbitrary points on the PES (except for stationary points) has been proposed by the group at Oviedo led by Martín-Pendás [16]. This approach partitions the energy contributions (as defined in the molecular Hamiltonian) atomically and does not suffer from the limitation of a non-vanishing virial contributions from the nuclear forces at other than stationary points on the PES. Interacting quantum atoms (IQAs) energy components are, hence, well defined at any point of the PES which allows one to trace the changes in these components, say, along a reaction path.

The IQA approach starts from QTAIM which it uses to define the atoms in the molecule then splits the total energy E into atomic self- and interaction pairwise energies. Thus, the total energy E is written as:

$$E = \sum_{A} E^{\mathrm{A}}_{\mathrm{self}} + \frac{1}{2}\sum_{A}\sum_{A\neq B} E^{\mathrm{AB}}_{\mathrm{int}}, \tag{8.11}$$

where

$$E^{\mathrm{A}}_{\mathrm{self}} = T^{\mathrm{A}} + V^{\mathrm{AA}}_{\mathrm{en}} + V^{\mathrm{AA}}_{\mathrm{ee}}, \tag{8.12}$$

and

$$E^{\mathrm{AB}}_{\mathrm{int}} = V^{\mathrm{AB}}_{\mathrm{nn}} + V^{\mathrm{AB}}_{\mathrm{en}} + V^{\mathrm{AB}}_{\mathrm{ne}} + V^{\mathrm{AB}}_{\mathrm{ee}}, \qquad A\neq B, \tag{8.13}$$

and where the type of interaction potential energy is indicated by the subscript and the corresponding superscript denotes the atom contributing to that. Thus, for example, the second term in eq. (8.13) expresses the energy of attraction between the electrons in basin A and the nucleus in basin B.

From the above definitions, an *additive atomic energy* is defined as the sum of the self-energy and half of all of that atom's interaction terms (in complete analogy with the atomic populations and delocalization indices (the reader is invited to examine the first equality in eq. 6.13 of Chapter 6 which, if summed over all atoms in the molecule, yields the total number of electrons N and assumes a mathematical form identical to eq. (8.11) which yields the total energy of the molecule E). Thus, the additive energy of an atom in a molecule is defined as:

$$E^{\mathrm{A}}_{\mathrm{add}} = E^{\mathrm{A}}_{\mathrm{self}} + \frac{1}{2}\sum_{A\neq B} E^{\mathrm{AB}}_{\mathrm{int}}. \tag{8.14}$$

A triglycine molecule (Gly_1-Gly_2-Gly_3) has been chosen to trace how KEM achieves the accuracy in energy prediction by tracing the individual atomic and atom–atom energy terms as defined within the IQA approach [17].

Hartree–Fock (HF)//6-311G(*d,p*) level calculations delivered the wave functions for the full molecule and for the kernels which were analyzed to obtain their IQA energy contributions using the AIMAll package [18]. The KEM error is defined:

$$\Delta P \equiv P(\mathrm{exact}) - P(\mathrm{KEM}), \tag{8.15}$$

which measures the discrepancy of property P calculated directly and its approximate value obtained from KEM.

Figure 8.5 shows the kernel split along with the errors in the additive energies in kcal/mol. Skipping the details that can be found in the original reference [17], here a few key findings are highlighted:

(a) The error in the total energy is 0.89 kcal/mol, that is, KEM total energy is within conventional chemical accuracy.
(b) The error in the additive atomic IQA energies sum to 0.06 kcal/mol which is remarkable given the wider range of errors displayed in Fig. 8.5 and which fetch +5.39 kcal/mol for N6 and −2.64 kcal/mol for C9. However, the *sum* of the additive energies exhibits an error of only 0.89 kcal/mol (point (a)).
(c) The sum of all self-energy errors ($\Delta E^{\mathrm{A}}_{\mathrm{self}}$) is −6.16 kcal/mol while that of all the interaction errors ($\Delta E^{\mathrm{A}}_{\mathrm{int}}$) is +7.05 kcal/mol. These two summed and oppositely signed errors compensate to a large extent and yield a total error of +0.89 kcal/mol KEM. Note that this KEM energy is lower than the exact energy since KEM as such is not variational). However, it has been shown recently how KEM can be *made* variational [19]. Variational-KEM delivers smaller overall errors than "raw/uncorrected" KEM and these errors always go in the correct direction, that is, the variational-KEM energies are always higher than the corresponding exact energies as a case study on a number of water clusters demonstrates [19].

From the above remarks, *individual* additive atomic energies can be in error by an order of magnitude larger than the error in the total KEM energy. There appears, thus, to be a cancellation of errors underpinning the accuracy of the KEM [17].

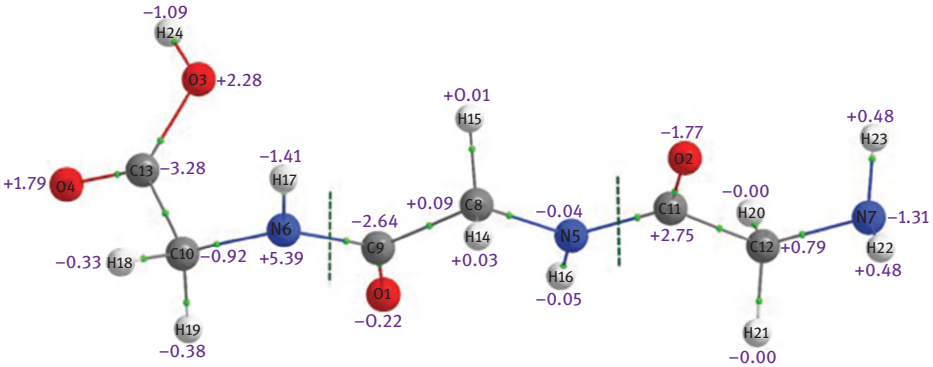

Fig. 8.5: The molecular graph of triglycine obtained from a HF/6-311G(d,p)//6-311G(d,p) calculation. The kernel splitting is indicated by the green dashed vertical lines and the numbers displayed are the errors in additive atomic IQA energies relative to the full system calculation rounded to two decimals in kcal/mol.

8.3 The Clinton iterative melding of assembled electron densities and of molecular aggregates

The idea of the reconstruction of the electron density maps from fragments is not new. Matta, for example, uses a reconstruction scheme whereby properties are directly summed to obtain the full-molecular properties from those of fragments [20]. If one is to reconstruct the full electron density scalar field from fragments calculated in molds using atoms-in-molecules extracted at their zero-flux surfaces, one is faced with the question as to how to meld these slightly mismatched zero-flux interatomic surfaces? One approach is to use a "pressure" applied on the interatomic surface from both sides as if it were an "elastic membrane," an approach led by Brenemann et al. [21–23]. An alternative and elegant approach has been proposed by Hernández-Trujillo and Bader [24] who use the properties of quantum projectors to enforce N-representability (by imposing idempotency of the density matrix, $\mathbf{P}^2 = \mathbf{P}$) and, in doing so, assemble large molecules from QTAIM fragments melding them at their zero-flux interatomic surfaces. The interatomic surfaces are "melded" through the application of Clinton iterative equations [24] (Fig. 8.6).

In another study, Polkosnik and Massa (P&M) use kernel recombination into an augmented density matrix of full systems consisting of a number of differently sized water clusters [19] instead of extracting density fragments and sticking them together at their nearly matching zero-flux interatomic surfaces (as done by Hernández-Trujillo and Bader). The clusters studied by P&M have the general formula $(H_2O)_n$, $n = 3–20$, and which were obtained from the earlier work of Gadre et al. [25]. Figure 8.7 displays one of the larger water clusters considered in that study.

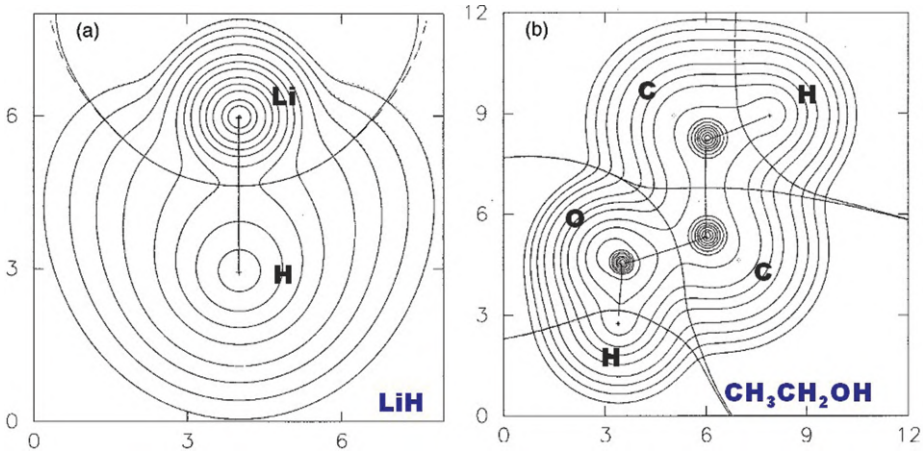

Fig. 8.6: Assembled versus direct Hartree–Fock electron densities contour representation with the zero-flux interatomic surfaces intersections with the planes of the drawings for an ionic system (LiH, left) and an organic polar system (ethanol, right). Assembled densities contours are the solid lines while the dashed contours are those obtained from the direct calculation. The two sets of contours and interatomic surfaces are hardly distinguishable. Distances are in atomic units (au) (Adapted with permission from Ref. [24], © 2001 *American Physical Society*).

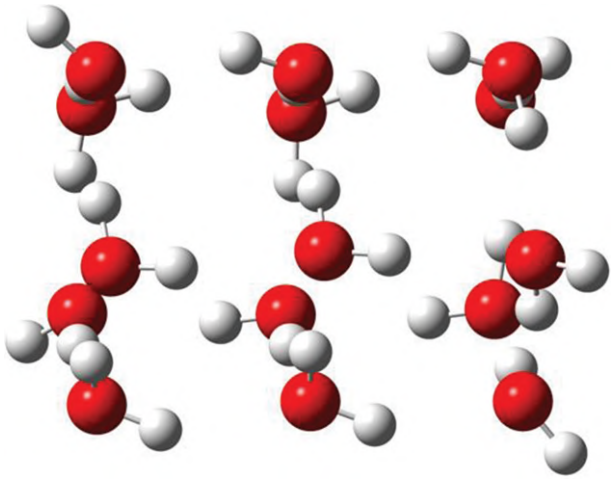

Fig. 8.7: An example of the water clusters with the formula $(H_2O)_{15}$ used to test the effect of imposing idempotency on the density matrix on the KEM error.

Since each water molecule was taken as a single kernel and all pairs of water molecules were taken as double kernels, there is no need – in this case – to include any capping hydrogen atoms since there are no severed covalent bonds. Three sets of calculations were done on these clusters: Set (I) which consists of direct calculations

on the full system, set (II) of traditional KEM calculations, and set (III) in which the KEM calculations were performed with the imposition of the idempotency constraint on the density matrix. This last set, III, can be termed "variationally constrained KEM" or simply "variational KEM."

Water clusters with $n = 10$, 12, 14, 15, 16, and 20 are of particular interest. This is so since only clusters with $n = 10$, 12, 14, and 15 were found to violate the variational principle and clusters with $n = 16$ and 20, while not violating the variational principle (their energies are higher than the corresponding exact energies) they, nevertheless, exhibited the highest magnitudes of errors [19]. To keep the discussion focused, it will be centered on those clusters to underscore the rectifying effect of the imposition of the idempotency on the density matrix.

Table 8.1 lists the errors in type II calculations ($E_{\mathrm{KEM}} - E_{\mathrm{full}}$) and contrasts it with the results of type III calculations on the same cluster ($E_{[\mathbf{P}_{\mathrm{projector}}]} - E_{\mathrm{full}}$). As already mentioned, the values listed in the table show four cases where $E_{\mathrm{KEM}} - E_{\mathrm{full}}$ is negative, violating the variational principle. The last two entries in the table exhibit the largest magnitudes of the errors in the uncorrected KEM (calculations II).

A comparison of the error in set II and set III calculations, tabulated in Tab. 8.1, reveals that, in contrast with set II (the second column of the table), the entries in the last column representing set III are all positive as required. It is further remarked that the errors in set III are smaller, in general, those of set II. Hence, the average absolute errors for set II is 2.8 ± 2.5 and is reduced to 1.2 ± 0.5 kcal/mol for set III. In conclusion, the imposition of N-representability has, as a consequence, the satisfaction of the variational theorem and a decrease in the magnitude of the errors inherent in the KEM approximation [19].

Tab. 8.1: Error in the KEM total energies without the imposition of N-representability ($E_{\mathrm{KEM}} - E_{\mathrm{full}}$, set II) and with the imposition of this quantum constraint ($E_{[\mathbf{P}_{\mathrm{projector}}]} - E_{\mathrm{full}}$, set III) in kcal/mol (Data obtained from Ref. [19] based on RHF/6-31G calculations).

H_2O_n	$E_{\mathrm{KEM}} - E_{\mathrm{full}}$	$E_{[\mathbf{P}_{\mathrm{projector}}]} - E_{\mathrm{full}}$
$n = 10$	−0.4	0.7
$n = 12$	−3.8	0.8
$n = 14$	−0.5	0.8
$n = 15$	−1.0	1.5
$n = 16$	6.4	1.9
$n = 20$	4.4	1.6
A.a.e.*	2.8 ± 2.5	1.2 ± 0.5

*A.a.e. = average absolute error (±standard deviation)

8.4 The density (matrix) in momentum space

Momentum density is unattainable from the electron density in position space alone, that is, $\rho(\mathbf{r}) \not\rightarrow \rho(\mathbf{p})$. The position space one-matrix $\rho_1(\mathbf{r}, \mathbf{r}')$, however, can be readily converted into a momentum one-matrix $\rho_1(\mathbf{p}, \mathbf{p}')$ through a six-dimensional Fourier transform:

$$\rho_1(\mathbf{p}, \mathbf{p}') = \iint \rho_1(\mathbf{r}, \mathbf{r}') \mathrm{e}^{-2\pi i(\mathbf{p}\cdot\mathbf{r} + \mathbf{p}'\cdot\mathbf{r}')} d\mathbf{r}\, d\mathbf{r}', \tag{8.16}$$

the diagonal elements of which represents the density in momentum space, that is

$$\rho(\mathbf{p}) = \rho_1(\mathbf{p}, \mathbf{p}')|_{\mathbf{p}'\to\mathbf{p}}. \tag{8.17}$$

8.5 The total energy

A most important quantum mechanical property is the total energy. It is expressed as an expectation value:

$$E = \langle \hat{H} \rangle = \int \Psi^* \hat{H} \Psi d\tau, \tag{8.18}$$

where Ψ is an antisymmetric and normalized many-electron wave function.

The expectation value of the Hamiltonian $\langle \hat{H} \rangle$ is expressible in terms of the one- and two-electron density matrices as:

$$E = \langle \hat{T}\rho_1 \rangle + \langle \hat{V}_{ext}\rho \rangle + \langle \hat{V}_{ee}\rho_2 \rangle, \tag{8.19}$$

which underscores the necessity of the three different density matrices to evaluate the total energy. The first term, the kinetic energy, is obtained from averaging a one-particle operator acting on the one-body density matrix. The second term, the external potential, is represented by a multiplicative operator acting on the electron density. The third and last term, the average of the electron-electron potential, is obtained from the action of a two-body nonlocal operator on two-body density matrix.

From these considerations, clearly, the electron density alone that one typically gets from the X-ray diffraction experiment cannot deliver the total energy. This is where the advantage of quantum crystallography is brought to the fore. By applying Clinton's iterative procedure, with an adopted basis set, one can construct experimentally consistent density matrices ρ, ρ_1, and ρ_2 from the scattering data. With these at hand, all properties follow, including the total energy.

8.6 Atomic virial energies

The following integral delivers the kinetic energy of an atom in a molecule $T(\Omega)$ (in au):

$$T(\Omega) = -\frac{1}{2}\int_{\Omega} \nabla^2 \rho_1(\mathbf{r}, \mathbf{r}')|_{\mathbf{r}'\to\mathbf{r}}\, d\mathbf{r}. \tag{8.20}$$

As discussed in Chapter 7, Bader postulated [26] and later proved [13, 27–29] the atomic statement of the virial theorem. As mentioned above, when the virial of all the forces on the nuclei vanish, the virial theorem assumes its simple form in eq. (8.10) and, correspondingly, the atomic virial theorem discussed in Chapter 7 also assumes the analogous simple form:

$$V(\Omega) = -2\ T(\Omega), \tag{8.21}$$

which, as we have seen earlier in this monograph, leads to the important result which states that for a system in equilibrium the atomic energy is simply the negative of the kinetic energy, that is:

$$E(\Omega) = T(\Omega) + V(\Omega) = -T(\Omega), \tag{8.22}$$

a result that, by necessity, leads to additivity, that is:

$$E = \sum_{\Omega} E(\Omega). \tag{8.23}$$

Here again, and since the kinetic energy cannot be extracted from the density alone (eq. (8.20)), clearly one would need quantum crystallography to obtain the virial energies of QTAIM from the scattering data. The same can be said about the IQA energy components discussed earlier.

8.7 Excited-state electron densities from X-ray diffraction experiments

Philip Coppens pioneered time-resolved X-ray diffraction following a short excitation pulse in what came to be also known as photocrystallography [30–33]. In this approach, bright synchrotron X-ray sources are used to probe the crystal at several short time intervals immediately after an ultra-short exciting laser pulse. This procedure has delivered excited state densities, so now the question is how to best represent such excited states quantum mechanically?

Coppens has shown that one can collect scattering data immediately following laser pumping to an excited state. The Clinton equations can then be used to obtain a representation of excited state orbitals. The ground state orbitals can be obtained

in the usual way. The scattering experiment determines only occupied orbitals (virtual orbitals do not scatter X-rays). Meanwhile, occupied excited state orbitals are constrained to be orthogonal to those of the ground state. The constraints on the density matrix in this case would include the normalization and the orthogonality to the ground-state orbitals. The forms of the constraints:

$$\mathrm{tr}\,\mathbf{PO} = \left\langle \hat{O} \right\rangle, \tag{8.24}$$

to which an additional constraint of orthogonality is added, that is:

$$\mathrm{tr}\,\mathbf{P}_{\mathrm{exited}}\mathbf{P}_{\mathrm{ground}} = 0, \tag{8.25}$$

where $\mathbf{P}_{\mathrm{exited}}$ and $\mathbf{P}_{\mathrm{ground}}$ are the excited- and ground-state density matrices, respectively. In this scheme, each density matrix would be obtained from the corresponding scattering data emanating from the electronic state in question. The representation of the excited state appears to fall naturally within the framework of the Clinton equations.

8.8 Conclusions

The long argument of this monograph is that the complete quantum mechanics can be extracted from, or injected into, the X-ray scattering data in the form of ρ, ρ_1, and ρ_2. This goal of quantum crystallography achieves two further objectives: (1) It allows for the extraction, from the X-ray scattering data, of properties that are impossible to determine from classical crystallography alone. Such properties include the momentum density, and the energies (total, virial, IQAs, etc.) (2) The imposition of quantum mechanical constraints during the crystallographic refinements delivers electron density matrices that are *N*-representable (and hence quantum mechanically valid) which is otherwise not guaranteed no matter how flexible the refinement and/or accurate is the experimental procedure. Nonspherical refinement has been and still delivers supremely important electron density maps and properties, what is being proposed here is to go one step further and extract more information from the same X-ray scattering data.

References

[1] Huang, L, Massa, L, Matta, CF. A graphene flake under external electric fields reconstructed from field-perturbed kernels. *Carbon* 76, 310–320 (2014).

[2] Timm, MJ, Matta, CF, Massa, L, Huang, L. The localization-delocalization matrix and the electron density-weighted connectivity matrix of a finite graphene nanoribbon reconstructed from kernel fragments. *J. Phys. Chem. A* 118, 11304–11316 (2014).

[3] Bader, RFW, Zou, PF. An atomic population as the expectation value of a quantum observable. *Chem. Phys. Lett.* 191, 54–58 (1992).
[4] Bader, RFW, Matta, CF. Atomic charges are measurable quantum expectation values: A rebuttal of criticisms of QTAIM charges. *J. Phys. Chem. A* 108, 8385–8394 (2004).
[5] Matta, CF. Modeling biophysical and biological properties from the characteristics of the molecular electron density, electron localization and delocalization matrices, and the electrostatic potential. *J. Comput. Chem.* 35, 1165–1198 (2014).
[6] Arabi, AA, Matta, CF. Bioisosteric groups in methylsquarate and carboxylic acid: The similarities of their electrostatic potentials and average electron densities. *Future Med. Chem.* 8, 361–371 (2016).
[7] Matta, CF, Arabi, AA. Electron-density descriptors as predictors in quantitative structure activity/property relationships and drug design. *Future Med. Chem.* 3, 969–994 (2011).
[8] Matta, CF, Bader, RFW. Atoms-in-molecules study of the genetically-encoded amino acids. III. Bond and atomic properties and their correlations with experiment including mutation-induced changes in protein stability and genetic coding. *Proteins: Struct. Funct. Genet* 52, 360–399 (2003).
[9] Todeschini, R, Consonni, V. *Molecular Descriptors for Chemoinformatics (Second Edition*; Vols. I and II). Wiley-VCH Weinheim, Weinheim, (2009).
[10] Huang, L, Matta, CF, Massa, L. The kernel energy method (KEM) delivers fast and accurate QTAIM electrostatic charge for atoms in large molecules. *Struct. Chem.* 26, 1433–1442 (2015).
[11] Slater, JC. The virial and molecular structure. *J. Chem. Phys.* 1, 687–691 (1933).
[12] Parr, RG, Brown, JE. Toward understanding vibrations of polyatomic molecules. *J. Chem. Phys.* 49, 4849–4852 (1968).
[13] Bader, RFW. *Atoms in Molecules: A Quantum Theory*. Oxford University Press, Oxford, U.K., (1990).
[14] Matta, CF, Sadjadi, S, Braden, DA, Frenking, G. The barrier to the methyl rotation in cis-2-butene and its isomerization energy to trans-2-butene revisited. *J. Comput. Chem.* 37, 143–154 (2016).
[15] Keith, TA. Atomic response properties. Chapter 3 in: *The Quantum Theory of Atoms in Molecules: From Solid State to DNA and Drug Design*; Matta, CF, Boyd, RJ (Eds.), Wiley-VCH, Weinheim (2007), 61–94.
[16] Blanco, MA, Martín-Pendás, Á, Francisco, E. Interacting quantum atoms: A correlated energy decomposition scheme based on the quantum theory of atoms in molecules. *J. Chem. Theor. Comput.* 1, 1096–1109 (2005).
[17] Massa, L, Keith, T, Cheng, Y, Matta, CF. The kernel energy method applied to quantum theory of atoms in molecules – Energies of interacting quantum atoms. *Chem. Phys. Lett.* 734, Art. #136650, 1–4 (2019).
[18] Keith, TA. AIMAll / AIMStudio. *http://aim.tkgristmill.com/* (2019).
[19] Polkosnik, W, Massa, L. Single determinant *N*-representability and the kernel energy method applied to water clusters. *J. Comput. Chem.* 39, 1038–1043 (2018).
[20] Matta, CF. Theoretical reconstruction of the electron density of large molecules from fragments determined as proper open quantum systems: The properties of the oripavine PEO, enkephalins, and morphine. *J. Phys. Chem. A* 105, 11088–11101 (2001).
[21] Breneman, CM, Rhem, M. QSPR analysis of HPLC column capacity factors for a set of high-energy materials using electronic van der Waals surface property descriptors computed by transferable atom equivalent method. *J. Comput. Chem.* 18, 182–197 (1997).
[22] Breneman, CM, Thompson, TR, Rhem, M, Dung, M. Electron density modeling of large systems using the transferable atom equivalent method. *J. Comput. Chem.* 19, 161–179 (1995).

[23] Breneman, CM, Weber, LW. Transferable atom equivalents. Molecular electrostatic potentials from the electric multipoles of PROAIM. In: *NATO ASI Series: The Application of Charge Density Research to Chemistry and Drug Design*; Plenum Press, New York (1991).
[24] Hernández-Trujillo, J, Bader, RFW. Properties of atoms in molecules: Construction of one-density matrix from functional group densities. *J. Chem. Phys.* 115, 10595–10607 (2001).
[25] Maheshwary, S, Patel, N, Sathyamurthy, N, Kulkarni, AD, Gadre, SR. Structure and stability of water clusters $(H_2O)_n$, n = 8–20: An *ab initio* investigation. *J. Phys. Chem. A* 105, 10525–10537 (2001).
[26] Bader, RFW, Beddall, PM. Virial field relationship for molecular charge distributions and the spatial partitioning of molecular properties. *J. Chem. Phys.* 56, 3320–3329 (1972).
[27] Bader, RFW, Beddall, PM, Peslak, J, Jr. Theoretical development of a virial relationship for spatially defined fragments of molecular systems. *J. Chem. Phys.* 58, 557–566 (1973).
[28] Srebrenik, S, Bader, RFW. Towards the development of the quantum mechanics of a subspace. *J. Chem. Phys.* 63, 3945–3961 (1975).
[29] Srebrenik, S, Bader, RFW, Nguyen-Dang, TT. Subspace quantum mechanics and the variational principle. *J. Chem. Phys.* 68, 3667–3679 (1978).
[30] Coppens, P. What can time-resolved diffraction tell us about transient species?: Excited-state structure determination at atomic resolution. *Chem. Commun.*, 1317–1320 (2003).
[31] Coppens, P, Fomitchev, DV, Carducci, MD, Culp, K. Crystallography of molecular excited states. Transition-metal nitrosyl complexes and the study of transient species. *J. Chem. Soc., Dalton Trans.*, 865–872 (1998).
[32] Vorontsov, I, Graber, T, Kovalevsky, A, Novozhilova, I, Gembicky, M, Chen, Y-S, Coppens, P. Capturing and analyzing the excited-state structure of a Cu(I) phenanthroline complex by time-resolved diffraction and theoretical calculations. *J. Am. Chem. Soc.* 131, 6566–6573 (2009).
[33] Pressprich, MR, White, MA, Vekhter, Y, Coppens, P. Analysis of a metastable electronic excited state of sodium nitroprusside by X-ray crystallography. *J. Am. Chem. Soc.* 116, 5233–5238 (1994).

Chapter 9
The calculation of the energy

The late Charles Coulson, Professor of Mathematics at Oxford who because of his pioneering calculations on benzene may well be regarded as the father *of theoretical chemistry, entertained the hope of replacing the wave function in quantum mechanics by the two-matrix as the basic tool. In June, 1959, at a conference in Boulder, Colorado about "Molecular Structure Calculations" he stated*

> *There is an instinctive feeling that matters such as electron correlation should show up in the two-particle density matrix . . . . but we still do not know the conditions that must be satisfied by Γ(12;1'2'). Until these conditions have been elucidated, it is going to be very difficult to make much progress along these lines.*

The "conditions" to which Coulson alluded are the restrictions imposed on the 2-matrix by the requirement that it is associated with a system of N identical fermions or bosons. In other words, what are necessary and sufficient conditions that a reduced density matrix can be represented as the contraction of the von Neumann density matrix of a system of N identical fermions or bosons. A. J. Coleman & V. I Yukalov (2000)

(*Reduced Density Matrices – Coulson's Challenge, Springer-Verlag, Berlin, 2000*).

The point of *N*-representability is to ensure that a density matrix descends from, and therefore, is mappable back into an *N*-body antisymmetric wave function. The antisymmetry is the theoretical representation equivalent of the experimental indistinguishability of the electrons. Thus, for every quantum property calculated from density matrices, their *N*-representability is desirable. For no calculated property is this truer than in the case of the energy. In particular, the variational theorem which is so important in energy optimization can only be mandated to hold true on condition that the density matrices used for such purpose are guaranteed to be *N*-representable. In the case of very large molecules, it is computationally an advantage to have the one-body density matrix in a kernel energy single-determinant *N*-representable form. In such a case the two-body density matrix is a known functional of the one-body case. Here we display the explicit form of such a two-body density matrix and state how it is used to calculate a molecular energy. An additional consideration is presented which converts an X-ray projector density matrix indirectly into a molecular energy.

9.1 The case of *N*-representable $\rho_{2\text{-det}}$ extracted from KEM $\rho_{1\text{-det}}$

As discussed in Chapter 1, the coherent X-ray scattering from a crystal gives experimental structure factors which are Fourier transforms of the electron density, that is:

$$F(\mathbf{K}) = \int e^{i\mathbf{K}\cdot\mathbf{r}} \rho(\mathbf{r})\, d\mathbf{r} \tag{9.1}$$

where $\rho(\mathbf{r})$ is the electron density at position $\mathbf{r}$ and $\mathbf{K}$, the wave vector, is fixed by the direction of scattering.

https://doi.org/10.1515/9783110566673-010

The single determinant representation of the density matrix, as discussed in Chapter 3, is then:

$$\rho_1(\mathbf{r},\mathbf{r}') = 2\,\mathrm{tr}\;\mathbf{P}\boldsymbol{\psi}(\mathbf{r})\otimes\boldsymbol{\psi}^{\dagger}(\mathbf{r}'), \tag{9.2}$$

where factor 2 indicates a double occupancy of orbitals and $\mathbf{P}$ is the matrix representative of the density in the basis of orthonormal atomic orbitals $\boldsymbol{\psi}(\mathbf{r})$.

As discussed in Chapter 3, the projector matrix $\mathbf{P}$ requires that [1]:

$$\mathbf{P}^2 = \mathbf{P}, \tag{9.3}$$

$$\mathrm{tr}\,\mathbf{P} = N, \tag{9.4}$$

and

$$\mathbf{P} = \mathbf{P}^{\dagger}, \tag{9.5}$$

that is, the satisfaction of the idempotency, normalization, and Hermiticity conditions, respectively. The particular projector $\mathbf{P}$ which satisfies the experimental X-ray scattering data is delivered by the Clinton equations [1]:

$$\mathbf{P}_{n+1} = 3\mathbf{P}_n^2 - 2\mathbf{P}_n^3 + \sum_k \lambda_k^{(n)}\mathbf{O}_k, \tag{9.6}$$

where the Lagrangian multipliers λ_k are used to enforce the conditions of constraint including normalization and X-ray scattering (see Chapter 3), and matrix representatives of the constraints are the elements of the matrix $\mathbf{O}_k$.

If the single determinant one-body density matrix $\rho_{1\text{-det}}(\mathbf{r},\mathbf{r}')$ is obtained from the X-ray experiment, the corresponding diagonal elements of the two body spin-dependent density matrix $\rho_{2\text{-det}}(\mathbf{r},\mathbf{r}')$ are given by the following expression:

$$\rho_{2\text{-det}}(\mathbf{r},\mathbf{r}') = \begin{vmatrix} \rho_{1\text{-det}}(\mathbf{r}) & \rho_{1\text{-det}}(\mathbf{r},\mathbf{r}') \\ \rho_{1\text{-det}}(\mathbf{r}',\mathbf{r}) & \rho_{1\text{-det}}(\mathbf{r}') \end{vmatrix}. \tag{9.7}$$

In this chapter we are concerned with this last equation expressing the relation of $\rho_{2\text{-det}}(\mathbf{r},\mathbf{r}')$ and $\rho_{1\text{-det}}(\mathbf{r},\mathbf{r}')$ for the case of very large molecules. In that case we suggest that $\rho_{1\text{-det}}(\mathbf{r},\mathbf{r}')$ may be expressed in KEM form as:

$$\underset{(\mathrm{KEM})}{\rho_{1\text{-det}}} = \sum_{a=1}^{n-1}\sum_{b=a+1}^{n} \underbrace{\rho_{1(a,b)}}_{\substack{\text{Double}\\ \text{kernels}}} - (n-2)\sum_{c=1}^{n} \underbrace{\rho_{1c}}_{\substack{\text{Single}\\ \text{kernels}}}, \tag{9.8}$$

where the full molecule ρ_1 has been represented in a summation of fragment kernels, whether single kernels $\rho_{1\text{-single}}$ or double kernels $\rho_{1\text{-double}}$ (see Chapter 5 and Ref. [2–15]). The question arises given $\rho_{1\text{-det}}$ as in eq. (9.8), what is the corresponding $\rho_{2\text{-det}}$?

To answer the previous question, consider, for simplicity and without loss of generality, a single-determinant one-body density matrix ρ_1 that consists of two parts (as the many-particle ρ_1 reconstructed from the KEM procedure described by eq. (9.8)). In this case we write:

$$\rho_1 = a_1 + a_2 \tag{9.9}$$

Since the corresponding spinless two-body density matrix is:

$$\rho_{2\text{-det}}(\mathbf{r},\mathbf{r}') = \begin{vmatrix} \rho_1(\mathbf{r}) & \frac{1}{2}\rho_1(\mathbf{r},\mathbf{r}') \\ \rho_1(\mathbf{r}',\mathbf{r}) & \rho_1(\mathbf{r}') \end{vmatrix}, \tag{9.10}$$

and expanding ρ_1 into its parts we have:

$$\begin{aligned} \rho_{2\text{-det}}(\mathbf{r},\mathbf{r}') = &\begin{vmatrix} a_1(\mathbf{r}) & \frac{1}{2}a_1(\mathbf{r},\mathbf{r}') \\ a_1(\mathbf{r}',\mathbf{r}) & a_1(\mathbf{r}') \end{vmatrix} + \begin{vmatrix} a_2(\mathbf{r}) & \frac{1}{2}a_2(\mathbf{r},\mathbf{r}') \\ a_2(\mathbf{r}',\mathbf{r}) & a_2(\mathbf{r}') \end{vmatrix} \\ &+ \begin{vmatrix} a_1(\mathbf{r}) & \frac{1}{2}a_1(\mathbf{r},\mathbf{r}') \\ a_2(\mathbf{r}',\mathbf{r}) & a_2(\mathbf{r}') \end{vmatrix} + \begin{vmatrix} a_2(\mathbf{r}) & \frac{1}{2}a_2(\mathbf{r},\mathbf{r}') \\ a_1(\mathbf{r}',\mathbf{r}) & a_1(\mathbf{r}') \end{vmatrix}. \end{aligned} \tag{9.11}$$

Now generalizing ρ_1 to that sum of parts characteristic of the KEM form, we have:

$$\rho_1(\text{KEM}) = \underbrace{\sum \rho_{1D}}_{a_1} - \underbrace{(n-2)\sum \rho_{1S}}_{a_2}, \tag{9.12}$$

where the summation indices were dropped for simplicity and the notation simplified, as described above, with reference to the single (S) and double (D) kernels. Now, calling a_1 the double-kernel term and a_2 the single-kernel term, eq. (9.11) becomes:

$$\begin{aligned} \rho_{2\text{-det}}(\mathbf{r},\mathbf{r}') = &\begin{vmatrix} \sum \rho_{1D}(\mathbf{r}) & \frac{1}{2}\sum \rho_{1D}(\mathbf{r},\mathbf{r}') \\ \sum \rho_{1D}(\mathbf{r}',\mathbf{r}) & \sum \rho_{D}(\mathbf{r}') \end{vmatrix} + \begin{vmatrix} -(n-2)\sum \rho_{1S}(\mathbf{r}) & -\frac{(n-2)}{2}\sum \rho_{1S}(\mathbf{r},\mathbf{r}') \\ -(n-2)\sum \rho_{1S}(\mathbf{r}',\mathbf{r}) & -(n-2)\sum \rho_{1S}(\mathbf{r}') \end{vmatrix} \\ &+ \begin{vmatrix} \sum \rho_{1D}(\mathbf{r}) & \frac{1}{2}\sum \rho_{1D}(\mathbf{r},\mathbf{r}') \\ -(n-2)\sum \rho_{1S}(\mathbf{r}',\mathbf{r}) & -(n-2)\sum \rho_{1S}(\mathbf{r}') \end{vmatrix} \\ &+ \begin{vmatrix} -(n-2)\sum \rho_{1S}(\mathbf{r}) & -\frac{(n-2)}{2}\sum \rho_{1S}(\mathbf{r},\mathbf{r}') \\ \sum \rho_{1D}(\mathbf{r}',\mathbf{r}) & \sum \rho_{1D}(\mathbf{r}') \end{vmatrix}, \end{aligned} \tag{9.13}$$

where the subscripts "S" and "D" refer to single and double kernels, respectively.

If the summations are moved outside the determinant symbols we obtain:

$$\rho_{2\,\mathrm{det}}(\mathbf{r},\mathbf{r}') = \sum_{D,D'} \begin{vmatrix} \rho_{1D}(\mathbf{r}) & \frac{1}{2}\rho_{1D}(\mathbf{r},\mathbf{r}') \\ \rho_{1D'}(\mathbf{r}',\mathbf{r}) & \rho_{D'}(\mathbf{r}') \end{vmatrix} + (n-2)^2 \sum_{S,S'} \begin{vmatrix} \rho_{1S}(\mathbf{r}) & \frac{1}{2}\rho_{1S}(\mathbf{r},\mathbf{r}') \\ \rho_{1S'}(\mathbf{r}',\mathbf{r}) & \rho_{1S'}(\mathbf{r}') \end{vmatrix}$$
$$- (n-2) \sum_{D,S} \begin{vmatrix} \rho_{1D}(\mathbf{r}) & \frac{1}{2}\rho_{1D}(\mathbf{r},\mathbf{r}') \\ \rho_{1S}(\mathbf{r}',\mathbf{r}) & \rho_{1S}(\mathbf{r}') \end{vmatrix} - (n-2) \sum_{D,S} \begin{vmatrix} \rho_{1S}(\mathbf{r}) & \frac{1}{2}\rho_{1S}(\mathbf{r},\mathbf{r}') \\ \rho_{1D}(\mathbf{r}',\mathbf{r}) & \rho_{D}(\mathbf{r}') \end{vmatrix}. \tag{9.14}$$

This last equation, eq. (9.14), is the main result of this section. Given the KEM representation of the one-body density matrix eq. (9.8), then eq. (9.14) is an exact representation of the corresponding two-body density matrix.

Having this last equation (eq. (9.14)), giving ρ_2 broken into explicit kernel contributions, in addition to ρ_1 similarly expressed in terms of kernels, the total energy becomes:

$$E = \left\langle \hat{h}_1 \left(\sum \rho_{1D}(\mathbf{r}) - (n-2) \sum \rho_{1S}(\mathbf{r}) \right) \right\rangle$$
$$+ \left\langle \hat{h}_{12} \left[\sum_{D,D'} \begin{vmatrix} \rho_{1D}(\mathbf{r}) & \frac{1}{2}\rho_{1D}(\mathbf{r},\mathbf{r}') \\ \rho_{1D'}(\mathbf{r}',\mathbf{r}) & \rho_{D'}(\mathbf{r}') \end{vmatrix} + (n-2)^2 \sum_{S,S'} \begin{vmatrix} \rho_{1S}(\mathbf{r}) & \frac{1}{2}\rho_{1S}(\mathbf{r},\mathbf{r}') \\ \rho_{1S'}(\mathbf{r}',\mathbf{r}) & \rho_{1S'}(\mathbf{r}') \end{vmatrix} \right.\right.$$
$$\left.\left. - (n-2) \sum_{D,S} \begin{vmatrix} \rho_{1D}(\mathbf{r}) & \frac{1}{2}\rho_{1D}(\mathbf{r},\mathbf{r}') \\ \rho_{1S}(\mathbf{r}',\mathbf{r}) & \rho_{1S}(\mathbf{r}') \end{vmatrix} - (n-2) \sum_{D,S} \begin{vmatrix} \rho_{1S}(\mathbf{r}) & \frac{1}{2}\rho_{1S}(\mathbf{r},\mathbf{r}') \\ \rho_{1D}(\mathbf{r}',\mathbf{r}) & \rho_{D}(\mathbf{r}') \end{vmatrix} \right] \right\rangle. \tag{9.15}$$

The advantage of this expression is, of course, that no energy calculation is more complicated than that corresponding to kernels which may be chosen to be dramatically smaller than for the molecule as a whole (see Chapter 5 where the time-saving aspects of KEM are discussed in some length). And if the KEM form of ρ_1 is chosen to be single-determinant N-representable then so too is ρ_2 exactly N-representable. In this case, the energy delivered by the last equation (eq. (9.15)) is mandated to satisfy the variational theorem.

As usual, the X-ray structure factors are fixed by the crystal's electron density. Now if that density is expressed in terms of kernels, then we have:

$$F(\mathbf{K}) = 2\,tr\left[\sum \mathbf{P}_D - (n-2)\sum \mathbf{P}_S\right]\mathbf{f}(\mathbf{K}), \tag{9.16}$$

in which each kernel contributes to a given structure factor:

$$F'(\mathbf{K}) = 2\,\mathrm{tr}\,\mathbf{P}'\mathbf{f}(\mathbf{K}), \tag{9.17}$$

where $\mathbf{P}'$ is the population matrix of a kernel, whether a single or a double kernel. The accuracy of the KEM calculated density can then be gauged by the magnitude of the *R-factor*:

$$R\text{-}factor = \frac{\sum \big| \, |F_{\text{obs}}| - |F_{\text{calc}}| \, \big|}{\sum |F_{\text{obs}}|}. \tag{9.18}$$

The energy represented in this section is based upon a single determinant expression of the experimental density. A single determinant of orbitals is sufficient to represent the exact density, as in DFT, although of course it is not an exact wave function. The energy is not exact, but importantly it obeys the variational theorem because the KEM density matrix is *N*-representable.

9.2 The energy from X-ray quantum crystallographic density?

The fundamental equation of X-ray crystallography allowing solution of molecular structure is eq. (9.1) where in the spherical atoms approximation, as discussed in Chapter 1, a promolecular electron density is expressed [16,17]:

$$\rho^{\text{pro}} = \sum_{i=1}^{M} \rho_i, \tag{9.19}$$

where the ρ_i is a spherical atomic density of atom i at its position in the modeled molecule which is typically obtained from Hartree–Fock calculations on free atoms in their ground electronic states. In more sophisticated treatments, the density is represented as a sum of radial and multipolar functions for a more accurate modeling [18] – as explained in Chapter 1.

The above expression of the density, whether expressed in terms of spherical atoms or multipoles, is not generally *N*-representable. For an electron density to be *N*-representable this means that it is mapable bijectively to an *N*-body antisymmetric wave function (see Chapter 3). The case of single-determinant *N*-representability is ensured by the conditions expressed in eqs. (9.3)–(9.5) with $\rho_1(\mathbf{r}, \mathbf{r}')$ expressed as in eq. (9.2).

The Clinton equations, expressed in eq. (9.6) above, are used to find projectors $\mathbf{P^2 = P}$ which simultaneously satisfy the constraints of X-ray scattering and normalization. The projector $\mathbf{P}$ has the property of being factorizable [1,19], that is, $\mathbf{P = C^{\dagger}C}$, and $\boldsymbol{\varphi} = \mathbf{C}\boldsymbol{\psi}$, so that ρ_1, ρ, and $\boldsymbol{\varphi}$ may all be obtained by measurements of the X-ray structure factors $\{F(\mathbf{K})\}$. (The atomic orbitals (AOs) basis, $\boldsymbol{\psi}(\mathbf{r})$, can be chosen to be orthonormal).

Density functional theory allows the information captured by the density matrix projector from X-ray scattering data to be transformed into a corresponding Kohn-Sham energy. The first Hohenberg-Kohn Theorem asserts that the density, were the Hohenberg-Kohn functional known, determines the exact energy. But the Hohenberg-Kohn functional is not known. However, the Kohn-Sham equations provide an approximate way to calculate the energy as a functional of the electron density, that is, $E = E[\rho]$. The Kohn-Sham functional can be expressed as:

$$E_{KS}[\rho] = T_s[\rho] + E_{ext}[\rho] + E_H[\rho] + E_{xc}[\rho], \tag{9.20}$$

where the first terms on the right-hand-side $T_S[\rho]$ is the Kohn-Sham kinetic energy followed, in order, by energy terms stemming from density-weighted 3D space integrals of the external potential (giving $E_{ext}[\rho]$), of the Hartree (Coulombic) classical potential (giving $E_H[\rho]$), and of the exchange-correlation potential (giving $E_{xc}[\rho]$).

The Kohn-Sham kinetic energy (T_S) is the "exact" kinetic energy of the true density but made-up of non-interacting (independent) particles. The dependence of all the terms on the right-hand-side of eq. (9.20) on the ground-state electron density are known exactly except $E_{xc}[\rho]$ which is famously an unknown functional of the density. Nevertheless, a great many $E_{xc}[\rho]$ functionals have been suggested as reasonable approximations. Such approximations can be used to obtain an approximate Kohn-Sham energy by substitution of the X-ray crystallographic electron density information $\rho(\mathbf{r})$ directly into the Kohn-Sham expression given above (eq. 9.20). Thus that density matrix obtained by approximate representation of the X-ray scattering provides all information needed for the Kohn-Sham energy of the experimental density.

9.3 Discussion and conclusion

In the first section of this chapter, it is emphasized that when the system becomes sufficiently large it becomes advantageous, computationally, to represent the molecule as a sum of kernel fragments as in eq. (9.8). Since the kernels may be taken to be much smaller than the full molecule, the computations using the kernels become much simpler. It has been shown in Chapter 5 how the KEM summation defining $\rho_{1\text{-det}}$ can be enforced to be N-representable by a single determinant. Of course, given such an N-representable $\rho_{1\text{-det}}(\mathbf{r},\mathbf{r}')$ which is a sum of kernels the question arises what is the corresponding N-representable single determinant for $\rho_{2\text{-det}}(\mathbf{r},\mathbf{r}')$. The answer must arise from eq. (9.10). In the last part of the first section that answer has been elaborated and results in eq. (9.14).

In closing this chapter and this book, the Clinton equations are shown to provide a pathway to extract from the X-ray scattering experiment an N-representable single-determinant density matrix which contains the experimental (& therefore "exact") density. The experimental projector density matrix $\mathbf{P}$ is factorizable, $\mathbf{P} = \mathbf{C}^{\dagger}\mathbf{C}$, and

therefore delivers orbitals giving the "exact" density, which is also characteristic of the KS orbitals. As long as the number of linearly independent X-ray constraints exceeds the number of independent elements of **P**, that is, $\kappa(m,N) = N(m - N)$,[1] the X-ray data fixes the electron density $\rho(\mathbf{r})$, the density matrix $\rho_1(\mathbf{r},\mathbf{r}')$, and the set of orbitals $\{\varphi(\mathbf{r})\}$. The experimental $\{\varphi(\mathbf{r})\}$ may therefore be considered an approximation within the basis used to the KS orbitals. Therefore they may be used to calculate an X-ray-derived molecular energy.

References

[1] Clinton, WL, Galli, AJ, Massa, LJ. Direct determination of pure-state density matrices. II. Construction of constrained idempotent one-body densities. *Phys. Rev.* 177, 7–12 (1969).

[2] Huang, L, Massa, L, Karle, J. Kernel energy method: Application to DNA. *Biochemistry* 44, 16747–16752 (2005).

[3] Huang, L, Massa, L, Karle, J. Kernel energy method: Application to insulin. *Proc. Natl. Acad. Sci. USA* 102, 12690–12693 (2005).

[4] Huang, L, Massa, L, Karle, J. Kernel energy method illustrated with peptides. *Int. J. Quantum Chem.* 103, 808–817 (2005).

[5] Huang, L, Massa, L, Karle, J. The kernel energy method: Application to a tRNA. *Proc. Natl. Acad. Sci. USA* 103, 1233–1237 (2006).

[6] Huang, L, Massa, L, Karle, J. Kernel energy method: Basis functions and quantum methods. *Int. J. Quantum Chem.* 106, 447–457 (2006).

[7] Huang, L, Massa, L, Karle, J. The kernel energy method of quantum mechanical approximation carried to fourth-order terms. *Proc. Natl. Acad. Sci. USA* 105, 1849–1854 (2008).

[8] Huang, L, Massa, L, Karle, J. Kernel energy method applied to vesicular stomatitis virus nucleoprotein. *Proc. Natl. Acad. Sci. USA* 106, 1731–1736 (2009).

[9] Huang, L, Massa, L, Karle, J. Quantum kernels and quantum crystallography: Applications in biochemistry. Chapter 1 in: *Quantum Biochemistry: Electronic Structure and Biological Activity, Vol. 1*; Matta, CF (Ed.), Wiley-VCH, Weinheim (2010), 3–60.

[10] Huang, L, Bohórquez, H, Matta, CF, Massa, L. The kernel energy method: Application to graphene and extended aromatics. *Int. J. Quantum Chem.* 111, 4150–4157 (2011).

[11] Huang, L, Krupkin, M, Bashan, A, Yonath, A, Massa, L. Protoribosome by quantum kernel energy method. *Proc. Natl. Acad. Sci. USA* 110, 14900–14905 (2013).

[12] Timm, MJ, Matta, CF, Massa, L, Huang, L. The localization-delocalization matrix and the electron density-weighted connectivity matrix of a finite graphene nanoribbon reconstructed from kernel fragments. *J. Phys. Chem. A* 118, 11304–11316 (2014).

[13] Huang, L, Massa, L, Matta, CF. A graphene flake under external electric fields reconstructed from field-perturbed kernels. *Carbon* 76, 310–320 (2014).

[14] Huang, L, Matta, CF, Massa, L. The kernel energy method (KEM) delivers fast and accurate QTAIM electrostatic charge for atoms in large molecules. *Struct. Chem.* 26, 1433–1442 (2015).

[15] Massa, L, Keith, T, Cheng, Y, Matta, CF. The kernel energy method applied to quantum theory of atoms in molecules – energies of interacting quantum atoms. *Chem. Phys. Lett.* 734, Art. #136650, 1–4 (2019).

1 See eq. (3.34) of Chapter 3.

[16] Hirshfeld, FL. Bonded-atom fragments for describing molecular charge densities. *Theor. Chim. Acta* 44, 129–138 (1977).
[17] Spackman, MA, Maslen, EN. Chemical properties from the promolecule. *J. Phys. Chem.* 90, 2020–2027 (1986).
[18] Stewart, RF. Electron population analysis with rigid pseudoatoms. *Acta Cryst. A* 32, 565–574 (1976).
[19] McWeeny, R. Some recent advances in density matrix theory. *Rev. Mod. Phys.* 32, 335–369 (1960).

Epilogue

For Aristotle, reality was a cosmos, an ordered universe where two regions of different nature could be distinguished: the supra-lunar world, which is the domain of the stars, composed of ether, perfect and immutable, and the sub-lunar world, composed of the four elements, air, water, earth, and fire, corruptible and in permanent change. Each of these two regions was ruled by its own laws. This ontological division lasted until the times of Galileo and Kepler, manifesting itself in the difference between physics, devoted to explaining what had been the Aristotelian sub-lunar world, and astronomy, devoted to the description of heavens. It was not until Newton, with his *Mathematical Principles of Natural Philosophy* of 1687, that the unification between the laws of Earth and the laws of heavens was achieved. From then on, physics acquired a single face, that of Newtonian mechanics.

Chemistry followed a completely different historical path. Its origins go back to alchemy during the Middle Ages, with its interest in the composition and properties of matter. It was with Boyle, in the 17th century, that the gradual separation of chemistry from alchemy started, and chemistry began to acquire an independent status. In turn, with Lavoisier in the 18th century, chemistry acquired a strict quantitative nature, allowing reliable predictions on the basis of precise measurements. Nevertheless, far from the theoretical character of physics, until the 18th century chemistry remained an eminently practical discipline, with its interest in obtaining medicines, food, pigments, among many other resources.

The first half of the 19th century found a scenario in which science has already completely branched off from philosophy and the different scientific disciplines have acquired their own identity. It is in this environment that Comte presented his famous hierarchy of sciences: mathematics, astronomy, physics, chemistry, biology, and sociology. The scale goes from the general to the particular, and from the simple to the complex: moving from mathematics to sociology, generality decreases and complexity increases. The influence of Comte's positivism was so strong that even today many still distinguish between fundamental and phenomenological disciplines, between primary and secondary sciences.

But already in the second half of the 19th century, the apparent simplicity of the hierarchy of the sciences began to fade out. In fact, different theoretical fields with their own epistemic and experimental strategies soon began to appear within each discipline. As a result, in the 20th century one can no longer speak of physics, but rather of classical mechanics, thermodynamics, quantum mechanics, electromagnetism, general relativity, etc. Nor can one speak simply of chemistry, but of organic chemistry, biochemistry, inorganic chemistry, analytical chemistry, physical chemistry. And although some are still anchored to the nineteenth-century hierarchy, it is now clear that the relationships between theoretical domains do not necessarily lead

https://doi.org/10.1515/9783110566673-011

to a “chain” where each “link” connects only two immediately adjacent ones. On the contrary, the different domains of science form a “network”, where each node can be connected to two or more others in a different way in each case. For example, classical mechanics is connected by completely different links with classical statistical mechanics, with special relativity and with quantum mechanics. In this reticular structure, traditional disciplinary boundaries become unimportant, as the links cross them in many different ways.

At present, as we have fully entered the 21st century, even the network picture goes into crisis. In fact, in that picture knowledge still seems to be mainly concentrated in the well-defined nodes, and the relationships between them only aim at unification. By contrast, the current panorama of science shows that, although the theoretical nodes survive, the largest production of knowledge takes place in the spaces between them. The boundaries between different theories and scientific disciplines become blurred and fluid, and it is precisely in these places of fluidity that present-day science is finding its greatest achievements. The case of quantum chemistry is a paradigmatic example: it is neither chemistry nor quantum physics, but it integrates elements of both disciplines, as well as new mathematical and computational resources. It is a discipline that grows by itself, delineated on the basis of a certain shared working methodology. However, in the general map of science it has diffuse borders and very diverse relationships with the different knowledges it incorporates. It makes no sense to ask a quantum chemist whether she is a physicist or a chemist: these categories are no longer valid for this new approach to the scientific practice.

The present book is framed precisely in this context: here classical crystallography merges with the theoretical resources of quantum mechanics. Thus, concepts such as atom, interatomic distance, chemical structure, electronic density, wave function, and Hamiltonian, among many others, coexist peacefully, regardless of the discipline in which they were originally proposed. From this fruitful combination, new explanations stem out, which are not available in traditional X-ray diffraction crystallography, but which quantum mechanics cannot provide in isolation either. In addition to the relevant scientific results this book offers, it is a perfect example of the scientific knowledge that is produced in the regions of fluidity and, as a consequence, points to a new way of conceiving the scientific enterprise, no longer constrained by the boundaries of traditional disciplines.

Olimpia Lombardi
Senior Researcher
University of Buenos Aires - CONICET

Appendix 1
Historical note: *N*-representability

> *The history of the exclusion principle is thus already an old one, but its conclusion has not yet been written. The essential advance of physics rests on the creative imagination of the experimental as well as the theoretical investigator, and, contrary to expensive applications of known principles, cannot be forced by planning on a grand scale. Therefore it is not possible to say beforehand where and when one can expect the further development of the basic principles of present-day physics, of which the problem of the exclusion principle is a part.*
>
> Wolfgang Pauli (1946)
> ("Remarks on the History of the Exclusion Principle," *Science* 103, 213–215, 1946)

The idea of *N*-representability was invented within the theory of quantum mechanics. It was at the time very far from the practice of X-ray crystallography. Elementary particles such as fermions exhibit experimental indistinguishability that requires theoretical expression. For this class of particles, to which electrons belong, *N*-body solutions of the Schrödinger equation must be antisymmetric in the exchange of particle pairs. The wave function is a probability amplitude but density matrices are formulated directly as probability quantities. John von Neumann [1] and Paul A. M. Dirac [2, 3] were among the first to recognize and use density matrices. Their invention of the concept is independent of one another.

Given the *N*-body density matrix, which emanates from the square of the full *N*-body Schrödinger wave function, one has a probability object which contains vastly more information than is required in order to calculate the expectation values of one- and two-electron quantum mechanical properties. These are, after all, those of maximal physical interest, including all powers of particle position and momentum coordinates. K. Husimi [4] was the first to realize, at least a decade before the introduction of the direct methods of crystal structure determination by H. Hauptman and J. Karle [5] were realized, that *N*-particle density matrices can be simplified without loss of their essential one-body and two-body information. Husimi invented one- and two-body reduced density matrices obtained by integration over all particles in the *N*-particle density matrix except for either one or two of the particles, respectively. It is the reduced density matrices that are those of greatest interest. Although the simplest density matrices of an *N*-particle system, no matter what the magnitude of *N* may be, they are yet sufficient to deliver all one- and two-particle expectation values of the system. That of course underlies their great interest.

The importance of the *N*-representability property of reduced density matrices was uncovered almost by accident. It was realized that the two-particle density matrix was all that is needed to calculate the molecular energy expectation value. Of course, the best energy would be expected to follow from miminization of that energy with respect to variation of the two-particle density matrix. Surprisingly, such a numerical optimization carried out by the noted statistical mechanician Joseph E. Mayer yielded, in one

https://doi.org/10.1515/9783110566673-012

case, a molecular energy that violated the variational principle of quantum mechanics [6]. The optimized molecular energy was well below the known "exact" value for the ground-state energy. But of course as touted in quantum mechanics textbooks, it is simply mathematically impossible. A short time later, R. H. Tredgold was able to trace the difficulty with the violation of the hard-and-fast rule of the variational theorem to the use of an expansion of the two-particle density matrix that was not *N*-representable [7]. However, the vocabulary term "*N*-representable" was not used by Tredgold as it has not yet been launched into the lexicon of quantum mechanics. That term was first used, as is to be mentioned, years later. But contemporaneously with the numerical difficulty associated with the variation of the variational principle, Per-Olov Löwdin began an influential study of density matrix formalism [8], which has contributed greatly to the formalism and understanding of reduced density matrices. Löwdin organized a famous series of annual Sanibel theoretical symposia during which many of his ideas related to the reduced density matrices were disseminated and have had a lasting impact in the field. These include the idea of natural orbitals whose occupation numbers fall in the range between 0 and 1. He pushed the idea that finding those conditions relating the two-particle density matrix to an antisymmetric *N*-particle wave function would ensure the satisfaction of the variational theorem. John Coleman [9, 10] participated in some of the Sanibel Symposia and enunciated what came to be called the "Coleman Theorem" regarding the one-particle density matrix. That is to say, those one-particle density matrices, which are *N*-representable, must have eigenvalues which fall in the range between 0 and 1. The extreme values of that range correspond to single determinant *N*-representability. Coleman, for may years, organized annual meetings held at Queen's University (Kingston, ON) whose purpose was to discuss the general problem of *N*-representability, especially as regards the case of the two-particle density matrix. In the same period, many important general and expansive views of the subject have entered the literature. Here, only a few of the most important cases are mentioned, which include the works of Ugo Fano [11], Dirk ter Haar [12], and Ernst R. Davidson [13].

Roy McWeeny published important reviews concerning density matrices [14, 15]. He also invented iterative equations whose purpose is to purify a matrix to idempotency. The McWeeny matrix equations may be considered a precursor to the equations named after William L. Clinton [16–22]. The purpose of Clinton's equations is to convert an initial guessed matrix to one which is, both, a normalized projector and also satisfies conditions of constraints, such as experimentally derived X-ray structure factors.

Derivation of the Clinton equations and their application to crystallography introduced the concomitant idea of *N*-representability into the literature of crystallography. The term "quantum crystallography" logically follows [23–28].

References

[1] Von Neumann, J. *Mathematical Foundations of Quantum Mechanics, (English Translation)*. Princeton University Press, Priceton, (1955).

[2] Dirac, PAM. Note on the interpretation of the density matrix in the many-electron problem. *Math. Proc. Cambridge Phil. Soc.* 27, 240–243 (1931).

[3] Dirac, PAM. *The Principles of Quantum Mechanics, Third Edition*. Oxford University Press, Oxford, (1958).

[4] Husimi, K. Some formal properties of the density matrix. *Proc. Phys. Math. Soc. Japan* 22, 264–310 (1940).

[5] Hauptman, H, Karle, J. Crystal-structure determination by means of a statistical distribution of interatomic vectors. *Acta Cryst*. 5, 48–59 (1952).

[6] Mayer, JE. Electron correlation. *Phys. Rev.* 100, 1579–1586 (1955).

[7] Tredgold, RH. Density matrix and the many-body problem. *Phys. Rev.* 105, 1421–1423 (1957).

[8] Löwdin, P-O. Quantum theory of many-particle systems. I. Physical interpretations by means of density matrices, natural spin-orbitals, and convergence problems in the method of configurational interaction. *Phys. Rev.* 97, 1474–1489 (1955).

[9] Coleman, AJ. Structure of fermion density matrices. *Rev. Mod. Phys.* 35, 668–686 (1963).

[10] Coleman, AJ, Yukalov, VI. *Reduced Density Matrices: Coulson's Challenge*. Springer, Berlin, (2000).

[11] Fano, U. Description of states in quantum mechanics by density matrix and operator techniques. *Rev. Mod. Phys.* 29, 74–93 (1957).

[12] Haar, DT. Theory and applications of the density matrix. *Rep. Prog. Phys*. 24, 304–362 (1961).

[13] Davidson, ER. *Reduced Density Matrices in Quantum Chemistry*. Academic Press, Inc., New York, (1976).

[14] McWeeny, R. Some recent advances in density matrix theory. *Rev. Mod. Phys*. 32, 335–369 (1960).

[15] McWeeny, R, Sutcliffe, BT. *Methods of Molecular Quantum Mechanics*. Academic Press, New York, (1969).

[16] Clinton, WL, Galli, AJ, Massa, LJ. Direct determination of pure-state density matrices. II. Construction of constrained idempotent one-body densities. *Phys. Rev.* 177, 7–12 (1969).

[17] Clinton, WL, Galli, AJ, Henderson, GA, Lamers, GB, Massa, LJ, Zarur, J. Direct determination of pure-state matrices. V. Constrained eigenvalue problems. *Phys. Rev.* 177, 27–33 (1969).

[18] Massa, LJ, Clinton, WL. Antisymmetric wavefunction densities from coherent diffraction data. *Trans. Am. Cryst. Ass.* 8, 149–153 (1972).

[19] Clinton, WJ, Massa, LJ. The cusp condition: Constraint on the electron density matrix. *Int. J. Quantum Chem.* 6, 519–523 (1972).

[20] Clinton, WL, Massa, LJ. Determination of the electron density matrix from X-ray diffraction data. *Phys. Rev. Lett.* 29, 1363–1366 (1972).

[21] Clinton, WL, Frishberg, CA, Massa, LJ, Oldfield, PA. Methods for obtaining an electron-density matrix from X-ray data. *Int. J. Quantum Chem*. 7, 505–514 (1973).

[22] Clinton, WL, Frishberg, CA, Goldberg, MJ, Massa, LJ, Oldfield, PA. Density matrix model for coherent X-ray diffraction: Study of experimental factors related to idempotency. *Int. J. Quantum Chem*. 24, 517–525 (1983).

[23] Wikipedia. *Quantum Crystallography (*https://en.wikipedia.org/wiki/Quantum_crystallography*)* (2023).

[24] Massa, L, Huang, L, Karle, J. Quantum crystallography and the use of kernel projector matrices. *Int. J. Quantum. Chem.* 56, 371–384 (1995).

[25] Huang, L, Massa, L, Karle, J. Quantum crystallography. *J. Mol. Struct.* 474, 9–12 (1999).
[26] Huang, L, Massa, L, Karle, J. Quantum crystallography applied to crystalline maleic anhydride. *Int. J. Quantum Chem.* 73, 439–450 (1999).
[27] Huang, L, Massa, L, Karle, J. Quantum crystallography, a developing area of computational chemistry extending to macromolecules. *IBM J. Res. & Dev.* 45, 409–415 (2001).
[28] Huang, L, Massa, L, Karle, J. Quantum kernels and quantum crystallography: Applications in biochemistry. Chapter 1 in: *Quantum Biochemistry: Electronic Structure and Biological Activity*; Matta CF (Ed.), Wiley-VCH, Weinheim (2010), 3–60.

Appendix 2
Comments regarding new discussions of quantum crystallography

On admire près de soi. L'admiration des médiocres caractérise les envieux. L'admiration des grands poètes est le signe des grands critiques. Pour découvrir au-delà de tous les horizons les hauteurs absolues, il faut être soi-même sur une hauteur.

Ce que nous disons là est tellement vrai qu'il est impossible d'admirer un chef-d'œuvre sans éprouver en même temps une certaine estime de soi. On se sait gré de comprendre cela. Il y a dans l'admiration on ne sait quoi de fortifiant qui dignifie et grandit l'intelligence. Victor Hugo (1860)

[Engl. trans.:
One admires close to oneself. The admiration of the mediocre characterizes the envious. The admiration of great poets is the mark of great critics. To discover beyond all horizons the absolute heights, one must be, oneself, standing high.

What we are saying here is so true that it is impossible to admire a masterpiece without at the same time feeling a certain self-esteem. We are grateful to understand that. There is in admiration something fortifying, who knows what, that dignifies and expands intelligence.]. Victor Hugo (1860)

(*Utilité du beau, et autres textes* [Engl. trans.: *The Utility of the Beautiful, and other texts*], Littéra, Éditions Manucius, Paris, 2018, p. 39)

A small but influential meeting occurred in 2017 at the Université de Lorraine in Nancy (France). The conference, named CECAM Discussion Meeting – Quantum Crystallography: Current Developments and Future Perspectives, was organized under the auspices of the Centre Européen de Calcul Atomique et Moléculaire in the period 19–20 June 2017. Perhaps two dozen scientists, widely ranged from around the globe, among those most interested in quantum crystallography were called together to discuss the status of the subject. Much of the discussion was predicated upon knowledge of the contemporaneous paper by Grabowsky, Genoni, and Bürgi (GGB) [1].

The paper by GGB so influenced the conference where it was under discussion, and the subsequent progress of the field subsequently seems relevant to refer for the readers of this monograph a bit of the paper's contents, with the hope that the paper itself will be consulted for its full impact.

This important paper reviews the history of quantum crystallography development and then goes on to point to the directions in which it may be expected to develop. Central to the paper's message regarding what is it that defines the workings of quantum crystallography are two figures that summarize the authors' view as presented and discussed in some detail in the paper. One of the figures in this paper (reproduced here as Fig. A2.1) points to a pair of different ways to encapsulate the field of quantum crystallography.

Our own view of alternative attack on quantum crystallography may be expressed as depending on whether quantum mechanics, as a formalism, is used to *extract* information *from* or to *inject* information *into* the X-ray scattering experiment.

https://doi.org/10.1515/9783110566673-013

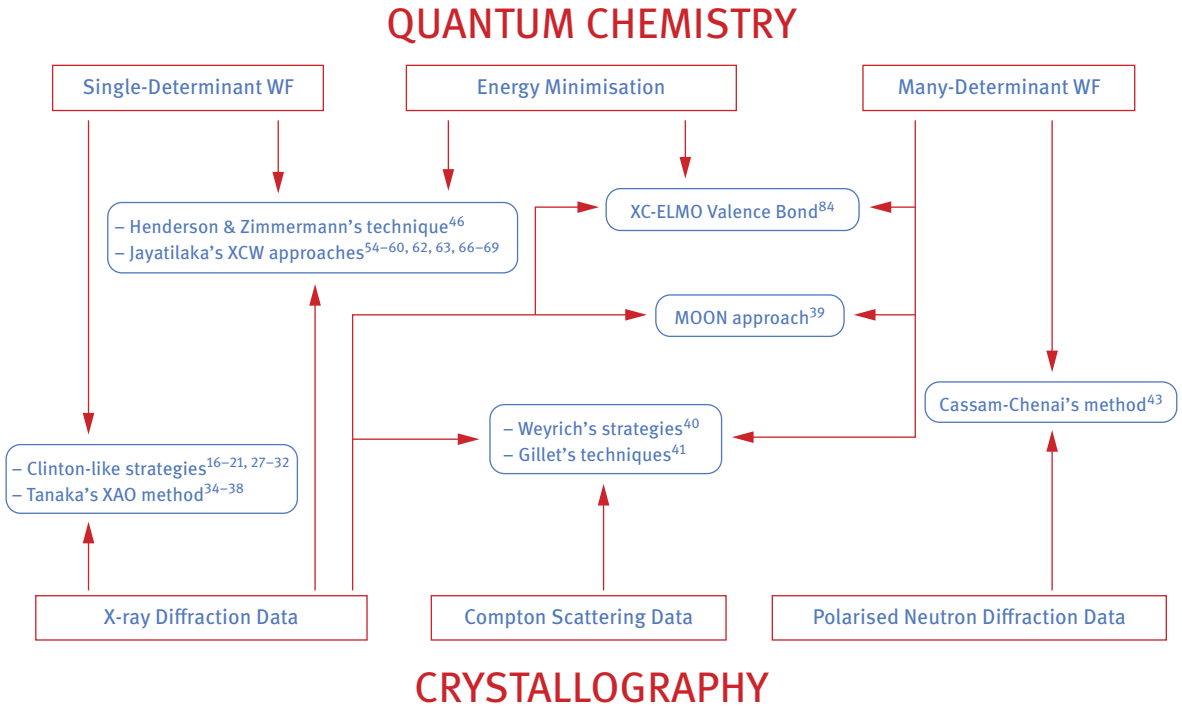

Fig. A2.1: A hierarchically organized flow chart where the lower the position of a box indicates lesser input from quantum chemistry and *vice versa*. Red and blue frames denote, respectively, the *features* and *principal methodologies* as stipulated from the "first definition of quantum crystallography" (reproduced from Ref. [1] with permission of the copyright holder).

These ideas have been presented in this monograph, in particular in Chapters 3 and 4, wherein the discussion was one of *extracting* the quantum mechanics from the X-ray scattering experiment. The emphasis in Chapters 5 and 6 is especially concerned with *injecting* the quantum mechanics into the crystallography by using the nuclear coordinates of a classical structure determination and calculating the *ab initio* density matrix via quantum chemical calculations.

In addition to the paper by GGB, the reader is strongly encouraged to consult the additional publications which are representative of the current trend in this evolving field of research [2–5]. These references (and the literature cited therein) capture much of the current mood of the direction in which the new field of quantum crystallography is moving.

References

[1] Grabowsky, S, Genoni, A, Bürgi, H-B. Quantum crystallography. *Chem. Sci.* 8, 4159–4176 (2017).

[2] Genoni, A, Bučinský, L, Claiser, N, Contreras-García, J, Dittrich, B, Dominiak, PM, Espinosa, E, Gatti, C, Giannozzi, P, Gillet, J-M, Jayatilaka, D, Macchi, P, Madsen, AØ, Massa, L, Matta, CF, Merz, KM, Jr., Nakashima, P, Ott, H, Ryde, U, Scherer, W, Schwarz, K, Sierka, M, Grabowsky, S. Quantum crystallography: Current developments and future perspectives. *Chem. Eur. J.* 24, 10881–10905 (2018).

[3] Macchi, P. The connubium between crystallography and quantum mechanics. *Crystallogr. Rev.* 26, 209–268 (2020).

[4] Gatti, C, Macchi, P. *Modern Charge Density Analysis*. Springer, Germany, (2012).

[5] Macchi, P. *Quantum Crystallography: Expectations vs Reality*, Springer, Switzerland, (2022).

Appendix 3
Publications on quantum crystallography by the authors

> *La perfección existe, porque es imaginable, pero no es perfecta, porque es inalcanzable.* Jorge Wagensberg (2002)
>
> *[Engl. trans.: Perfection exists, because it is imaginable, but it is not perfect, because it is unreachable]*. Jorge Wagensberg (2002)
>
> (*Si la naturaleza es la respuesta, ¿cuál era la pregunta? y otros quinientos pensamientos* [Engl. trans.: *If nature is the answer, what was the question? and five hundred other thoughts*], Fabula Tusquets Editores, Barcelona, 2008, p. 50)

This appendix lists the publications by the authors of this monograph, to date, related to the development and uses of quantum crystallography. No body of work is ever perfect or complete and this one is no exception. The publications listed further are suggestive of "work in progress" in this rapidly developing subfield of crystallography. From the outset, it has been stated that this is a *monograph* and not a textbook-style book that reviews the entire landscape of quantum crystallography. The exposition is, hence, biased by the interests and slanted toward the contributions of the authors to the field. This appendix starts by listing recently edited collective works on the topic followed by journal articles and chapters in books and is intended as a convenient bibliography of the work upon which this monograph is based.

1. Edited special journal issues on quantum crystallography

[1] Matta, CF (Guest Editor). Special issue: Honoring Professor Lou Massa – A Path through Quantum Crystallography. *Struct. Chem.* 28(5), 1277–1605 (October 2017).

[2] Matta, CF, Massa, L (Guest Editors). Special issue: Quantum Crystallography – Part 1 of 2. *J. Comput. Chem.* 39(17), 1013–1075 (30 June 2018).

[3] Matta, CF, Massa, L (Guest Editors). Special issue: Quantum Crystallography – Part 2 of 2. *J. Comput. Chem.* 39(18), 1077–1167 (5 July 2018).

2. Journal articles and chapters in books on quantum crystallography

[1] Massa, L, Castanedo, LAM, Fahimi, P, Matta, CF. Applications of *in-silico* quantum chemical calculations to large systems: The kernel energy method. Chapter 7 in: In-silico *Approaches to Macromolecular Chemistry*, Thomas, J., Thomas, S., Kornweitz, H., and Thomas, M. (Eds.), Elsevier, The Netherlands (2023), 199–215.

https://doi.org/10.1515/9783110566673-014

[2] Massa, L, Fahimi, P, Castanedo, LAM, Matta, CF. *In silico* approaches and challenges for quantum chemical calculations on macromolecules. Chapter 6 in: In-silico *Approaches to Macromolecular Chemistry*, Thomas, J., Thomas, S.; Kornweitz, H., Thomas, M. (Eds.), Elsevier, The Netherlands, 2023, 185–197.
[3] Matta, CF, Massa, L. *A two projector triple product in quantum crystallography. Int. J. Quantum Chem*. 122, Article # e26838 (2022).
[4] Matta, CF, Huang, L, Massa, L. Quantum crystallography: *N*-representability big and small. *Isr. J. Chem.* 62, Article # e202100108 (2022).
[5] Keith, TA, Massa, L, Cheng, Y, Matta, CF. The kernel energy method applied to quantum theory of atoms in molecules – energies of interacting quantum atoms. *Chem. Phys. Lett.* 734, 136650 (2019).
[6] Polkosnik, W, Matta, CF, Huang, L, Massa, L. Fast quantum crystallography. *Int. J. Quantum Chem.* 119, e25986 (2019).
[7] Genoni, A, Bučinský, L, Claiser, N, Contreras-García, J, Dittrich, B, Dominiak, PM, Espinosa, E, Gatti, C, Giannozzi, P, Gillet, M, Jayatilaka, D, Macchi, P, Madsen, AØ, Massa, LJ, Matta, CF, Merz, KM, Jr., Nakashima, P, Ott, H, Ryde, U, Scherer, W, Schwarz, K, Sierka, M, Grabowsky, S. Quantum crystallography: Current developments and future perspectives. *Chem. Eur. J.* 24, 10881–10905 (2018).
[8] Massa, L, Matta, CF. Quantum crystallography: A perspective. *J. Comput. Chem.* 39, 1021–1028 (2018).
[9] Massa, L, Matta, CF. Exploiting the full quantum crystallography. *Can. J. Chem.* 96, 599–605 (2018).
[10] Matta, CF, Massa, L. Quantum crystallography in medicinal chemistry. *Future Med. Chem.* 10, 1525–1527 (2018).
[11] Matta, CF. Quantum crystallography: From the intersection to the union of crystallography and quantum mechanics. *J. Comput. Chem.* 39, 1019–1020 (2018).
[12] Massa, L, Matta, CF. Quantum crystallography (QCr): A perspective. *J. Comput. Chem.* 39, 1021–1028 (2018).
[13] Polkosnik, W, Massa, L. Single determinant *N*-representability and the kernel energy method (KEM) applied to water clusters. *J. Comput. Chem.* 39, 1038–1043 (2018).
[14] Matta, CF. A path through quantum crystallography: A short tribute to Professor Lou Massa. *Struct. Chem.* 28, 1279–1283 (2017).
[15] Massa, L. A zigzag path through quantum crystallography. *Struct. Chem.* 28, 1293–1296 (2017).
[16] Matta, CF. On the connections between the quantum theory of atoms in molecules (QTAIM) and density functional theory (DFT): A Letter from Richard F. W. Bader to Lou Massa. *Struct. Chem.* 28, 1591–1597 (2017).
[17] Huang, L, Matta, CF, Massa, L. The kernel energy method (KEM) delivers fast and accurate QTAIM electrostatic charge for atoms in large molecules. *Struct. Chem.* 26, 1433–1442 (2015).
[18] Timm, MJ, Matta, CF, Massa, L, Huang, L. The localization–delocalization matrix and the electron density–weighted connectivity matrix of a finite graphene flake reconstructed from kernel fragments. *J. Phys. Chem. A* 118, 11304–11316 (2015).
[19] Huang, L, Massa, L, Matta, CF. Graphene flake under external electric fields reconstructed from field-perturbed kernels. *Carbon* 76, 310–320 (2014).
[20] Huang, L, Massa, L, Krupkin, M, Bashan, A, Yonath, A. Protoribosome by quantum kernel energy method *Proc. Natl. Acad. Sci. USA* 110, 14900–14905 (2013).
[21] Huang, L, Massa, L. Quantum kernel (KEM) applications in biochemistry. *Future Med. Chem.* 4, 1873–1875 (2012).

[22] Huang, L, Bohórquez, H, Matta, CF, Massa, L. The kernel energy method: Application to graphene and extended aromatics. *Int. J. Quantum Chem.* 111, 4150–4157 (2011).
[23] Huang, L, Massa, L. Kernel energy method applied to an energetic nitrate ester. *Int. J. Quantum Chem.* 111, 2180–2186 (2011).
[24] Huang, L, Massa, L. The kernel energy method: Construction of 3&4 tuple kernels from a list of double Kernel interactions. *J. Mol. Struct.* 962, 72–79 (2010).
[25] Huang, L, Massa, L. Kernel energy method: Drug target interaction energies for drug design. *Int. J. Quantum Chem.* 110, 2886–2893 (2010).
[26] Weiss, SN, Huan, L, Massa, L. A generalized higher order kernel energy approximation method. *J. Comput. Chem.* 31, 2889–2899 (2010).
[27] Huang, L, Massa, L, Karle, J. Quantum kernels and quantum crystallography: Applications in biochemistry. Chapter 1 in: *Quantum Biochemistry: Electronic Structure and Biological Activity (Vol. 1)*; Matta, CF (Ed.), Wiley-VCH, Weinheim (2010), 3–60.
[28] Huang, L, Massa, L, Karle, I, Karle, J. Calculation of strong and weak interactions in TDA1 and RangDP52 by kernel energy method. *Proc. Natl. Acad. Sci. USA* 106, 3664–3669 (2009).
[29] Huang, L, Massa, L, Karle, J. Kernel energy method applied to vesicular stomatitis virus nucleoprotein. *Proc. Natl. Acad. Sci. USA* 106, 1731–1736 (2009).
[30] Huang, L, Massa, L, Karle, J. The kernel energy method of quantum mechanical approximation carried to fourth order terms. *Proc. Natl. Acad. Sci. USA* 105, 1849–1854 (2008).
[31] Huang, L, Massa, L, Karle, J. Kernel energy method: The interaction energy of the collagen triple helix. *J. Chem. Theory Comput.* 3, 1337–1341 (2007).
[32] Huang, L, Massa, L, Karle, J. Drug target interaction energies by the kernel energy method: Aminoglycoside drugs and ribosomal A site RNA target. *Proc. Natl. Acad. Sci. USA* 104, 4261–4266 (2007).
[33] Huang, L, Massa, L, Karle, J. The kernel energy method: Application to tRNA. *Proc. Natl. Acad. Sci. USA* 103, 1233–1237 (2006).
[34] Huang, L, Massa, L, Karle, J. The kernel energy method: Basis functions and quantum methods. *Int. J. Quantum Chem.* 106, 447–457 (2006).
[35] Massa, L, Huang, L, Karle, J. The kernel energy method illustrated with peptides. *Int. J. Quantum Chem.* 103, 808–817 (2005).
[36] Huang, L, Massa, L, Karle, J. The kernel energy method: Application to insulin, *Proc. Natl. Acad. Sci. USA* 102, 12690–12693 (2005).
[37] Massa, L. Approximate *N*-representability by correlated – determinant wavefunctions. In: *Reviews in Modern Quantum Chemistry: A Celebration of Contributions of Robert G. Parr (Vol. I)*; Sen, KD (Ed.), World Scientific, Singapore (2002), 666–683.
[38] Huang, L, Massa, L, Karle, J. Form factors for core electrons useful in the quantum crystallography (QCr) of organic molecules. *Acta Cryst. A* 58, 410–411 (2002).
[39] Huang, L, Massa, L, Karle, J. Quantum crystallography, a developing area of computational chemistry extending to macromolecules. *IBM J. Res. Develop.* 45(3/4), 409–415 (2001).
[40] Soirat, AJA, Massa, L. The number of independent parameters defining a projector: Proof in matrix representation and resolution of previously conflicting arguments. Chapter 8 in: *Electron, Spin and Momentum Densities and Chemical Reactivity*; Mezey, PG, Robertson, BE (Eds.), Kluwer Academic Publishers, Dordrecht (2000), 127–146.
[41] Huang, L, Massa, L, Karle, J. Quantum crystallography applied to crystalline maleic anhydride. *Int. J. Quantum Chem.* 73, 439–450 (1999).
[42] Karle, J, Huang, L, Massa, L. Quantum crystallography: Features and application. Chapter 1 in: *Current Challenges on Large Supramolecular Assemblies*; Tsoucaris, G (Ed.), NATO Science Series C: Mathematical and Physical Sciences, vol. 519 (1999), 1–5.
[43] Huang, L, Massa, L, Karle, J. Quantum crystallography. *J. Mol. Struct.* 474, 9–12 (1999).

[44] Karle, J, Huang, L, Massa, L. Quantum crystallography, a technique for extending the concept of structure. *J. Pure Appl. Chem.* 70, 319–324 (1998).
[45] Huang, L, Massa, L, Karle, J. Kernel projector matrices: Application to Leu[1] – Zervamicin. In: *Encyclopedia of Computational Chemistry*, Schleyer, Pv-R (Ed.), John Wiley & Sons, New York, 1457–1464 (1998).
[46] Huang, L, Massa, L, Karle, J. Kernel projector matrices for Leu[1]-Zervamicin. *Int. J. Quantum Chem.* 60, 1691–1700 (1996).
[47] Massa, L, Huang, L, Karle, J. Quantum crystallography and the use of kernel projectors matrices. *Int. J. Quantum Chem.* 29, 371–384 (1995).
[48] Soirat, AJA, Massa, L. Number of independent parameters needed to define a projector. *Phys. Rev. B* 50, 3392 (1994).
[49] Soirat, A, Flocco, M, Massa, L. Approximately *N*-representable density functional density matrices: The case of large *N*. *Proc. Indian Acad. Sci. (Chem. Sci)* 106(2), 209–216 (1994).
[50] Soirat, A, Flocco, M, Massa, L. Approximately *N*-representable density functional density matrices. *Int. J. Quantum Chem.* 49, 291–298 (1994).
[51] Flocco, M, Gao, XQ, Massa, L. A study of the Colle-Salvetti formula for the calculation of the correlation – energy. *Int. J. Quantum Chem.* 38(24), 213–223 (1990).
[52] Massa, L, Flocco, M, Soirat, A. Reduced density matrices *N*-representable by correlated determinant wavefunctions. *J. Mol. Struct.* 199, 337–342 (1989).
[53] Massa, L. XOOM crystallography in relation to other problems. In: *Molecular Structure*; Stezowski, JJ, Huang, J-L, Shao, M-C (Eds.), Oxford University Press, Oxford (1988).
[54] Massa, L, X-ray orthonormal orbital model for crystallography. In: *Proceedings of the Coleman Symposium: Density Matrices and Density Functionals*, Erdahl, R, Smith, V, Reidel, D, (Eds.), Springer Netherlands, 707–716, (1987).
[55] Massa, L, Boehme, RF, LaPlaca, SJ. X-ray imaging of quantum electron structure. In: *Patterson and Pattersons – A Fifty Year Celebration of the Patterson Function, Proceedings of A Symposium Held at the Fox Chase Cancer Center, Philadelphia, PA, USA, Nov. 13–15 1984*; Glusker, JP, Patterson, BK, Rossi, M (eds), Oxford University Press, Oxford (1986), 427–449.
[56] Massa, L. Quantum model of coherent X-ray diffraction. *Chem. Scr.* 26, 469–472 (1986).
[57] Cohen, L, Frishberg, C, Lee, C, Massa, L. Correlation energy for a slater determinant fitted to the electron density. *Int. J. Quantum Chem.* 28(Suppl. 19), 525–533 (1985).
[58] Massa, L, Boehme, RF, LaPlaca, SJ. X-ray imaging of quantum electron structure, *I.B.M. Research Report* RC 11159 (#49854) (1985).
[59] Massa, L. Sufficiency conditions for *N*-representability by correlated-determinant wavefunctions, *I.B.M. Research Report* RC 11593 (#52101) (1985).
[60] Massa, L. Correlation energy formalism: Correlated – determinant wavefunctions, *I.B.M. Research Report* RC 11591 (#52099) (1985).
[61] Massa, L, Goldberg, M, Frishberg, C, Boehme, RF, LaPlaca, SJ. Wave functions derived by quantum modeling of the electron density from coherent diffraction: Beryllium Metal. *Phys. Rev. Lett.* 55, 622–625 (1985).
[62] Massa, L, Goldberg, M, Frishberg, C, Boehme, RF, LaPlaca, SJ. Wave functions derived by quantum modeling of the electron density from coherent diffraction; Beryllium Metal, *I.B.M. Research Report* RC 10863 (#48481) (1984).
[63] Clinton, WL, Frishberg, CA, Goldberg, MJ, Massa, L, Oldfield, PA. Density matrix model for coherent X-ray diffraction: Study of experimental factors related to idempotency. *Int. J. Quantum Chem.* 24(Suppl. 17), 517–525 (1983).
[64] Goldberg, MJ, Massa, L. Quantum model of coherent X-ray diffraction: Extension to Bloch orbitals. *Int. J. Quantum Chem.* 24, 113–126 (1983).

[65] Frishberg, CA, Massa, L. Density matrix equation for crystals. *Int. J. Quantum Chem.* 23, 85–89 (1983).
[66] Frishberg, CA, Goldberg, MJ, Massa, L. Quantum model of the coherent diffraction experiment: Recent generalizations and applications. In: *Electron Distributions and the Chemical Bond*; Coppens, P, Hall, M (Eds.), Plenum Press, New York, 101–110, (1982).
[67] Frishberg, CA, Massa, L. Numerical applications of a quantum model for the coherent diffraction experiment. *Acta Cryst. A* 38, 93–98 (1982).
[68] Frishberg, CA, Massa, L. Idempotent density matrices for correlated systems from X-ray diffraction structure factors. *Phys. Rev. B* 24, 7018–7024 (1981).
[69] Massa, L, Cohen, L. A local energy method based on the reduced density matrix equations. *Int. J. Quantum Chem.* 18(14), 167–173 (1980).
[70] Frishberg, CA, Massa, L. Notes on density matrix model for coherent X-ray diffraction. *Int. J. Quantum Chem.* 13, 801–810 (1978).
[71] Clinton, WL, Frishberg, CA, Massa, L, Oldfield, PA. Electron densities consistent with coherent diffraction data, diffraction studies of real atoms and real crystal. In: *International Crystallography Conference on Diffraction Studies of Real Atoms and Real Crystals*, Melbourne (Australia), 19–23 August 1974. [Unpublished].
[72] Clinton, WL, Frishberg, C, Massa, L, Oldfield, PA. Methods for obtaining an electron density matrix from X-ray diffraction data. *Int. J. Quantum Chem.* 7(Suppl. 7), 505–514 (1973).
[73] Clinton, WJ, Massa, L. The cusp condition: Constraint on the electron density matrix. *Int. J. Quantum Chem.* 6, 519–523 (1972).
[74] Clinton, WJ, Massa, L. Antisymmetric wavefunction densities from coherent diffraction data. *Trans. Am. Crystallogr. Assoc.* 8, 149 (1972).
[75] Clinton, WJ, Massa, LJ. Determination of the electron density matrix from X-ray diffraction data. *Phys. Rev. Lett.* 29, 1363–1366 (1972).
[76] Clinton, WL, Galli, AJ, Henderson, GA, Lamers, GB, Massa, LJ, Zarur, J. Direct determination of pure-state matrices. V. constrained eigenvalue problems. *Phys. Rev.* 177, 27–33 (1969).
[77] Clinton, WL, Galli, AJ, Massa, LJ. Density matrices, II. Construction of constrained idempotent one body densities. *Phys. Rev.* 177, 7–12 (1969).

Index

This index covers the keywords in the text which include the names of authors that are cited by name therein. It does not cover author or keywords in the reference lists appended to each chapter or appendix.

https://doi.org/10.1515/9783110566673-015